DISCLAIMER

This report was prepared as an account of work sponsored by an agency of the United States Government. Neither the United States Government nor any agency thereof, nor any of their employees, makes any warranty, express or implied, or assumes any legal liability or responsibility for the accuracy, completeness, or usefulness of any information, apparatus, product, or process disclosed, or represents that its use would not infringe privately owned rights. Reference herein to any specific commercial product, process, or service by trade name, trademark, manufacturer, or otherwise does not necessarily constitute or imply its endorsement, recommendation, or favoring by the United States Government or any agency thereof. The views and opinions of authors expressed herein do not necessarily state or reflect those of the United States Government or any agency thereof. Reference herein to any social initiative (including but not limited to Diversity, Equity, and Inclusion (DEI); Community Benefits Plans (CBP); Justice 40; etc.) is made by the Author independent of any current requirement by the United States Government and does not constitute or imply endorsement, recommendation, or support by the United States Government or any agency thereof.

Grid Resiliency with a 100% Renewable Microgrid

Final Technical Report (FTR)

DE-EE0009027

Laurence Abcede, Kimberly McGrath, Jose Cardenas, Beverly Glory, Taha Mustafa, Mary Cortez, Maison Cowley, Nagadev Shanmukh, Alejandra Jacquez

San Diego Gas & Electric Company®, San Diego, California, United States

Annabelle Pratt, Kumaraguru Prabakar, Jing Wang, Yaswanth Nag, and Martha Symko-Davies

National Renewable Energy Laboratory, Golden, Colorado, United States

Acknowledgements

This material is based upon work supported by the U.S. Department of Energy's Office of Energy Efficiency and Renewable Energy (EERE) under the Solar Energy Technologies Office (SETO) Fiscal Year 2019 Funding Program Award Number DE-EE0009027.

The authors would like to thank EERE SETO Technology Advisor, Robert Reedy for his depth of experience and insights throughout the project, and Thomas Bialek, previously Chief Engineer at SDG&E, whose leadership and insights drove innovations at the Borrego Springs Microgrid.

Executive Summary

San Diego Gas & Electric Company (SDG&E) installed America's first and largest utility-scale microgrid in Borrego Springs in 2013. The first generation Borrego Springs Microgrid utilized diesel generators to form and stabilize the microgrid island, with support from grid-scale batteries and local solar photovoltaic (PV) generation.

In this project, SDG&E in partnership with National Renewable Energy Laboratory (NREL) demonstrated through modeling, simulation and utility field testing that blackstart and islanding of the microgrid can be led with 100% renewable, inverter based resources (IBRs), to help reduce community reliance on conventional generation resources.

Through equipment upgrades, grid-forming island leader capability was transitioned to a battery IBR instead of the Borrego Springs Microgrid diesel generators. A new microgrid controller was integrated to the microgrid and programmed to control and manage multiple energy storage systems. Synchrophasor and other power quality data verified autonomous, high-speed response of the IBRs through blackstart, islanding, and load step testing. Results of project field evaluations provide distribution systems operators (DSO) with increased confidence that renewable, IBR can replace traditional generators to blackstart and island microgrids and rapidly establish stable island frequency with rapid changes in peak power demand.

Importantly, the project validated the integration feasibility of a distributed energy resource management system (DERMS) controller that manages multiple grid-forming and grid-following IBRs, establishing a standard design interface to reduce the complexity of integrating new DERs in the future and supporting replication by the industry. As a result of learnings in this project, SDG&E has implemented the microgrid controller strategy at multiple other microgrid sites, thereby validating the replicability of the solution.

Hardware-in-the-loop (HIL) simulations including power and controller HIL hardware — along with electromagnetic transient (EMT) simulations of Borrego Springs Microgrid — informed adjustments to inverter parameters and were important to characterize the performance of the IBRs in relevant operating conditions before deployment. The EMT and HIL simulations of islanding the entire community are important contributions in providing confidence in IBR performance prior to future islanding of the community in the field. **High-fidelity EMT and/or HIL simulation of IBRs can de-risk field operations, and its relevance and importance as a tool is increasing as distribution grids and microgrids become more complex and dynamic with an increasing proportion of renewable generation, distributed energy storage, and two-way power and energy flows.**

Table of Contents

Background

The community of Borrego Springs (Figure 1) is in a rural desert region of San Diego County, California, located at the end of a long, radial electric transmission line. The major local resources of power generation include two third-party owned solar photovoltaic (PV) generation plants, one 26 MW_{ac} transmission interconnected, one 6.3 MW_{ac} distribution interconnected, as well as ~8.6 MW of customer rooftop PV. The community's location within the transmission grid, combined with a high proportion of local PV generation, creates a low-inertia grid environment; there is a shortfall of spinning mass normally provided by rotating turbines to stabilize any deviations in the power system's frequency. At the same time, the Borrego Springs community is subject to extreme weather conditions including high heat, high winds, and monsoon flooding. These conditions result in an increased risk for Public Safety Power Shutoff (PSPS) events, unplanned outages, and/or planned outages for compliance maintenance. Historically, outages can last from hours to multiple days.

With the need to increase community resiliency, SDG&E installed America's first and largest utility-scale microgrid in Borrego Springs in 2013.[1] A key operational outcome of the first generation microgrid was demonstrating that the community could be islanded with the generators as the island leaders, with support from renewable resources. The purpose of this project was to advance the capability of the microgrid, to demonstrate that blackstart and islanding of the microgrid can be undertaken with 100% renewable, IBR, thereby reducing reliance on conventional generators.

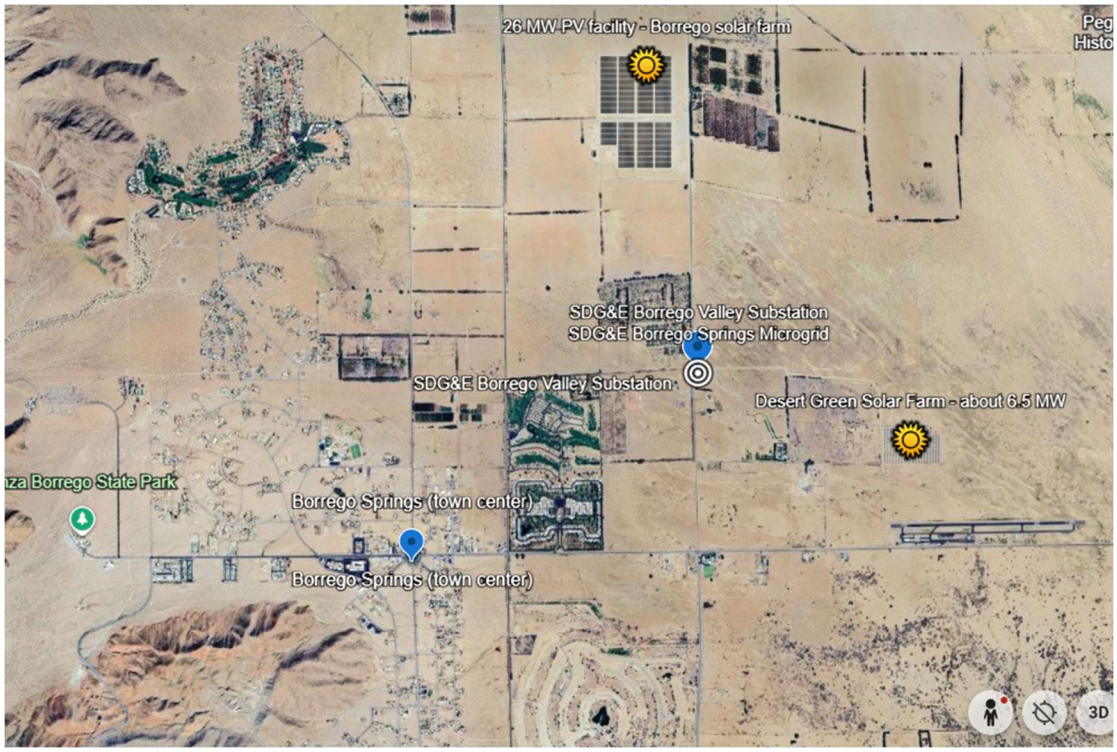

Figure 1: Aerial view of Borrego Springs from Google Earth.

State-of-the-art

The deployment of state-of-the-art distributed energy resources (DERs) and control strategies in utility grids and microgrids must be undertaken carefully with stepwise validation to mitigate risks of customer service disruptions. Studies to date have been concerned with modeling, simulation, and limited-scale field tests. Hardware-in-the-loop (HIL) simulations have previously demonstrated they can de-risk microgrid deployments and provide early insights by testing conditions that are not yet demonstrated during field operations. [1,2] Other laboratory HIL and field results have demonstrated blackstart using a grid-forming (GFM) battery and PV, with staged load pickup and re-synchronization routines, with GFM inverters establishing voltage and frequency references in a zero voltage network and able to pick up priority loads and then synchronize additional devices.[3] Simulation studies have indicated that further development of inverter control techniques, such as soft starting techniques, can expand the conditions under which IBRs can provide black-start support.[4] Integrated synchronization control for microgrid disconnection and reconnection has been developed for GFM inverters to smooth angle changes and reduce transients at the point of common coupling (PCC), and related work compares strategies for seamless reconnection of additional GFM units into an already energized inverter-based island.[5]

A recent interoperability systematic review highlighted that most microgrid interoperability research still concentrates on the communications layer, with relatively less emphasis on physical/electrical interoperability, and that adoption of common industry standards is one of the important strategies for ensuring interoperability, enabling microgrid systems to function effectively and reliably.[6]

Project Advancements

This project is built on previous Borrego Springs Microgrid development and addresses multiple technological and operational knowledge gaps identified for the deployment of coordinated renewable IBRs at scale and under conditions relevant to microgrid and distribution system operations.

Power hardware in the loop (PHIL) and controller hardware in the loop (CHIL) experiments using equipment and conditions matching field operation: Relevant HIL experiments were performed with PHIL and CHIL interfaces for GFM inverters and a microgrid control system, respectively. A PHIL interface to enable simulations of seamless transitions between islanded and grid-connected operation had to be developed, because inverters need to switch modes (i.e., between grid-following (GFL) and GFM) as the microgrid transitions between grid-connected and islanded operation. In this project, the relevant Borrego Springs Microgrid GFM inverter and microgrid control system was installed at NREL's Energy Systems Integration Facility (ESIF) to conduct PHIL and CHIL simulations to characterize and validate microgrid operations. A laboratory test plan was developed and executed that simulated different relevant field scenarios, including testing the ability of the GFM battery inverter to provide fast frequency response during islanding and load and/or insolation transient conditions. These tests were intended to demonstrate how advanced GFM inverter controls can contribute to grid stability and resiliency and reduce PV curtailment due to islanding operations with fast frequency response and maintaining frequency variations within

±0.5 Hertz under load variations ranging from 10% to 100% of full load at different time scales.

Modeling and simulation at scale: There is a need for richer physical/electrical validation beyond communications-layer interoperability. Studies which are small-scale (single feeders) and/or use simplified device and load models limit external validity to larger, unbalanced distribution networks that include power electronic devices. One objective of this project was to demonstrate the effectiveness of the GFM battery inverter controls through a more comprehensive simulation of the Borrego Springs Microgrid to validate how DERs contribute to grid stability and resilience by establishing frequency and maintaining voltage magnitude during transient conditions. Electromagnetic transient (EMT) simulations are complementary to simulations on the HIL platform to test the microgrid stability and reliability under dynamic events, especially for scenarios that are hard to complete in HIL due to potential hardware damage. EMT simulations in this project sought to elucidate the stability and reliability of the Borrego Springs Microgrid under various dynamic scenarios.[8,9] In this project, 20 grid-following PV inverter models were used to simulate the 26 MW_{ac} PV installation, including their controls, along with the two battery energy storage systems (one GFM and one GFL) and at least 80 customer-owned solar installations, some of which have smart inverter functions. This simulation therefore exceeded 100 inverters and contained many nodes.

Making DERMS used as a microgrid control system controller software more configurable and interoperable: This project systematically evaluated the design of a standard interface for various DERs to decrease the complexity of interfacing between a DERMS and the edge device. The development goal was to shorten the time needed to integrate and interface a DERMS controller with distribution system operations, thereby enabling the incorporation of additional DERs.

Real-world utility evaluation of 100% renewable blackstart and island: To the team's knowledge, this project was the first of its kind to upgrade an existing battery inverter based resource with grid forming and island leader capability and establish control parameters to coordinate that resource with a grid following battery and grid following ultracapacitor through a DERMS used as a microgrid controller. Conventional generators, once the island leaders, were deprioritized to backup systems only. Results of utility field evaluations represent a key step to improve the operational effectiveness of microgrids and provide operational confidence that renewable resources can replace fossil generators to blackstart and island microgrids and maintain stable island frequency with rapid changes in real power demand.

Project Objectives

Goals & Objectives

The primary goal of this project was to demonstrate islanding and blackstart of the Borrego Springs Microgrid with 100% renewable resources, validating that inverter-based resources (IBRs) can contribute to grid stability and resilience by establishing frequency and maintaining voltage magnitude during transient conditions, especially during microgrid islanding. Field implementation and validation of these advanced resources helps operators gain confidence that IBRs can capture more value in renewable microgrids and improve the stability and resilience of the electric system. The broader impact was to establish a replicable model that developers and utilities can use to deploy renewable microgrids that combine solar generation, energy storage, and coordinated control to increase resilience and reduce reliance on fossil-fuel generation.

Significant advancements in the state of the art of modeling, simulation, and field integration of grid forming and grid following battery IBRs were required to achieve the project goals and objectives. A high-fidelity HIL platform incorporating power and controller hardware akin to field equipment, utilized under realistic operating conditions at Borrego Springs Microgrid, was needed to de-risk field implementation of new technology by assessing new grid-forming and grid-following distributed energy resource control schemes and supporting adjustments to inverter parameters. HIL testing supports the safe rollout of an increasing share of inverter and other power electronic IBRs into distribution systems.

The capability developed in this project has tremendous nationwide impact as distribution networks add increasing amounts of PV generation, battery energy storage, and electrification of transportation, where system dynamics become faster, nonlinear, and require tight coupling to communications and protection settings. The HIL platform developed enables utilities and other users to exercise real controllers and power-electronics firmware against feeder- and microgrid island scenarios before deployment. By validating interoperability under realistic contingencies, HIL can demonstrate reducing integration risk and preventing adverse interactions that threaten stability and power quality.

The operation of multiple grid-forming and grid-following inverters within a microgrid power system are not well understood under dynamic operating conditions, such as islanding. It is particularly relevant to demonstrate effectiveness of coordinated IBRs to form and maintain stable microgrids in more complex operating environments such as the Borrego Springs Microgrid, which ties to a low inertia environment grid, has a high proportion of renewable generation, and experiences large intermittent loads. Therefore, this project conducted dynamic modeling evaluations to study the behavior of transitioning island-leader functionality to an IBR from a conventional generating resource under dynamic conditions such as islanding, load changes, and solar insolation variation.

The Borrego Springs Microgrid is rural and remote. Therefore, development of a standard, more configurable control software interface for various distributed energy

resources (DERs) was important to decrease the complexity of interfacing between DERMS and IBRs. Demonstration of coordinated control of these assets through DERMS was an important aspect of this project to reduce the need for on-site manual operation and demonstrate control from SDG&E's distribution operations center over 100 miles away.

Dissemination of the details of HIL test capabilities, field test setups, simulations, and test results were an important outcome in this project to support broader and further technical advancements in the integration and operation of IBR in electric distribution grids and microgrids.

Task and Milestone Summary

This report reflects the results of work performed by SDG&E and NREL for this project. The various tasks designate the lead entity performing the task. Developments in this project proceeded across four major workstreams, namely HIL Advancements, Software Simulation Enhancements, Power Conversion System (PCS) Upgrades and Utility Field Demonstrations.

HIL Advancements

Table 1 summarizes the HIL workstream and milestones. Deploying new technologies in the field has inherent risk, especially to customers in the area where the field commissioning of new control systems and inverters is carried out. The objectives of this task are to enhance the HIL capabilities used in conjunction with simulation tools to perform pre-field demonstration work in NREL's ESIF laboratory. Successful pre-field demonstrations in the laboratory decrease the risks associated with field commissioning of new control systems and inverters, ensuring that operational procedures are validated and accurate, and enhance overall safety and reliability in the field.

Table 1: HIL workstream tasks and milestones.

Workstream and Tasks	Technical Milestones
HIL Advancements **Tasks 1 and 10:** HIL Enhancement **Tasks 4, 13, 18:** HIL Test Plan Development and Execution	• BP1-6-T1: Complete HIL setup with capacitor bank controller, regulator controller and LTC controller. • BP2-10-T10: The HIL setup with selected hardware should operate seamlessly with the CHIL devices added. • BP2-16-T10: Accepted paper in conference/journal. • BP2-13-T13: HIL Test Plan completed. • BP2-15-T13: Complete initial testing with the complete integrated HIL evaluation platform setup with test cases. • BP3-22-T18: Completed 25 % of the experiments outlined in the HIL Test Plan. • BP3-24-T18: Complete execution of the HIL Test Plan. • BP3-25-T18: Create report detailing the results of the HIL simulations outlined in the test plan. • BP3-26-T18: Accepted paper in conference/journal. • BP3-30-T18: Define additional HIL simulations based on field tests. • BP3-31-T18: Perform additional HIL simulations and document results. • BP3-35-T18: NREL CRADA

Software Simulation Enhancements

Table 2 summarizes the software simulation workstream and milestones. The objectives of these tasks were to update the existing Borrego Springs RSCAD model to integrate the enhanced HIL capabilities from Task 1 to enable real time digital simulation (RTDS) work, providing a realistic representation of the field. The RSCAD model developed provides a high-fidelity simulation capability to test the different novel control and hardware developments.

The operation of multiple grid-forming and grid-following inverters within a power system are not well understood under dynamic operating conditions, such as islanding. The objectives of full scale simulation are to demonstrate the effectiveness of the GFM inverter controls through a more comprehensive simulation of the Borrego Springs Microgrid, and to study the behavior of multiple grid-forming and grid-following inverters under dynamic conditions such as black start, islanding, load and solar insolation changes.

Table 2: Software simulation tasks and milestones.

Workstream and Tasks	Technical Milestones
Software Simulation Advancements Tasks 2 and 11: RSCAD Modeling of Borrego Springs Microgrid Tasks 5, 14, and 19: Full Scale Simulation	• BP1-9-T2: RCSAD model should operate properly in grid connected mode and islanded mode for simple test cases. • BP2-20-T11: The complete HIL platform is ready for use. • BP2-19-T14: Complete full scale RSCAD simulation models including explicit models of grid-forming inverters. • BP3-23-T19: Execute full-scale simulation plan and analyze results. • BP3-29-T19: Execute full-scale simulation plan, including contingency scenarios and analyze results.

Power Conversion Systems (PCS) Upgrades

Table 3 summarizes the PCS upgrade workstream and milestones. The purpose of Tasks 6 and 15 were to establish baseline operating performance before system improvements are made and then complete the design upgrade requirements. The process enhances overall system design and ensures operational procedures are drafted and tested appropriately. Tasks 7 and 16 enable GFM capabilities for the IBRs and will enhance voltage and frequency stability for the Borrego Springs Microgrid, including upgrades to the site power meter, engineering of the interface to the new inverter control system, and evaluation of the operability of the new interface.

Table 3: PCS Upgrade tasks and milestones.

Associated Tasks	Technical Milestones
PCS Upgrades Task 6 and 15: Engineering Assessment of Existing ESS PCS and Upgrade Design Task 7 and 16: PCS Control Upgrade Task 8: Standard Interface Development	• BP1-1-T6: Assessment of existing battery. • BP1-3-T6: Upgraded battery specification defined. • BP1-2-T8: Review interface points list. • BP1-4-T8: Review communication protocols and cyber security requirements. • BP1-7-T8: Standard interface proposed. • BP2-14-T16: Battery control system constructed, commissioned and energized. • BP2-18-T16: Test concurrence by a major vendor and SDG&E.

Utility Field Demonstrations

Table 4 summarizes the utility field demonstration tasks and milestones. Tasks 9, 17 and 20 are related to field testing and microgrid operations. Task 9 conducts a comprehensive review of historic island operations at Borrego Springs Microgrid, assessment of the control and process changes needed to operate the microgrid with IBR, and field testing. Tasks 17 and 20 are for preparation and execution of field testing to validate 100% renewable microgrid blackstart and islanding.

Table 4: Utility field demonstration tasks and milestones.

Associated Tasks	Technical Milestones
Utility Field Demonstrations Tasks 9, 17, and 20: Field Tests	• BP1-5-T9: Review historical islanding events. • BP2-12-T17: Schedule field tests. • BP3-21-T20: Evaluation of battery-inverter resource response through microgrid controller for blackstart and island. • BP3-27-T20: Install pre-charge circuit on ultracapacitors and confirm operation. • BP3-28-T20: Evaluation of battery-inverter resource and ultracapacitor response through microgrid controller for blackstart and island. • BP3-32-T20: Conduct community-wide field demonstration. • BP3-33-T20: Analyze field test and demonstration results. • BP3:24-T20: Final report

Project Go/No-Go Decision Points

Go/No-Go Decision Point	Validation
1: Complete validation of upgraded model. (Tasks 1 and 2)	The RSCAD model is validated, and test results are documented.
2: Battery control system designed. (Tasks 6, 7, 8, and 9)	SDG&E subject matter experts, vendor and microgrid controller provider agree to new design.
3: Initial RSCAD model with controller HIL set up and tested. (Tasks 1 and 2)	Initial model is tested with simple test cases.

Table 5 summarizes the project Go/No-Go decision points with associated tasks and validation method.

Table 5: Project decision points.

Go/No-Go Decision Point	Validation
1: Complete validation of upgraded model. (Tasks 1 and 2)	The RSCAD model is validated, and test results are documented.
2: Battery control system designed. (Tasks 6, 7, 8, and 9)	SDG&E subject matter experts, vendor and microgrid controller provider agree to new design.
3: Initial RSCAD model with controller HIL set up and tested. (Tasks 1 and 2)	Initial model is tested with simple test cases.

Project Results and Discussion

Overview of the Borrego Springs Microgrid and Distributed Energy Resources
Referring to Figure 2, the Borrego Springs community is served by three 12 kV distribution circuits, and the Borrego Springs Microgrid yard is located directly next to the substation, which steps down voltage to 12 kV from the 69 kV transmission line. A 26 MW_{ac} PV plant is interconnected to the 69 kV bus, and a 6.3 MW_{ac} concentrating PV array is interconnected to one of the 12 kV circuits. Presently, these PV assets are unavailable during microgrid operations. The community also has approximately 8.6 MW of rooftop PV generation, which contributes to the microgrid's renewable generation during operations, but is not controllable or controlled by SDG&E.

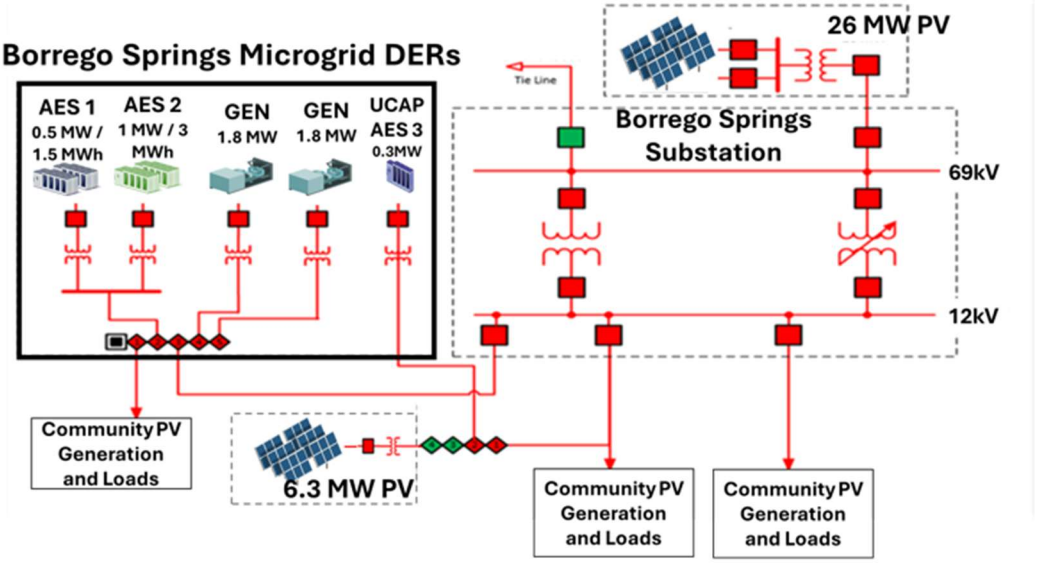

Figure 2: Diagram of the Borrego Springs Microgrid.

Figure 3 shows the existing and developed resources within the Borrego Springs Microgrid yard (dark blue), as well as existing local PV generation resources (light blue). Existing resources in the yard include a 1 MW/3 MWh battery energy storage system (AES2), a 0.5 MW / 1.5 MWh battery energy storage system (AES1), two modern 2.15 MW diesel generators (recently replacing legacy 1.8 MW generators), a 300 kW ultracapacitor system (AES3) and a 3 MW/3 MVAr load bank. Prior to this project, the older generators were utilized to blackstart and undertake island transitions, with battery energy storage serving a support role. The yellow area is a planned expansion of the microgrid. SDG&E aims to operate the Borrego Springs Microgrid in islanded mode either without diesel generators (when the BESS can meet the net load) or with the generators in load-following mode (when their capacity is needed to meet the net load). To achieve this, the 1-MW BESS, AES2, was upgraded with a GFM inverter that operates as the voltage and frequency leader when the microgrid is islanded and that is operated in GFL mode when the microgrid is connected to the grid. The 0.5-MW BESS inverter, AES1, is always operated in GFL mode. The ultracapacitor system, AES3, operates in GFL mode with a frequency-watt curve. The team implemented a microgrid controller to command the assets and provide a visual real-time status of the energy storage systems and other microgrid assets.

Figure 3. SDG&E Borrego Springs Microgrid assets.

Task 1: Hardware-in-the-Loop (HIL) enhancement (Task Lead: NREL)
Error! Reference source not found. shows the HIL test bed at the NREL Energy Systems Integration Facility (ESIF) enhanced during this project. The setup expands upon an earlier test bed that was developed for the Borrego Springs Microgrid with diesel generators and grid-following (GFL) inverters. [2,8] The distribution system is simulated in an RTDS Simulator with the time step set to 95 microseconds.

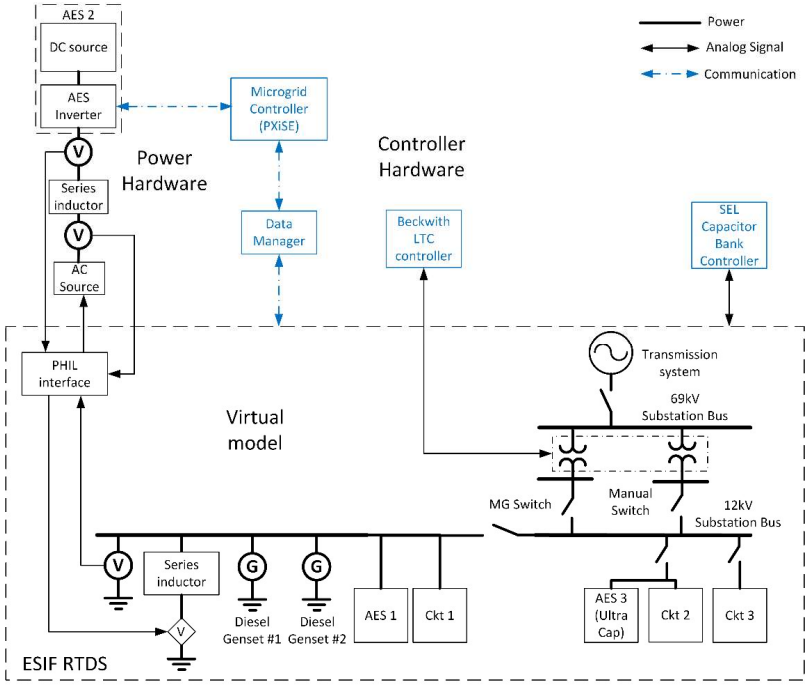

Figure 4: Diagram of the HIL test bed.

The power system model includes a simple representation of the transmission system; the substation transformers and load tap changers (LTCs); the microgrid (MG) switch; the three distribution feeders (Ckt 1, Ckt 2, and Ckt 3), all of which include rooftop PV systems; the two diesel generators, the GFL BESS, AES1; and the ultracapacitor system, AES3, on Ckt 2; and interfaces to the hardware. Each asset, AES1, AES2, AES3, Genset #1 and Genset #2, is connected to its own switch position to ensure safety and flexibility during operations and maintenance. Two LTC controllers, one capacitor bank controller, and the same microgrid controller that is deployed in the field are interfaced with the RTDS as controller-hardware-in-the-loop (CHIL). In Subtask 1.1 the team successfully incorporated load tap changer and capacitor bank controllers into the HIL test bed and demonstrated command functionality. This augmentation of the HIL testbed was important to increase the fidelity of the setup to study dynamic events in the microgrids. These two CHIL devices were not present in the previous version of the HIL setup at NREL's energy systems integration facility (ESIF).

Figure 5 pictures the two LTC controllers and two capacitor bank controllers installed at NREL's ESIF facility. This rack also hosts the RTDS analog input/output cards necessary to interface between the controllers and the model in RSCAD. The screen shows the pulse command sent from a capacitor bank controller to the RSCAD model. *Milestone 6 was achieved through completion of the HIL setup with capacitor bank controllers and LTC controllers.*

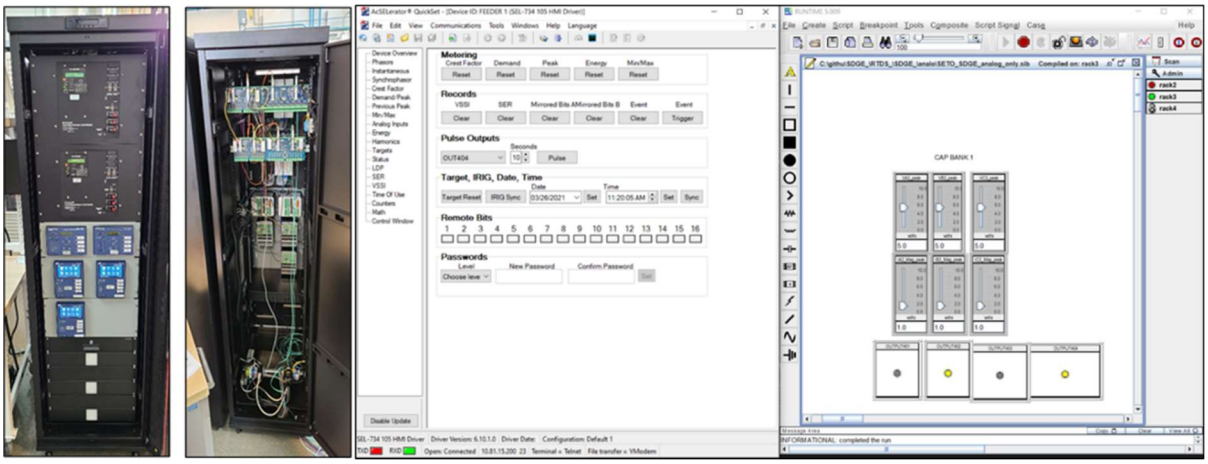

Figure 5: Rack with Beckwith load tap changers and SEL capacitor bank controllers. Capacitor bank controller operation through SEL quickset and the signals observed in RSCAD for a pulse command shown (RSCAD GUI Lights turning on for a pulse command).

NREL ran the RSCAD model with the Beckwith Load Tap Changer controllers and the SEL Capacitor Bank Controllers. Commands were sent from the Beckwith and SEL graphical user interfaces (GUIs), respectively. Figure 6Error! Reference source not found. shows the LTC controller sending tap up command from the controller to the

RSCAD model. Figure 6 also shows this signal in the RSCAD HMI, and the tap position increased from 0 (as shown in Figure 1) to position 1.

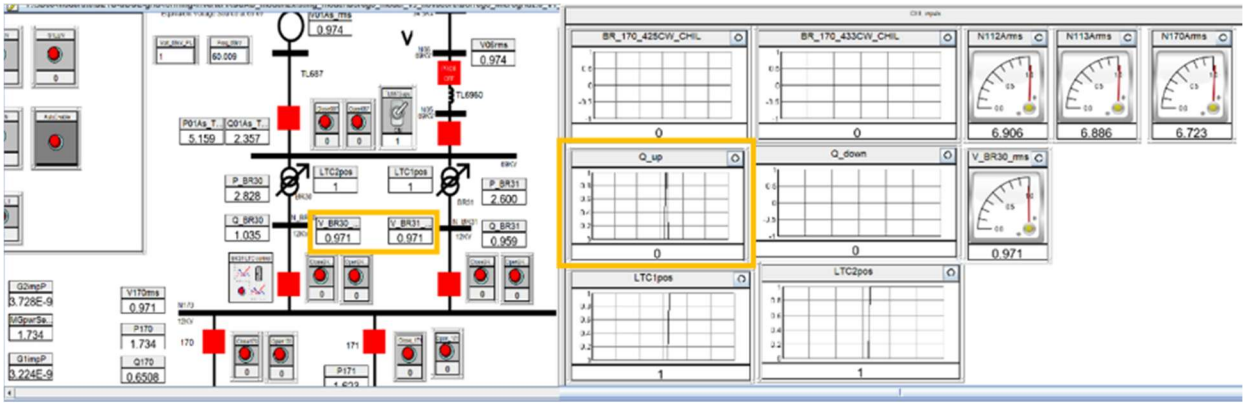

Figure 6: RSCAD HMI screen indicating LTC controller sending tap up signal to LTC transformers and the voltage increasing on the secondaries (indicated by the yellow boxes).

Figure 7 shows the SEL capacitor bank controller HMI setting indicating the voltage and current values measured from the RSCAD model. Figure 7 also shows the capacitor controller sending a close command to the capacitor bank to turn on the circuit breaker and connect the capacitor bank to the microgrid.

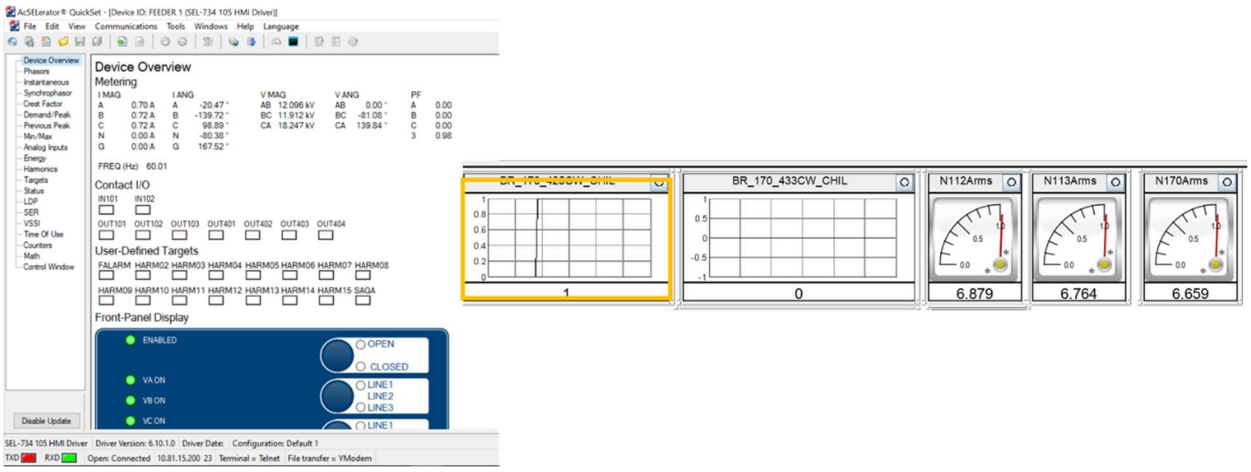

Figure 7: SEL capacitor bank HMI indicating voltage and current measurements from RSCAD model and capacitor bank controller turning on the capacitor bank in the Borrego Springs model.

In subtask 1.2, enhanced PV inverter simulation models were added into the HIL evaluation platform. Previously, distributed PV inverters were modeled using the net load at the circuit head. This approach did not yield reliable results as net load captures only the steady state performance and not the transient response. Figure 8 shows the dynamic PQ injection block available in RSCAD enabling inverter ride-through programming to represent the field response of grid-following inverters. The project team used this block to represent the rooftop PV inverters distributed on the three circuits at Borrego Springs Microgrid. In the field, the SDG&E microgrid controller does not control the third-party 6.3

MW_{ac} asset and thus this asset was not modeled in detail in the RSCAD model. This model allows the team to program the ride through settings of the inverters in the field and represent the field response of the inverters more accurately.

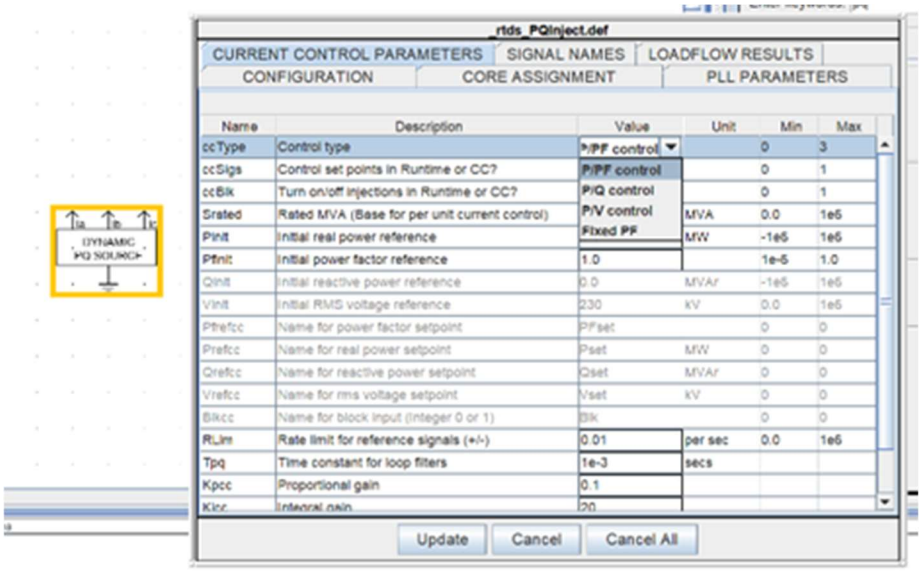

Figure 8: Dynamic PQ injection block utilized to represent the PV inverters.

Related to information dissemination regarding HIL setup development, NREL and SDG&E submitted the paper "Impact of Load Tap Changer Control Operation Under Microgrid Conditions" to IEEE, which was accepted and presented at the 2022 IEEE Power & Energy Society General Meeting (Milestone 16).

Task 2: RSCAD Modeling of Borrego Springs Microgrid (Task Lead: SDG&E)

The purpose of this task was to enhance the existing Borrego Springs RSCAD model to provide a very realistic representation of the field, incorporating opportunities to leverage NREL's HIL capabilities. In Subtask 2.1, RSCAD model updates were made reflecting the updated configuration of the microgrid, and data from observed microgrid events were used to verify the updates. First, updates were made to the Borrego Springs RSCAD model to consolidate recent topological, configuration settings, and firmware update changes in the field, adding more detail to the model to be able to recreate certain events observed in the field, and to allow for future additions/changes. The most significant model changes made were:

- Conversion of model to run on NovaCOR, the current generation of the RTDS Simulator's main processing hardware, for improved accuracy, performance, and scalability.
- Addition of switches and downstream loads to allow for accurate execution of sectionalizing steps of the islanding and blackstart distribution operating procedures.

The model was then tested against data collected from two past field events identified in Task 6:

- Planned island operation on 05/15/2018: data available included lower resolution load profile and MG output information useful for studying the response of the test environment.
- Blackstart operation on 12/19/2019: data available included higher resolution voltage and frequency information useful for DER transient studies.

5/15/18 Field Data vs. Simulation Results:
Figure 9 andFigure 10 show the comparison between the microgrid net load and the active and reactive power generation by the microgrid assets as dispatched by the DERMS between the field and the test environment across ~5 hours. The input to the test environment was the load profile from the 05/15/2018 event. There is a close match seen across this event except during time T1 during which the simulation reactive demand was different than the input provided. This was due to a limitation on the model where injection of reactive power is currently not supported.

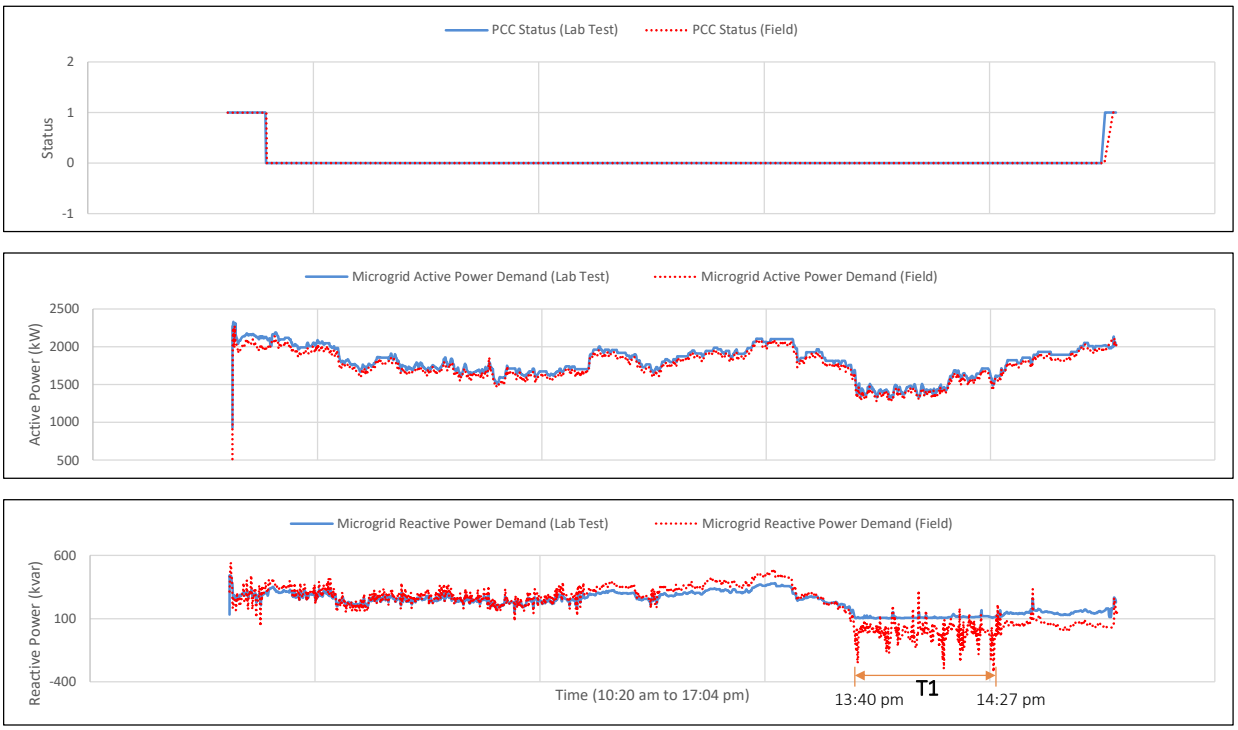

Figure 9: 5/15/18 Field Data vs. Simulation Results – microgrid active and reactive power.

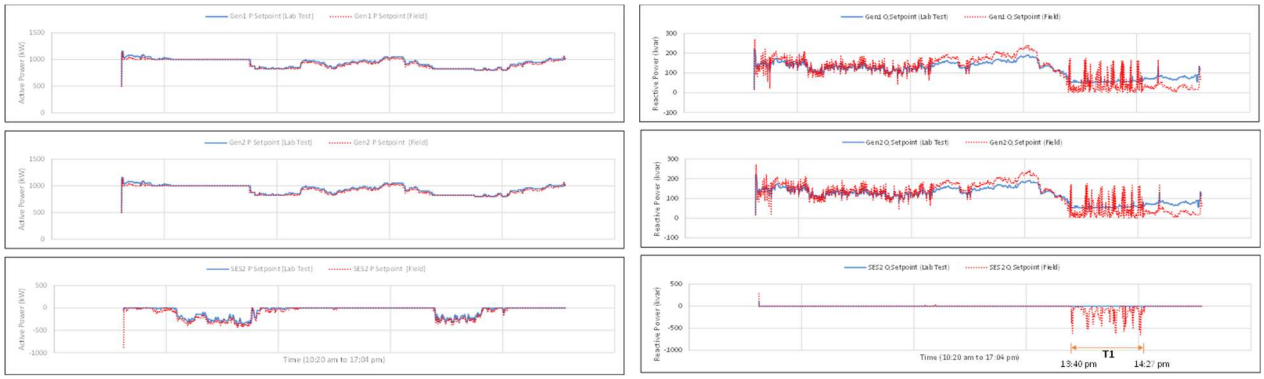

Figure 10: 5/15/18 Field Data vs. Simulation Results – generator and AES2 P setpoint active and reactive power (left), and Q setpoint active and reactive power (right).

Observations and conclusions from the 12/19/2019 event:

With higher resolution data being available for this event, this allowed for frequency and voltage transients comparisons in addition to time taken to return to steady state as shown below. Figure 11 and Figure 12 compare the field and test environment when blackstarting – demonstrating a close match between active and reactive power load response. Continued refinements were made to the governor and exciter control parameters in the model to improve the model fidelity of frequency and voltage transient response in the test environment.

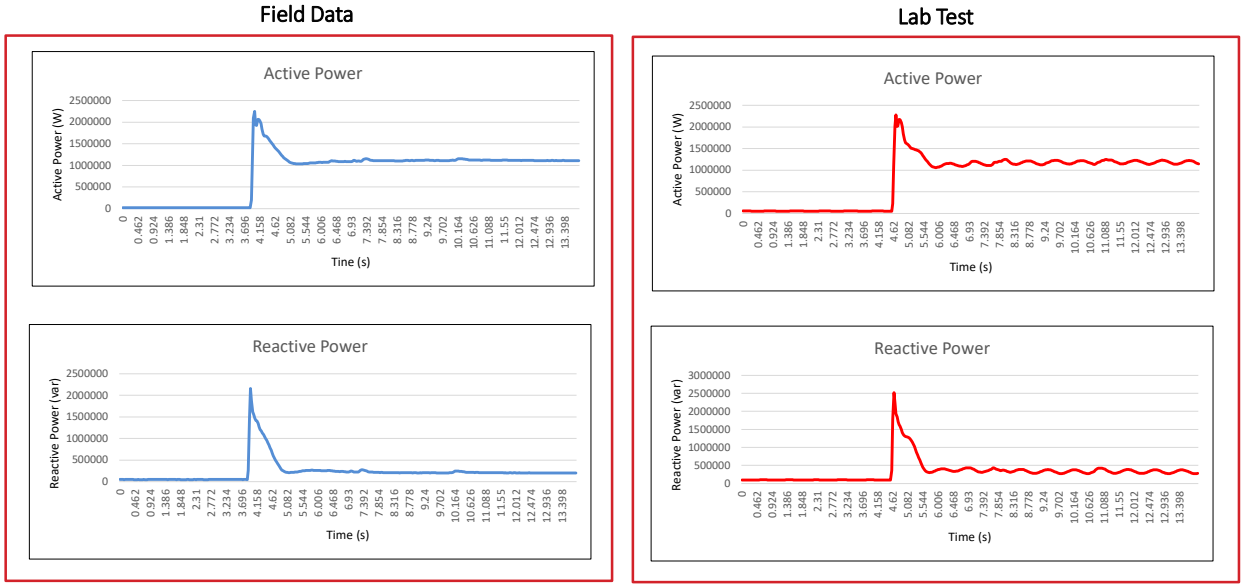

Figure 11: 12/19/19 Field Data vs. Simulation Results – active and reactive power.

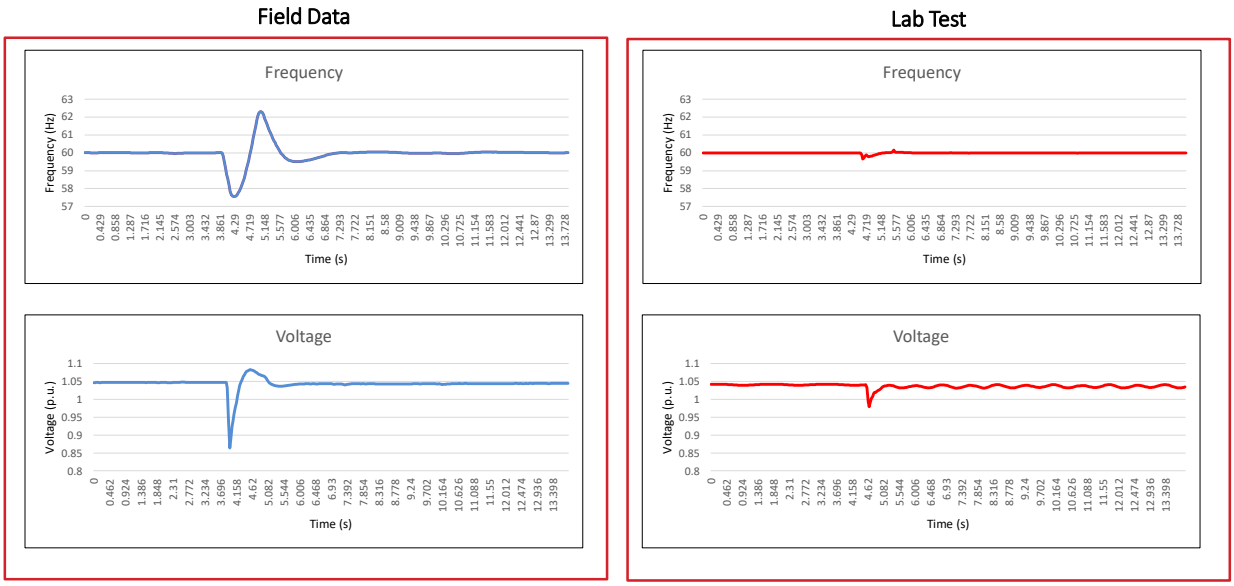

Figure 12: 12/19/19 Field Data vs. Simulation Results – frequency and voltage.

In Subtask 2.2 led by NREL, the Borrego Springs RSCAD model was updated with analog and digital IOs for the LTC and capacitor bank controller CHIL. This updated model was used at ESIF and the PHIL interface for the GFM battery inverter power hardware was added to it in Task 4. Figure 13 shows the processor assignment of the updated Borrego Springs model with the necessary analog, digital IOs for CHIL setup. Examples from the CHIL experiments are shown in the Task 1 results.

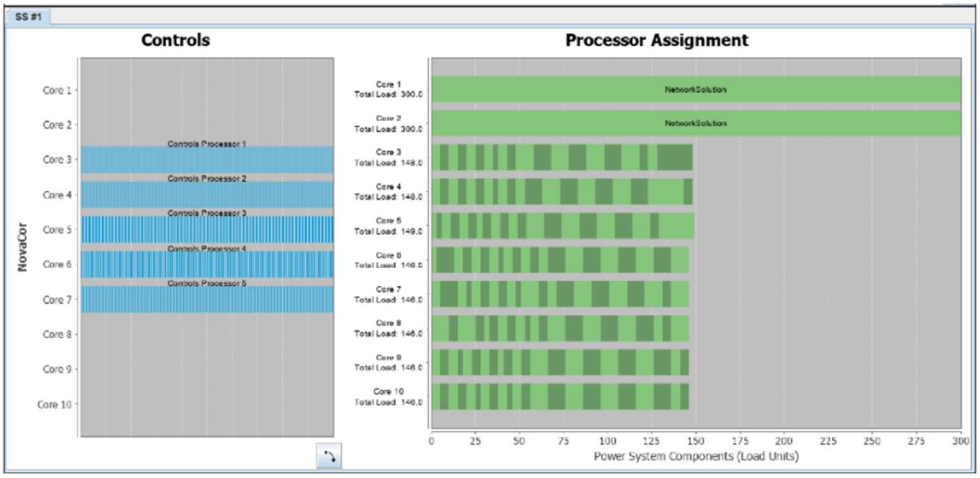

Figure 13: Successful processor assignment of Borrego Springs model at ESIF's 10 core NovaCOR rack.

Successful completion of this task achieved Milestone 9 of the project, demonstrating RSCAD model operated properly in grid connected mode and islanded mode for simple test cases. Based on the outcomes of Tasks 1 and 2, the team reached a Go decision for DP1: validation of upgraded model complete; executed against field test cases and documented, as well as DP3: Initial RSCAD model with controller HIL set up and tested. The updated RSCAD model ran RTDS at ESIF with the LTC controller and the capacitor bank controller connected to the RTDS hardware.

Task 3: Remote HIL setup between NREL's ESIF and SDG&E's Integrated Test Facility

Task 3 was de-scoped from this project before work initiated, related to unanticipated NREL operating costs for remote HIL setup between NREL and SDG&E. In addition, there were technical difficulties anticipated in the connection between a national lab and a private entity. SETO agreed that use of the revised hardware-in-the-loop setup at Energy Systems Integration Facility provided adequate validation for the operation evaluation

Tasks 4: HIL Test Plan Development (Task Lead: NREL)

The purpose of Task 4 was to identify HIL test plan requirements through the review of previous Borrego Springs Microgrid events, and to perform a review of site equipment and controls and identify needed inverter and controller hardware equipment to be installed from Task 6. There were three components of the ESIF evaluation platform: 1) the virtual model, 2) the controller hardware, and 3) the power hardware. For the virtual model, the Borrego Springs distribution system was simulated in real time using the RTDS digital real-time simulator. SDG&E provided the model, updated in Task 2, to NREL in the RTDS proprietary simulation software format, RSCAD, and NREL made the necessary modifications for integrating it with the hardware. The platform is shown in Figure 2 and includes:

- A simple representation of the transmission system
- The microgrid (MG) switch
- The three feeders (Ckt 1, Ckt 2, and Ckt 3) that include rooftop PV systems
- Two 1.8-MW diesel generators
- One utility-scale battery energy storage system (AES1) rated at 500 kW/1.5 MWh
- One ultracapacitor system (AES3) rated at 300 kW/30 sec on Ckt 2
- Interfaces to hardware.

Rooftop PV system models will capture the trip characteristics of the PV systems. The 26 MW_{ac} transmission interconnected PV facility, and the 6.3 MW_{ac} distribution interconnected PV facility are not planned to be operated during microgrid operation, and they are not included in the RSCAD model. The 6.3 MW_{ac} distribution PV facility is owned and operated by a third party and is non-dispatchable and non-controllable by SDG&E. Therefore, during a transmission line outage, only the rooftop PV is available amongst all three PV resources nearby.

For the controller hardware, two LTC controllers, two capacitor bank controllers, as well as a microgrid controller, identical to the field controller, was interfaced with the RTDS as CHIL. The microgrid controller was active during all the tests and its performance was captured as part of all the simulations.

For the power hardware, the GFM battery inverter, AES2, was implemented as power-hardware-in-the-loop (PHIL) using the same battery inverter model that is installed in the field. It was interfaced with the RTDS through a controllable AC source in series with an inductor and through a battery emulator that supplies DC power to the inverter. The

measured currents were scaled to represent the 88-kW inverter hardware as a 1-MW /3-MWh system. The hardware used in the evaluation setup is listed in Table 6**.**

Table 6: HIL hardware component selections.

Functional Component	Manufacturer	Part No.	Ratings
Controllable AC source/sink	Regatron	TC.100.690.144-ACS-19036-A	100kVA, bidirectional, 3 x 0 to 305 V AC
Controllable DC source/sink	NH Research	9300	100 kW bidirectional, 0–1,200 V DC, 334 A DC
BESS inverter (with internal transformer)	Hitachi Energy	EssPro PCS	88 kW, 300–420 V DC, 210–294 A DC 480 V/ 3 P / 60 Hz / 150 A Coupling voltage = 190 V AC
Inductor	CTM Magnetics	Custom	~1 mH
Simulation computer	RTDS	Rack system (x 2)	Total of 10 x cores
LTC controller	Beckwith	M-2001D	
Capacitor bank controller	Schweitzer Engineering Laboratories	734B	

Task 5: Full Scale Simulation (Task Lead: NREL)

The purpose of Task 5 was to identify full scale simulation requirements. Subject-matter experts from NREL and SDG&E worked together to define requirements and the team identified the necessary measurement points in the PSCAD model, different test scenarios, and models that need to be built in addition to the PSCAD model converted from the RSCAD model.

The power system model of the Borrego Springs Microgrid has more than 300 nodes. The three advanced energy storage systems (AES1, AES2, and AES3) were modeled in detail. In addition, 20 GFL PV inverters at the 26 MW_{ac} PV installations are modeled explicitly in PSCAD, including their controls. The 6.3 MW_{ac} PV facility is modeled in detail because it is part of normal grid-connected operation. More than 80 customer-owned rooftop solar installations are modeled in detail as well. The simulation therefore exceeds 100 inverters and 400 nodes. The original power system model for Borrego Springs was established in the existing model data format known as Synergi. An off the shelf conversion tool is not available to convert Synergi to PSCAD data format, so the team deemed it necessary to manually develop the power system model based on the updated RSCAD model that was developed in Task 2.

To complete the detailed model of the Borrego Springs microgrid, the team established three steps: (1) Start with the passive network and ensure that the power flow matches the passive network model in RSCAD; (2) Add the dynamic model of DER and verify the DER models one by one; and (3) Evaluate the overall stability and power quality of the microgrid model for both grid-connected and islanded mode. To build such a complex

model, the team identified the major challenges, which are summarized in Table 7 with the corresponding solutions to proceed with model development in Task 14.

Table 7: Challenges and solutions for Borrego Springs EMT simulations.

Challenges	Solutions
Simulation of full network with 105 DERs	The network is divided into three projects in PSCAD interlinked through a cable model.
Blackstart of the grid connection	An accelerated black-start sequence is performed to reduce the overall simulation time. For example, the rooftop PV is reconnected to the grid 5 seconds after the grid voltage is back rather than 5 minutes based on the IEEE 1547-2003 requirements.
Borrego Springs network stability	Control parameters of the PID controller of the AES2 GFM inverter are tuned to simulate the stable cases.

Task 6: Engineering Assessment of PCS and Upgrade Design (Task Lead: SDG&E)

The objectives of Task 6 were to review and analyze existing Borrego Spring Microgrid energy storage system resource designs, and frequency and voltage response of the existing Borrego Springs microgrid, to inform the project's field power conversion system (PCS) engineering upgrades and establish baseline performance characteristics. In Task 6.1, the team assessed frequency and voltage excursions from select past islanding events collected in Task 9. V and *f* analysis from historic islanding operations is critical to quantify improved resiliency and reliability in the planned upgrade, utilizing IBRs to provide fast frequency response in lieu of conventional generators. The islanding operation conducted on 12/19/2019 was selected for the most detailed analysis, because this event collected high resolution (33 ms intervals) phasor measurement (PMU) data at the Trayer switch; 1-minute or longer interval data is likely too infrequent to capture actual frequency maxima and minima. The 12/19/2019 islanding operation was a planned outage to conduct compliance maintenance, initiating at 9:27am and ending at 19:35pm. The on-site diesel generators were used to conduct the island transition.

Real power events were identified and characterized in grid parallel pre-island (over the course of approximately 2.5 hours) and during island (approximately 11 hours). Referring to Figure 14, six power events were captured pre-island, and 15 events were captured during island.

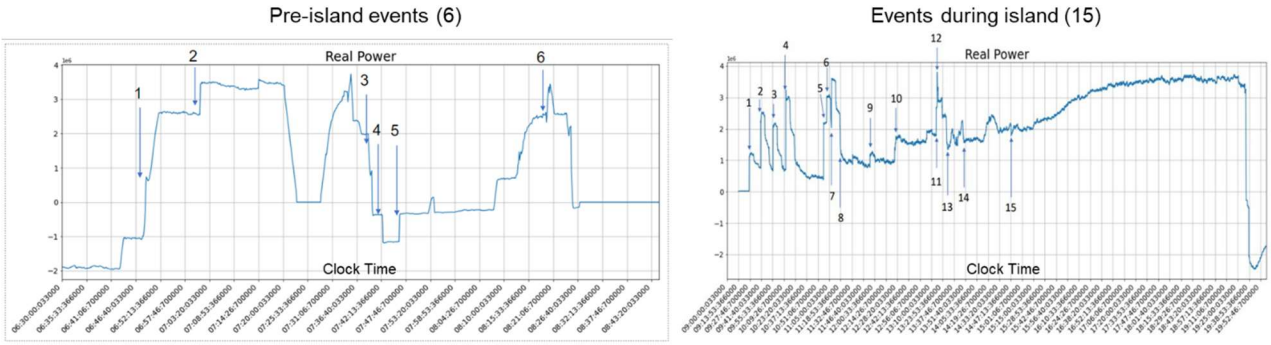

Figure 14: 12/19/19 Islanding operation - events captured pre-island and during island.

Table 8 summarizes voltage and frequency characteristics pre-island operation. Frequency and voltage remain in-bounds.

Table 8: Voltage and frequency characteristics of the microgrid, before islanding.

Bus	V1 (V)	VA (V)	VB (V)	VC (V)
Min	6979.21	6962.21	6975.05	7000.21
Max	7097.00	7071.11	7100.26	7125.90
Mean	7061.08	7039.54	7060.14	7083.62
Stdev	13.48	13.15	14.20	13.89

f min (Hz)	**59.995**
f max (Hz)	60.015
Mean	59.955
St Dev	**0.0149**
% Pnts > 60.6	0
% Pnts <59.4	0

Table 9 summarizes voltage and frequency characteristics during the island operation, in which rapid changes in power and frequency are observed with changes in real power. Power change events had significant impact to frequency, often exceeding 10% bounds of upper and lower frequency limits - 59.4 and 60.6 Hz, respectively.

Table 9: Voltage and frequency characteristics of the microgrid, during island.

Bus	V1 (V)	VA (V)	VB (V)	VC (V)
Min	6292.50	6152.60	6184.51	6125.72
Max	7450.33	7407.30	7437.83	7533.03
Mean	7180.11	7175.65	7157.65	7207.19
Stdev	24.06	25.20	37.28	39.29

f min (Hz)	**55.568**
f max (Hz)	62.096
Mean	60.000
St Dev	**0.0359**
% Pnts > 60.6	0.0083%
% Pnts <59.4	1.2720%

Referring to Figure 15, the island transition took 3.33 seconds to settle, with significant out of bound frequency excursion.

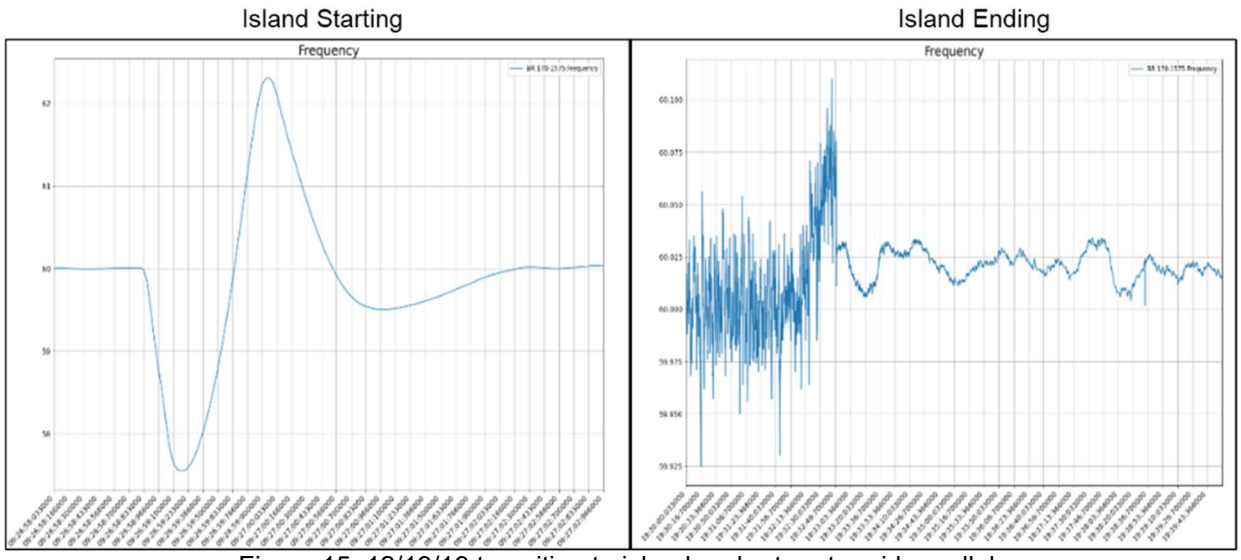

Figure 15: 12/19/19 transition to island and return to grid parallel.

Change in frequency per change in real power (d_{Hz}/d_{MW}) is an indicator of power system state of health for frequency stability. Table 10 summarizes the main power events during the island. During island, frequency exceeds 10% bounds of 59.4-60.6Hz utilizing conventional generation assets. Average range of frequencies is average 1.864x that of the change in real power. The events take on average 712.375 ms to settle to within 2% error of a 60Hz baseline. These reference points were utilized as benchmarks to gauge the effectiveness of the planned upgrades in the project, particularly the performance of an IBR to blackstart and form an island.

Table 10: 12/19/19 event frequency characteristics with load change.

Power Event	Real Power Change (MW)	dHz/dMW	Rise Time (ms)	Max (Hz)	Min (Hz)	Settling Min (Hz)	2% Settling Time (ms)
1	2.234	2.126	57	62.3	57.55	59.51	700
2	2.193	1.975	57	61.65	57.32	59.39	763
3	1.18	1.834	43	61	58.84	59.44	657
4	2.55	2.094	93	61.03	55.69	59.47	1100
5	1.148	1.477	50	60.72	59.02	59.19	623
6	1.166	2.012	57	61.01	58.66	59.62	690
7	1.177	1.856	53	60.84	58.65	59.24	583
12	1.182	1.54	73	60.66	58.84	59.18	583
Mean	1.604	1.864	60.375	61.151	58.071	59.380	712.375
Stdev	0.568	0.227	14.671	0.518	1.076	0.151	157.321
Max	2.55	2.126	93	62.3	59.02	59.62	1100
Min	1.148	1.477	43	60.66	55.69	59.18	583

In Task 6.2, the team conducted a review of the existing PCS topology and energy storage system design and then identified the updates needed to achieve the project objectives. Key design updates and features are upgrade of the AES2 battery inverter to serve as the island master, programmed functionality of AES2 to enable a 100% renewable blackstart, upgrade of the AES3 (ultracapacitor) inverter to higher power, and implementation of a microgrid controller for automatic islanding (considering the Task 8 objective of a standard, interoperable platform), upgrade to all inverter firmware and control panels, and power line communications (PLCs).

AES3 was programmed to serve as an out of bounds frequency arrestor, operating in GFL mode with a frequency envelope with a deadband of +/- 0.06 Hz, with maximum output power at 59.408 Hz and 60.592 Hz, as shown in Figure 16. **Error! Reference source not found.** summarizes the existing assets, upgrades, and features enabled by the upgrades. The design was reviewed and confirmed by SDG&E and project vendors.

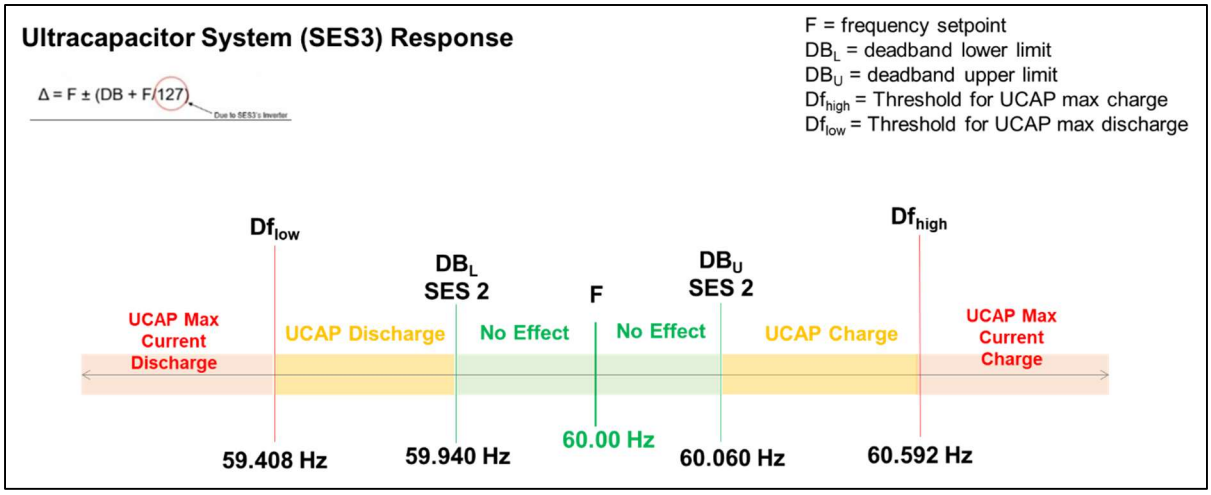

Figure 16: AES3 (ultracapacitor) operating principle.

Table 11: Summary of Existing PCS, upgrades required, and features enabling renewable operation of the microgrid.

ASSET	UPGRADE	FEATURES ENABLING RENEWABLE MICROGRID
Microgrid Controller	**Install New Microgrid Controller** Enables automatic, seamless islanding	• Software solution is scalable and replicable, supporting interoperability. Able to coordinate many DERs • High speed control
AES2 Li-ion (NCA) 1MW/3MWh **ISLAND MASTER** ***Energy Storage*** - Backup power - PV firming - Blackstart - Generator ramping/bridging	**Update Inverter Firmware, add Control Panel** Update inverter firmware and control panel to enable desired functionality and communication with other storage assets and the microgrid controller. **Upgrade ESS Controller and battery PLC** • Adaption of SEC functionality for communication with microgrid controller • Upgrade battery management system PLCs to improve communication between individual battery containers, enhance battery data logging.	• Enables grid forming functionality for seamless islanding, with programmable blackstart and grid fault detection. • Coordinated operation of all energy storage assets. • Ability for dynamic P and Q control, low voltage ride through, peak shaving, smoothing, battery state of charge management, *f*, and V control, blackstart • Programmed as island master • Enhances stability and fidelity across storage assets, all storage assets communicating locally via Modbus TCP/IP

AES1 **Li-ion (NCA)** **0.5MW/1.5MWh** ***Energy Storage*** - Backup power - PV Firming - Generator ramping/bridging	**Install New Inverters and Control Panel** Replace existing inverters and protections with 4 x 250 kW inverters	• Grid forming functionality for seamless islanding • Updated firmware enables unified operation of all energy storage assets.
	Upgrade ESS Controller and battery PLC • Add SEC to enable communication with LADC • Addition and upgrade of battery BMS PLCs – CAN bus communication between containers.	• Ability for dynamic P and Q Control, LVRT, peak shaving, smoothing, SOC management, *f,* and V control • Enhances stability and fidelity across storage assets, all storage assets communicating locally via Modbus TCP/IP
AES3 **UCAP** **0.5MW** ***Power Support*** - Islanding - Voltage stabilization - Fast Frequency Support	**Install New Inverters and Control Panel** - Add 500kW inverter for power upgrade (300kW derated), upgrade transformer to achieve higher power rating.	Addition of fast responding storage asset into rapidly inject power, provide fast frequency support during island transition and islanding operations
	Add Energy Controller (SEC) and UCAP PLC Develop local interface and site energy controller to establish connection with microgrid controller.	• Ability for dynamic P and Q Control, LVRT, SOC management, *f,* and V control • Enhances stability and fidelity across storage assets, all storage assets communicating locally via Modbus TCP/IP

In Task 6.3, the team evaluated renewable and load intermittency and possible grid interruptions, due to loss of generation, increased loading and possible faults on primary and secondary system. Fast-acting grid forming inverters paired with energy storage can mitigate outage due to PV variability, primarily through voltage support, secondarily through bridging power until PV generation is restored. Sitting on a single, long transmission line, the Borrego Springs Microgrid is susceptible to disruptions even in grid connected mode with a sudden loss of PV. Figure 17 exemplifies a fault due to unplanned loss of 26 MW_{ac} PV (voltage sag and tripping of breaker). Borrego Springs additionally has >8 MW of rooftop PV, with some intermittency related to cloud coverage and monsoon weather events. On average, the shape of the Borrego Springs Microgrid load is highly predictable, with agriculture operations representing approximately 25% of total load, peaking in the evenings. However, given the low inertia environment of the islanded microgrid, rapid changes in load even in magnitude of 1.5-2.5 MW observed during historic islanding operations, may cause out of bound frequency and voltage excursions and can potentially trip existing conventional generation assets depending on setpoints.

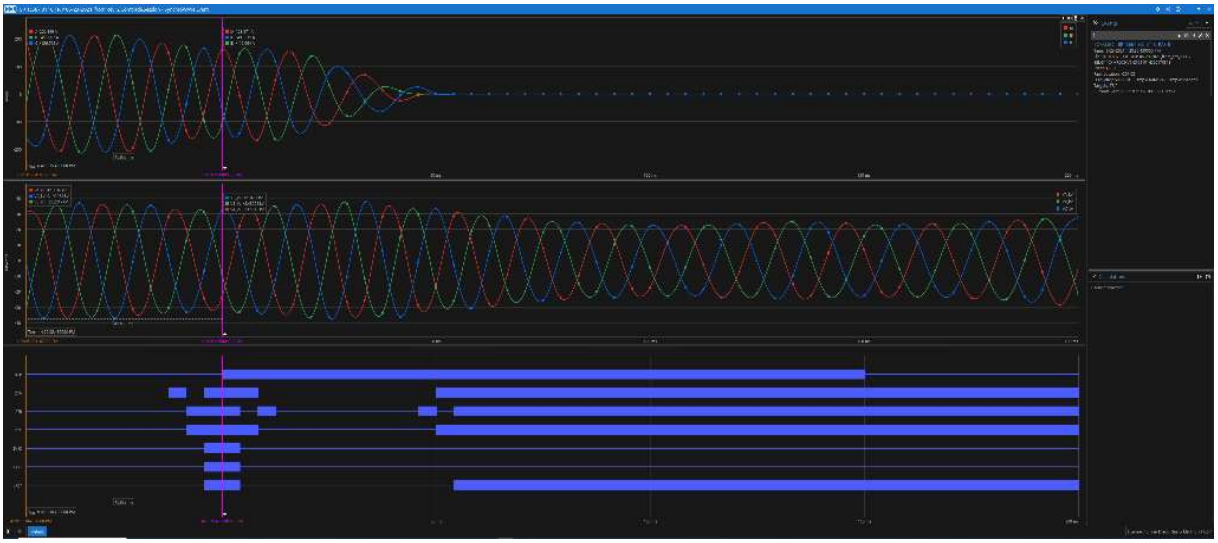

Figure 17: Impact of loss of 26 MW PV system on microgrid voltage (top) and current (bottom).

The existing energy storage system performance was assessed in Task 6.4 to review nameplate ratings, capabilities, functionality and historical operating performance.

Table 12: Assessment of energy storage systems, before upgrades.

	AES 1 (Li-ion)	AES 2 (Li-ion)	AES 3 (Ultracapacitor)
Power Rating (kW)	500	1000	250
Energy Rating (kWh)	1500	3000	12.5 (3 minutes)
SOC (%)	20-85%	20-85%	0-100%
Assessment	Meets specification, validate by cycling performance.	Meets specification, validate by cycling performance.	Meets specification, validate by cycling performance, will be upgraded with 500kW inverter to serve as a higher power, shorter duration system

summarizes the specification and performance of each of the storage assets, and the assets were validated by cycling performance (current and voltage), confirming that AES 1, 2, and 3 performance specifications met the requirements for operation in the project.

Table 12: Assessment of energy storage systems, before upgrades.

	AES 1 (Li-ion)	AES 2 (Li-ion)	AES 3 (Ultracapacitor)
Power Rating (kW)	500	1000	250
Energy Rating (kWh)	1500	3000	12.5 (3 minutes)
SOC (%)	20-85%	20-85%	0-100%
Assessment	Meets specification, validate by cycling performance.	Meets specification, validate by cycling performance.	Meets specification, validate by cycling performance, will be upgraded with 500kW inverter to serve as a higher power, shorter duration system

Milestones 1 and 3 were achieved through successful completion of ESS assessment in Task 6.1 and upgraded battery specification defined in Task 6.2 and 6.4.

Task 7: PCS Control Upgrade (Task Lead: SDG&E)
The purpose of this task was to develop the energy storage inverter control interfaces to the microgrid controller and confirm interoperability, in anticipation of completing the design, engineering and programming in Tasks 15 and integration in Task 16. Power quality metering was established to analyze power quality and digitally record faults.

Task 8: Standard Interface Development (Task Lead: SDG&E)
In Task 8, a standard design interface for DERs was established to decrease the cost and complexity of integrating these resources with a DERMS controller. As a first step (Task 8.1), the team reviewed existing and potential new microgrid applications. These applications include energy resiliency, alternative service models and reduction of Public Safety Power Shutoff (PSPS) events. Additional applications included marketplace participation and opportunities to support the grid, while in parallel. Table 13 summarizes applications, capabilities and benefits. These benefit streams were disseminated during stakeholder engagements and tours of the Borrego Springs Microgrid.

Table 13: Review of DER microgrid applications, capabilities, and values.

Applications	Direct (green) or Indirect Value (blue)	Description	Microgrid Capabilities	Ratepayer and Societal Value
Reduce Local Fossil Fuel Consumption	1) Fuel Savings 2) Future reduction in number and/or size of on-site generators.	Renewable DER assets provide the required power and energy reliability such that traditional generators deployed in microgrids can be turned off or downsized/eliminated in new projects.	**Grid Forming Inverters + ES** '- Seamless transition to island - Blackstart - Acting island master - Voltage support - Frequency Response (+Frequency Reg) **Controller** '- Real-time generation and load balancing (increase intelligence of resource aggregation, informs grid planning and operations) - Interoperability of grid-edge DERs (standard interface), adaptable controller **Protocols** - Integrated control and management between LADC and DSO - Information transparency - local, control center, system operator	Reduced cost of energy Reduced demand charges Reduction in GHG emissions Increased power quality and reliability Insultation from price volatility of fuel and electricity Reduced power outages Avoidance of economic, equipment damage losses associated with power quality issues Avoidance of losses due to business interruption and loss of production/scrap Service continuity during PSPS Back up and emergency power availability Market participation
Reduce purchase of G, T, & D services	Energy cost savings	Microgrid renewable DER assets providing local power reduces purchases of grid electricity.		
Reduce purchase of ancillary services and provide ancillary services	Energy cost savings	Support grid voltage, frequency, deliver capacity when called upon.		
Mitigate Curtailment	Energy cost savings (increased energy utilization)	Peak energy captured and utilized during peak demand via energy storage, or directly utilized for value-added activity (e.g., hydrogen generation, wastewater treatment, desalination)		
Improved Security and Safety	1) Maintain local critical facility operations during outages 2) Emergency service support during outages 3) Decentralization of power supply reduces risk of successful infrastructure attack; critical security loads seamlessly powered in island operations.	**Islanded operations during PSPS events provide continuity of service - especially important to critical loads such as healthcare facilities. MG acts as "energy hub" during emergency events. Ability to partition power to critical and/or most sensitive loads.**		
Enhancement of Grid Resiliency and Stability	1) Provide contingent capacity, fast frequency response and/or ensure power quality when the grid is unavailable 2) Deferral of T&D capacity investment 3) Reduce T&D capacity losses 4) Support deployment of new renewable generation	Seamless transition to island with ability to operate in island mode for prolonged periods of time. Use of DERs to reduce grid energy use during peak hours, thereby reducing need for additional T&D lines.		
Reduction in operating reserve requirement	Deferral of new plant new construction	Use of resources within a microgrid defers need to install additional peaking capacity		
Scalability, Flexibility, and Evolution	Responsiveness to evolving consumer requirements	Ease of integration of DERs at the grid edge facilities integration of new and/or additional utility, third-party, or customer owned assets which the utility can optimally dispatch.		

Next, the team established a points list for new and upgraded energy storage IBRs to be integrated into the microgrid (Subtask 8.2). Formalization of standardized points is the basis for providing universal guidance for DERMS-distribution system operator interface, supporting interoperability of a variety of DERMS assets. Feedback was provided from project hardware and software vendors that were engaged by SDG&E to assist with this project. For existing equipment, SDG&E updated its points list to ensure consistency with SDG&E standards. For new equipment, a standardized points list was generated. Points were added and eliminated as necessary within limitations of existing

setup and scope of this program. Table 14 summarizes changes to the control modes of the energy storage assets.

Table 14: Summary of control mode changes of energy storage assets.

ESS Asset	Inverter	Device Controller	Action Taken	Control Mode
AES2 GFM	Existing	Existing	Updated existing points list.	To operate as the grid forming resource for the microgrid. Grid connected: Voltage source inverter (VSI) Power Quality (PQ) Microgrid: Voltage source inverter (VSI) Voltage Frequency (VF)
AES1 GFL	New	New (matched to AES2)	New points list generated, aligned with standards of existing SDG&E points lists.	Current source inverter (CSI) base mode with P and Q setpoints
AES3 GFL	New	New	New points list generated, aligned with standards of existing SDG&E points lists.	Current source inverter (CSI) Frequency Regulation mode

Milestone 2 was completed with the review of the interface points list.

In subtask 8.3 MODBUS TCP/IP was selected as the local communications protocol for the individual energy storage DER assets to be implemented based on the practical and technical criteria of interoperability, ease of use, configurability, and cost.

- The protocol supports a multi-vendor ecosystem, in that it is vendor-neutral and standardized, enabling “plug and play” integration of different DER components such as inverters, energy storage, controllers, and meters.
- It is straightforward to implement MODBUS TCP/IP on embedded devices and strong for real-time monitoring and control where complex messaging is not needed. Further, it has clear function codes making it easier to debug and maintain.
- It utilizes existing standard internet protocol based infrastructure and allows devices to communicate over local area networks (LAN), fiber, or through virtual private networks (VPN). Therefore, it supports integration with SCADA systems, HMI panels and PLCs over standard networks.
- It is low cost and open source, scalable and has a mature ecosystem of open source protocol analyzers.

A noted disadvantage of MODBUS TCP/IP is that it has no authentication, encryption, or session control. So, it must be secured externally with network segmentation, firewalls, VPNs, or secure proxies. Per subtask 8.4 SDG&E reviewed the protocol with the SDG&E cybersecurity team confirming there were no additional cybersecurity requirements needed to deploy the strategy (Subtask 8.4). Information security standards require encryption of any communication that happens between different zones (for example between a site and a data center). In the case of the Borrego Springs Microgrid, MODBUS communications between the DERs and the controller all occur on the site, within the same zone.

Subtask 8.5 established the standard interface. SDG&E shared the points list with the microgrid controller vendor and PCS equipment provider. The team disseminated information for future sharing of the points list and other recommended procedures. *Communication protocols were deemed compatible and facilitate DER interoperability. Existing SDG&E cybersecurity requirements were applied to the new energy storage specifications, completing Milestones 4 and 7.*

Task 9: Field Tests (Task Lead: SDG&E)

This task undertook a comprehensive data collection and review process of historic islanding events at the Borrego Springs Microgrid, to select the events to be analyzed in Subtask 6.1. Table 15 summarizes the historic islanding events.

Table 15: Historic islanding events at Borrego Springs Microgrid (as of June 2021.)

Date	Event Type	Island Duration
Sept 6-7, 2013	Emergency Outage - Storm	6 hours
5/21/2015	Planned Outage - Maintenance	8 hours
3/13/2016	Planned Outage - Maintenance	90 seconds
5/17/2016	Planned Outage - Testing	1 hour
10/4/2017	Planned Outage - Testing	5 hours
5/5/2018	Planned Outage - Maintenance	4.5 hours
10/9/2018	Planned Outage - Maintenance	3 hours
12/19/2019	Planned Outage – Relay Calibration &Transmission Pole Replacements	12 hours
2/5/2020	Planned Outage – Relay Calibration & Transmission Pole Maintenance	5 hours

Referring to Figure 18, with an understanding that high resolution data would be necessary to measure frequency and voltage excursions for calculation of rate of frequency response and rate of change per unit of real power, the team identified two events for further analysis. The event of 5/5/2018 collected data at 1-minute intervals, and the 12/19/2019 even collected data at 33 ms intervals.

Figure 18: Down selection process for Vand *f* analysis.

Milestone 5 was completed with historic islanding events reviewed, and events down selected for analysis.

Figure 19 presents the Borrego Spring Microgrid updated topology enabled by the battery control scheme established in the above tasks. Per the design, AES2 with a GFM inverter will serve as the island leader. Key features of selected PCS equipment, energy storage, and microgrid controller were confirmed to meet the needs of the microgrid upgrade, which enabled final design of the battery control system.

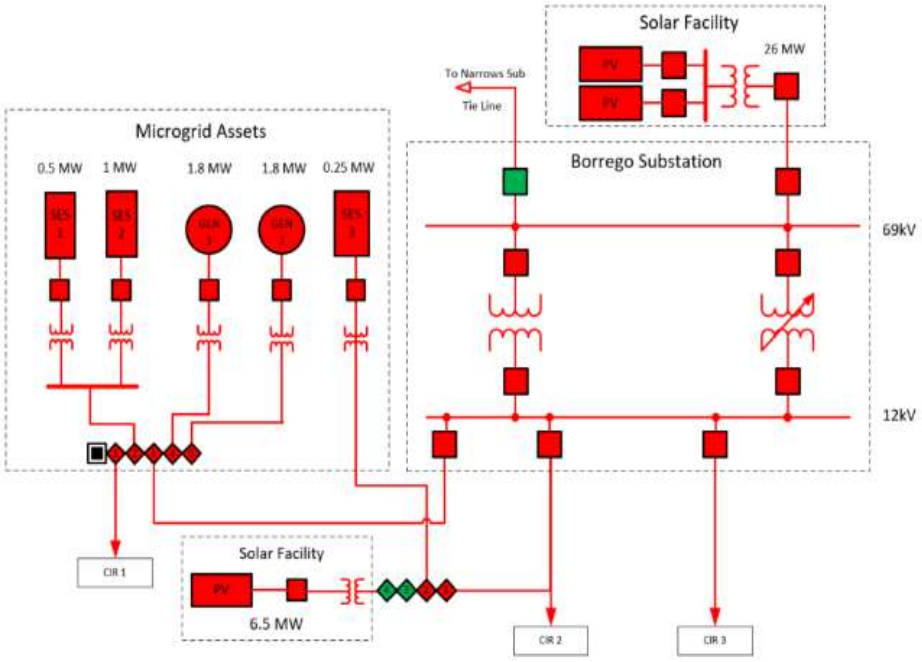

Figure 19: Updated topology of the Borrego Springs Microgrid.

Decision Point 2 "Go" was achieved with the battery control system designed and agreed to with vendors, ready for integration into PHIL.

Task 10: HIL Enhancement (Task Lead: NREL)

As a continuation of efforts from Task 1, the purpose of Task 10 was to integrate the field-relevant grid-forming battery inverter into the HIL evaluation platform (subtask 10.1), ensure accuracy in the setup by minimizing reactive power tracking errors (subtask 10.2), and set up real-time visualization and data collection for the HIL platform (subtask 10.3). NREL established the PHIL experimental setup shown in Figure 20. The inverter manufactured by CE+T between the AC source and inverter is not used in this setup. Two custom-built measurement boxes with voltage and current transducers are shown on the floor with oscilloscopes on top. One box also houses an SEL 751 feeder protection relay with synchronization capabilities to control the simulated microgrid switch. The allowable frequency, voltage amplitude, and phase differences were set to 1 Hz, 2V, and 8 degrees, respectively. The 100-kVA power inductor was manufactured to a specification of 1 mH by CTM Magnetics. SDG&E provided a Hitachi ABB PCS100 inverter. A 100-kW Regatron TopCon TC.ACS voltage amplifier was used for the AC source, and an NH Research 9300 controllable DC source was used to provide a fixed DC voltage to the inverter.

Through implementation of lead compensation and a proportional resonant controller, the voltage values match between the hardware and model, and the real and reactive power errors between the model and the hardware setup were reduced (Figure 21).

The real power is approximately 40 kW (three phase), and the reactive power is approximately 7.2 kVAr (three phase). The real power values without lead compensation and with lead compensation match the hardware values. This is understandable as the delay only impacts the reactive power. The reactive power values do not match the hardware results without the lead compensator (Qhil is approximately 3.8kVar). With the implemented lead compensation and PR controller, the values in the model match the reactive power from the hardware setup.

Per subtask 10.3, NREL integrated PHIL visualization with the Borrego Springs model. This step enabled ease of operation and troubleshooting of the testbed (Figure 22).

Figure 20: PHIL experimental setup with the inverter on the right (to the left of the large computer screens), the AC source in the center, and the power inductor on the left. Photo by NREL.

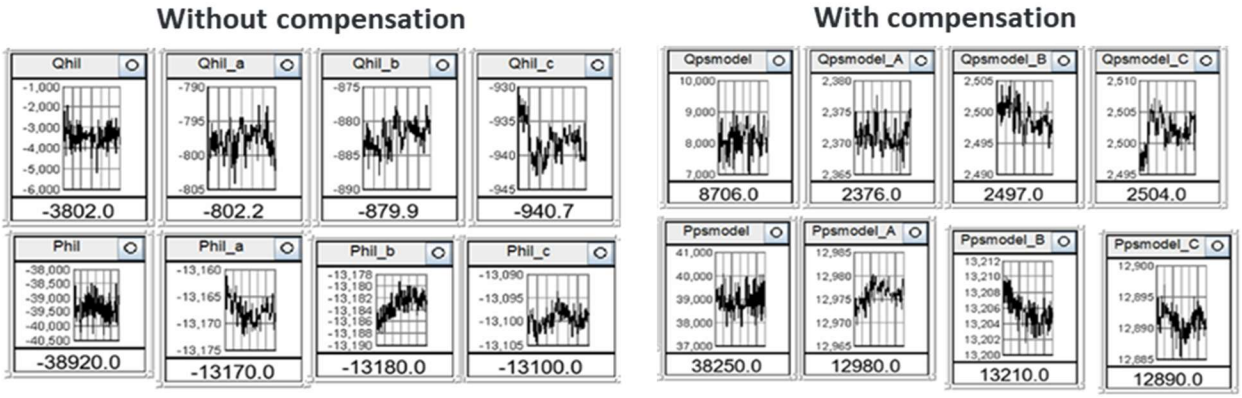

Figure 21: Real and reactive power measurements showing the reduction in reactive power errors between the model and hardware setup.

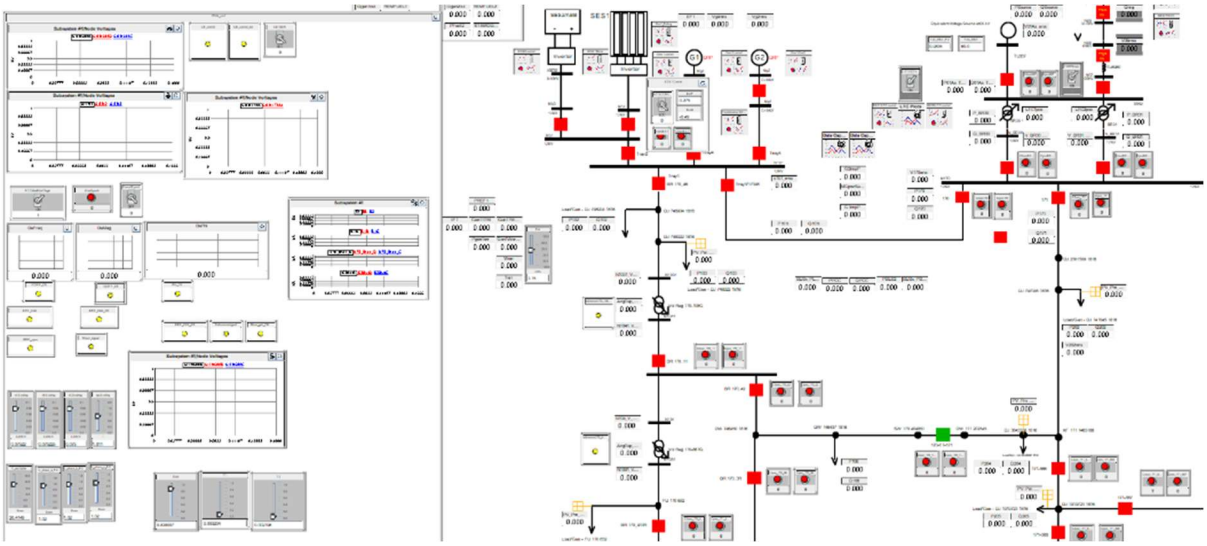

Figure 22: PHIL visualization group included in the Borrego Springs model.

The HIL setup with selected hardware was demonstrated to operate seamlessly with the CHIL devices added with inverter PHIL integration in GFM and GFL modes at different loads per Milestone 10.

PHIL setup learnings were disseminated in the paper "Power-Hardware-in-the-Loop Interfaces for Inverter-Based Microgrid Experiments Including Transitions" *(Milestone 26*).[10]

Please see Appendix A for additional technical details on the HIL setup and PHIL interface development.

Task 11: RSCAD Modeling of Borrego Springs Microgrid (Task Lead: SDG&E)
Building upon Task 2, the RSCAD model was updated to contain all controllable microgrid resources including the energy storage IBRs and tested for fidelity based on regression and functional tests from planned islanding and loss of generation tests. Once the Borrego Springs Microgrid model was fine-tuned, test cases were conducted. Figure 23 represents the microgrid response during the planned islanding test, response at the time of transitioning with 2.1 MW, 0.45 kVAr load, Gen1 (1MW, 150 kVAr) and AES1 (500 kW, 0 kVAr) used for GFL support. AES2 is in island leader mode with droop setpoints set to 0. Figure 24 represents the microgrid response during loss of generation test, response with loss of generation from AES1 Test with 2.1 MW, 0.45 kVAr load, Gen1 (1.5 MW, 250 kVAr) and AES1 (500 kW, 0 kVAr) used for GFL support. AES2 is in island leader mode with droop setpoints set to 0.

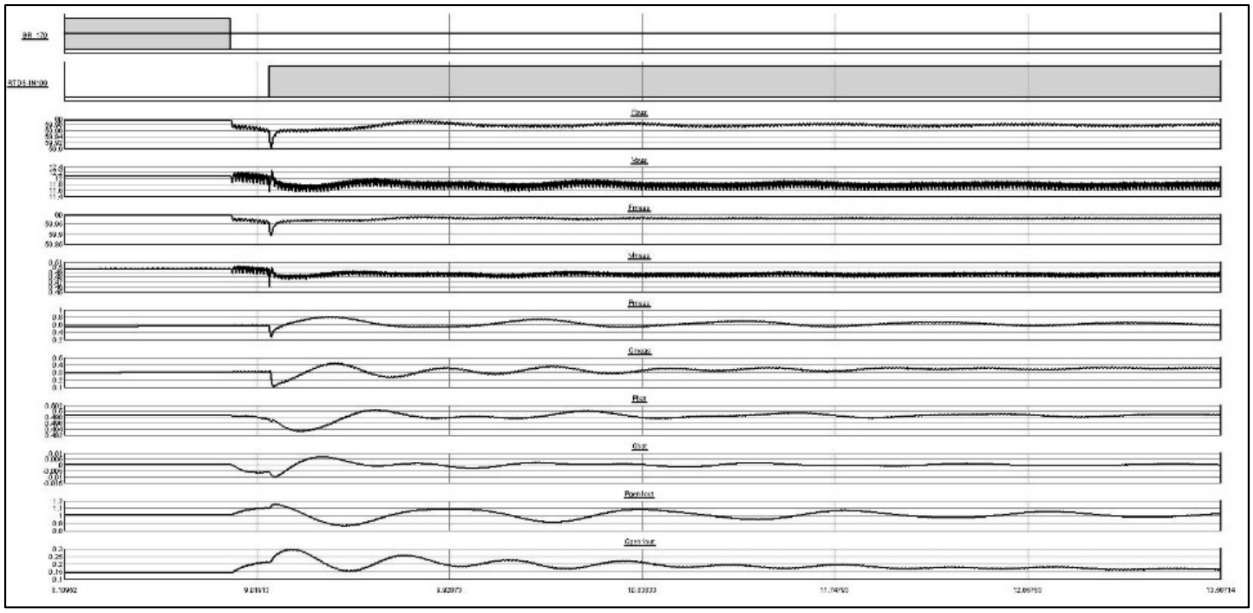

Figure 23: Microgrid response during planned islanding test.

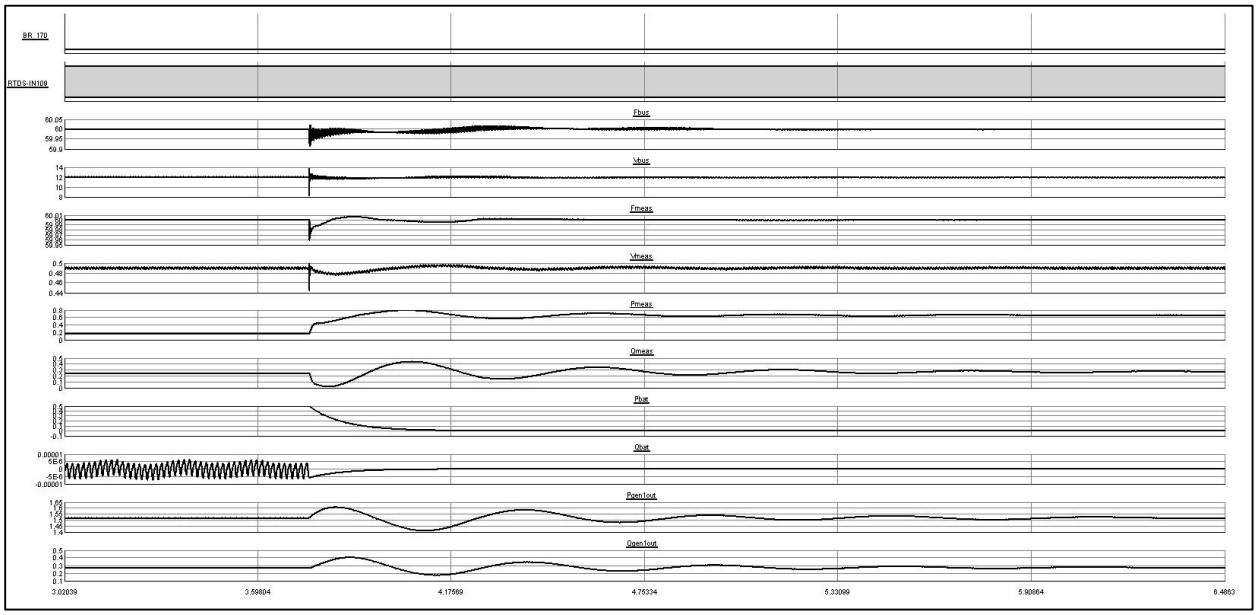

Figure 24: Microgrid response during loss of generation test.

Subtask 11.2, led by NREL, established the sequence of operations for the HIL platform. The GFM battery inverter (power hardware) is started in GFM mode (VSI-VF mode of operation). The start-up sequence of the model is presented below.

- Step 1: Initiate the power hardware experiment with the controllable AC supply (grid simulator) voltage fed by the voltage at the PCC circuit breaker in the RTDS model (signal 1 in Figure 25). Start the inverter hardware in GFM mode.
- Step 2: Turn on the voltage regulator in the RTDS to reduce the voltage errors introduced by grid simulator
- Step 3: Close the breaker using the SEL sync check.

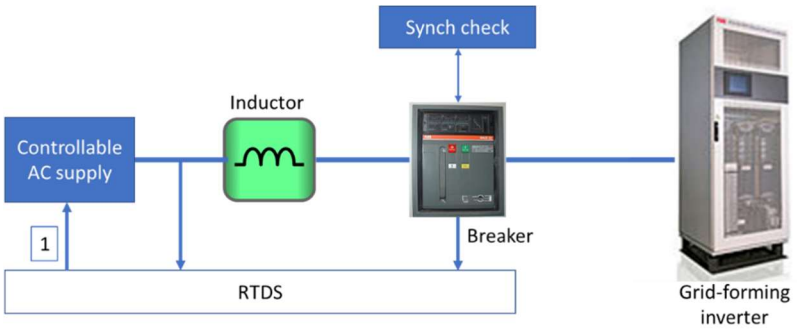

Figure 25. Simplified power hardware-in-the-loop (PHIL) setup for grid-forming inverter.

After completing these steps, the voltage, frequency, and power flow were verified for grid-connected operation. Then circuit 1 (Ckt 1, see Figure 4) was separated to form an island with the two battery energy storage systems (GFL inverter modeled in RTDS and the GFM inverter emulated in power hardware) by opening the PCC breaker (MG switch). Under this operation, the diesel generators were turned off and the entire Ckt 1 was supported by the two battery energy storage systems. This model was tested up to 500 kW of simulated loads in Ckt 1 and the model maintained stable operation. A synchronization relay was modeled in RTDS to transition this island back to grid-connected operation through the PCC breaker. Transition from grid-connected to islanded operation and from islanded to grid-connected operation was satisfactory under manual operation of the microgrid. The island also survived for load values up to 500 kW.

Referring to Figure 26, the microgrid controller was integrated with the HIL platform (subtask 11.3, led by NREL). Communications channels were tested between NREL's RTDS (running the Borrego Springs model) and the microgrid controller through a SEL real-time automation controller (RTAC).

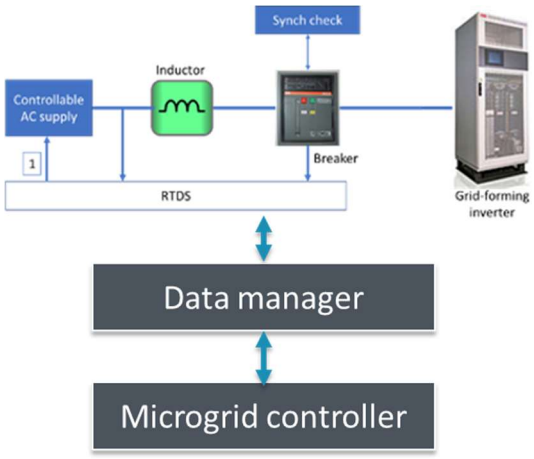

Figure 26: Simplified PHIL controller hardware in the loop (CHIL) setup for the microgrid controller.

Task 12: Continue Remote HIL setup between NREL's ESIF and SDG&E's ITF

Task 12 was to be a continuation of Task 3 and was de-scoped from this project before work initiated, related to unanticipated NREL operating costs for remote HIL setup between NREL and SDG&E. In addition, there were technical difficulties anticipated in the connection between a national lab and a private entity. The revised hardware-in-the-loop setup at Energy Systems Integration Facility provided adequate validation for the operation evaluation

Task 13: HIL Test Plan Development and Execution (Task Lead: NREL)
The HIL Test Plan was prepared in Task 13 to identify specific test cases for validating the ability of the GFM battery to reduce the frequency variability during planned islanding and blackstart, to improve the likelihood of the formation of a stable microgrid when islanding occurs with only renewable, IBR, i.e., in a low-inertia environment. *The HIL Test Plan was prepared in iterative feedback loops between SDG&E and NREL, summarized in this section. The plan was reviewed and approved by the project's DOE Program Manager before testing was initiated, satisfying Milestone 13, completion of the HIL Test Plan.* The NREL team utilized the HIL evaluation platform as described and shown in Figure 4.

A stepwise process was established for the laboratory evaluation procedure:

1. Configure the power system simulation: Load the load profile and insolation profiles for the feeder. Configure the predetermined DER states, including the battery state of charge.
2. Configure the utility-scale DER: Select the available resources and capabilities for dispatch in the microgrid controller.
3. Configure the HIL components: Verify the configuration and control scheme on the hardware. Energize the power amplifiers as needed and start up the controller hardware.
4. Enable the data collection and management systems: Enable the data collection system that will be used to collect and record data from the various hardware components and the software-based simulation platforms.
5. Perform the simulation: Initialize the data collection and visualization. Let the RTDS step through the load and insolation profiles and simulate the selected scenario.

Evaluation Scenarios and Criteria
Planned Islanding
All simulations were conducted in NREL's ESIF laboratory. Islanding simulations were planned for a few different load conditions, including heavy and light load during the daytime and nighttime. Simulations were planned to run for at least 3 minutes of operation after islanding. Additionally, NREL simulated different generation sources online. AES1 (grid following BESS) and AES2 (grid forming BESS) were always online, and AES1 always operated in VSI-PQ (voltage source inverter—power flow control) mode. AES2 was always operated in VSI-PQ mode when grid-connected and VSI-VF (voltage source inverter—voltage and frequency control) mode when islanded. For the

baseline simulations, the diesel generators were online and operated in grid-following mode, i.e., AES2 is always the voltage and frequency leader. The diesel generators were also online in load-following mode for heavy load scenarios because the renewable resources do not have adequate capacity. When AES3 was online, it operated in GFL mode with the frequency envelope setting enabled. The initial state of charge of the batteries for AES1 was set to 70%, and the initial state of charge of the AES3 ultracapacitor was set to 90%.

It was also planned to simulate two scenarios where a disturbance is added during islanding, either by applying a load transient (representing turning on or off agricultural pumps), or by a solar insolation transient (such as a cloud passing over), or by opening or closing a line switch or a circuit breaker. Table 16 summarizes the scenarios for planned islanding.

Table 16: Test case scenarios for planned islanding.

Scenario No.	Loading	AES2	AES3	Diesel Generators	Other
Baseline 1	Heavy	VSI-VF	Offline	Online	
Baseline 2	Light	VSI-VF	Offline	Online	
Baseline 3	Night	VSI-VF	Offline	Online	
1	Heavy	VSI-VF	Online	Online	
2	Heavy	VSI-VF	Online	Online	Load step
3	Light	VSI-VF	Offline	Offline	
4	Light	VSI-VF	Online	Offline	
5	Light	VSI-VF	Online	Offline	Cloudy solar
6	Night	VSI-VF	Offline	Offline	
7	Night	VSI-VF	Online	Offline	

For each scenario, the team evaluated the voltage and frequency performance guided by the metrics listed in Table 17. The transient metrics for frequency are illustrated in Figure 27. If the island collapses, NREL recorded the time from the islanding event until the frequency dropped below 58 Hz.

Table 17: Evaluation metrics for planned islanding.

	Metric	Description
Transient	ΔV_{max}	The largest voltage deviation from the pre-event voltage
	dv/dt	The rate of change of voltage at the start of the dynamic event
	Voltage settling time	Time until the voltage transient stays within an acceptable band of 0.95–1.05 p.u.
	Δf_{max} (nadir)	The largest frequency deviation from the pre-event frequency
	df/dt	The rate of change of frequency at the start of the dynamic event
	Frequency settling time	Time the frequency enters the acceptable band of 0.95–1.05 p.u.
	$V_{steady\text{-}state}$	The steady-state voltage in RMS after the transition
Steady state	ΔV	The deviation of the steady-state voltage from the nominal voltage
	Voltage standard deviation	$\sigma_v = \sqrt{\frac{\sum(V_{meas,i} - V_{steady-state})^2}{N}}$
	$f_{steady\text{-}state}$	The steady-state frequency after the transition
	Δf	The deviation of the steady-state frequency from the nominal frequency
	Frequency standard deviation	$\sigma_f = \sqrt{\frac{\sum(f_{meas,i} - f_{steady-state})^2}{N}}$

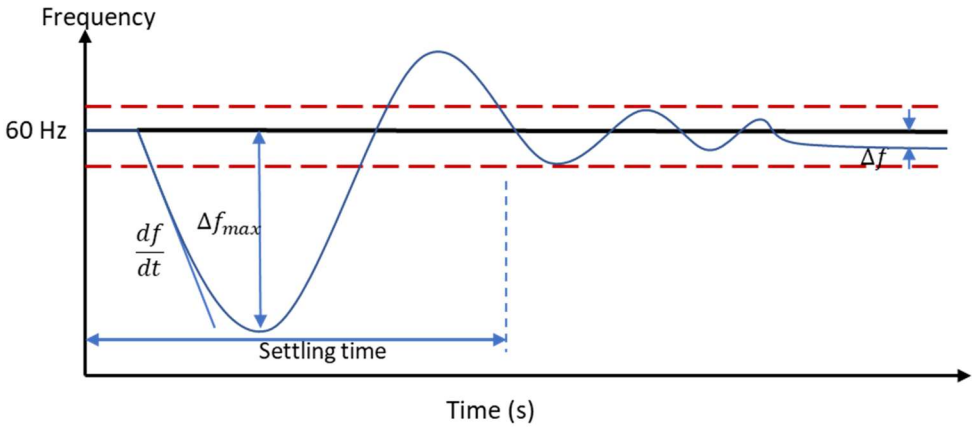

Figure 27: Frequency response after a dynamic event.

Blackstart

For the simulation of black start, HIL simulations were planned to follow the proposed sequence of restoration steps provided by SDG&E. The main intent was to evaluate whether AES2 can successfully restore power to the microgrid without using the diesel generators. AES2 is a GFM and black-start-capable battery inverter that will act as the island leader. Simulation was planned for a few different load conditions, including heavy and light load during the daytime and nighttime. The evaluation criterion was whether stable operation of the energized portion of the circuit is achieved after each

step in the black-start sequence. Stable operation was defined as a voltage and frequency standard deviation below 5% after the settling time of a transient.

Data collection

Data was collected from the RTDS using standard measurement blocks provided by RTDS as part of their RSCAD software. The types of data collected included voltage, current, power, and frequency. The voltage/current waveforms were captured at 1,000 Hz. Other data was captured at a rate of 60 Hz, which refers to the rate at which the team read the values from the RTDS. Root-mean-square (RMS) values were collected using single-phase RMS meters that calculate the RMS value over a half cycle. Frequency was collected from single-phase frequency meters that use a zero-crossing method and from simulated PMUs, and phase-angle data was collected from three-phase phase-angle difference meters. Real and reactive power measurements were collected from three-phase power meters. Battery state of charge was calculated in the RTDS based on data from the NH Research controllable DC source/sink that was programmed to emulate a battery.

Setup Validation

NREL evaluated the steady state accuracy of the PHIL interface for the Borrego Springs HIL setup using the simple microgrid model shown in **Error! Reference source not found.**. The team took measurements at several power levels and calculated the average inductance and resistance values of the power inductor, $\boldsymbol{Z_h}$, following the procedure described in Appendix A. The final values we used for $\boldsymbol{Z_h}$ are 1.3 mH and 75 mohm, based on experimental testing.

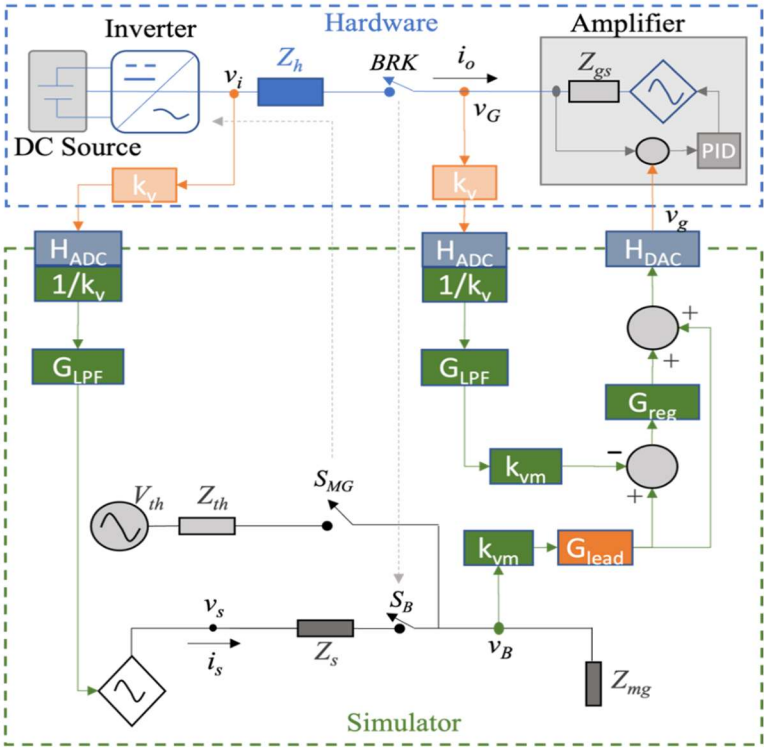

Figure 28: Simplified experimental setup with voltage amplifier and inductor for islanded and grid-connected operation.

The 88-kW hardware inverter was scaled to represent a 1-MW inverter to match the power rating of AES2. The scale-up factor, ***K***, utilized was 11.36, and the simulated inductor value was calculated as $\boldsymbol{Z_s = Z_h / K}$.

Table 18 shows accuracy results for active power, where $\boldsymbol{P_i}$ is the output power of the hardware inverter and $\boldsymbol{P_{sim}}$ is the output power of the equivalent voltage source representing the inverter in the simulation. We achieved an acceptable error at medium to high power, but accuracy deteriorated at lower power, and this warrants future work, such as introducing adaptive gains.

Table 18: Table 1. Steady-state accuracy for active power.

P_i [kW]	Q_i [kVar]	P_i [%]*	P_{sim}/K	Error [kW]	Error [%]**
7.1	2.3	8	4.78	2.32	33
14.7	2.9	17	13.38	1.32	9
22.4	3.96	25	21.92	0.48	2
30.4	5.49	35	30.11	0.29	1
38.79	7.28	44	38.24	0.55	1
47.36	9.47	54	46.16	1.20	3

* Percentage of hardware inverter power rating ** Percentage of *Pi*

Dynamic accuracy of the PHIL interface for the Borrego Springs HIL setup used data from a planned islanding experiment that used the Borrego Springs Microgrid power system model. The dynamic accuracy is good, as shown in Figure 29 that compares the scaled hardware and simulated GFM inverter output power for phase A. Similar performance was observed for the other phases.

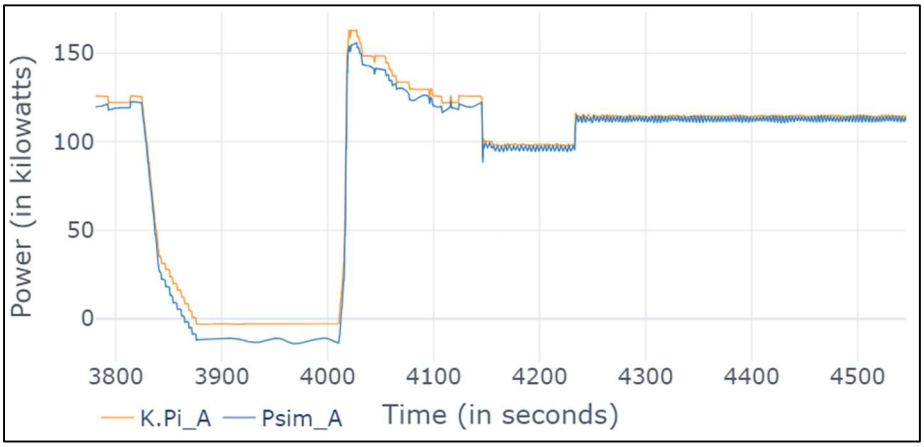

Figure 29: Comparison of scaled hardware and simulated inverter output active power for phase A under dynamic conditions.

Milestone 15, complete initial testing with the complete integrated HIL evaluation platform setup with test cases. was achieved with completion of this task.

Task 14: Full Scale Simulation (Task Lead: NREL)

As a continuation of Task 5, the team expanded the RSCAD model from Task 2 with explicit inverter models representative of the Borrego Springs Microgrid including planned battery PCS upgrades with GFM capability and established the Full Scale Simulation Test Plan. The simplified one-line diagram is show in Figure 30.

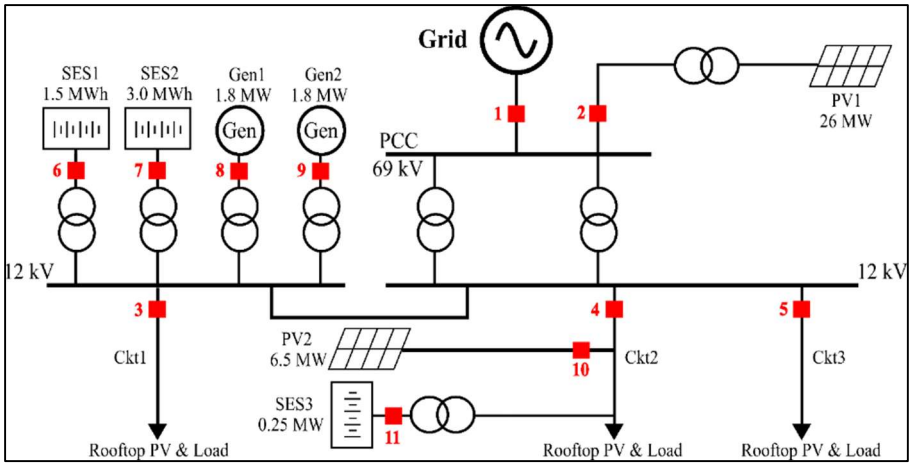

Figure 30: Simplified one-line diagram of Borrego Springs Microgrid used in the model.

PV Models

Explicit models and controls of at least 20 of the GFL PV inverters at the PV1 installation (subtask 14.1), and explicit models of at least 80 customer-owned PV systems (subtask 14.2) were added to the full simulation model. The model for the GFM battery inverter including controls was incorporated.

PV1, PV2, and the rooftop PV were modeled as GFL inverters. All GFL inverters are average models of a controlled voltage source followed by a filter. The control block diagram is shown in Figure 31. The inverter receives the power set points (Pref, Qref), which generate the direct-quadrature (dq) current references (Id*, Iq*) using the Park transformation and are passed through the dynamic current limiter. The referenced currents generated from the power references are compared to the derived currents (Id_mea, Iq_mea), which are calculated from the current measurements. The current controller consists of a proportional-integral (PI) controller and grid voltage feed-forward terms that together minimize the error and generate the dq voltage references (Vd, Vq). These voltages in the synchronous reference frame are then converted to natural reference frame voltages (abc) using the inverse Park transformation.

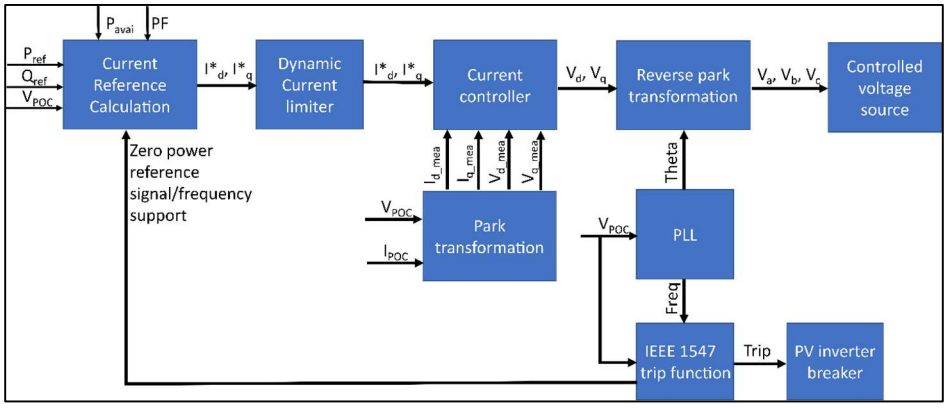

Figure 31: PV GFL inverter control block diagram.

The PV1 model has an LCL filter, consisting of two series inductors and a shunt capacitor connected at the midpoint between the inductors, with the parameters

obtained from the field. This model can work in either PQ control mode or with a smart inverter function (volt-VAR with VAR priority and active power maximum power point tracking). PV2 is a legacy and noncontrollable facility, and it works in unity power factor mode. The distributed rooftop PV units operate in unity power factor mode. PV2 and the rooftop PV are modeled using an L filter.

PV1 consists of 54 inverters of 500 kW each in the field, but it is aggregated and modeled using 20 inverters of 1.3 MW each in PSCAD. 4.5 MW of rooftop PV are distributed at customer sites in the field, but the rooftop PV is aggregated in PSCAD. There are 22 total rooftop PV systems in the RSCAD model, which were disaggregated and modeled using 82 inverters of different ratings and placed at the same locations as in the RSCAD model. The voltage and frequency trip and ride-through settings are included in the PSCAD model. The inverters of PV1 comply with the Institute of Electrical and Electronics Engineers (IEEE) Std 1547-2018 in the field, and therefore those settings are used in PSCAD. [11] The rooftop PV units are a mix of legacy and more modern inverters, but because they are aggregated in the PSCAD model, that could not be reflected, and therefore they are all modeled as IEEE Std 1547-2003 compliant.

Grid-forming Inverter Model

In subtask 14.2, a model of a GFM battery inverter, including controls, was added to the full-scale simulation model. AES1, AES2, and AES3 were modeled as GFM inverters. The PSCAD model of the GFM inverter was developed to represent the state of the art in GFM inverters. We were unable to use an inverter model provided by the manufacturer, so we used a model developed by NREL that was reviewed and approved as sufficiently representative of the field inverter by the manufacturer and SDG&E. The control diagram of the GFM inverter model is shown in Figure 32. This GFM inverter model has a traditional double-loop structure with an outer loop for power control (PQ control) or voltage control (VF control), depending on the operation mode, and an inner current loop. There are three operation modes of the inverter model: startup (VF control), grid-connected (PQ control), and islanding leader (VF control). The model can shift between the operation modes based on the PCC circuit breaker status. In PQ control mode, the GFM inverter is IEEE Std 1547-2018 compliant.

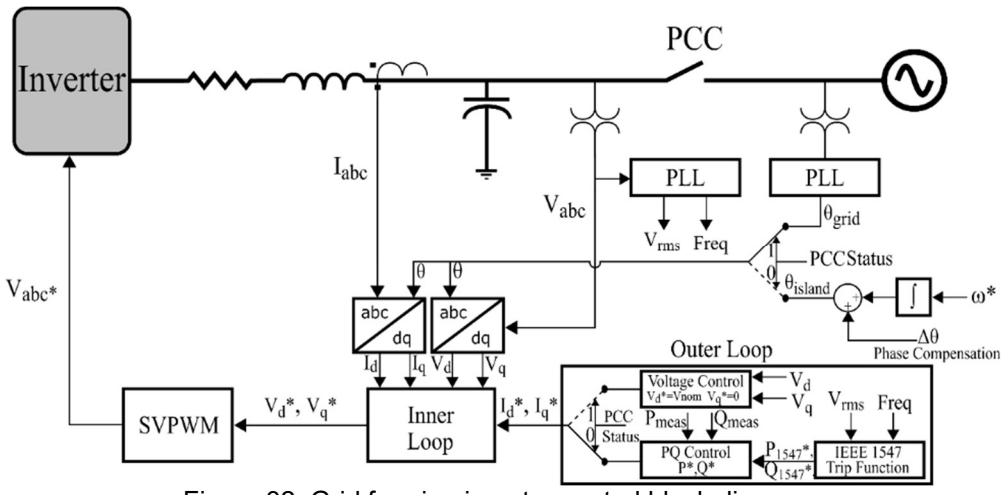

Figure 32: Grid forming inverter control block diagram.

The GFM inverter is initialized in VF control to start up and connect to the network by closing the PCC breaker after synchronization. When the PCC breaker is closed, the outer loop control shifts from VF to PQ mode following the power set points. If the inverter is the island leader and it is in islanded operation, it shifts from PQ to VF mode when the PCC breaker is opened, and then ω is determined from the selected operation mode, i.e., isochronous mode or droop relationship. One important feature of this control structure is that the phase angle for the Park transformation (abc/dq0) switches between a grid-connected GFL angle (θgrid) and an islanded self-generated angle (θisland). To have a smooth islanding transition, the phase angle difference between the grid phase angle and the self-generated phase angle is calculated and added to the GFM inverter phase angle after the PCC circuit breaker is opened. [6] The current references generated from the outer loop (Id*, Iq*) are passed onto the inner current loop, which include a PI control and a grid voltage feed-forward term. Finally, the voltage references from the inner current loop are converted to three-phase voltage signals for the pulse-width modulation (PWM) generation to control the average switching model.

The inverter model is also equipped with additional grid-supporting functions in GFL mode:

- **Active/reactive power priority**: Under normal operation, GFL inverters track the power reference commands subject to the maximum current limit. During frequency or voltage contingency events, inverters are required to support the grid by generating/absorbing active or reactive power; therefore, the active power (P) or reactive power (Q) reference command is implemented using current-limiting logic to prioritize one over the other. In an active power priority scenario, the model prioritizes the active power set point, and the reactive power is limited to the remaining device capacity. With reactive power priority, the model provides reactive power output in response to the voltage measurements at the terminal. The amount of power injection is determined from a predefined volt-VAR curve subject to the device rating. The reactive power output is changed once per second to minimize the oscillations. At the same time, the active power is curtailed if there is less capacity of active power than the commanded active power because of VAR

priority. Note that SES3 uses a frequency fast response function to support and maintain the frequency during islanding operation.

- **Ride-through mode:** During grid-connected mode, inverter tripping under grid disturbances can cause grid instability, leading to blackouts; therefore, interconnection standards require inverters to ride through disturbances and restore power to the pre-disturbance levels [9]. During voltage disturbances, voltage sags at the inverter terminals trigger voltage ride-through mode. For voltages outside the continuous operating range, the model stays connected in constant power mode or enters cessation mode. During frequency disturbances, the model responds by increasing/decreasing the active power based on a droop relationship. The magnitude of the active power is calculated from the equations described in Table 23 of IEEE Std 1547-2018.

IEEE Std 1548-2018 Ride-Through Modeling

GFM and utility-scale inverters are equipped with IEEE Std 1547-2018 ride-through and trip settings. The ride-through and trip requirements for voltage and frequency are defined according to IEEE Std 1547-2018. Category III requirements are selected for modeling. The ride-through requirements for voltage and frequency are modified for undervoltage and frequency to avoid gaps in the default settings, as shown in Table 19 and
Table 20, respectively.

Table 19: Modified voltage ride-through requirements.

Voltage Range (p.u.)	Operating Mode	Minimum Ride-Through Time (s)	Maximum Response Time (s)
V > 1.20	Cease to energize	N/A	0.16
1.10 < V ≤ 1.20	Momentary cessation	12	0.083
0.88 ≤ V ≤ 1.10	Continuous operation	Infinite	N/A
0.50 ≤ V < 0.88	Mandatory operation	21	N/A
V < 0.50	Momentary cessation	1	0.083

Table 20: Modified frequency ride through requirements.

Frequency Range (Hz)	Operating Mode	Minimum Ride-Through Time (s)
f > 62	N/A	N/A
61.2 < f ≤ 62	Mandatory operation	300
58.5 ≤ f ≤ 61.2	Continuous operation	Infinite
56.5 ≤ f < 58.5	Mandatory operation	300
f < 56.5	N/A	N/A

With incorporation of PV and GFM inverters including controls, Milestone 19 was achieved.

Please see Appendix B for full details.

Task 15: Engineering Assessment of Existing ESS PCS and Upgrade Design (Task Lead: SDG&E)

Building on Task 6, this task completed the design of the microgrid controller integration and initiated validation of the control design. Figure 33 provides the completed control upgrade design scheme and protection scheme. Microgrid controller provides visual real time status of all DERs, commands based on use cases and asset availability. The DER RTAC aggregates individual DER assets and executes action, utilizing commands from the microgrid controller. The system RTAC receives key information from the DERs for system protection and provides top-level supervisory control via SCADA. Beyond this project, this interoperable configuration enables microgrid operators to have autonomy and flexibility to deploy a variety of assets in different configurations.

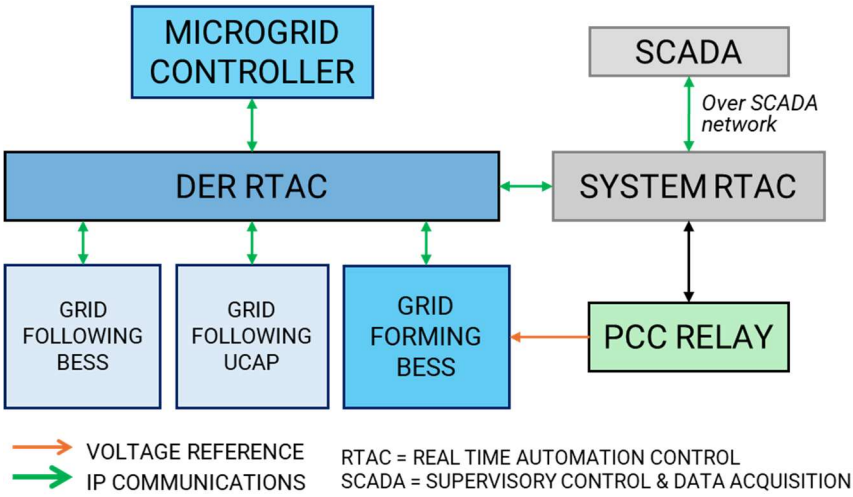

Figure 33: Microgrid control scheme.

The control design was validated through successful planned islanding with the GFM inverter HIL controlled through microgrid controller in controller hardware in the loop (CHIL) experiments. Communication channels were successfully tested between NREL's RTDS (running the Borrego Springs Microgrid model) and the microgrid controller through an SEL real-time automation controller (RTAC)**.** Figure 34 provides a view of the microgrid controller user interface (large screen), and the Borrego Springs RSCAD model (small screen on left). *The complete HIL evaluation platform was then ready for execution of the HIL Test Plan (Milestone 20).*

Figure 34: HIL setup operating with CHIL devices and inverter PHIL integration.

Task 16: PCS Control Upgrade (Task Lead: SDG&E)

Continuing from Task 7, final PCS design details were established, the energy storage inverter systems were upgraded and commissioned, and the resources were integrated into the field microgrid controller. Figure 35 pictures the three energy storage systems - AES2 (1 MW/3 MWh Li-ion BESS), AES1 (0.5MW/1.5 MWh Li-ion BESS), and AES3 (0.3MW) ultracapacitor. These systems were commissioned with concurrence from the inverter hardware vendor. Figure 36 presents the control interface, whose testing was in concurrence with the microgrid controller vendor. Operations are made possible through conformance to the permission exchange standard and operations procedures developed by SDG&E, with a view of interoperability and integrating more renewable DERs which could act as island masters in the future.

Figure 35: Borrego Springs Microgrid upgraded energy storage IBRs.

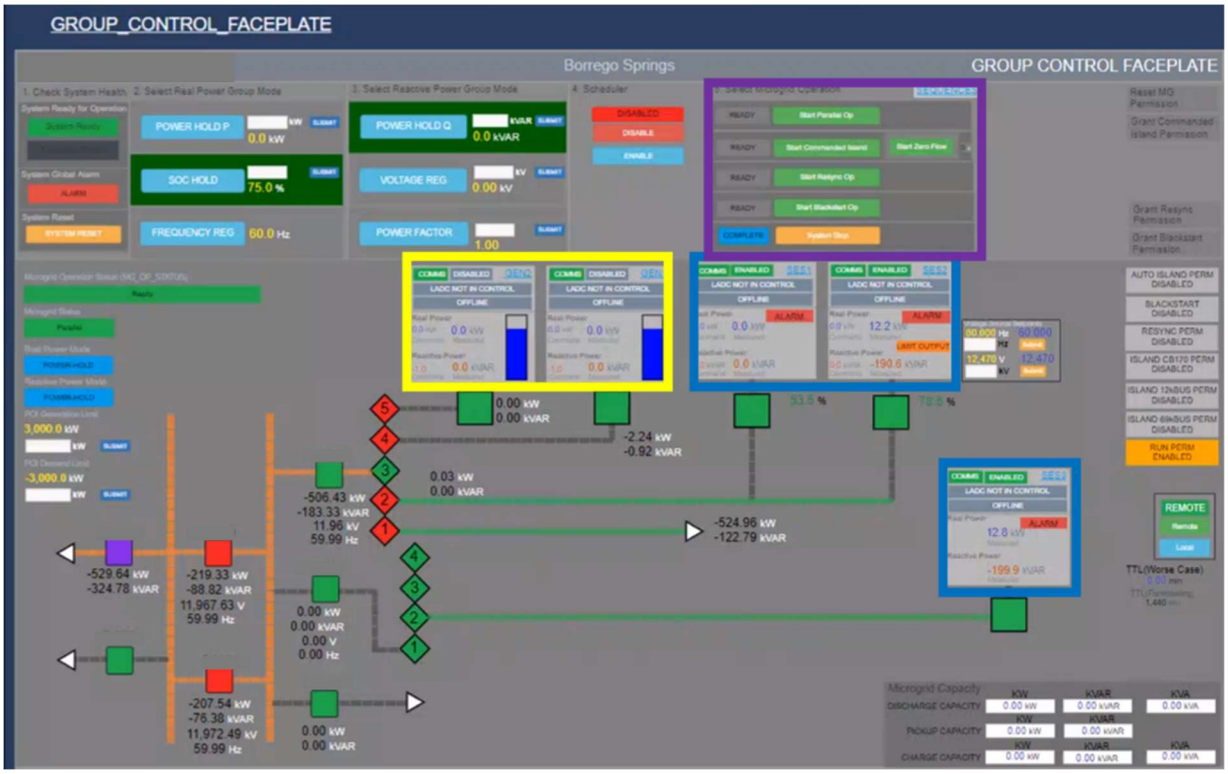

Figure 36: Microgrid standard interface.

Task 17: Field Tests (Task Lead: SDG&E)

With completion of the battery inverter field upgrades and equipment commissioning as well as microgrid control and control point integration, blackstart test procedures were established (subtask 17.1). Importantly, NREL's Borrego Springs simulations uncovered updates needed to inverter parameters, highlighting the importance and value of HIL testing. A switch plan was submitted to the SDG&E Electric Distribution Operations and was scheduled for a field operation in November 2023 (subtask 17.2 and Milestone 12). Results of field tests are described under Task 20.

Task 18: HIL Test Plan Development and Execution (Task Lead: NREL)

In this task, HIL experiments were executed per the test plan, with results indicative of microgrid stability utilizing the GFM battery inverter to blackstart, island, and support large load steps. Completion of testing per the test plan achieves Milestones 22 and 24. Full data are provided in *Appendix A (Milestones 22, 24, and 25), with a summary presented here.*

Blackstart Results

Blackstart simulation was performed under light load conditions with the ultracapacitor, AES3, and diesel generators offline. NREL dispatched the GFL inverter, AES1, manually, and closed the breakers manually in the RSCAD simulation. Results demonstrate stable formation of an island, and the voltage and frequency are maintained within limits throughout all load and generation changes. The most significant transition is when the first load is added. There is a significant transient in

frequency and voltage, but they are within voltage limits and within 100 msec of settling time.

Figure 37 shows the microgrid voltage and frequency, measured at the 12-kV bus, during the blackstart experiment, showing formation of the island and stable operation. Before the inverter initiates the blackstart mode, the voltage at the bus is zero, and there is no waveform from which the frequency could be measured. Therefore, the frequency value oscillates around 60 Hz before the frequency measurement gets an actual voltage waveform.

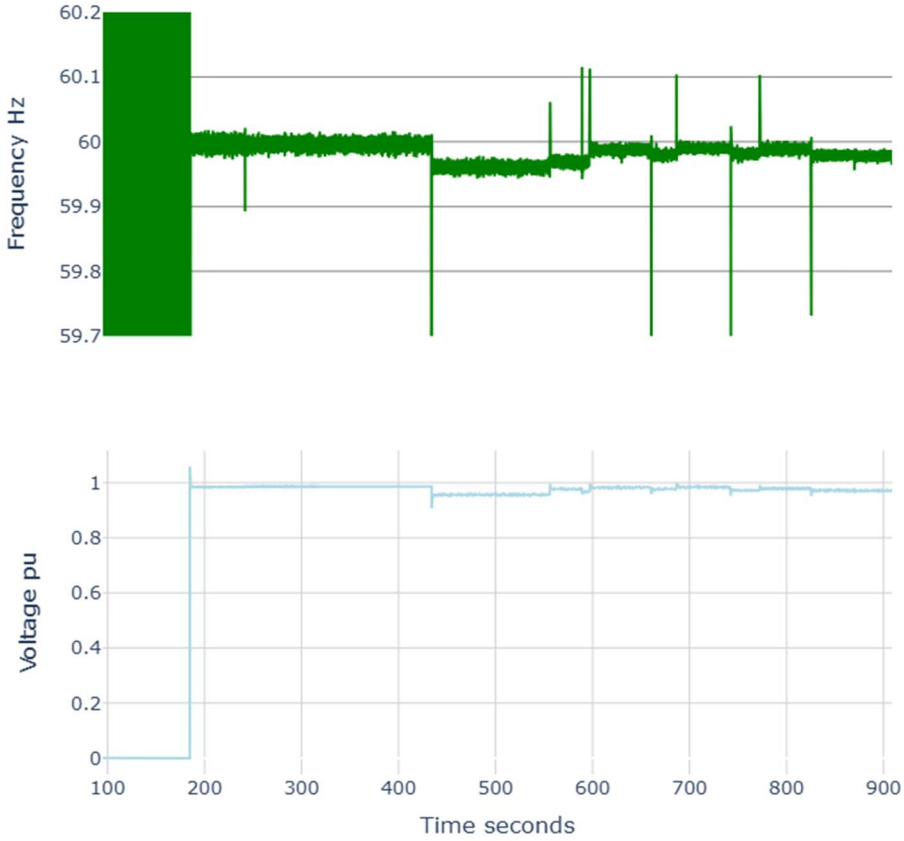

Figure 37: Microgrid frequency (top) and voltage (bottom) during the black-start experiment, showing the establishment of voltage and frequency for the microgrid.

Figure 38 shows the microgrid frequency, inverter output power, and microgrid voltage for the portion of the experiment after the 12-kV bus is energized. Before ~ 430 s, there are no energized loads. The GFM inverter, AES2, output power increases at ~430 s to supply power to the first energized section. The GFL inverter, AES1, is manually dispatched at ~ 550 s, resulting in a change in output power of the GFM inverter to maintain generation-load balance. The PV systems in the first energized section are activated at ~ 590 s, causing a slight reduction in the output power of AES2. PV inverters would take between 1 and 5 min to come online in the field; here they are brought online sooner for the sake of limiting the duration of the experiment and the amount of data to collect.

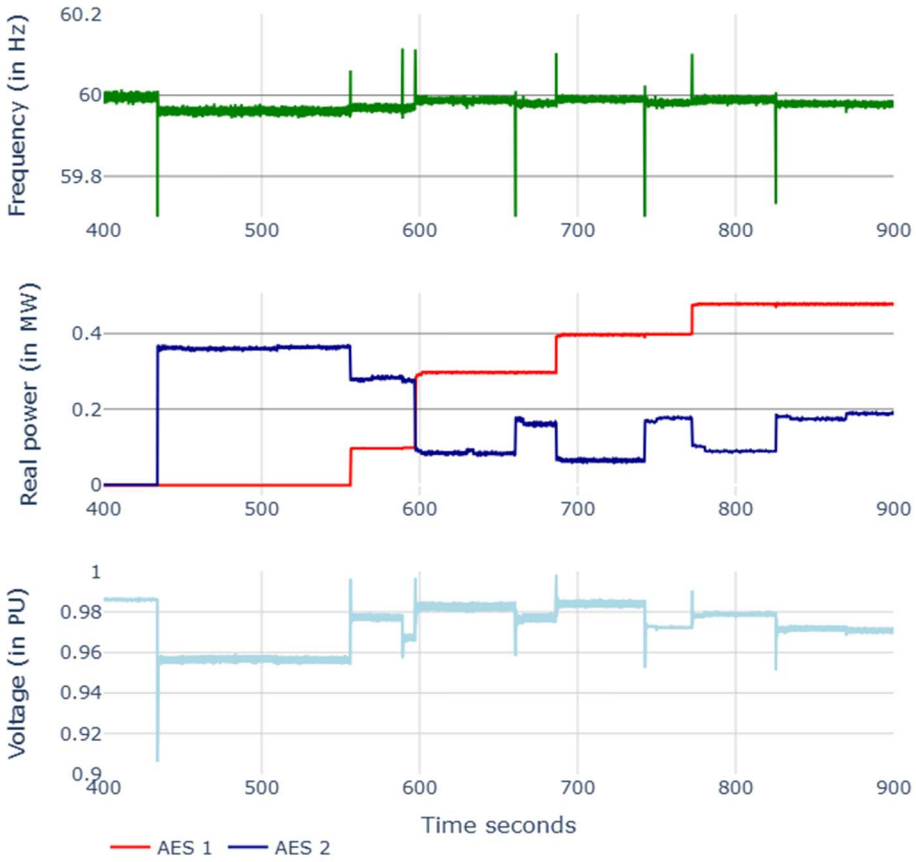

Figure 38: The microgrid frequency (top); inverter output powers (center); and microgrid voltage during the black-start experiment, after the island has been established.

The output power of AES1 is manually increased at ~ 600 s, which is prior to closure of the next breaker to ensure that enough generation capacity is online. Then another breaker is closed at ~ 670 s and the GFM inverter picks up that load. The next set of PV systems are brought online shortly afterward, resulting in a small drop of power provided by AES2. This sequence is repeated with GFL inverter dispatch at ~690 s, closure of another breaker at ~750 s, and PV systems online at ~760 s; and then again with a GFL inverter dispatch at ~780 s, closure of another breaker at ~820 s, and PV systems online at ~830 s. There are smaller changes in AES2 output power due to load and PV profile changes every 1 min.

The voltage and frequency are maintained within limits throughout all load and generation changes. The most significant transition is when the first load is added (360kW), shown in more detail in Figure 39 over 4 s. There is a significant transient in frequency and voltage, but they are within voltage limits and within 100 msec settling time.

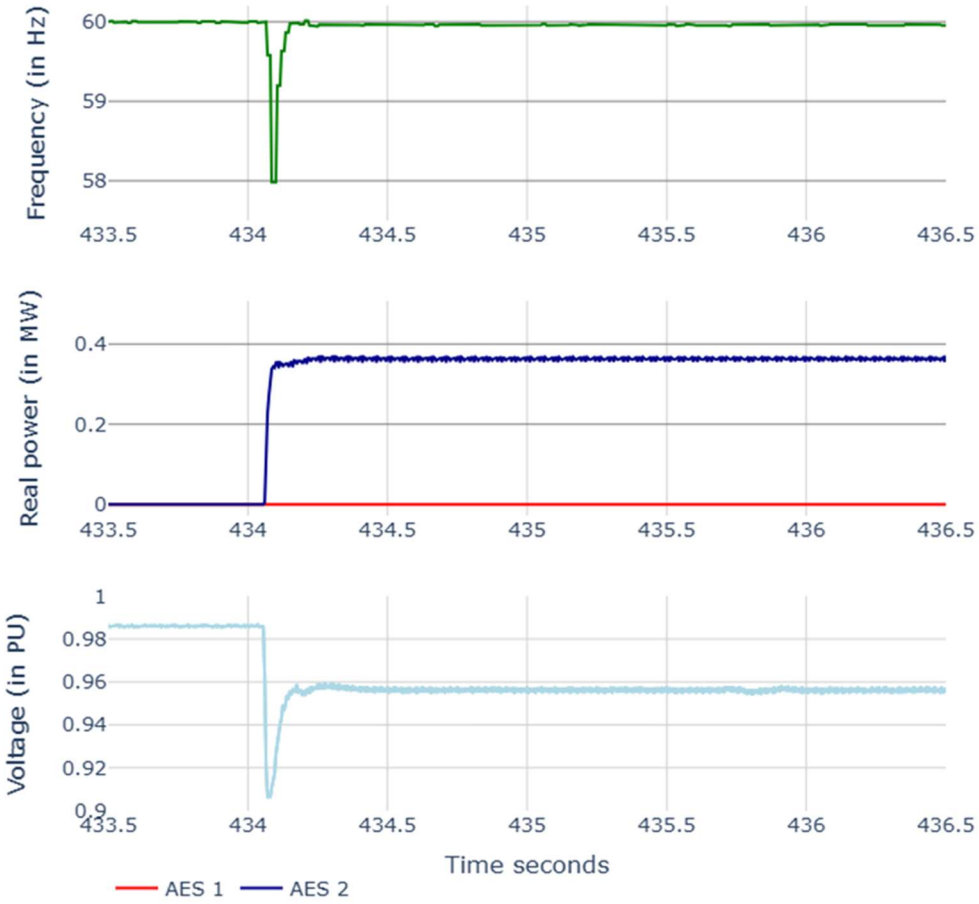

Figure 39: The microgrid frequency (top); inverter output powers (center); and microgrid voltage during the black-start experiment, when the first load is picked up.

Planned Islanding Results

AES2 is operated in GFL mode when grid-connected and in GFM mode with a frequency droop setting of 0.2% and a voltage droop setting of 1% when islanded. AES 1 is always operated in GFL mode. When AES3 is online, it operates in frequency regulation mode (GFL mode with a frequency-watt curve). The state of charge (SOC) of the ultracapacitor is maintained near 90% when it is not actively responding to an underfrequency or overfrequency condition.

Resources are dispatched by the microgrid controller except for the diesel generator, which is dispatched manually. The diesel generators were used only in the heavy load scenarios, in GFL mode, when the battery resources do not have adequate capacity.

The team used data from 1–2 a.m. for night load, 8–9 a.m. for light load, and 5–6 p.m. for heavy load based on historical data from July 29, 2019.

At the start of the zero-power flow step in the planned islanding process of the MGC, the grid-following BESS, AES1, is dispatched to supply the load up to its rated power of 500 kW and any remaining load is carried by the GFM BESS, AES2, up to half of its

rated power, which is the maximum allowed by the MGC during a planned islanding scenario. Once the power flow through the microgrid switch is less than +/- 50 kW, the microgrid controller will allow the operator to island the microgrid.

The simulations were run for at least 3 min of operation after islanding to confirm the stability of the island. Table 21 presents a summary of planned island events. Green shading indicates when the different battery inverter resources are online. All scenarios yielded a stable island utilizing the battery inverter in GFM mode.

Table 21: Summary of planned islanding results.

Load profile	AES2 (GFM)	AES3	AES1 (GFL)	Diesel Generator	Result
Night	120 kW	Offline	500 kW	Offline	Stable island.
Night	160 kW	Online	500 kW	Offline	Stable island, AES3 not triggered.
Light	100 kW	Offline	500 kW	Offline	Stable island.
Light	150 kW	Online	500 kW	Offline	Stable island. No observable response from AES3.
Light, Cloudy	200 kW	Online	500 kW	Offline	Stable island. No observable response from AES3.
Night	0 kW	Offline	240 kW	350 kW	Stable island, AES1 dispatch lowered. Small steady state oscillations observed in DER output before and during island.
Light	0 kW	Offline	300 kW	350 kW	Stable island, AES1 dispatch lowered. Steady state oscillations observed in DER output before and during island.
Heavy	400 kW	Offline	500 kW	550 kW	Stable island with significant steady state oscillations observed in DER output before and during island.
Heavy	400 kW	Online	500 kW	550 kW	Stable island with significant steady state oscillations observed in DER output before and during island. No discernible response from AES3 due to oscillations.

Load Step Results – Light Load

For load steps under light load conditions, NREL used constant loads and PV outputs in the simulation. The starting net load is about the same as during the planned islanding experiment under light load conditions. The load is stepped up from 685 kW to 885 kW (i.e., a step up of 200 kW). The results are shown in Figure 40. The MGC dispatches the GFL inverter, AES1, at its rated output power of 500 kW. The AES3 output power changes from charging at about 25 kW to discharging, peaking at about 32 kW, when the load is stepped up. The frequency drops as low as 59.58 Hz and is restored above 59.94 Hz within 75 msec; it is above 59.9 Hz by the time AES3 would have reached its maximum discharge rate. The response rates are similar for AES2 and AES3, which is to be expected because they use inverters from the same manufacturer and family of products but with different ratings.

The RSCAD model of AES3 used frequency measured by a phase-locked loop (PLL) followed by a filter with a time constant of 0.01 s. This technique filtered out fast frequency transients, so AES3 did not respond to frequency transients. NREL therefore replaced the frequency input to the ultracapacitor model with the frequency captured

from a simulated PMU to speed up the ultracapacitor response. However, frequency with the PMU measurement input to AES3 showed significant oscillations after a load step, so further study is warranted with a filtered PMU measured frequency as an input. AES2 regulates the frequency quickly and accurately and AES3 contributes when the frequency is outside of its frequency dead band, but it does not reach its rated output power because its response time is longer than the dwell time of frequency below the frequency deadband.

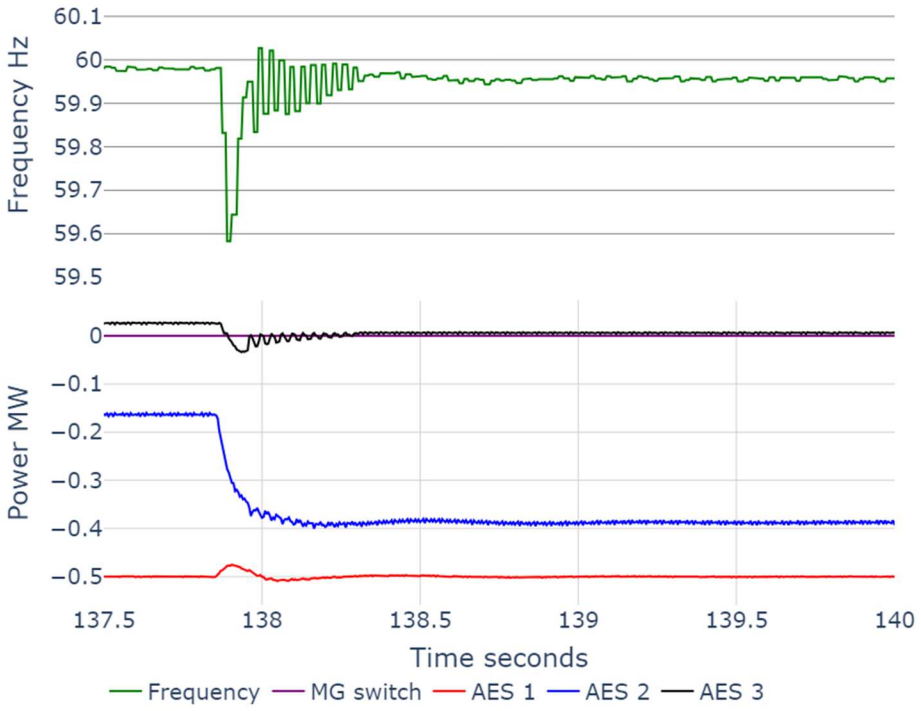

Figure 40: Microgrid frequency (top) and inverter powers (bottom) during a load step of 200 kW in islanded operation with the ultracapacitor under light load conditions.

Load Step Results – Heavy Load

For heavy load, NREL introduced load steps after the conclusion of the planned islanding experiment under the heavy loading conditions with the ultracapacitor. Figure 41 shows the load step down and load step up over 30 s.

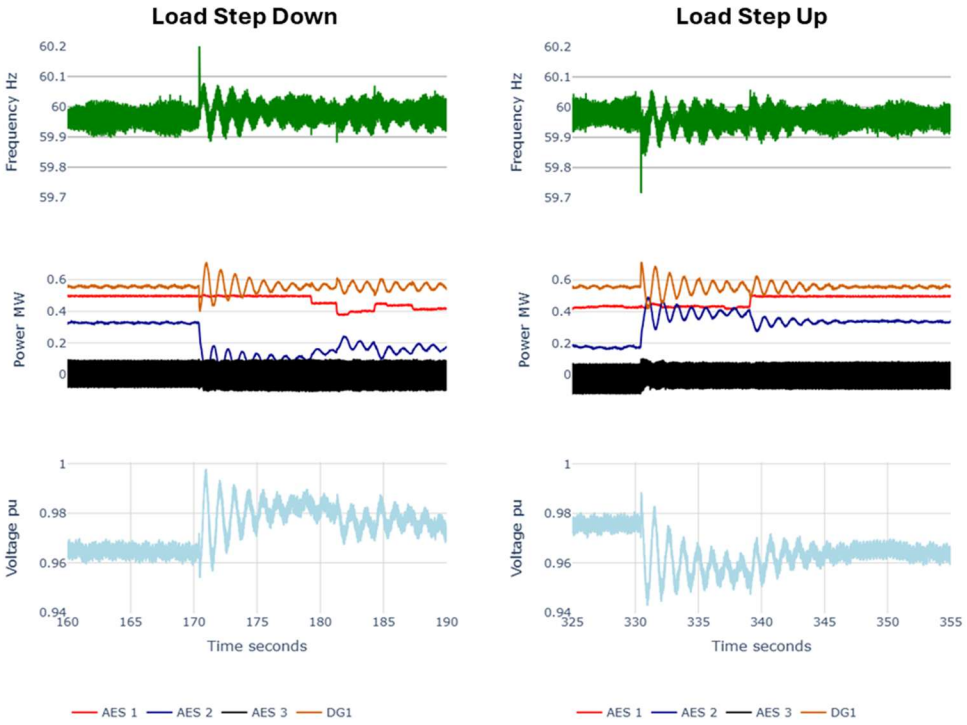

Figure 41: The microgrid frequency (top); inverter output powers and the power flow through the microgrid switch (center); and microgrid voltage (bottom) during a load step down and load step up in islanded operation with a diesel generator online and with the ultracapacitor under heavy loading conditions for about 30 s.

Stable operation is maintained, but significant oscillations are observed, and the frequency oscillations exceed the ultracapacitor deadband, so its ability to provide frequency support is negatively impacted. Further study is warranted on the interactions of the RSCAD generator model with other elements.

Results of this work were published and disseminated in the IEEE papers "Interoperable, Inverter - Based Distributed Energy Resources Enable 100% Renewable and Resilient Utility Microgrids" [10] and "Power-Hardware-in-the-Loop Experiments of a Microgrid With a Grid-Forming Battery Inverter" [11].

This task successfully completed the following milestones:

- *BP3-22-T18: Completed 25 % of the experiments outlined in the HIL Test Plan.*
- *BP3-24-T18: Complete execution of the HIL Test Plan.*
- *BP3-25-T18: Create report detailing the results of the HIL simulations outlined in the test plan.*
- *BP3-26-T18: Accepted paper in conference/journal.*

Related to the timing of field testing and budgetary limitations owing to the additional level of effort to build the HIL test platform, NREL could not complete follow-on simulations based on feedback/outcomes of SDG&E second field demonstration. Therefore, the following milestones were not completed.

- *BP3-30-T18: Define additional HIL simulations to be performed based on field tests.*
- *BP3-31-T18: Perform additional HIL simulations and document results.*
- *BP3-35-T18: NREL CRADA*

Task 19: Full Scale Simulation (Task Lead: NREL)
Comprehensive results of Full Scale Simulation are presented in Appendix B. Table 22 summarizes the testing scenarios:

Table 22: Simulation testing scenarios.

Scenario	Description
Black start	A black start is a very important scenario, especially to test the capability of the GFM and black-start-capable battery inverter and islanding leader, AES2. SDG&E provides the field sequence/restoration steps. This scenario has a series of dynamic operations of reconnecting DERs and load; therefore, the simulation time might be longer than 60 seconds. We also anticipate having to speed up the restoration sequence compared to what would be done in the field to keep the total simulation time reasonable.
Planned islanding	This is the most critical scenario to test for the Borrego Springs Microgrid. In this case, the microgrid controller reduces the power flow across the PCC to near zero before opening the microgrid switch. A disconnection logic is developed to control the PCC circuit breaker. Three different load conditions are simulated: morning, noon, and night. For each load condition, a combination of the availability of different grid assets is designed to investigate all possible situations.
Unplanned islanding	Unplanned islanding might happen, and it is important to test the stability of the microgrid system. For example, if a fault happens in the main grid, the PCC relay will open the PCC switch. Three different load conditions are simulated: morning, noon, and night. For each load condition, a combination of the availability of different grid assets is designed to investigate all possible situations.
Contingency events	This tests the islanded microgrid under selected disturbance events to evaluate the disturbance metrics of the microgrid. Events include: • Faults (line to ground [LG], double line to ground [LLG], triple line to ground [LLLG]) • Loss of generation (e.g., AES1) • Load rejection. For each event, three different load conditions are simulated: morning, noon, and night.

The most important learnings from the full-scale simulation are:

- A blackstart with only renewable resources can pick up the critical load in Ckt 2 even at night, and the diesel generator can be successfully brought online to pick up more load.
- AES2, the islanding leader and the only GFM source, can support the microgrid operation well enough to handle normal operations (e.g., planned islanding and black starts) and some abnormal operations (LG fault and some unplanned islanding).
- It is hard for the system to survive unplanned islanding. If one more GFM source can be added, the system might be capable of handling abnormal operations.

- It is hard for the system to survive an LLG fault, but it can ride through LG faults, and the system can maintain stability with a large load rejection.
- AES2 has a faster settling time than the diesel generator as the GFM source, and it can perform equivalent to the diesel generator; therefore, using a GFM inverter could replace the traditional diesel generator to make a 100% renewable microgrid feasible.

Results for planned and unplanned islanding are summarized below. For more detail on these, and results from blackstart and contingency event simulations, see Appendix B.

Planned Islanding

During planned islanding, the PCC of the microgrid (at 69 kV) is dispatched to minimize the power flow and avoid the transition operation transients. Table 23 describes the planned islanding scenarios evaluated and
Table 24 provides the learnings and outcomes of each case.

Table 23: Planned islanding test cases.

Test No.	Loading	26-MW PV Facility	6.5-MW PV Facility	Rooftop PV	Diesel	SES1 and SES2	SES3
1	Morning	On	On	On	On	Offline	Offline
2	Morning	On	Offline	On	Offline	On	On
3	Morning	On	Offline	On	On	Offline	Offline
4	Morning	On	On	On	Offline	On	On
5	Morning	On	On	On	Offline	On	Offline
6	Morning	On	Offline	On	Offline	On	Offline
7	Noon	On	On	On	Offline	On	On
8	Noon	On	On	On	On	Offline	Offline
9	Noon	On	Offline	On	On	Offline	Offline
10	Noon	On	Offline	On	Offline	On	On
11	Noon	On	On	On	Offline	On	Offline
12	Noon	On	Offline	On	Offline	On	Offline
13	Night	Offline	Offline	Offline	Offline	On	On
14	Night	Offline	Offline	Offline	Offline	On	Offline

Table 24: Summary Results of planned islanding simulations.

Test No.	Results	Learnings and Findings
1	*Successful planned islanding operation with diesel generator as GFM asset.* When the PCC circuit breaker is opened, the active and reactive power at the PCC are close to 500 kW and 500 kVAR, respectively. The PCC voltage and frequency reach steady state in about 6 seconds. The voltages at the	(1) The 26-W PV facility is curtailed from 0.2 to 0.1 due to excess generation. (2) The PCC voltage and frequency exhibit small oscillations and reach steady state within 6 seconds due to the slow response of the governor and AVR.

	end of the three circuits are maintained above 0.95 p.u.	
2	*Successful planned islanding operation, but the system exhibits some oscillations*. When the PCC circuit breaker is opened, the active and reactive power at the PCC are close to zero and 500 kVAR, respectively. The microgrid reaches steady state within 4 seconds after the PCC circuit breaker is opened. The PCC voltage and frequency show oscillations even after reaching steady state. SES2 absorbs a small amount of excessive active power and generates approximately 500-kVAR reactive power after the islanding operation. The voltages at the end of the three circuits are maintained above 0.95 p.u.	(1) The 26-MW PV facility is less curtailed (from 0.2 to 0.15) because the 6.5-MW PV facility is offline. (2) SES2 can act as a slack bus to balance the generation and load to maintain the system. (3) Before the islanding operation, the PCC frequency and head of circuits already exhibit some oscillations, and the oscillations worsen after the islanding operation.
3	*Successful planned islanding operation*. When the PCC circuit breaker is opened, the active and reactive power at the PCC are close to 200 kW and 550 kVAR, respectively. The PCC voltage settles at 0.98 p.u. from the islanding event. The PCC frequency overshoots to 60.3 Hz the moment the PCC breaker opens and settles at 60.1 Hz within 6 seconds. The voltages at the end of the three circuits are maintained above 0.95 p.u.	(1) The 26-MW PV facility is curtailed from 0.2 to 0.16. (2) The PCC voltage and frequency exhibit small oscillations and reach steady state within 6 seconds due to the slow response of the governor and AVR.
4	*Successful planned islanding operation*. When the PCC circuit breaker is opened, the active and reactive power at the PCC are close to zero and 550 kVAR, respectively. The microgrid reaches steady state within 4 seconds after the PCC circuit breaker is opened. The microgrid voltage and frequency show smooth transients with a small undershoot (0.97 p.u.) in voltage, and the microgrid frequency nadir is 60 Hz and overshoots to 60.42 Hz. (The frequency is 60.18 Hz in grid-connected mode.) The voltages at the end of the three circuits are maintained above 0.95 p.u.	Low load and low PV. (1) The PCC power flow needs to be minimized during the islanding operation. (2) The 26-MW PV facility needs to be curtailed (from 0.2 to 0.1) to reduce the excessive active power. (3) The transformers in the microgrid consume a significant amount of reactive power, and the capacitor banks need to turn on to supply the reactive power demand. AES1 can be used to buffer and fine-tune to balance the reactive power demand and generation.
5	*Successful planned islanding operation*. When the PCC circuit breaker is opened, the active and reactive power at the PCC are close to zero and 550 kVAR, respectively. The microgrid reaches steady state within 4 seconds after the PCC circuit breaker is opened. The PCC voltage and frequency show smooth transients with a small undershoot (0.97 p.u.) in voltage, the PCC frequency nadir of 60 Hz (60.18 Hz in grid-connected mode), and an overshoot of 60.42 Hz. The voltages at the end of the three circuits are maintained above 0.95 p.u.	Unlike Scenario 1, AES3 is offline. The frequency is stable and maintained close to nominal, so there is no need to use AES3.
6	*Successful planned islanding operation.* When the PCC circuit breaker is opened, the active and reactive power at the PCC are close to zero and 550 kVAR, respectively. The microgrid reaches steady state within 4 seconds after the PCC circuit breaker is opened. The PCC voltage and frequency show smooth transients with a small undershoot (0.97 p.u.) in voltage, the PCC frequency nadir of 60 Hz (60.18 Hz in grid-connected mode), and an overshoot of 60.42 Hz. There are no oscillations in the PCC voltage and frequency. The voltages at the end of the three circuits are maintained above 0.95 p.u.	Unlike Scenario 2, AES3 is offline. (1) The 26-MW PV facility is less curtailed (from 0.2 to 0.167) because PV2 is offline. (2) AES2 can act as a slack bus to balance the generation and load to maintain the system. (3) Each circuit has one capacitor bank on. (4) There is no need to use AES3.

7	*Successful planned islanding operation*. When the PCC circuit breaker is opened, the active and reactive power at the PCC are 450 kW and 500 kVAR, respectively. The microgrid reaches steady state within 4 seconds after the PCC circuit breaker is opened. The PCC voltage and frequency show smooth transients with a small undershoot (0.95 p.u.) in voltage, the PCC frequency nadir of 60 Hz (60.18 Hz in grid-connected mode), and an overshoot of 60.42 Hz. There are no oscillations in the PCC voltage and frequency. The voltages at the end of Ckt1 and Ckt3 are maintained above 0.95 p.u., and the end-of-circuit voltage for Ckt2 is 0.923 p.u.	There is high load and high PV. The general rule for reactive power dispatch: If the reactive power demand is less than 300 kVAR, AES2 is used; if the demand is between 300 and 500 kVAR, AES1 is used; otherwise, the 26-MW PV facility is used. (1) The 26-MW PV facility needs to be completely curtailed (from 0.9 to 0) to reduce the excessive active power. (2) AES1 is dispatched to generate 500-kVAR reactive power after the islanding operation. (3) Ckt1 has two capacitor banks on, and Ckt2 and Ckt3 each have one capacitor bank on. (4) A reactive power generation source with flexible dispatchability is needed to regulate the voltage at Ckt2, such as turning on the volt-VAR smart inverter function of the rooftop PV.
8	*Unsuccessful planned islanding operation*. When the PCC circuit breaker is opened, the active and reactive power at the PCC are -400 kW and 500 kVAR, respectively. The PCC voltage exhibits oscillations for 6 seconds before settling at 1 p.u. The PCC frequency increases beyond the operation limit, so the planned islanding is not successful.	(1) The 26-MW PV facility is curtailed from 0.9 to 0 because minimum power from the facility is 10% of capacity. The dispatched power is less than 10% of the 26-MW PV plant's capacity, so the facility is curtailed fully.
9	*Successful planned islanding operation.* When the PCC circuit breaker is opened, the active and reactive power at the PCC are 800 kW and 500 kVAR, respectively. The PCC voltage settles at 0.98 p.u. within 6 seconds. The PCC frequency shows a nadir of 59.6 Hz and exhibits oscillations before reaching steady state. The Ckt2 end-of-feeder voltage is slightly less than 0.95 p.u.	(1) The 26-MW PV facility is curtailed from 0.9 to 0.18. The 26-MW PV facility supplies the power generated by the 6.5-MW PV facility and additional active power to reduce the active power across the PCC breaker. (2) The diesel generator active and reactive power plots show the high oscillations compared to other scenarios.
10	*Successful planned islanding operation, but the system exhibits some oscillations*. When the PCC circuit breaker is opened, the active and reactive power at the PCC are 300 kW and -500 kVAR, respectively. The microgrid reaches steady state within 5 seconds after the PCC circuit breaker is opened. The PCC voltage and frequency show oscillations before the island operation and worsen after the islanding operation. The PCC voltage is steady before the islanding operation, but it shows oscillations after the islanding operation. SES2 absorbs a small amount of excessive active power and generates approximately 500-kVAR reactive power after the islanding operation. The voltages at the end of the three circuits are maintained above 0.95 p.u.; however, they exhibit very large oscillations (magnitude of 0.14 p.u.).	(1) The 26-MW PV facility is curtailed from 0.9 to 0.25. The 26-MW PV facility supplies the power generated by the 6.5-MW PV facility in Scenario 5 and additional active power to reduce the active power across the PCC breaker. It also supplies approximately 1-MVAR reactive power to take the power generated in AES1 from Scenario 5. (2) SES2 can act as a slack bus to balance the generation and load to maintain the system. (3) Ckt1 has two capacitor banks on, and Ckt2 and Ckt3 each have one capacitor bank on.
11	*Successful planned islanding operation.* The results are the same as Scenario 7.	Compared to Scenario 5, in this scenario, AES3 is offline. Because the frequency is maintained close to nominal, there is no need for AES3, and the system functions well without it.
12	*Successful planned islanding operation, but the system exhibits some oscillations*. When the PCC circuit breaker is opened, the active and reactive power at the PCC are close to zero. The microgrid	Compared to Scenario 6, in this scenario, AES3 is offline, and the PCC power flow is closer to zero. This helps reduce the harmful

	reaches steady state within 5 seconds after the PCC circuit breaker is opened. The PCC voltage and frequency show oscillations after the islanding operation, but the oscillations are smaller than those in Scenario 6. SES2 has active and reactive power output close to zero. The voltages at the end of the three circuits are maintained above 0.95 p.u. with reduced oscillations compared to Scenario 6.	transients during the islanding operation and avoids saturation of AES2.
13	*Successful planned islanding operation*. When the PCC circuit breaker is opened, the active and reactive power at the PCC are 2.4 MW and 2 MVAR, respectively. The microgrid reaches steady state within 0.5 seconds after the PCC circuit breaker is opened. The PCC voltage and frequency show smooth transients with an undershoot (0.85 p.u.) in voltage and a PCC frequency overshoot of 60.15 Hz. There are no oscillations in the PCC voltage and frequency.	There is high load and no PV. (1) Most load is disconnected because only 1.5 MW of power is available. (2) Significant effort is made to tune the voltage control of AES2. PID control must be used to maintain voltage stability. (3) This scenario shows an extreme case where there is not enough generation and there is very little flexibility to balance the generation and load; however, with careful dispatch and tuning of AES2, the microgrid system survives this planned islanding operation.
14	*Successful planned islanding operation*. The results are similar to Scenario 9.	Because the frequency is maintained as stable, there is no need for AES3; therefore, this scenario (with AES3 offline) shows the same results as Scenario 9.

Unplanned Islanding

During unplanned islanding, the power flow at PCC (the 69 kV bus) is not zero because the event is caused by suddenly tripping off the breaker at PCC due to a fault condition. Table 25 describes the unplanned islanding scenarios evaluated and Table 26 provides the learnings and outcomes of each case.

Table 25: Unplanned islanding test cases.

Test No.	Loading	6.5MW PV	Rooftop	Diesel	AES1 and AES2	AES3
1	Morning	On	On	Offline	On	On
2	Noon	On	On	Offline	On	On
3	Night	Offline	Offline	Offline	On	On

Table 26: Summary Results of unplanned islanding simulations. *

Test	Results	Learning and findings
1	Unsuccessful unplanned islanding operation	Since AES1 is assumed to be offline, there is not enough generation to support the load. With BESS as grid-forming resource, any under/over generation is leading to increase/decrease in voltage. There is voltage-power coupling which is contrary to synchronous machines power-frequency coupling.
2	Borderline successful unplanned islanding operation	Due to excess generation, PCC voltages increase maximum operating voltage. Any change in generation can put it over the maximum allowable operating voltage.
3	Unsuccessful unplanned islanding operation.	With 1 MVA AES2 capacity, there is not enough generation available to support unplanned islanding. Adding diesel can help to pick up critical loads.

* Note that the 26MW (PV1) array is not considered here because “Unplanned” means the 69kV T/L tripped unexpectedly, disconnecting the 26 MW PV facility.

This task successfully completed Milestones 23 and 29 related to execution of the full-scale simulation, contingency scenarios and results analysis. The NREL team had desired to run additional contingency scenarios relevant to Borrego Springs, including the impact of PV intermittency or large load, however budget constraints related to the additional effort of this task prevented additional scenarios.

Task 20: Field Tests (Task Lead: SDG&E)

Field Operation #1:

In November 2023, the SDG&E team conducted an evaluation of the battery IBRs to assess inverter response and capability to maintain system frequency (within 60 Hz ± 0.5% (60.3-59.7 Hz) during blackstart, islanding, and load step variations, and to validate the automation and logic of the microgrid controller. Tests were performed on a sectionalized circuit of the Borrego Springs Microgrid (no impact to customers). AES2 (as island leader) and AES1 were the only resources used for the test; AES3, was not yet commissioned with the new controller and the diesel generators were offline and unavailable to participate. All commands were sent from the microgrid controller to also validate the automation and logic developed. SDG&E conducted testing on an isolated section of circuit such that no customers were impacted by testing.

All operations were successful, and demonstrated that the IBR, AES2 could blackstart and island the microgrid working in conjunction with AES1, a GFL support resource through the microgrid controller.

<u>Blackstart</u>

Blackstart results are shown in Figure 42. The frequency before blackstart is zero, but the data capture system retains the last frequency point before communications were lost and therefore shows it as 60 Hz. The minimum frequency observed immediately after blackstart start was 59.79 Hz, with a follow-on excursion to 59.73 Hz approximately 10 s later, which is attributable to the load of certain high-power air-conditioning loads in the microgrid yard coming back online after a precheck delay. The maximum rate-of-change-of-frequency (RoCoF) response observed was 2.22 Hz/s, and the island achieved stability within less than 2 min.

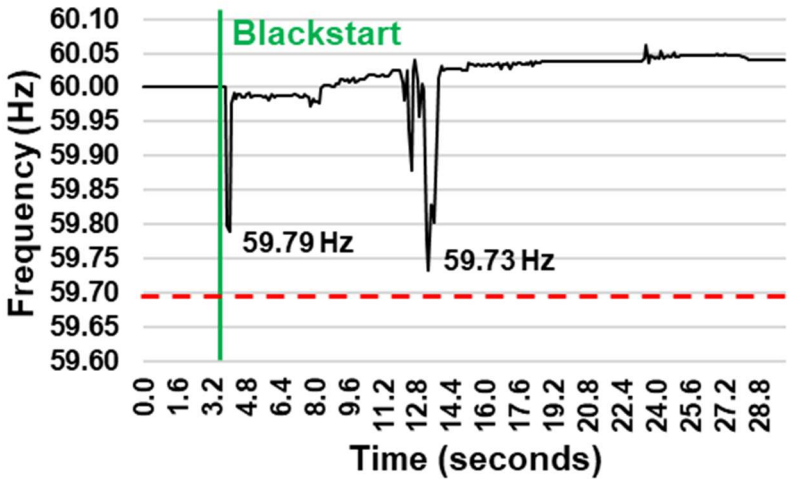

Figure 42: Measured frequency during blackstart test.

Islanding

Preliminary evaluations of the AES2 inverter response and the capability to maintain system frequency within 60 Hz ± 0.5% (60.3-59.7 Hz) during blackstart, islanding and load step operations were performed on a circuit section of the Borrego Springs Microgrid, which was configured to ensure no customer impacts. AES2 and AES1 were the only resources used for the test; the UCAP, AES3, was not yet commissioned with the new controller and the diesel generators were offline and unavailable to participate. All commands were sent from the microgrid controller to also validate the automation and logic developed.

For the islanding evaluation, AES2 was derated to 400 kW from its nameplate of 1 MW to provide headroom during the tests. AES1 was used as a baseload, set to 380 kW. Frequency changes throughout these events were collected through synchrophasor (PMU) data acquisition with a 33-millisecond sampling rate.

Referring to Figure 43, the minimum frequency observed during the planned islanding with a 380-kW load (from AES1) was 59.98 Hz, with a maximum RoCoF of 0.24 Hz/s, indicating that AE 2 well maintains frequency within the tolerance band of +/- 0.5% of 60 Hz, as indicated in Figure 43. The island was monitored for 10 minutes following the transition, and frequency was maintained within bounds thought the operation. Primary stability was achieved in 40ms.

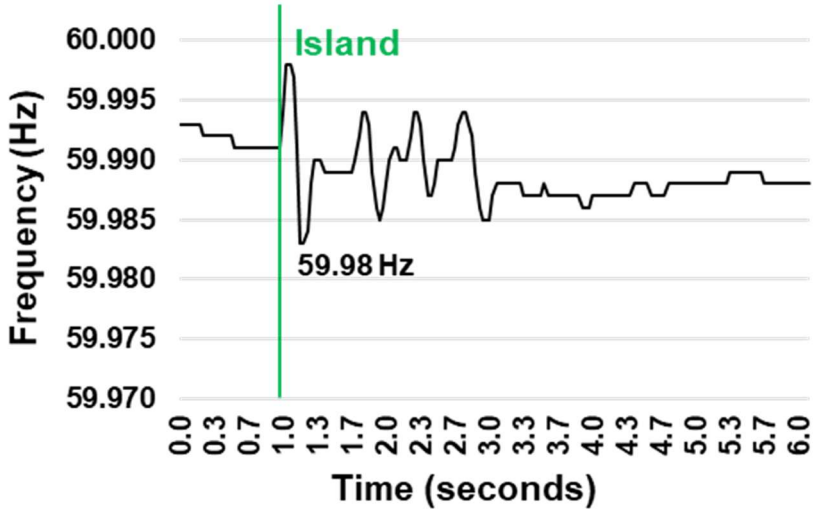

Figure 43: Measured frequency during the islanding event.

Large load step

System frequency was also evaluated for large change in load during island operation, a relevant condition given the high-power demands of local agricultural equipment (rapid load increase), or customer rooftop PV systems coming back online after an outage (rapid load decrease). For these evaluations, AES2 was dispatched at 75% of full rating (750 kW) and AES1 was dispatched at 380 kW. Figure 44 provides the system frequency response with addition and removal of a 400kW load. Minimum frequency observed was 58.563 Hz, with a RoCoF of 4.27 Hz/sec for load addition, and maximum frequency observed was 60.72 Hz, having a 5.76 Hz/sec, with loss of the load. In both cases, the island was preserved.

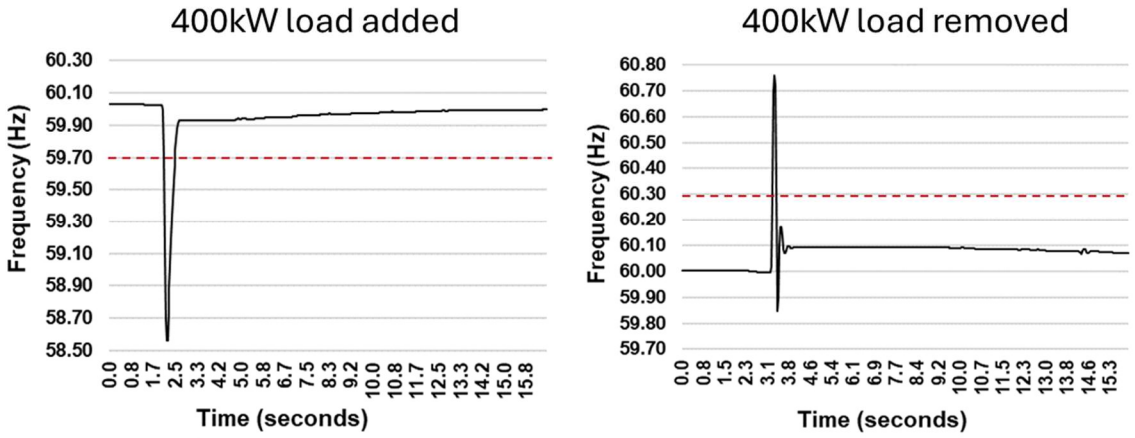

Figure 44: 400kW load response.

Table 27 summarizes the tests. Based on historic operational data analysis presented in Table 9, conventional generating resources do not appear to react as fast as the IBRs evaluated.

Table 27: Summary results of Field Operation #1.

Operation	*f* max (Hz)	*f* min (Hz)	RoCoF (dHz/dt)	Restoration time to in-bound frequency
Parallel → Island	60.01	59.98	0.24 Hz/s	*f* remained in bounds
Island → Parallel	60.02	59.98	0.15 Hz/s	*f* remained in bounds
Blackstart	60.04	59.73	2.22 Hz/s	*f* remained in bounds
400kW load addition		58.61	4.27 Hz/s	430ms
400kW load loss	60.72		5.76 Hz/s	200ms

This field test met Milestone 21, Evaluation of battery-inverter resource response through microgrid controller for blackstart and island. Findings were also presented in the IEEE paper "Interoperable, Inverter - Based Distributed Energy Resources Enable 100% Renewable and Resilient Utility Microgrids".[10]

Installation of AES3 pre-charge circuit

For operation of AES3 through the microgrid controller, the team identified the need to install a pre-charge circuit to automate ultracapacitor charging to the voltage level of the inverter, with a customizable setpoint (% of 600V DC max). The circuit was installed and then its operation checked before proceeding with field tests (Figure 45), meeting Milestone 27.

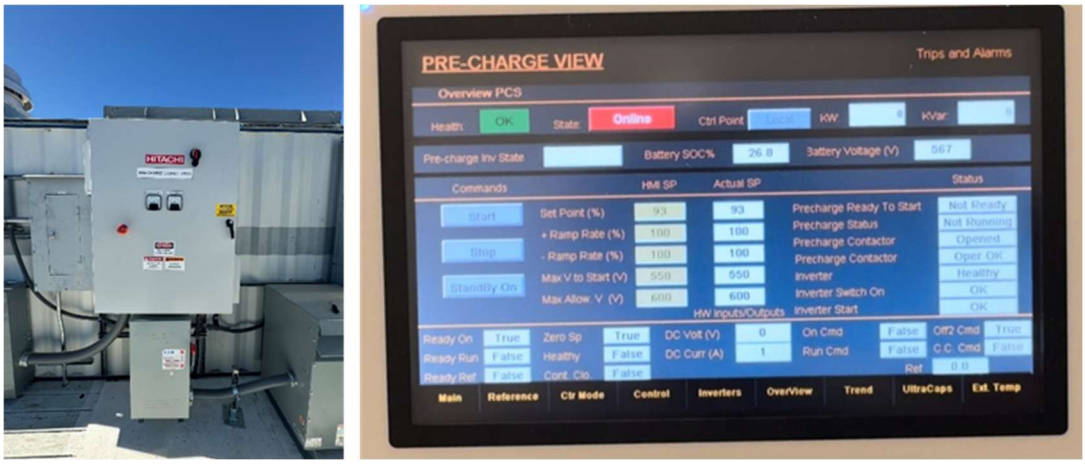

Figure 45: AES3 pre-charge circuit DC drive and user interface screen.

Field Operation #2:

The SDG&E team conducted an evaluation of the battery IBRs to assess inverter response and capability to maintain system frequency (within 60 Hz ± 0.5% (60.3-59.7 Hz) during blackstart, islanding, and load step variations, and to validate the automation and logic of the microgrid controller. Building upon the previous field operation, this field evaluation included the ultracapacitor, AES3 with control callability through the microgrid controller. Tests were performed in the Borrego Springs Microgrid yard (no impact to customers). AES2 (as island leader) and AES1 were utilized, in addition to the ultracapacitor system AES3. Generators were offline, unless noted. All commands were sent from the microgrid controller to also validate the automation and logic developed. All tests were run at a power factor of 0.95 unless otherwise noted. AES1 was utilized to push and pull power during

the testing, and a load bank was utilized in certain tests. SDG&E conducted testing exclusively within the microgrid yard, such that no customers were impacted by testing.

Operations were successful, and demonstrated that the IBR, AES2 could blackstart and island the microgrid working in conjunction with AES1, a GFL support resource and AES3 as a frequency support resource through the microgrid controller.

Blackstart and island stability

Results of the blackstart test with AES2 as island leader are shown in Figure 46, with a subsequent 500kW load pickup. Maximum frequency observed was 60.157 Hz and minimum frequency observed was 59.196 Hz, within bounds. Rate of change of frequency, dHz/dt, was 0.108 Hz/s with 2% settling time of 389.84 ms and settling min of 19.492 seconds. AES3 was not triggered during the operation.

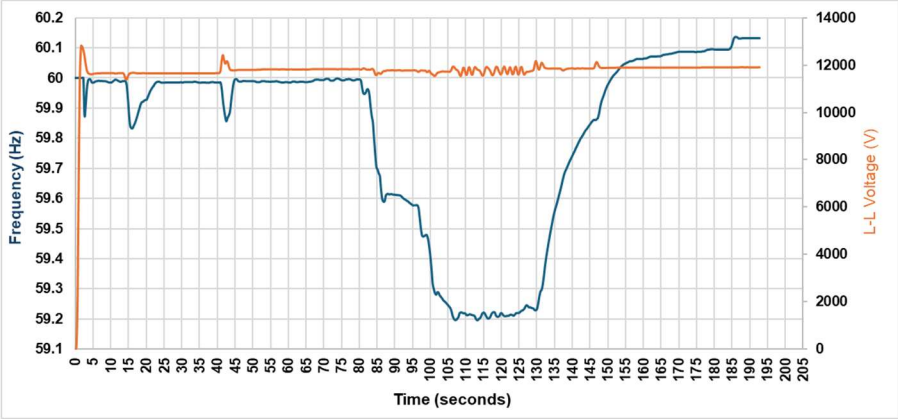

Figure 46: Blackstart operation with AES2 island leader.

Load step tests – AES2 island leader with AES3 frequency support

Table 28 summarizes the conditions for light load step tests. These tests utilized AES2 as the island leader and AES3 was activated as a frequency support system, available to support when triggered per the setpoints noted in Figure 16. AES1 was set to 0 kW to start. When the load bank is turned on although the setpoint is set to 0KVA, it still has a load of ~33kW due to its fans running. Power factor setting of the load bank was 0.95. Generators were offline for these experiments.

Table 28: Load step tests with AES2 island leader, AES3 active and generators offline

Event	Time	Incremental Load Change (kW)	Load bank Setpoint (KVA)	AES 3 Status	AES 1 setpoint
1	3:30	685	721.05	available	0 kW
2	3:34	200	931.58	available	0 kW
3	3:35	-200	721.05	available	0 kW
4	3:38	300	1036.84	available	0 kW
5	3:39	-600	210.53	available	0 kW
6	3:40	600	842.11	available	0 kW
7	3:42	800	0	available	0 kW
8	3:43	1000	1052.63	available	0 kW
9	3:45	-1000	0	available	0 kW
10	3:54	850	1263.16	available	350kW
11	3:55	-850	0	available	350kW
12	3:56	850	1263.16	available	350 kW
13	3:56	-850	0	available	350 kW

Table 29 summarizes the cases where the ultracapacitor, AES3 was triggered to support microgrid frequency, observed when load step real power changes were larger than ≥600kW. Orange color notes where frequency fell outside of bounds of IEEE 1547-2003, which has tighter underfrequency and overfrequency protection settings (59.3 Hz and 60.5 Hz, respectively) It is important to evaluate performance under these more stringent bounds considering that a portion of customers served during microgrid operation have older vintage rooftop PV inverters on which could potentially fault during an over or underfrequency event.

Table 29: Frequency response assessment of events where AES3 was triggered.

Event	Real Power Change (MW)	RoCoF (dHz/MW), Hz/MW	SES3 Triggered value (kW)	F max (Hz)	F min (Hz)	RoCoF (dHz/dt), Hz/s	settling min (ms)	2% settling time (ms)
1	0.685	0.196	120	59.960	59.826	0.917	778	15.56
6	0.600	0.305	140	59.953	59.770	0.785	561	11.22
7	0.800	0.501	-275	60.377	59.976	2.99	600	12
8	1	0.277	220	59.910	59.633	1.67	391	7.82
11	0.850	0.918	-270	60.765	59.985	5.86	750	15
12	0.850	0.318	260	59.907	59.637	2.45	500	10
13	0.850	0.869	-270	60.669	59.930	5.74	724	14.48

Figure 47 and Figure 48 plot the frequency response for the 600kW load step change and settling period, with an expanded view of the first few seconds of the step change.

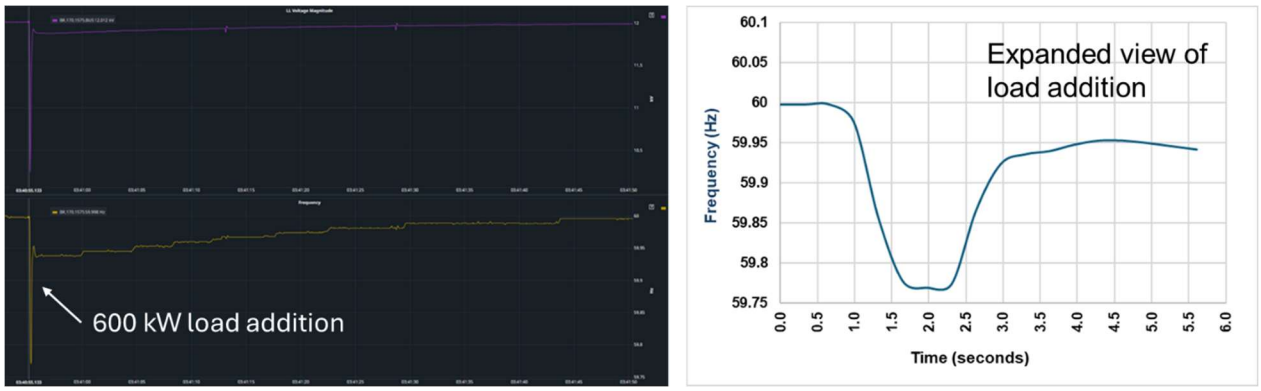

Figure 47: 600kW load applied.

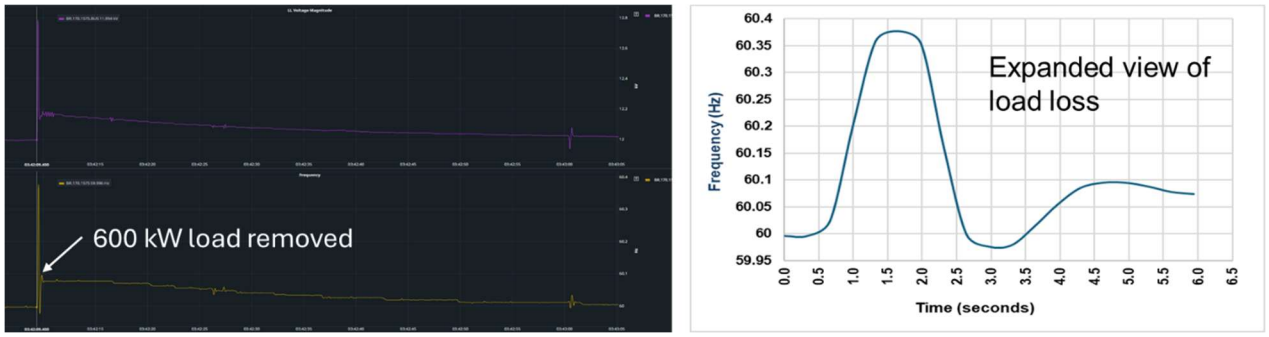

Figure 48: 600kW load removed.

Figure 49 and Figure 50 plot the frequency response for the 850 kW load step change and settling period, with an expanded view of the first few seconds of the step change.

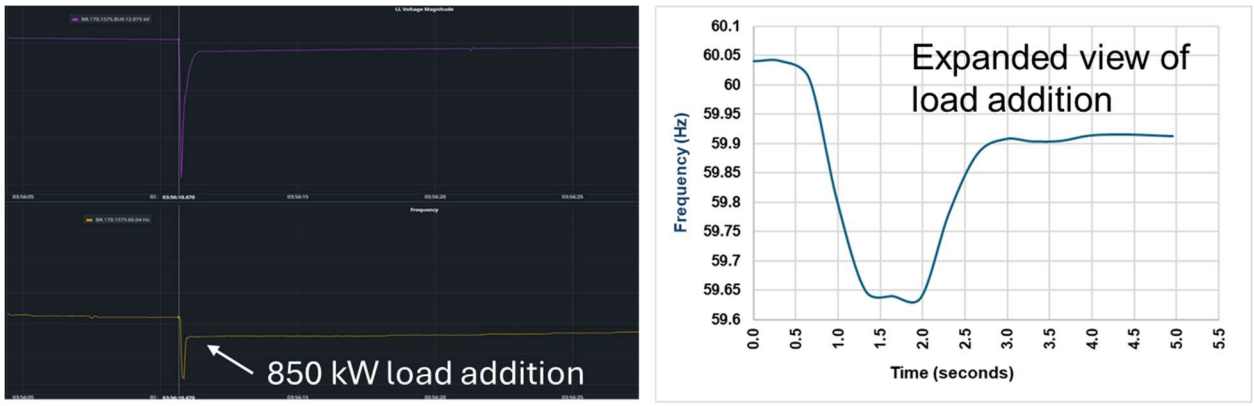

Figure 49: 850kW load applied.

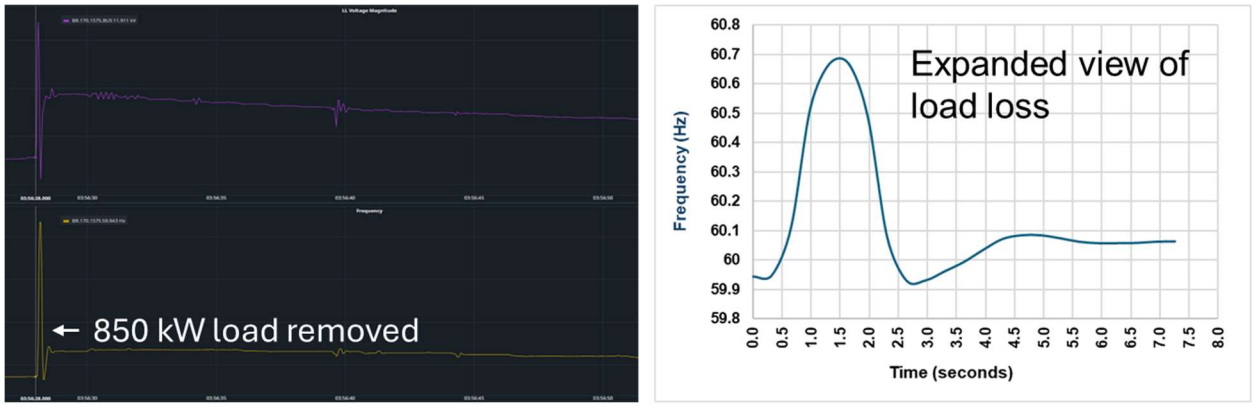

Figure 50: 850kW load removed.

In the case of 800 and 850kW, AES3 had a shortfall in power to maintain frequency in bounds. Figure 51 highlights the rapid, maximum power injection of AES3 in response to the 850kW load demand (left) and power absorption during load loss (right).

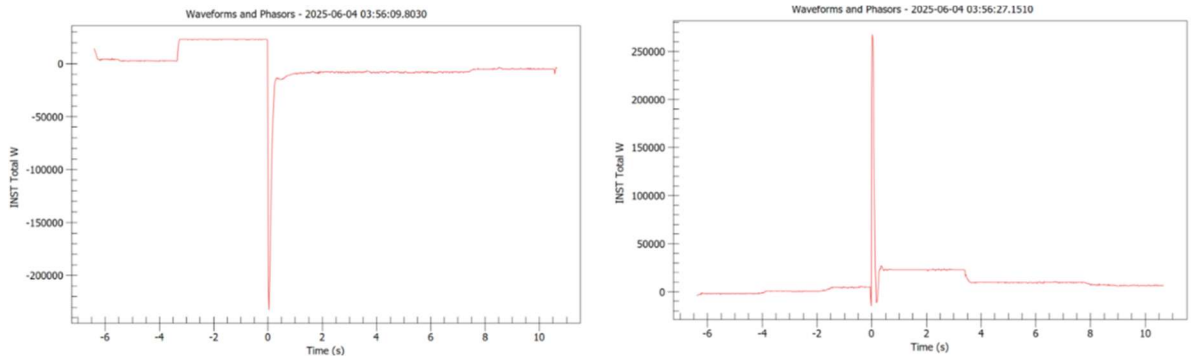

Figure 51: AES3 power injection/absorption in response to 850kW load addition (left) and loss (right).

The team attempted a 1MW load step test twice (Table 30). Given the shortfall in power of the energy storage resources to perform this test in the test configuration, the generator was activated as a backup resource. Generator 1 was set to dispatch 1MW at 0.95 PF at 04:00. Shortly afterwards at 04:04 the load bank setpoint of 1052.63 KVA at 0.95 PF was pushed, AES2 was set to 0 W and so was AES1. It was deemed to be too big of a load step (owing to the relatively low power rating of the energy storage systems) since shortly afterwards the generator tripped in both cases.

Table 30: Conditions for 1MW load test.

Event	Time	Load bank Setpoint	Gen Setpoint	AES 1 setpoint	AES 2 setpoint
14	04:04	1052.63 at 0.95 PF	1MW at 0.95PF	-240 kW	0 kW
15	04:18	2105.26.63 at 0.95 PF	1MW at 0.95PF	0 kW	-1 MW

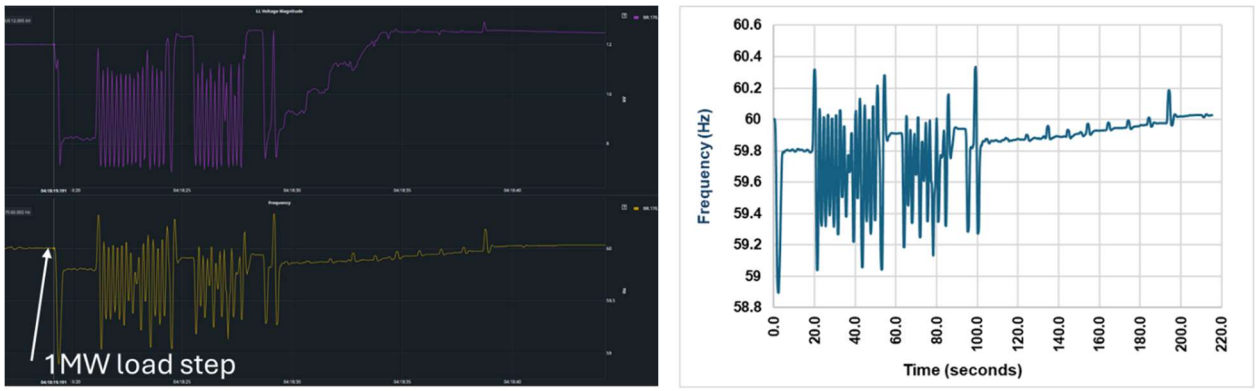

Figure 52: 1MW load step attempt.

Table 31: Frequency response characteristics for 1MW load step test (event 15).

Event	Real Power Change (MW)	RoCoF (dHz/dMW), Hz/MW	F max (Hz)	F min (Hz)	RoCoF (dHz/dt), Hz/s	settling min (ms)	2% settling time (ms)
14	1	0.966	60.396	59.430	0.026	38067	761.34
15	1	1.441	60.335	58.894	0.105	21716	434.32

Figure 53 provides the microPMU data for the ultracapacitor illustrating its attempt to support the operation by triggering. We see the system immediately injecting at its maximum rate to support the first seconds, then repeated charge and discharge in response to the destabilizing impact of the generator shortfall. It is possible that the generators would not have tripped had the ultracapacitor been able to deliver higher power for a longer duration.

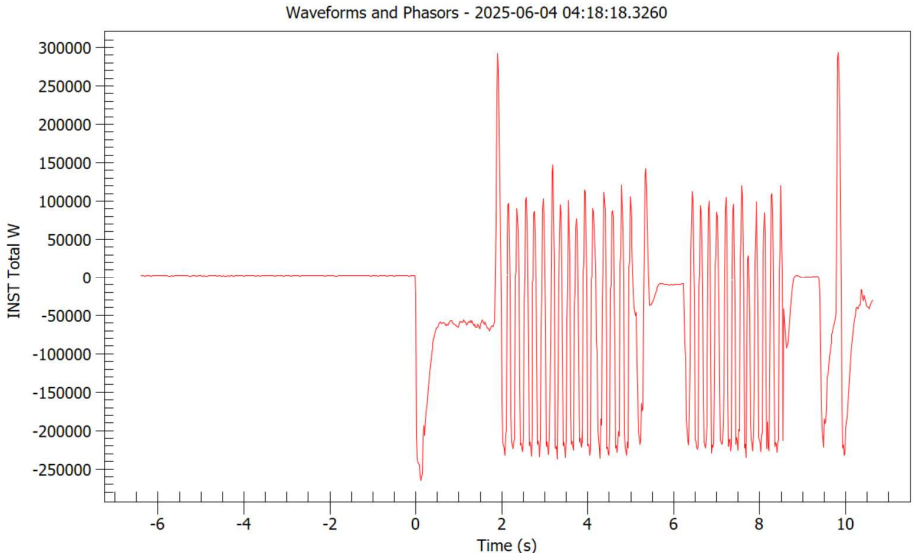

Figure 53: AES3 ultracapacitor response to support 1MW load.

Results from the second field evaluation provided further support that the IBR AES2, including support from AES3, can arrest the rate of change of frequency of the microgrid faster than conventional generators, resulting in a lower change of frequency per unit of real power. Comparing the load step of AES2 w/ AES3 to closest comparable load events of a historic microgrid operation with conventional generators (Table 10, events 3 and 5-12), the change in frequency per change in real power is substantially reduced using AES2, with faster settling time, indicating higher overall microgrid stability. Building on the confidence gained from this 100% IBR evaluation of the microgrid for blackstart, island, and large load pickup, additional battery energy storage resources are being added to Borrego Springs Microgrid to support larger amounts of load in the community.

This task successfully completed Milestone 28 and 33, evaluation of battery-inverter resource and ultracapacitor response through microgrid controller for blackstart and island and analyze field test and demonstration results. During the time window that the upgraded microgrid resources were being validated and the end of the project, there were no unplanned outages in Borrego Springs nor a scheduled maintenance operation in the area. Therefore, customers were not affected, but there was also not an opportunity to conduct a community-wide field demonstration per Milestone 32.

Significant Accomplishments and Conclusions

In this project, GFM capabilities were successfully transitioned from existing diesel generators to battery IBRs, and a new interoperable DERMS microgrid control system demonstrated control and management of multiple GFM and GFL inverters. Through synchrophasor and other power quality data, the upgraded Borrego Springs Microgrid resources demonstrated 100% renewable capability to stabilize microgrid frequency for blackstart, islanding operations, and large load addition or removal. Broadly, the project developed and validated an interoperable integration strategy for inverter-based distributed energy resources to a standard design interface to reduce the complexity of integrating new DERs.

Full scale EMT simulation and HIL testing advanced the state of -the-art by demonstrating how intelligent control of distributed assets can improve local system reliability and resilience and reduce PV curtailment during islanding operations. Importantly, HIL tests informed updates to inverter parameters and de-risked the deployment of IBRs to support further industry utilization of HIL as technique to minimize the deployment risk of equipment in microgrids in the grid.
Project information and outcomes were disseminated in technical publications and presentations, workforce training sessions, and in general presentations the Borrego Springs community. Significantly, the IBR control strategy developed in this project has been utilized at additional SDG&E microgrid sites, highlighting the extensibility and replicability of the solution.

This project met its three primary end of project goals. Firstly, it was demonstrated that 100% renewable blackstart and islanding functionality is possible at the Borrego Springs Microgrid, utilizing a battery IBR. AES2, the battery island leader, provided the necessary frequency response functionality to stabilize the microgrid in response to variability from changes in load as evidenced by smaller changes in frequency versus changes in real power compared to conventional generators, and faster frequency settling time. To our knowledge, this project was the first to be able to directly evaluate the performance of at-scale IBR versus conventional generators in a utility microgrid, with the benefit of a decade of historic operational context. This project has demonstrated the technology evolution of IBRs and has increased the confidence that in-front-of-the-meter (IFM) microgrids can be operated, safely and efficiently, to enhance grid resiliency. In addition, this demonstration project has allowed system operators to reduce their dependency on fossil-fueled, conventional generation to engineer, design and operate microgrids. Renewable, IBRs can now provide grid-support, while grid-connected, without concerns of refueling or emissions, and provide resiliency during system stress, emergencies and compliance system maintenance, while it operates in islanded mode.

The project team established an interoperable microgrid control system enabling operation of multiple IBRs, which could be operated on site or remotely. Remote operation is especially important for microgrids located in rural and remote areas to help avoid delays in grid operation related to the additional time it takes to travel to these

sites to address any issues. As a direct outcome of learnings and confidence gained in IBRs during this project, SDG&E deployed four additional microgrids with the same control platform, highlighting the replicability of the solution. Since 2013, the lessons learned at the Borrego Springs Microgrid have supported the development of permanent and temporary microgrids to enhance reliability and resiliency. These lessons learned span system architecture, equipment specifications, microgrid layout, modeling and simulations, commissioning techniques and community outreach.

The capability established in this project through HIL and EMT simulations of Borrego Springs microgrid supported important adjustments for microgrid field procedures to inverter parameters and were important to characterize the responsiveness of IBRs. This project demonstrated the capability of simulation to de-risk field operations and more broadly become increasingly important as distribution grids and microgrids become more complex and dynamic with increasing proportions of renewable generation.

NREL extended a previously developed PHIL interface for GFM inverters to enable HIL simulations of seamless transitions between islanded and grid-connected operation. Such interfaces are particularly challenging when the inverters need to switch modes, i.e., between GFL and GFM as the microgrid transitions between grid-connected and islanded operation. The PHIL interface used is suitable for those who need a solution that uses a voltage-mode power amplifier. NREL identified that further work is warranted on improving the accuracy of this interface at low power levels.

EMT simulation of the Borrego Springs network with 105 inverters was challenging. The strategy to divide the network into three sections to simulate them in parallel was an efficient approach. The sections are defined so that the DERs are distributed roughly equally across the three sections to reduce the overall simulation time. In this project, NREL developed and utilized its own inverter model because the inverter manufacturer was unable to provide a PSCAD model. It was not anticipated that the inverter manufacturer would be unable to provide a PSCAD model and this slowed down progress. While the NREL inverter model is representative of state-of-the-art GFM inverters, findings related to the inverter controls cannot be directly applied to field inverters. Adaptive PID control in the GFM inverter might be needed to adaptively tune the PID control parameters to work with all the scenarios.

Remote HIL setup between NREL ESIF and SDG&E ITF (Tasks 3 and 12) were descoped from the project before the project kicked off, because NREL ESIF cost recovery was underestimated during the proposal phase and to keep NREL’s total budget the same, scope had to be reduced, and it was jointly decided that these were the least critical of NREL’s tasks.

Overall, the level of effort required in simulation was higher than anticipated. Logistics in field work at certain points in the project related to vendor availability to conduct on-site work created some delays given the remote location of Borrego Springs. During the time window that the upgraded microgrid resources were validated and the end of the

project, there were no unplanned outages in Borrego Springs nor a scheduled maintenance operation in the area. Therefore, there was not an opportunity to conduct a community-wide field demonstration (BP3-32-T20). SDG&E plans to utilize the IBRs to support customers during future planned outages, once scheduled, and unplanned outages, should the microgrid be used to support outages called upon.

Path Forward

Based on the results of this project's field evaluations and conclusions from NREL's EMT and HIL simulations, SDG&E is adding six more battery containers to the Borrego Springs Microgrid having a total rating of 7 MW/14 MWh. This IBR will become the new island leader, enabling prolonged operation of the microgrid on 100% renewable energy, and the ability to support most, if not all, of the community load. This resource will be integrated into the microgrid controller established during this DOE project, representing an extensibility of the platform. As part of its sustainability strategy, SDG&E is consistently reviewing the infrastructure needs of its remote communities and will continue to work with the Borrego Springs community to implement its lessons learned from this project and further strengthen the resilience of Borrego Springs. SDG&E will share with the DOE the outcomes and lessons learned from these operations that it presents to the community of Borrego Springs. The results of this work indicate that conventional generators may only be needed as a backup resource. During the day, the microgrid can harness energy from local solar plants and rooftop solar, as well as use batteries to power the entire community. During the night, the expanded capacity of the microgrid's batteries can help power critical load areas.

HIL simulations provided valuable insights to set inverter parameters and de-risk field tests and operations. Broadly, NREL sees promising results to improve the ability of grid operators to integrate increasing amounts of solar generation into the grid in a cost-effective, secure, resilient, and reliable manner. NREL is continuing to build on the PHIL experimental setup established in this project and leveraging the platform to study grid integration of GFM fuel cell inverters. Continued research efforts include study of the PHIL interfaces with multiple GFM inverters in a microgrid, and addressing PHIL interface accuracy deterioration at lower power, possibly by adding adaptive gains.

The PSCAD EMT model established in this project can serve as a baseline model for the Borrego Springs Microgrid to add more IBRs to the system as SDG&E plans to integrate more renewable resources, especially GFM inverters. Possible areas of exploration include:

- Study the best operation modes and droop settings for multiple GFM inverters with different capacities. Currently, a single islanding leader, a GFM inverter, is used even though other battery inverters are also GFM-capable. If multiple GFM inverters run in parallel, the best droop settings need to be investigated, especially under the worst scenario, e.g., unplanned islanding. Moreover, secondary control can be studied as well because reactive power sharing is a problem when multiple GFM inverters run in parallel.
- Troubleshoot and investigate any observed instability/oscillations in the field. A high-fidelity EMT model reflects the real-world power system, and the EMT model

can recreate the instability/oscillations observed in the field. Through targeted troubleshooting, those observed problems can be mitigated.

- Perform specific EMT simulations to evaluate the capabilities of the microgrid with more IBRs, such as a black start and planned and unplanned islanding. For a black start, the most straightforward measure of the microgrid capability is how much load can be picked up under different loading conditions (morning, noon, and night). Planned and unplanned islanding tests whether the microgrid can survive under those conditions.
- Model the GFM to be 2800-2022 compliant and study the GFM inverter's ride-through performance under different transients and events.

Products

Publications and papers produced under the award

Authors	Article Title	Publication	DOI	OSTI ID
Pratt, Annabelle; Prabakar, Kumaraguru; Symko-Davies, Martha	**Power-Hardware-in-the-Loop Experiments of a Microgrid with a Grid-Forming Battery Inverter**	2025 IEEE Power & Energy Society General Meeting (PES GM)	Not yet available	Not yet available
Abcede, Laurence; Blankenship, Alie; Moradpour, Andrew; Aragon, Mary; Cardenas, Jose; Shamukh, Nagadev; McGrath, Kimberly; Pratt, Annabelle; Prabakar, Kumaraguru; Symko-Davies, Martha	**Interoperable, Inverter - Based Distributed Energy Resources Enable 100% Renewable and Resilient Utility Microgrids**	2025 IEEE PES Grid Edge Technologies Conference & Exposition (Grid Edge)	10.1109/GridEdge61154.2025.10887429	2558970
Meyers, Toby; Prabakar, Kumar; Pratt, Annabelle; Tiwari, Soumya; Fossum, John	**PHIL Interface Design For Use with a Voltage-Regulated Amplifier**	2023 IEEE PES Conference on Innovative Smart Grid Technologies (ISGT Latin America)	10.1109/ISGT-LA56058.2023.10328333	2001481
Pratt, Annabelle; Prabakar, Kumaraguru; Ganguly, Subhankar; Tiwari, Soumya	**Power-Hardware-in-the-Loop Interfaces for Inverter-Based Microgrid Experiments Including Transitions**	2023 IEEE Energy Conversion Congress and Exposition (ECCE)	https://doi.org/10.1109/ECCE53617.2023.10362806	2324597
Velaga, Yaswanth Nag; Wang, Jing; Pratt, Annabelle; Abcede, Laurence; Shanmukh, Nagadev	**Transient Stability Study of a Real-World Microgrid with 100% Renewables**	2022 IEEE Energy Conversion Congress and Exposition (ECCE)	10.1109/ECCE50734.2022.9947656	1916449
Prabakar, Kumaraguru; Meyers, Toby; Fossum, John; Pratt, Annabelle; Symko-Davies, Martha; Shanmukh, Nagadev; Menvielle, Michelle; Abcede, Laurence; Bialek, Tom	**Impact of Load Tap Changer Control Operation Under Microgrid Conditions**	2022 IEEE Power & Energy Society General Meeting (PES GM)	https://doi.org/10.1109/PESGM48719.2022.9916915	1909412

Information Dissemination and Workforce Development
Over 20 tours of the microgrid were conducted to highlight the innovations of this project, including: the Borrego Springs Infrastructure Committee and Community Sponsor Group, La Jolla Tribal Council, Oregon State University Alfred P. Sloan Foundation, MCAS Miramar, Consumers Energy, Commission for Environmental Cooperation, Southern California Edison, SDG&E wildfire mitigation team, and Department of Energy. Additionally, information was communicated on an annual basis to the community of Borrego Springs during Borrego Days events.

Seven workforce training sessions were conducted in this project, including at SDG&E Apprentice Night School. Training topics included power quality and metering training, real time automation and control, harmonics standards and indices, and SDG&E Troubleshooter Emergency Training.

Project Team and Roles

San Diego Gas & Electric Company

- Laurence Abcede, Principal Investigator
- Kimberly McGrath, Program Manager
- Borrego Springs Microgrid Development, Engineering, and Operations Team:
    - Jose Cardenas
    - Beverly Glory
    - Taha Mustafa
    - Mary Cortez
    - Maison Cowley
    - Nagadev Shanmukh
    - Steven Prsha
    - Alejandra Jacquez
    - Andrew Moradpour
    - Alie Blankenship
    - Michelle Menvielle
    - Harrison Kim
    - Devon Yousif

National Renewable Energy Laboratory

Hardware in the loop platform design, development and PHIL/CHIL testing:

- Annabelle Pratt
- Kumaraguru Prabakar

Full scale simulation

- Jing Wang
- Yaswanth Nag Velaga
- Martha Symko-Davies – Laboratory manager and advisor

Solar Energy Technologies Office (SETO)

- Robert Reedy – TechnologyAdvisor
- Guohui Yuan - Program Manager, Systems Integration

References

[1] Hilal Katmale, Sean Clark, Thomas Bialek, and Laurence Abcede, “Borrego Springs: California’s First Renewable Energy-Based Community Microgrid,” CEC-500-2019-013, Feb. 2019. [Online]. Available: https://www.energy.ca.gov/sites/default/files/2021-05/CEC-500-2019-013.pdf

[2] J. Wang, A. Pratt, K. Prabakar, B. Miller, and M. Symko-Davies, “Development of an integrated platform for hardware-in-the-loop evaluation of microgrids prior to site commissioning,” *Applied Energy*, vol. 290, p. 116755, May 2021, doi: 10.1016/j.apenergy.2021.116755.

[3] K. Prabakar, Y. N. Velaga, R. Flores, J. Brouwer, J. Chase, and P. Sen, “Enhancing distribution system resiliency using grid-forming fuel cell inverter,” in Proc. 2022 IEEE Rural Electric Power Conference (REPC), pp. 38–42.

[4] G. Skaria *et al*., "Experiences and Lessons from Field Demonstration of Grid-forming Inverter in An AC Microgrid," *2024 IEEE Power & Energy Society General Meeting (PESGM)*, Seattle, WA, USA, 2024, pp. 1-5, doi: 10.1109/PESGM51994.2024.10689195.

[5] Jain, Himanshu, Gab-Su Seo, Eric Lockhart, Vahan Gevorgian, and Benjamin Kroposki. 2020. Blackstart of Power Grids with Inverter-Based Resources: Preprint. Golden, CO: National Renewable Energy Laboratory. NREL/CP-5D00-75327. https://www.nrel.gov/docs/fy20osti/75327.pdf

[6] Wang, Jing, Annabelle Pratt, and Murali Baggu. 2019. Integrated Synchronization Control of Grid-Forming Inverters for Smooth Microgrid Transition: Preprint. Golden, CO: National Renewable Energy Laboratory. NREL/CP-5D00-72756. https://www.nrel.gov/docs/fy20osti/72756.pdf

[7] A. Suryani, I. Sulaeman, O. A. Rosyid, N. Moonen and J. Popović, "Interoperability in Microgrids to Improve Energy Access: A Systematic Review," in *IEEE Access*, vol. 12, pp. 64267-64284, 2024, doi: 10.1109/ACCESS.2024.3396275

[8] K. Prabakar, A. Pratt, et al., “Site-specific evaluation of microgrid controller using controller and power-hardware-in-the-loop,” in *Proc. 2019 45th Annual Conference of the IEEE Industrial Electronics Society (IECON)*, pp. 6463–6468.

[9] IEEE Standard for Interconnection and Interoperability of Distributed Energy Resources with Associated Electric Power Systems Interfaces,” IEEE. doi: 10.1109/IEEESTD.2018.8332112.

[10] L. Abcede *et al*., "Interoperable, Inverter - Based Distributed Energy Resources Enable 100% Renewable and Resilient Utility Microgrids," *2025 IEEE PES Grid Edge Technologies Conference & Exposition (Grid Edge)*, San Diego, CA, USA, 2025, pp. 1-5, doi: 10.1109/GridEdge61154.2025.10887429.

[11] A. Pratt, K. Prabakar and M. Symko-Davies, "Power-Hardware-in-the-Loop Experiments of a Microgrid With a Grid-Forming Battery Inverter," *2025 IEEE PES General Meeting*, Austin, TX, USA, 2025.

APPENDIX A NREL Grid Resiliency With a 100% Renewable Microgrid: Hardware-in-the-Loop Tasks

APPENDIX B – NREL Full Scale Simulation Report: Transient Stability Study of Borrego Springs Microgrid With 100% Renewables

Grid Resiliency With a 100% Renewable Microgrid: Hardware-in-the-Loop Tasks

Abstract—The NREL team conducted hardware-in-the-loop (HIL) experiments to de-risk the field deployment of a battery inverter at the Sen Diego Gas & Electric Company Borrego Springs Microgrid that was upgraded with grid-forming (GFM) capability to serve as the island leader. We need power-hardware-in-the-loop (PHIL) interfaces for GFM inverters to enable simulations of seamless transitions between islanded and grid-connected operation. Such interfaces are particularly challenging when the inverters need to switch modes (i.e., between grid-following (GFL) and GFM as the microgrid transitions between grid-connected and islanded operation). This report presents the HIL experimental results from an HIL test bed for the Borrego Springs Microgrid that uses a PHIL interface with a power inductor that was previously developed for PHIL simulations of microgrids wherein the inverters need to switch modes (i.e., between GFL and GFM as the microgrid transitions between grid-connected and islanded operation). This interface is suitable for those who need a solution that uses a voltage-mode power amplifier. We present details on the interface and HIL simulation results of planned islanding, black start and load steps in islanded operation to show the effectiveness of the inverters in managing the voltage and frequency.

1 Introduction

The island leader role of the multimegawatt Borrego Springs Microgrid operated by San Diego Gas & Electric Company (SDG&E) in Borrego Springs, California, was transitioned to a grid-forming (GFM) battery inverter through hardware upgrades and a new microgrid controller.

The deployment of state-of-the-art distributed energy resources (DERs) and control strategies in utility grids and microgrids must be undertaken carefully with stepwise validation to mitigate risks of customer service disruptions. Hardware-in-the-loop (HIL) simulations can de-risk microgrid deployments and provide early insights by testing conditions not yet demonstrated during field operations [1][2]. SDG&E is employing HIL simulations of the Borrego Springs Microgrid at the National Renewable Energy Laboratory's (NREL's) Energy Systems Integration Facility (ESIF) to evaluate the frequency response behavior of the microgrid with an inverter-based resource (IBR) serving as island leader under practical operating conditions to build confidence that the microgrid can be formed by an IBR and will be stable. This report presents the results from HIL experiments of the SDG&E Borrego Springs Microgrid operating with up to 100% renewable generation. Section 2 provides an overview of the HIL test bed, Section 3 describes the HIL simulation results, and Section 4 concludes and discusses future work.

2 HIL Test Bed Setup

2.1 HIL Test Bed Overview

Figure 2 shows the HIL test bed at the ESIF. The setup expands upon an earlier test bed that was developed for the Borrego Springs Microgrid with diesel generators and grid-following (GFL) inverters [1] [3]. The distribution system is simulated in an RTDS Simulator[1] with the time step set to 95 microseconds. SDG&E provided the model to NREL in the RTDS proprietary simulation software format, RSCAD, and NREL made the necessary modifications to integrate it with the controller and power hardware.

The Borrego Springs community is served by three 12 kV distribution circuits that contain approximately 8.6 MW of nondispatchable, noncontrollable customer rooftop photovoltaic (PV) generation. A 26-MW

[1] https://www.rtds.com/

alternating current (MW_{ac}) PV plant is connected to the 69-kV bus, and a 6.3 MW_{ac} concentrating PV plant is connected to a 12-kV circuit. Presently, these two PV plants are unavailable during microgrid operations and therefore not included in the model.

The microgrid has historically used two 1.8-MW diesel generators as the voltage and frequency leaders in islanded mode [1], and two GFL utility-scale battery energy storage systems (BESS), rated at 1 MW/3 MWh (AES 2) and 0.5 MW/1.5 MWh (AES 1), respectively. SDG&E aims to operate the Borrego Springs Microgrid in islanded mode either without diesel generators (when the BESS can meet the net load) or with the generators in load-following mode (when their capacity is needed to meet the net load). To achieve this, the 1-MW BESS, AES 2, was upgraded with a GFM inverter that operates as the voltage and frequency leader when the microgrid is islanded and that is operated in GFL mode when the microgrid is connected to the grid. The 0.5-MW BESS inverter is always operated in GFL mode. The microgrid also has an ultracapacitor system, AES 3 (0.3 MW/30 s), that operates in GFL mode with a frequency-watt curve. The team implemented a PXiSE Energy Solutions microgrid controller to command the assets and provide a visual real-time status of the energy storage systems and other microgrid assets.

The power system model includes a simple representation of the transmission system; the substation transformers and load tap changers (LTCs); the microgrid (MG) switch; the three distribution feeders (Ckt 1, Ckt 2, and Ckt 3), all of which include rooftop PV systems; the two diesel generators, the GFL BESS, AES 1; and the ultracapacitor system, AES 3, on Ckt 2; and interfaces to the hardware. Two load tap changer (LTC) controllers, one capacitor bank controller, and the same microgrid controller that is deployed in the field are interfaced with the RTDS as controller-hardware-in-the-loop (CHIL).

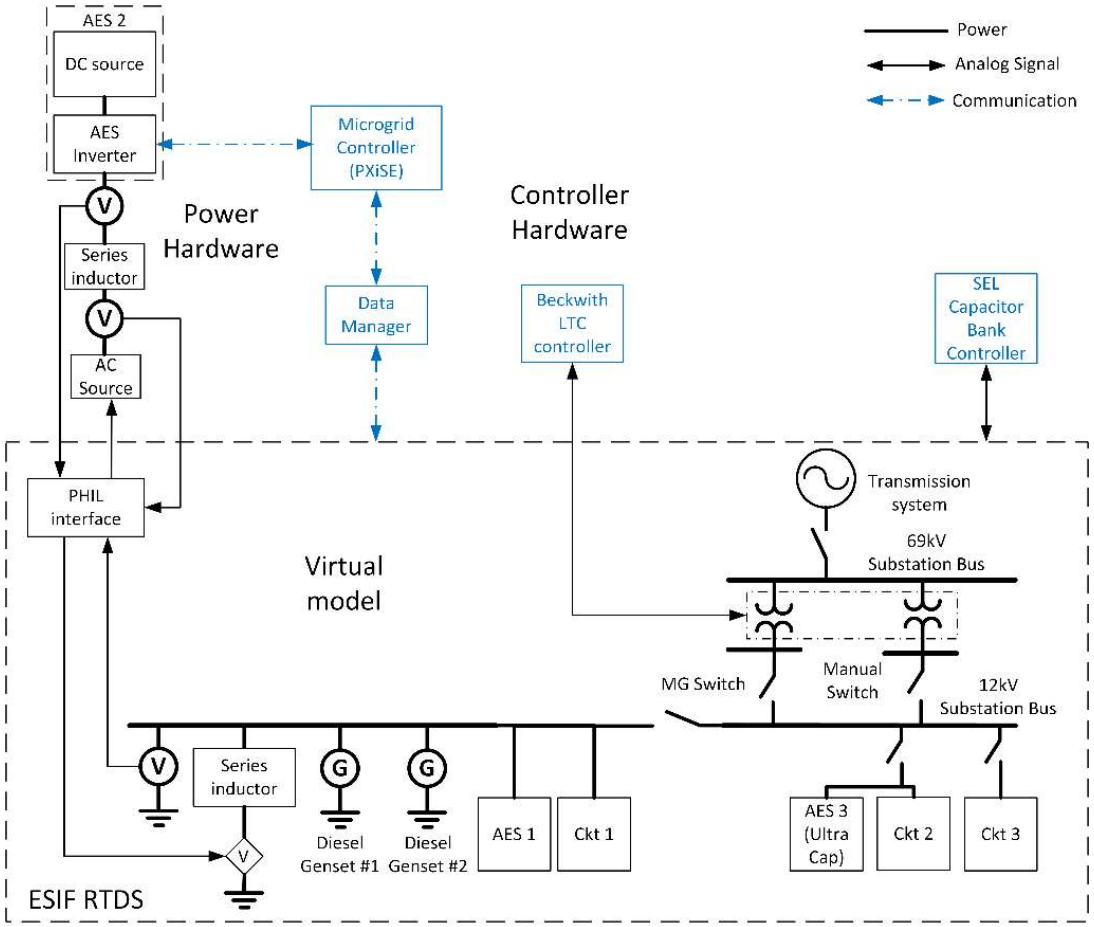

Figure 1. Diagram of the HIL test bed.

GFM inverter technology is rapidly advancing, and inverter performance is far from uniform across products, especially in how they respond to transitions between grid-connected and islanded operation. Therefore, we implemented AES 2 as PHIL using a GFM battery inverter from the same manufacturer and line of products as the inverters installed in the Borrego Springs Microgrid and with the same controls. It was interfaced with the RTDS through a controllable AC source in series with an inductor and connected to a controllable DC source that supplies DC power to the inverter, as described in [4].

Figure 3 shows the experimental setup in the ESIF. The inverter manufactured by CE+T between the AC source and inverter is not used in this setup. Two custom-built measurement boxes with voltage and current transducers are shown on the floor with oscilloscopes on top. One box also houses an SEL 751 feeder protection relay with synchronization capabilities to control the simulated microgrid switch. We set the allowable frequency, voltage amplitude, and phase differences to 1 Hz, 2V, and 8 degrees, respectively. The 100-kVA power inductor was manufactured to a specification of 1 mH by CTM Magnetics.

We used a Hitachi ABB PCS100 inverter; 100-kW Regatron TopCon TC.ACS voltage amplifiers for the AC source; and a NH Research 9300 controllable DC source that was set to a fixed DC voltage.

Figure 2. PHIL experimental setup with the inverter on the right (to the left of the large computer screens), the AC source in the center, and the power inductor on the left. Photo by NREL.

2.2 Power-Hardware-in-the-Loop Interface

HIL simulations can de-risk microgrid deployments, and they can test many conditions that are unsafe to test in the field [1]. Multiple HIL studies of more traditional microgrids with synchronous generators acting as the voltage and frequency leaders and that include inverters operating in GFL mode have been published [3]. GFM inverter performance is far from uniform across products, especially in how inverters respond to transitions between grid-connected and islanded operation. Therefore, it is valuable to include GFM inverters as PHIL simulations of microgrids. Because of the differences in GFM inverter controls and their behavior, it is also important to verify that the microgrid controller can manage the specific GFM inverter effectively, and therefore it is also recommended to include the actual microgrid controller in the HIL simulations. A PHIL interface is required between the GFM inverter and the power network model for both grid-connected and islanded operation and for transitions between the two. We first present the PHIL interface requirements to study microgrids with a GFM inverter acting as the voltage and frequency leader when the microgrid is islanded from the main grid. We considered only a single GFM inverter in this work, though we recognize that future work on multiple GFM inverters is warranted. We then present a PHIL interface that we developed and implemented in the ESIF and experimental results obtained with the PHIL interface and a simple power system model.

2.2.1 PHIL Interface Requirements

We require a PHIL interface that enables HIL experiments with a GFM inverter that operates in GFM mode when the microgrid is islanded and in GFL mode when the microgrid is connected to the grid, and that can transition between these two states. A standard PHIL interface that provides a voltage reference to the inverter hardware can be used for grid-connected operation with the inverter operating in GFL mode. Multiple such interfaces have been developed and extensively studied [5][6].

We recognize that there is a shift toward operating GFM inverters in GFM mode when they are connected to the grid [3], as a virtual synchronous generator (VSG), and that this would simplify the requirements on the PHIL interface [7], but there are real-world situations—as illustrated by the SDG&E project—in which GFM inverters are required to switch between GFM and GFL modes. The choice of which mode to operate GFM inverters in when grid-connected may be driven by inverter capabilities, microgrid controller capabilities, or by a utility's comfort level with GFM inverters.

In islanded mode, the GFM inverter acts as a voltage source because it is the voltage and frequency leader, and the HIL interface needs to represent the net load of the microgrid (i.e., it should represent a current source to the inverter). A method has been proposed for a PHIL interface for GFM inverters [8] that uses a simulated GFM inverter—connected at the same point of common coupling (PCC) as the hardware inverter—in the real-time simulator that behaves as a controllable voltage source, called a "virtual GFM." The authors state, "This can also be seen as moving one GFM inverter of a large system under test into the simulation side." This approach simplifies the requirements on the HIL interface because it presents a voltage reference to the inverter hardware; however, this approach is inadequate for the case that we are considering wherein there are no other GFM inverters in the microgrid.

One way to address this challenge is to use a power amplifier that can act as a controllable current source. This approach has been demonstrated [9] for islanded operation and a transition to grid-connected operation when the GFM inverter operates in GFM mode during grid-connected operation. If the inverter switches between GFM and GFL modes as the microgrid transitions between islanded and grid-connected operation, then the PHIL interface needs to switch from representing a voltage source in grid-connected mode to representing a current source in islanded mode through the transition.

The NREL team developed two PHIL interface methods to meet the requirements [10]. The first method uses two power amplifiers: one acting as a voltage amplifier and one as a current amplifier. Because not many laboratories have current amplifiers [8][4], for the second method we expanded upon an approach [4] that uses a voltage amplifier combined with a power inductor to perform PHIL simulations with a GFM inverter operating in islanded mode. We showed that the second method can also be used for grid-connected operation and for transitions between islanded and grid-connected operation. The two-amplifier method suffers from short delays when switching between the amplifiers, and we therefore chose to implement the voltage amplifier method for the Borrego Springs Microgrid HIL setup.

We first demonstrated successful implementation of the interface through PHIL experiments using a simple Thevenin equivalent of a power system and an aggregated microgrid load. In Section 3, we present experimental results with the hardware inverter integrated with the Borrego Springs Microgrid power system model.

2.2.2 Voltage Amplifier PHIL Interface

We extended the approach previously proposed in [4]—which interfaces a voltage amplifier to a GFM inverter through a power inductor in islanded operation—to handle operation in grid-connected mode as well as transitions between grid-connected and islanded operation.

The experimental setup we used to demonstrate the interface is shown in Figure 3. In islanded operation, S_{MG}, is open, and the inverter mode is set to isochronous GFM. The inverter sets the voltage, v_i, and this is fed back to a controlled voltage source, v_s, in the simulation through a potential transformer with a gain k_v, an ADC, H_{ADC}, a gain $1/k_v$, and a unity-gain low-pass filter, $G_{LP\,F}$.

We used a regulated voltage amplifier with a proportional integral derivative (PID) compensator, but a

higher accuracy than that provided by the amplifier is required. Therefore, we added regulation using the same methodology as that used for grid-connected operation as described in [5]. This approach ensures that the voltage amplifier output voltage, v_G, matches the simulated voltage, v_B. A gain of k_{vm} is applied to both v_B and the feedback path from v_G. The PHIL interface needs to ensure that the phase relationship of v_s to v_B is the same as that of v_i to v_G. This requires compensating for the calculation delay incurred by the simulator between the input signal to the voltage source, v_s, and v_B, and this was determined to be equal to 6 time steps of 95 microseconds, or a total of 12 degrees. We added a 12-degree phase lead compensator, G_{lead}, to achieve compensation for the calculation delay following [4]. By matching the impedance in the simulation, Z_s, to the impedance in the experimental setup, Z_h—which includes the physical inductor, the cables, and the breaker, *BRK*—the current in the simulation, i_s, matches the current in the hardware, io [4]. The simulated current, is, can be scaled up by scaling down the impedance in the simulation, Z_s, by the current scale-up factor, K.

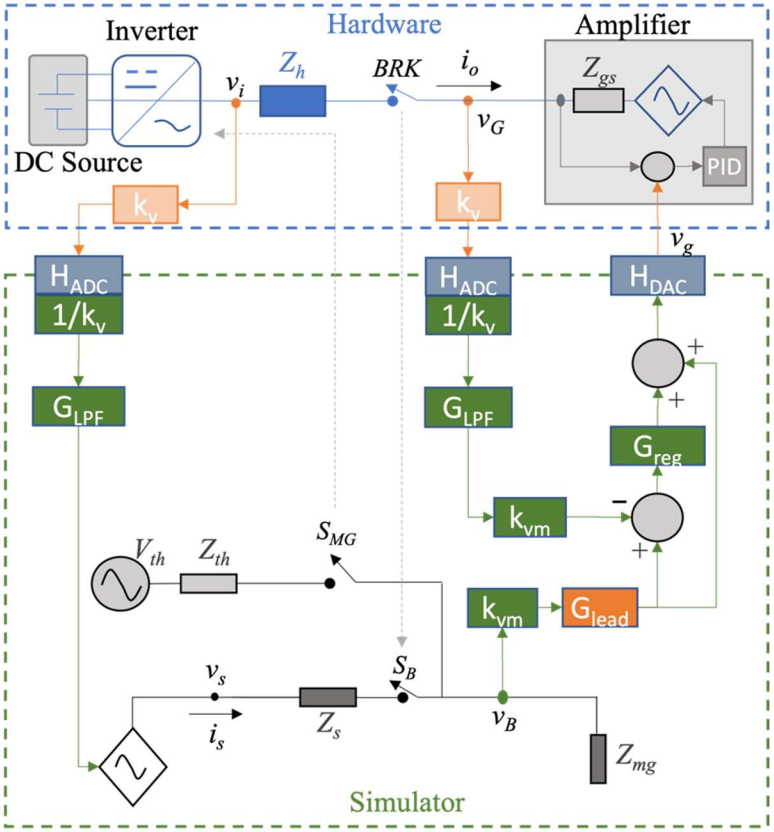

Figure 3. Experimental setup with voltage amplifier and inductor for islanded and grid-connected operation.

In grid-connected operation, S_{MG} is closed, and the inverter operates in GFL mode. Instead of feeding back current, as is typical for PHIL with a GFL inverter, we feed back voltage, v_B, to the simulation, and that voltage results in a scaled version of the current (and therefore power) in the hardware, using the same reasoning as in islanded mode for matching the currents.

We integrated the hardware inverter with the simple power system model using the voltage amplifier method.

2.2.3 Power Inductor Value Calculation

The impedance, $\boldsymbol{Z_h}$, is calculated using measurements of the voltages at the output of the inverter, $\boldsymbol{V_i}$, and at the output of the amplifier, $\boldsymbol{V_G}$, and the current, $\boldsymbol{I_o}$, through the power inductor, as follows:

$\boldsymbol{Z_h} = (\boldsymbol{V_i} - \boldsymbol{V_G})/\boldsymbol{I_o} = \Delta \boldsymbol{V}/\boldsymbol{I_o}$.

The vector diagram in Figure 4 shows the voltages and current with their respective phase relationships. We used a Yokogawa WT1806E power analyzer to obtain the per-phase amplitudes of the voltages and current and the phase angle between $\boldsymbol{V_i}$ and $\boldsymbol{I_o}$, denoted as γ, and between $\boldsymbol{V_G}$ and $\boldsymbol{I_o}$, denoted as φ. We then calculated $\boldsymbol{Z_h}$ for each phase, through the following steps:

First, we assume that:

- $\boldsymbol{V_G} = V_G + j0$.

Then we calculate:

- $\delta = \gamma - \varphi$.

We use those values to calculate:

- $\boldsymbol{Vi} = Vi.\cos(\delta) + \mathrm{j}\ Vi.\sin(\delta)$ and
- $\boldsymbol{I_o} = I_o.\cos(\varphi) + \mathrm{j}\ I_o.\sin(\varphi)$.

The voltage drop across inductor can be expressed as:

- $\Delta \boldsymbol{V} = \boldsymbol{V_i} - \boldsymbol{V_G} = Vi.\cos(\delta) + \mathrm{j}\ Vi.\sin(\delta) - V_G = (Vi.\cos(\delta) - V_G) + \mathrm{j}Vi.\sin(\delta)$.

The amplitude of the voltage drop across the inductor, ΔV, is:

- $\Delta V = \mathrm{sqrt}((V_i.\cos(\delta) - V_G)^2 + (V_i.\sin(\delta)^2))$.

From inspection of the vector diagram the phase angle of the voltage drop across the inductor, θ, is:

- $\theta = \arctan(V_i.\sin(\delta) \div (V_i.\cos(\delta) - V_G))$.

The amplitude of the impedance $\boldsymbol{Z_h}$ is:

- $Z_h = \Delta V / I_o$.

The phase angle of $\boldsymbol{Z_h}$ is:

- $(\theta - \varphi)$.

It follows that:

- $\boldsymbol{Z_h} = \Delta V / I_o.\cos(\theta - \varphi) + \mathrm{j}\ \Delta V / I_o.\sin(\theta - \varphi)$.

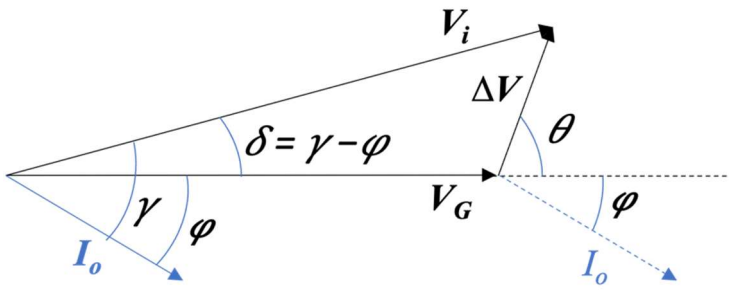

Figure 4. Vector diagram for inductor value calculation.

The simulated current, i_s, can be scaled up relative to the hardware current, i_o, by scaling down the impedance in the simulation, $\boldsymbol{Z_s}$, by the current scale-up factor, $K = i_s / i_o$, (i.e., $\boldsymbol{Z_s} = \boldsymbol{Z_h}/K$).

2.2.4 Experimental Results with Voltage Amplifier PHIL Interface

We demonstrated the proposed voltage amplifier PHIL interface with experimental results using an ABB PCS100 GFM fuel cell [2] inverter[2] rated at 100 kW. We scaled up this 100-kW hardware inverter to 1 MW by scaling down Z_s by a factor of 10. We use a 50-kW Regatron TopCon TC.ACS for the voltage amplifier for the experiments presented. For higher-power experiments, more Regatron amplifiers can be paralleled. The inverter is connected to a controllable DC source, a Webasto AV-900, that is set to a fixed DC voltage. We used an RTDS digital real-time simulator with the time step set to 95 microseconds. The 100-kVA power inductor was manufactured to a specification of 1 mH by CTM Magnetics. We calculated the total impedance, Z_h, of the physical inductor, cables, and breaker from measurements at medium power, as 1.2 mH with a resistance of 40 mohm, and we scaled this value down by a factor of 10 to use for Z_s.

Figure 5 shows the experimental setup in the ESIF, with the inverter in the back on the left, the amplifier in the front on the right, and the power inductor between them. The breaker is in a box mounted on a rack just behind the inductor.

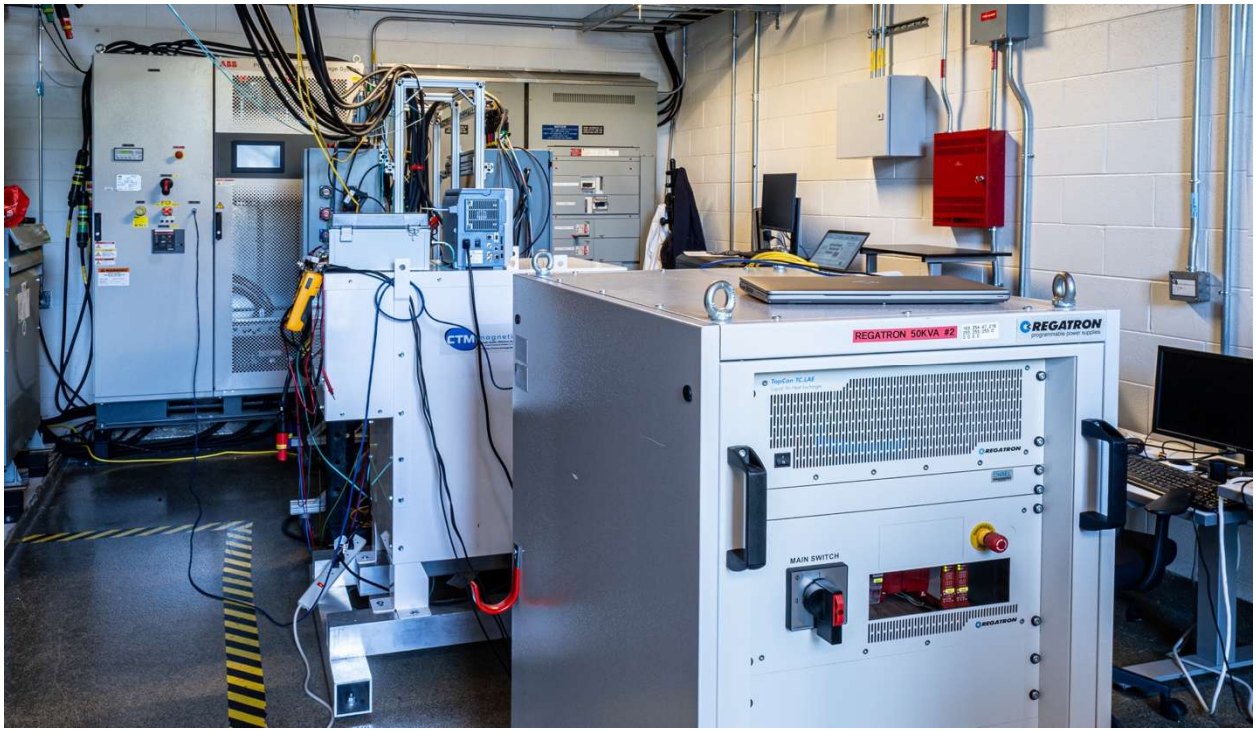

Figure 5. Experimental setup of voltage amplifier interface method. The inverter is in the back on the left, the amplifier is in the front on the right, and the power inductor is between them. Photo by NREL.

We used an SEL 751 feeder protection relay with synchronization capabilities for the breaker, *BRK*, and we set the allowable frequency, voltage amplitude, and phase differences to 1 Hz, 2 V, and 8 degrees,

[2] The fuel cell inverter used is from the same manufacturer and the same inverter series as the inverter used in Borrego Springs Battery Energy Storage System (i.e., the same model but with a lower DC input voltage range). We used it for evaluating the power-hardware-in-the-loop interface because it can accept a digital signal to change inverter modes between grid-forming and grid-following based on the microgrid switch status, as shown in Figure 3Figure 3. The battery inverter used in the Borrego Springs setup needs a signal from the PXiSE microgrid controller to change the inverter mode, which can incur a communications delay of a couple of hundred milliseconds.

respectively. We use the BRK status as an input to control the status of the S_B switch in the RSCAD model.

We started the experiment in grid-connected mode, and the sequence of operation is as follows:

1. Start RSCAD model with S_{MG} closed. This sets v_B.
2. Turn the amplifier on. This sets vv_G.
3. Turn the inverter on in GFM mode. This sets v_s.
4. Start synchronization for *BRK*, adjusting the inverter frequency as needed. When *BRK* closes, it closes S_B in the RSCAD model.

To switch to islanded mode, we open S_{MG}, and this switch status is provided as an input bit to the inverter to change from GFL to GFM mode. To switch back to grid-connected mode, we close S_{MG}, and this changes the inverter mode from GFM to GFL.

In all figures in this section, the bottom three traces show a zoomed-in view of the top three traces during the time period indicated by the white box. The top trace of three is the current measured at the power amplifier, the second trace from the top is the power amplifier voltage, and the bottom trace is the inverter voltage.

Figure 6 shows an inverter dispatch step change in grid-connected mode. The inverter is initially dispatched to provide 5 kW, and then the set point is increased to 30 kW. This is scaled up by a factor of 10 so that the simulated voltage source v_s changes from delivering 50 kW to 300 kW. The inverter has a ramp rate limit of 1 kW/second so the current ramps up over approximately 25 seconds (s).

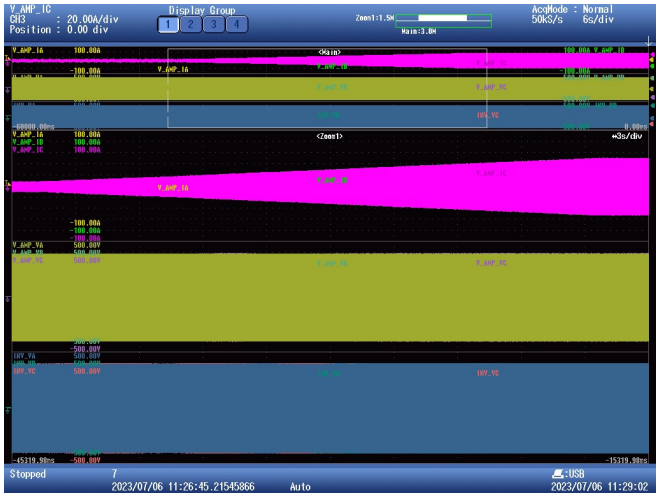

Figure 6. Scope capture of the inverter dispatch change in grid-connected operation showing the current (top), amplifier voltage (second from top), and inverter voltage (bottom).

A transition from grid-connected to islanded operation is shown in Figure 7, with the load in the RSCAD model, Z_{MG}, set to draw 100 kW at nominal voltage. This transition results in about 10 kW provided by the hardware inverter, and the inverter was set to dispatch 2 kW when in GFL mode, so the inverter current must increase suddenly when the microgrid switch, S_{MG}, is opened. This experiment simulates an unplanned islanding operation wherein the PCC current is not reduced to near zero before islanding. The inverter regulates the voltage in islanded operation and the voltages show a small dip after islanding and then they are regulated to the voltage set point.

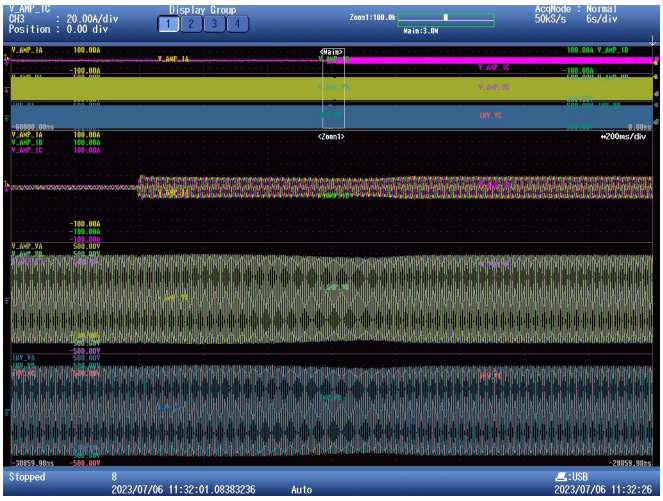

Figure 7. Scope capture of the transition from grid-connected to islanded operation showing the current (top), amplifier voltage (second from top), and inverter voltage (bottom).

The microgrid load, Z_{MG}, is increased from 50 kW to 300 kW in islanded operation, shown in Figure 8. The inverter current follows the load because it is the voltage and frequency leader.

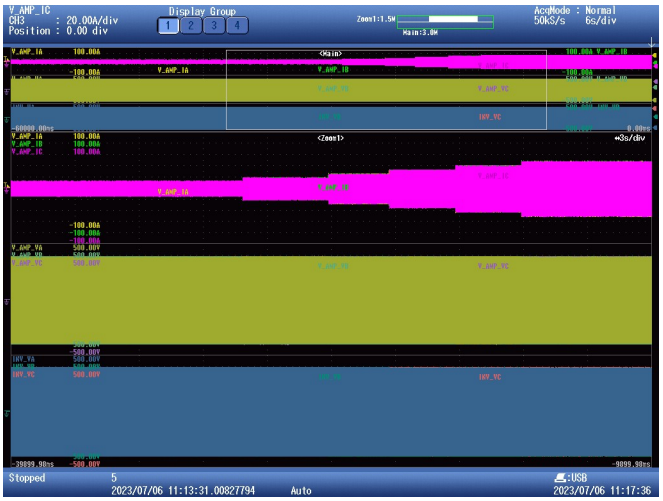

Figure 8. Scope capture of the load step change in islanded operation showing the current (top), amplifier voltage (second from top), and inverter voltage (bottom).

Figure 9 shows resynchronization for a transition from islanded to grid-connected operation with a 100-kW microgrid load, Z_{MG}, and the inverter set to dispatch 2 kW.

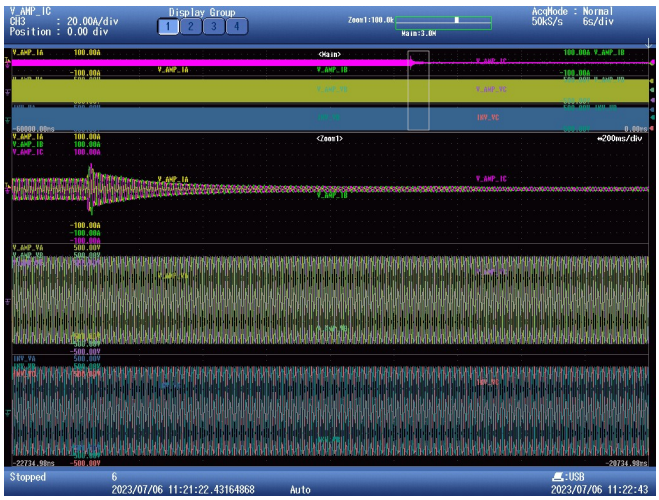

Figure 9. Scope capture of transition from islanded to grid-connected operation showing the current (top), amplifier voltage (second from top), and inverter voltage (bottom).

3 Borrego Springs Hardware-in-the-Loop Simulation Results

The main purpose of the HIL simulation was to evaluate the effectiveness of the inverters in limiting the frequency variability during planned islanding under various operating conditions to improve the likelihood of forming a stable microgrid with only IBRs—i.e., in a low-inertia environment. This section presents results from HIL simulations of planned islanding, expanding upon those presented in [11], as well as results from black start and load steps in islanded mode. First, we present results on the accuracy of the PHIL interface using the HIL setup for Borrego Springs, and then results from an experiment that we performed to evaluate the frequency response of the inverters.

3.1 PHIL Interface Accuracy Results

We evaluated the steady state accuracy of the PHIL interface for the Borrego Springs HIL setup using the simple microgrid model shown in Figure 3. We took measurements at several power levels and calculated the average inductance and resistance values of $\boldsymbol{Z_h}$ following the procedure described in Section 2.2.3. The final values we used for $\boldsymbol{Z_h}$ are 1.3 mH and 75 mohm, based on experimental testing.

We need to scale up the 88-kW hardware inverter to represent a 1-MW inverter to match the power rating of AES 2, so our scale-up factor, K, is 11.36, and $\boldsymbol{Z_s} = \boldsymbol{Z_h}/K$.

Table 1 shows accuracy results for active power, where P_i is the output power of the hardware inverter and P_{sim} is the output power of the equivalent voltage source representing the inverter in the simulation. We achieved an acceptable error at medium to high power, but accuracy deteriorated at lower power, and this warrants future work, such as introducing adaptive gains.

Table 1. Steady-state accuracy for active power

P_i [kW]	Q_i [kVar]	P_i [%]*	P_{sim}/K	Error [kW]	Error [%]**
7.1	2.3	8	4.78	2.32	33
14.7	2.9	17	13.38	1.32	9
22.4	3.96	25	21.92	0.48	2
30.4	5.49	35	30.11	0.29	1
38.79	7.28	44	38.24	0.55	1
47.36	9.47	54	46.16	1.20	3

* Percentage of hardware inverter power rating ** Percentage of *Pi*

We evaluated the dynamic accuracy of the PHIL interface for the Borrego Springs HIL setup using data from a planned islanding experiment that used the Borrego Springs Microgrid power system model. The dynamic accuracy is good, as shown in Figure 5 that compares the scaled hardware and simulated GFM inverter output power for phase A. Similar performance was observed for the other phases.

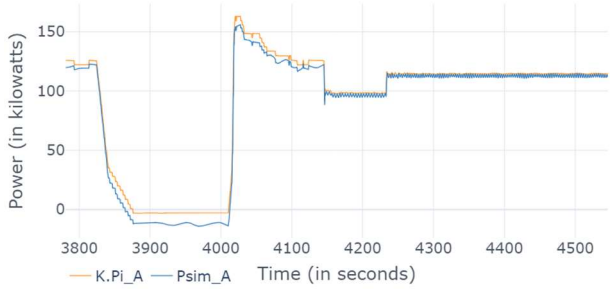

Figure 10. Comparison of scaled hardware and simulated inverter output active power for phase A under dynamic conditions.

3.2 Frequency Step Change With Ultracapacitor Results

First, we aimed to verify that the AES 3 ultracapacitor model performs as expected. We ran a simulation with the microgrid in grid-connected operation without AES 2 (i.e., a software simulation only). We used constant loads for this simulation.

The RSCAD model for the ultracapacitor, AES 3, allows for the selection of one of several modes and we used the Frequency Regulation Mode setting for active power in RSCAD.

AES 1 is always operated in GFL mode, and AES 2 is operated in GFL mode when connected to the grid and in GFM mode with a frequency droop setting of 0.2% and a voltage droop setting of 1% when islanded. When online, AES 3, the ultracapacitor, operates in GFL mode with a frequency envelope with a deadband of +/- 0.06 Hz and maximum output power of 200 kW at 59.408 Hz and 60.592 Hz, as shown in Figure 11. (Note: UCAP = ultracapacitor)

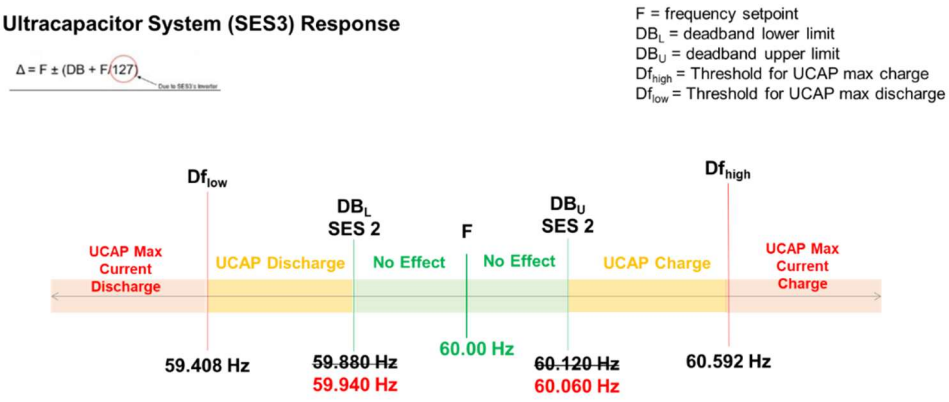

Figure 11. AES 3 frequency envelope settings.

The project team also published results [12] with a frequency droop setting of 2% for AES 2 and a frequency-watt curve deadband of either +/- 0.3 Hz or +/- 0.2 Hz for AES 3. The state of charge (SOC) of the ultracapacitor is maintained near 90% when it is not actively responding to an underfrequency or overfrequency condition. Further, the RSCAD model of AES 3 used in [12] used frequency measured by a phase-locked loop (PLL) followed by a filter with a time constant of 0.01 s. This technique filtered out fast frequency transients, so AES 3 did not respond. We therefore replaced the frequency input to the ultracapacitor model with the frequency captured from a simulated phasor measurement unit (PMU) to speed up the ultracapacitor response.

We then adjusted the grid frequency to 59.3 Hz in a step change. Figure 12 shows AES 3 power output in the top trace and the input frequency to AES 3 in the bottom trace. AES 3 reaches its maximum output power of 200 kW in 190 msec with the PMU frequency as an input to the ultracapacitor model. We performed the same experiment with the filtered PLL frequency input, and the ultracapacitor reached 200 kW output in 280 msec, so the response is faster with the PMU frequency input.

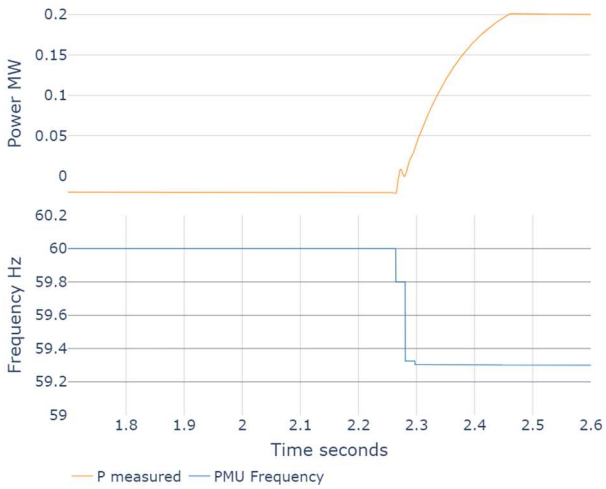

Figure 12. Ultracapacitor output power (top) and frequency used as input to ultracapacitor (bottom).

3.3 Planned Islanding Results

We performed planned islanding simulations for different load conditions, including heavy and light load during daytime and nighttime. The community of Borrego Springs has three distribution circuits. In our experiment, part of Ckt 2 was islanded based on the capacity of the available generation sources. We used varying load and PV profiles, with a resolution of 1 minute (min), based on historical data on July 29, 2019. Only net load data were available, so we estimated the PV output power based on solar insolation data from NREL's National Solar Radiation Database (https://nsrdb.nrel.gov/) and used that to estimate the native load. The estimated total native load and rooftop PV output power for Ckt 2 is shown in Figure 13. We normalized these data and applied the same profile to each load and rooftop PV system on Ckt 2 in the RSCAD model.

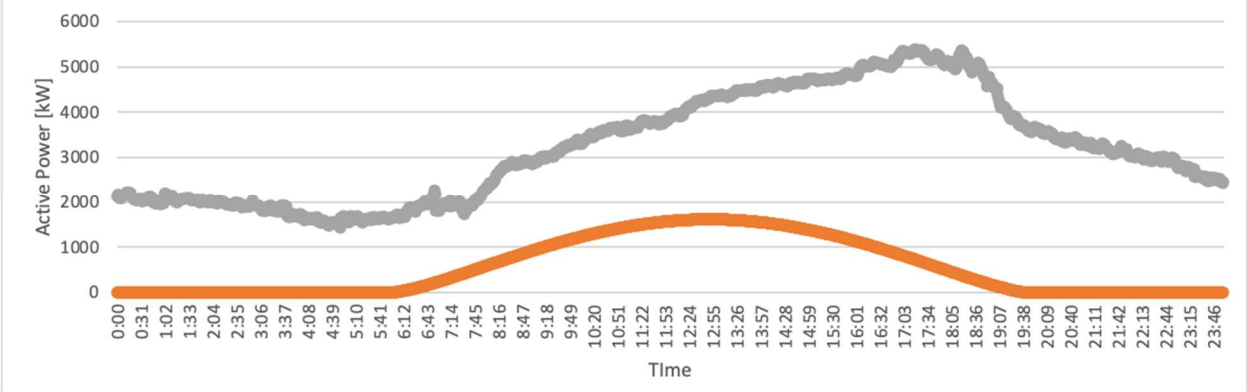

Figure 13. Estimated total native load (grey) and rooftop PV (orange) output power for Ckt 2 on July 29, 2019.

Table 2 lists the scenarios that were simulated for planned islanding. The diesel generators were offline for the first five scenarios and online for the last five. We used data from 1–2 a.m. for night load, 8–9 a.m. for light load, and 5–6 p.m. for heavy load. We also varied whether the ultracapacitor system, AES 3, is online or not.

Table 2. Experimental scenarios for planned islanding

Loading	**AES 3**	**Diesel Generators**	**Other**
Night	Offline	Offline	
Night	Online	Offline	
Light	Offline	Offline	
Light	Online	Offline	
Light	Online	Offline	Cloudy solar
Night	Offline	Online	
Light	Offline	Online	
Heavy	Offline	Online	
Heavy	Online	Online	
Heavy	Online	Online	Load step

The simulations were run for at least 3 min of operation after islanding to confirm the stability of the island. AES 1 is always operated in GFL mode, and AES 2 is operated in GFL mode when grid-connected and in GFM mode with a frequency droop setting of 0.2% and a voltage droop setting of 1% when islanded. AES 3 operates in GFL mode with a frequency-watt curve. It maintains the SOC of the ultracapacitors near 90% when it is not actively responding to an underfrequency or overfrequency condition. The diesel generators are used only in heavy load scenarios, in GFL mode, when the battery resources do not have adequate capacity.

At the start of the islanding process, the microgrid controller (MGC) dispatches the GFM inverter, AES 2, to charge at about 50 kW, and the GFL inverter, AES 1, is dispatched at zero output. At the start of the zero-power flow step in the planned islanding process of the MGC, the grid-following BESS, AES 1, is dispatched at its rated power of 500 kW and the remaining load is carried by the grid-forming BESS, AES 2, up to half of its rated power, which is the maximum allowed by the MGC during a planned islanding scenario. Once the power flow through the microgrid switch is less than +/- 50 kW, the MGC will allow the operator to island the microgrid.

3.3.1 Planned Islanding with Diesel Generators Offline

3.3.1.1 Night Load

We successfully islanded with and without the ultracapacitor, AES 3, under night loading conditions. We used data from 1–2 a.m. for night loading conditions. There is no PV generation and the load of the energized section of the feeder is approximately 600 kW.

3.3.1.1.1 Night Load Without Ultracapacitor

The output power, as recorded by three-phase power meters in RSCAD, of the two BESS, AES 1 and AES 2, and the power flow through the two breakers feeding the 12-kV bus, the microgrid (MG) switch and the manual switch, are shown in Figure 14 for planned islanding without the ultracapacitor under night loading conditions.

At the start of the islanding process of the microgrid controller, at ~2,500 s, the GFM inverter, AES 2, is dispatched to charge at about 50 kW, and the GFL inverter, AES 1, is dispatched at zero output. At the start of the zero-power flow step in the planned islanding process, at ~2,700 s, the grid-following BESS, AES 1, is dispatched at its rated power of 500 kW and the remaining load of ~120 kW is carried by the grid-forming BESS, AES 2. The manual switch is opened at ~2,880 s and islanding occurs by opening the microgrid switch at ~2,900 s. We ran the experiment for about 3 min (200 s) after islanding to ensure that a stable island was formed.

Figure 14. Inverter output powers and the power flow through the breakers feeding the 12-kV bus during planned islanding without the ultracapacitor under night loading conditions.

Figure 15 shows planned islanding under night loading conditions without the ultracapacitor over about 3 min, on the left, and over about 4 s, on the right. The microgrid frequency, captured from a simulated phasor measurement unit (PMU) in RSCAD, is shown at the top. It starts at 60 Hz and initially rises and then drops to 59.99 Hz because frequency droop is set to 0.2% for AES 2. The initial increase in frequency is due to a delay of about 200 msec for AES 2 to change modes from GFL to GFM (recall that the inverter mode for AES 2 switches from GFL to GFM when the microgrid is islanded). The increase in frequency is very small in this case, but in general, reducing this delay could improve the transient response, e.g., by lowering the overshoot.

The output power of the two BESS, AES 1 and AES 2, and the power flow through the microgrid switch are shown in the center. The power flow through the microgrid switch is very close to zero at islanding. The GFL inverter, AES 1, output power shows a brief transient. The inverter mode for AES 2 switches from GFL to GFM when the microgrid is islanded, and its output power adjusts to regulate the microgrid voltage and frequency. The microgrid voltage, drops from 1.02 p.u. when grid-connected to 0.985 p.u. when islanded.

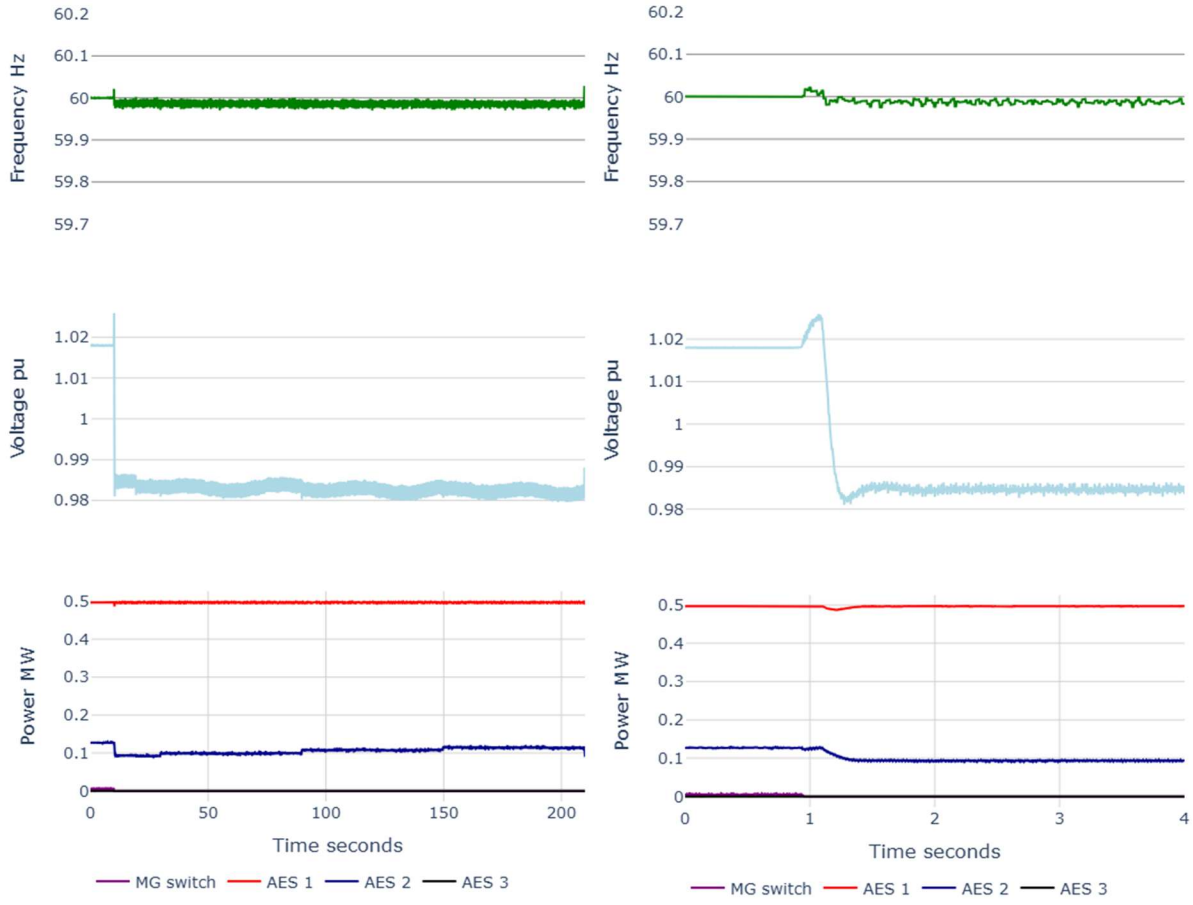

Figure 15. The microgrid frequency (top); microgrid voltage (center); and inverter output powers and the power flow through the microgrid switch (bottom) during planned islanding without the ultracapacitor under night loading conditions for about 3 min (left) and about 4 s (right).

3.3.1.1.2 Night Load With Ultracapacitor

The frequency does not vary much when islanding because of the zero-power flow condition that is established prior to opening the microgrid switch, and the light loading of AES 2. The ultracapacitor therefore does not respond during islanding.

Figure 16 shows a planned islanding event with the ultracapacitor, AES 3. The top subplot shows the microgrid frequency and the bottom subplot shows the microgrid voltage. The center subplot shows the output power for the inverters (AES 1, AES 2, AES 3) and the power flow through the microgrid switch. The microgrid controller reduces the power flow through the microgrid switch to near zero before opening it. It dispatches the GFL inverter AES 1 at its full power rating (500 kW), and it dispatches AES 2, which operates in GFL mode while grid-connected, to provide the rest of the net load (~160 kW) so that the power flow through the microgrid isolation switch is near zero. Note that, even though this and the previous experiment, described in Section 3.3.1.1.1, were both performed under night loading conditions, and AES 1 is dispatched at 500 kW in both cases, the output power of AES 2 is not the same because the timing of the islanding cannot be controlled exactly, so it can occur at any point during the night load profile.

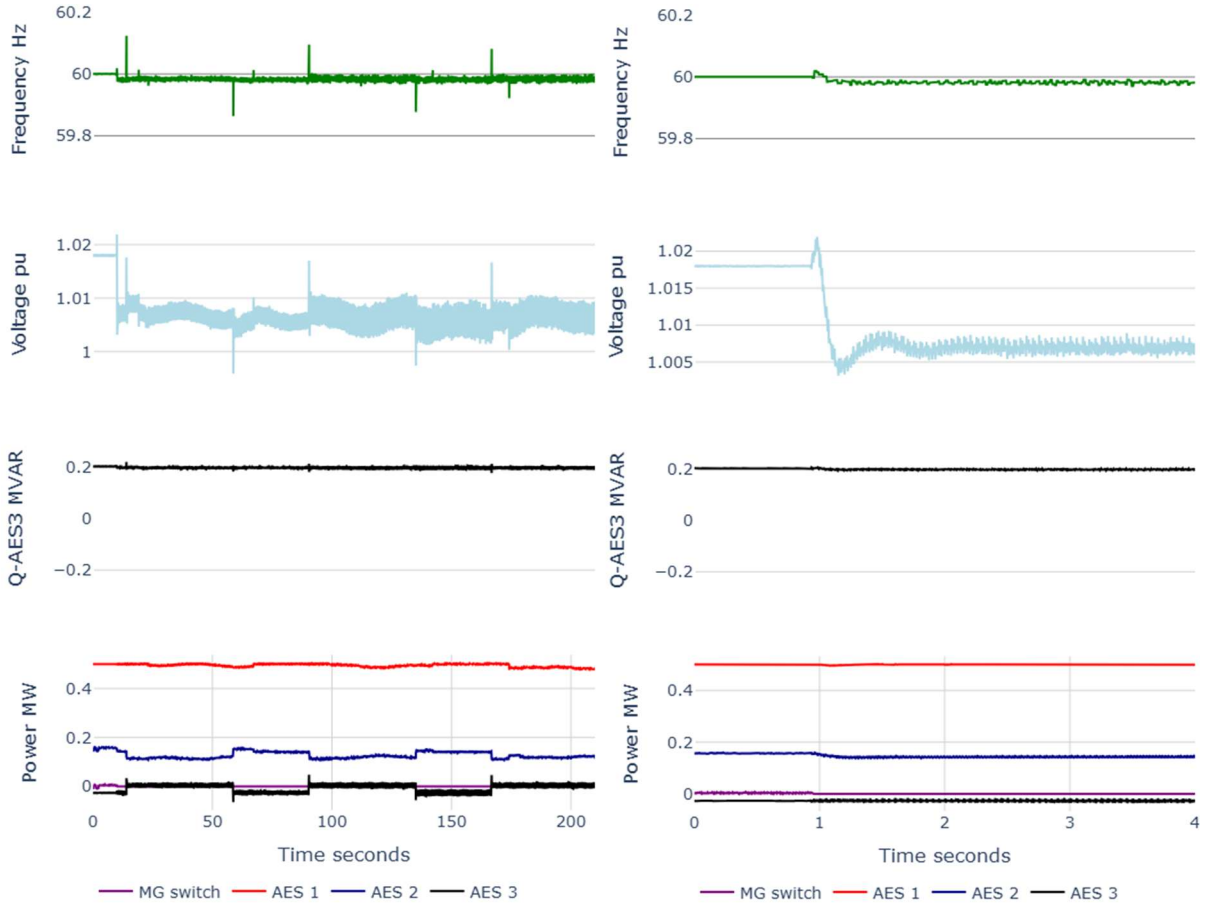

Figure 16. The microgrid frequency (top); microgrid voltage (second from top); reactive output power of the ultracapacitor (second from bottom); and inverter output powers and the power flow through the microgrid switch during planned islanding with the ultracapacitor under night loading conditions for about 3 min (left) and about 4 s (right).

AES 3 periodically charges (at about 20 kW) to maintain its target SOC, then its power drops to zero after it reaches its target SOC. For this experiment, it is charging at 20 kW when the microgrid is islanded. The power flow through the microgrid switch is close to zero at islanding. AES 1 output power shows a brief transient. The inverter mode for AES 2 switches from GFL to GFM when the microgrid is islanded, and its output power adjusts to regulate the microgrid voltage and frequency. The frequency initially rises, due to the delay in mode change described in Section 3.3.1.1.1 and then drops to 59.98 Hz because frequency droop

is set to 0.2% for AES 2.

The microgrid voltage, drops from 1.02 per unit (p.u.) when grid-connected to just below 1.01 p.u. when islanded. The voltage is higher during islanded operation than in the scenario without the ultracapacitor and we were not able to determine the exact mechanism that results in the voltage difference. When we run experiments without the ultracapacitor, we open a switch in the RSCAD model between the ultracapacitor model and the network model. We observed that when we close that switch and keep the ultracapacitor in idel mode, we still see higher voltages, so we think that the higher voltages are due to interactions between the ultracapacitor model in RSCAD and the rest of the system. In addition, the ultracapacitor provides 200 kVar of reactive power when it is online, as shown in Figure 16 which was unexpected. We think that the ultracapacitor reactive power control mode was inadvertently set to voltage regulation rather than to idle.

3.3.1.2 Light Load

We successfully islanded with and without the ultracapacitor, AES 3, under light loading conditions. We used data from 8–9 a.m. for light loading conditions. The net load of the energized section of the feeder is approximately 600 kW.

3.3.1.2.1 Light Load Without Ultracapacitor

Figure 17 shows results from planned islanding without the ultracapacitor at light load. The power flow through the microgrid switch is very close to zero at islanding. The GFL inverter, AES 1, output power shows a brief transient. The inverter mode for AES 2 switches from GFL to GFM when the microgrid is islanded, and its output power adjusts to regulate the microgrid voltage and frequency. The frequency starts at 60 Hz and drops to a low of 59.94 Hz and then stabilizes within 200 msec at 59.99 Hz because of frequency droop for AES 2. The voltage drops from 1.02 p.u. when grid-connected to 0.985 p.u. when islanded, because of voltage droop for AES 2.

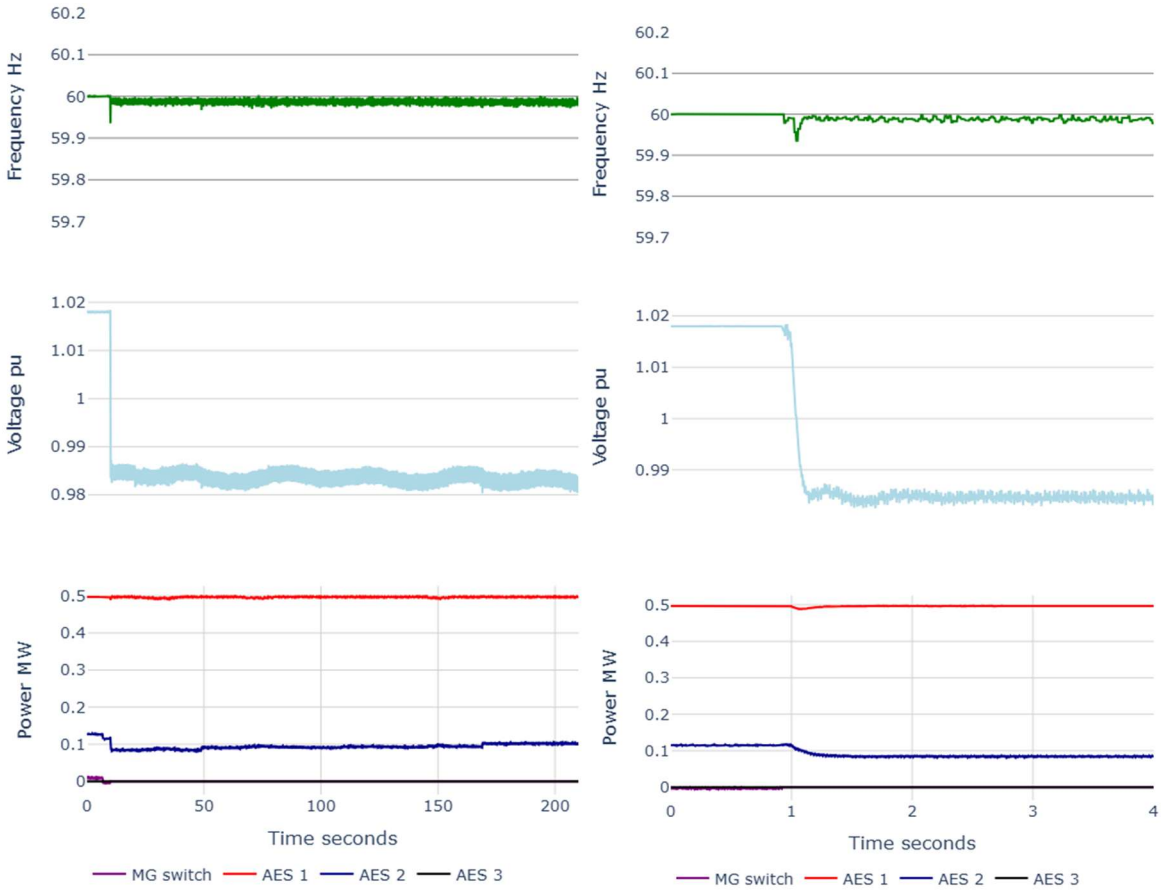

Figure 17. The microgrid frequency (top); microgrid voltage (center); and inverter output powers and the power flow through the microgrid switch during planned islanding without the ultracapacitor under light loading conditions for about 3 min (left) and about 4 s (right).

3.3.1.2.2 Light Load With Ultracapacitor

Figure 18 shows a planned islanding event with the ultracapacitor, AES 3. The microgrid controller reduces the power flow through the microgrid switch to near zero before opening the microgrid isolation switch. It dispatches GFL inverter AES 1 at its full power rating (500 kW), and it dispatches AES 2, which operates in GFL mode while grid-connected, to provide the rest of the net load (150 kW) so that the power flow through the microgrid isolation switch is near zero.

AES 3 periodically charges (at about 20 kW) to maintain its target SOC, then its power drops to zero after it reaches its target SOC. For this experiment, it is charging at 20 kW when the microgrid is islanded. The power flow through the microgrid switch is close to zero at islanding (about 40 kW). AES 1 output power shows a brief transient. The inverter mode for AES 2 switches from GFL to GFM when the microgrid is islanded, and its output power adjusts to regulate the microgrid voltage and frequency. The voltage drops from 1.02 p.u. when grid-connected to a low of 0.965 p.u. when islanded and then it settles at 1.005 p.u. because of voltage droop for AES 2. The frequency drops to 59.89 Hz after islanding and then settles at 59.98 Hz.

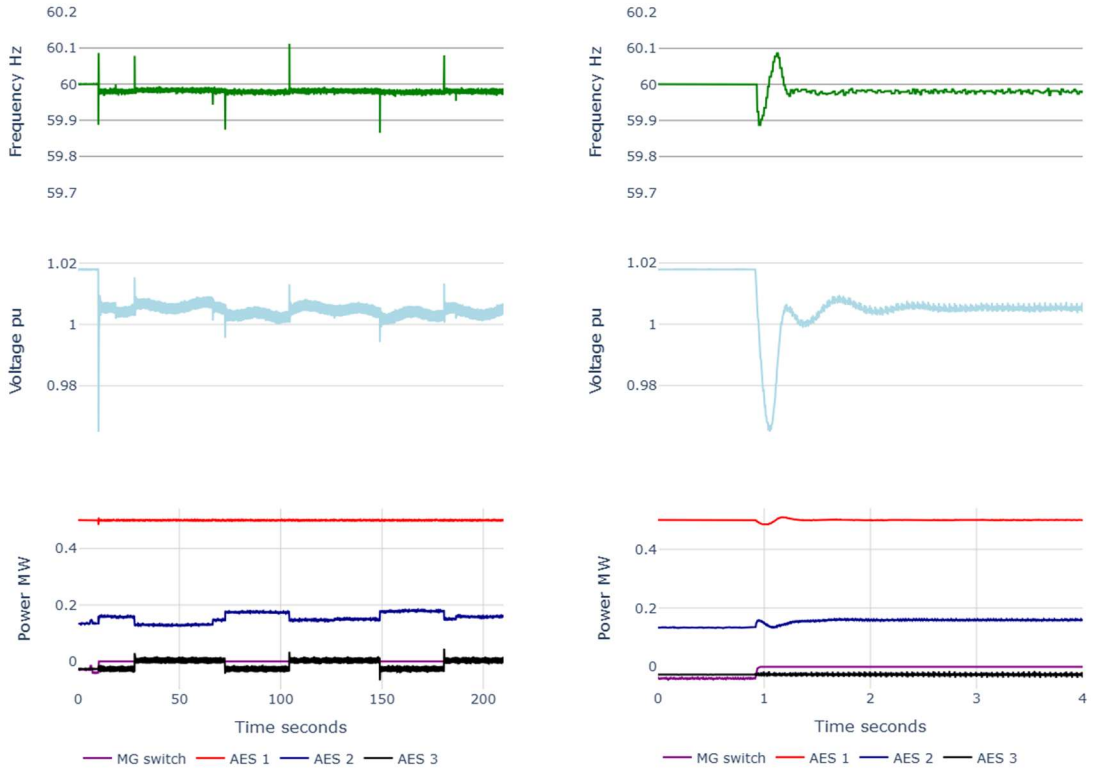

Figure 18. The microgrid frequency (top); microgrid voltage (center); and inverter output powers and the power flow through the microgrid switch during planned islanding with the ultracapacitor under light loading conditions for about 3 min (left) and about 4 s (right).

We expected AES 3 to respond to a frequency drop to 59.89 Hz by discharging at about 20 kW, based on the frequency-watt curve parameters shown in Figure 11, but there is no observable response. AES 2 responds almost immediately to stabilize the frequency, so the frequency is below 59.94 Hz for only 75 msec; and as discussed in Section 3.2 it takes AES 3 190 msec to reach its maximum output power of 200 kW. Therefore, the lack of response from AES 3 is believed to be due to the slower dynamic response in the ultracapacitor RSCAD model's controls.

There is a frequency transient every time AES 3 starts or stops charging. AES 3 also does not respond to the frequency transients when it stops and starts charging. The frequency is outside of the frequency envelope deadband for only about 25 msec.

We re-ran this scenario with cloudy solar data using the same load profile, from 8–9 a.m. on July 29, 2019, and solar insolation data from July 22, 2019 (1 week earlier), which was a cloudy day. The solar insolation data for the clear day, July 29, and the cloudy day, July 22, are compared in Figure 19.

.

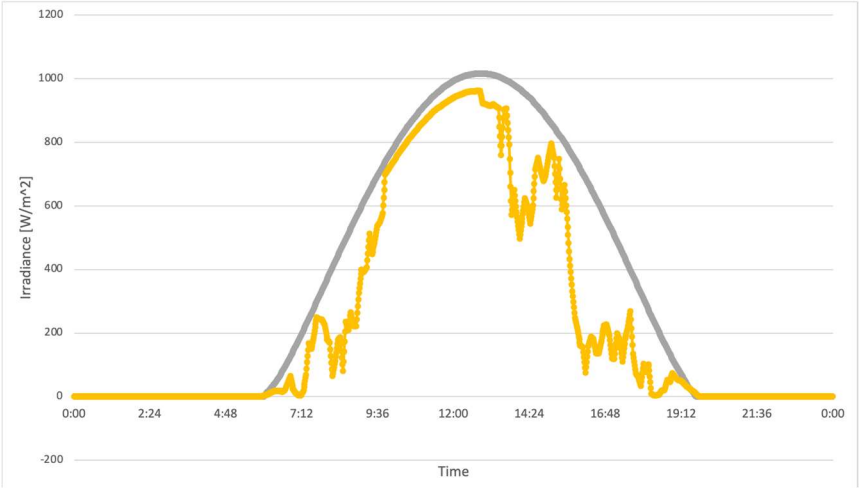

Figure 19. Solar insolation data used for the cloudy day scenario, compared to insolation used for the clear day scenario.

Results for planned islanding with the ultracapacitor for a cloudy day under light load conditions are shown in Figure 20. At the start of the islanding process of the microgrid controller, at ~1,750 s, the GFM inverter, AES 2, is dispatched to charge at about 50 kW, and the GFL inverter, AES 1, is dispatched at zero output. At the start of the zero-power flow step in the planned islanding process, at ~1,950 s, the grid-following BESS, AES 1, is dispatched at its rated power of 500 kW and the remaining load of ~200 kW is carried by the grid-forming BESS, AES 2. The manual switch is opened at ~1,600 s and islanding occurs by opening the microgrid switch at ~2,080 s. We ran the experiment for about 10 min (600 s) after islanding to observe the response of the GFM inverter to varying load and solar insolation conditions. A stable island was maintained despite the varying load and solar powers.

Figure 20. Inverter output powers and the power flow through the microgrid switch during planned islanding with the ultracapacitor under light loading and cloudy solar conditions.

Figure 21 shows the planned islanding event with the ultracapacitor, AES 3, for a cloudy day under light load conditions over about 3 min (left) and 4 s (right). The frequency drops initially to 59.96 Hz, which is a smaller drop than in the experiment with clear solar conditions described earlier because the power flow through the microgrid switch is very close to zero in this case, whereas it was close to 50 kW for the clear day simulation. This variation is to be expected because the microgrid controller will close the switch if the power flow through the microgrid switch is less than 50 kW. About 0.1 s after islanding there is another transient that is due to a reduction in the net load and the frequency increases to 60.01 Hz, and then the inverter mode is changed to GFM for AES 2 and the frequency drops due to the voltage droop setting.

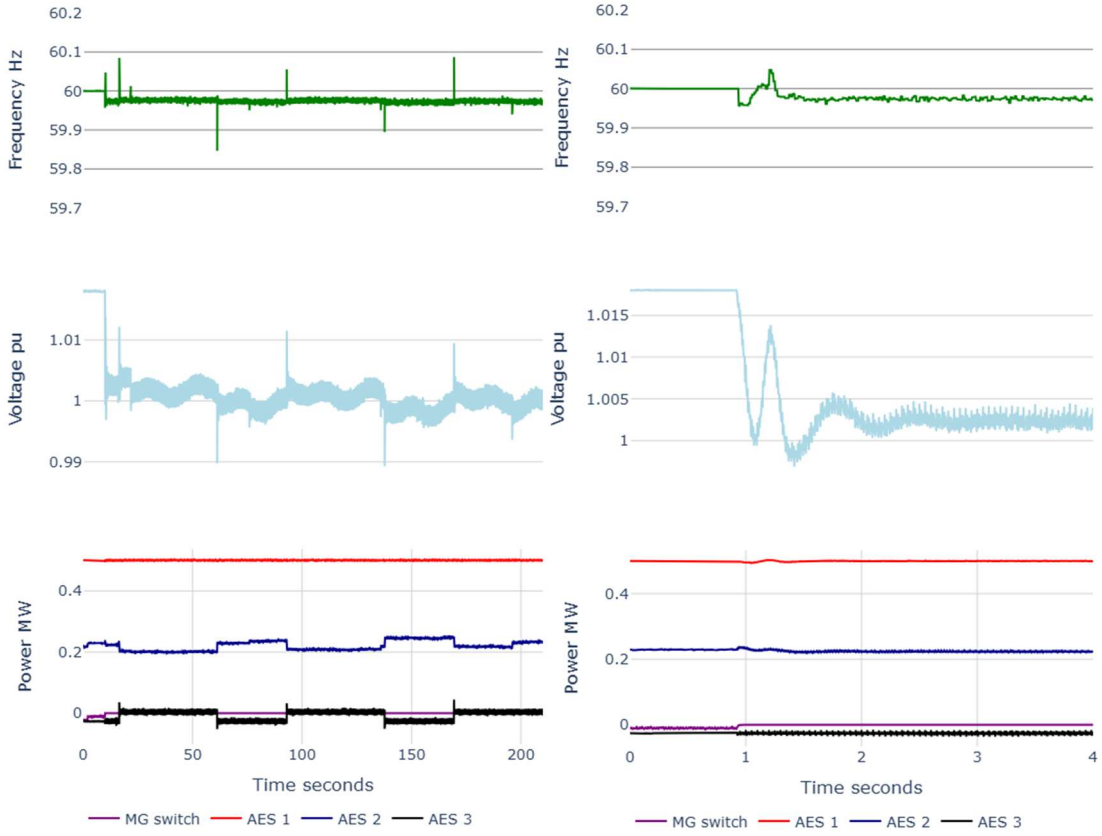

Figure 21. The microgrid frequency (top); microgrid voltage (center); and inverter output powers and the power flow through the microgrid switch during planned islanding with the ultracapacitor under light loading conditions for about 3 min (left) and about 4 s (right).

3.3.2 Planned Islanding with a Diesel Generator Online

We performed HIL simulations of planned islanding with one of the diesel generators—simulated in RSCAD with a rating of 2.2 MVA—online. We dispatched the diesel generator manually (i.e., it was not dispatched by the PXiSE microgrid controller). We performed simulations under night and light load conditions without the ultracapacitor using the same load and solar insolation profiles that we used in the simulations without the diesel generators. We also ran HIL simulations with a heavy load profile—with and without the ultracapacitor—that is not possible without a diesel generator because the load exceeds the capacity of the BESS and PV systems. When we ran the experiments with the diesel generator, we inadvertently set the grid voltage to a lower value of ~0.985 p.u. than for the experiments without the diesel generator, wherein the grid voltage was set to ~1.02 p.u. The lower voltage value does not impact the results in islanded mode, but has the effect of a greater change in voltage during islanding.

3.3.2.1 Night Load Without Ultracapacitor

The load under night loading conditions is approximately 600 kW and we dispatched the diesel generator at 350 kW so that it would provide about half of the required generation in islanded operation. Results for planned islanding without the ultracapacitor under night load conditions are shown in Figure 22.

At the start of the islanding process of the microgrid controller, at ~3,625 s, the GFM inverter, AES 2, is dispatched to charge at about 50 kW, and the GFL inverter, AES 1, is dispatched at zero output. During the zero-power flow step in the planned islanding process that starts at ~3,800 s, the GFL inverter, AES 1, is dispatched at about 240 kW and the GFM inverter is dispatched at about zero. Islanding occurs by opening the microgrid switch at ~3,925 s. A stable island is formed, and the MGC lowers the dispatch of the GFL inverter, AES 1, to about 200 kW at ~ 3,950 s. Some steady state oscillation in the diesel generator output power is observed during islanded operation, along with minor oscillations in the inverter output powers. No such oscillations were observed without the diesel generator. Prior to islanding, oscillations in the power flow through the microgrid switch are observed, and we suspect that there is some undesirable interaction between the diesel generator and the dynamic load models in RSCAD, but we did not have time to fully investigate this. We recommend that this be studied in more depth.

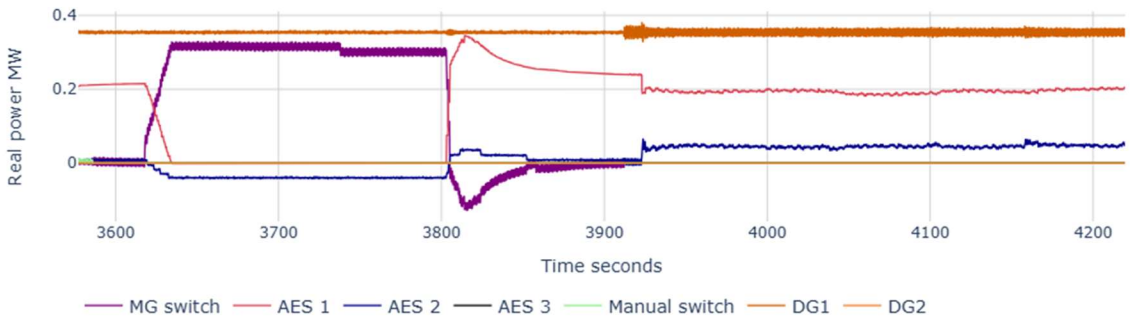

Figure 22. Inverter output powers and the power flow through the microgrid switch during planned islanding with a diesel generator online and without the ultracapacitor under night loading and conditions.

Figure 23 shows results from planned islanding without the ultracapacitor. The power flow through the microgrid switch is very close to zero at islanding and the GFL and GFM inverters, AES 1 and AES 2, output power has no observable transient. The frequency and voltage, while stable, exhibit oscillations in islanded operation that were not observed without the diesel generator.

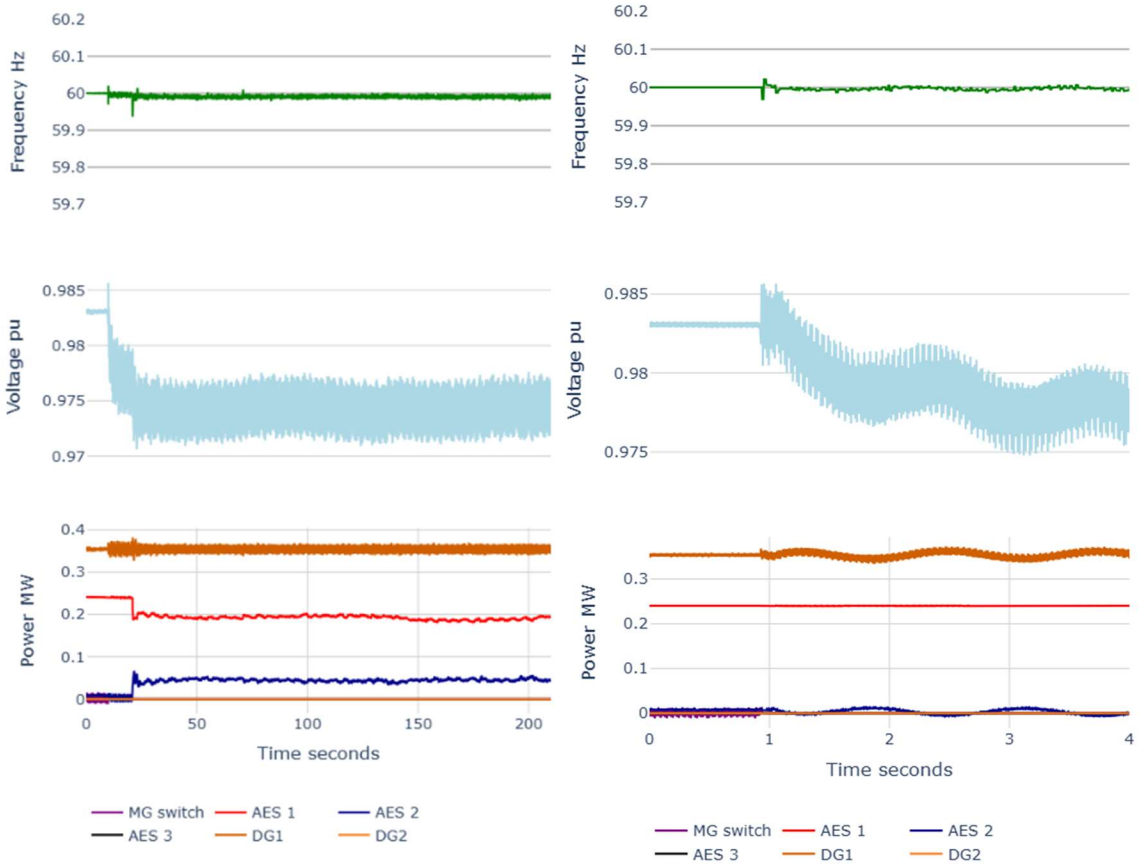

Figure 23. The microgrid frequency (top); microgrid voltage (center); and inverter output powers and the power flow through the microgrid switch during planned islanding with a diesel generator online and without the ultracapacitor under night loading conditions for about 3 min (left) and about 4 s (right).

3.3.2.2 Light Load Without Ultracapacitor

The net load under light loading conditions is a little higher than the night load at about 700 kW. We manually dispatched the diesel generator at 350 kW, and the MGC dispatched the GFL inverter, AES 1, at about 300 kW, and the GFM inverter, AES 2, at about zero. Islanding occurs by opening the microgrid switch, as shown in Figure 24. A stable island is formed, and the MGC lowers the dispatch of the GFL inverter, AES 1, by about 30 kW about 10 s after islanding. Steady state oscillations in the diesel generator output power, and also in the inverter output powers, are observed during islanded operation, along with oscillations in the microgrid frequency and voltage. Prior to islanding, some oscillation in the power flow through the microgrid switch is observed.

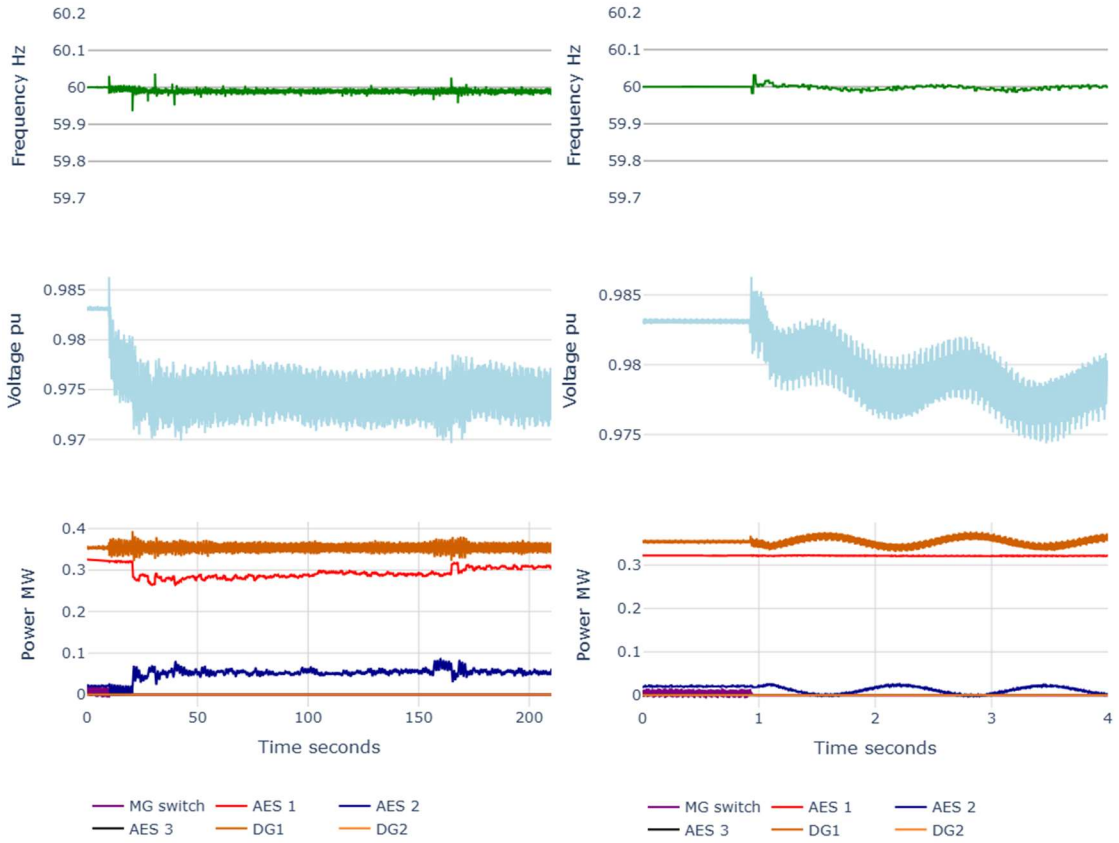

Figure 24. The microgrid frequency (top); microgrid voltage (center); and inverter output powers and the power flow through the microgrid switch during planned islanding with a diesel generator online and without the ultracapacitor under light loading conditions for about 3 min (left) and about 4 s (right).

3.3.2.3 Heavy Load

The net load with the heavy load profile is about 1.4 MW and we dispatched the diesel generator at 550 kW. The PXiSE MGC dispatched the GFL inverter, AES 1, at its rated power of 500 kW and the GFM inverter, AES 2, at about 400 kW to establish zero power flow.

3.3.2.3.1 Heavy Load Without Ultracapacitor

Islanding occurs by opening the microgrid switch at ~2,980 s, as shown in Figure 25 and Figure 26. A stable island is formed, but significant oscillations in the diesel generator output power, and also in the inverter output powers, are observed during islanded operation, along with oscillations in the microgrid frequency and voltage. Prior to islanding, we observe oscillations in the power flow through the microgrid switch. As noted earlier, we recommend further evaluation of the diesel generator model interactions.

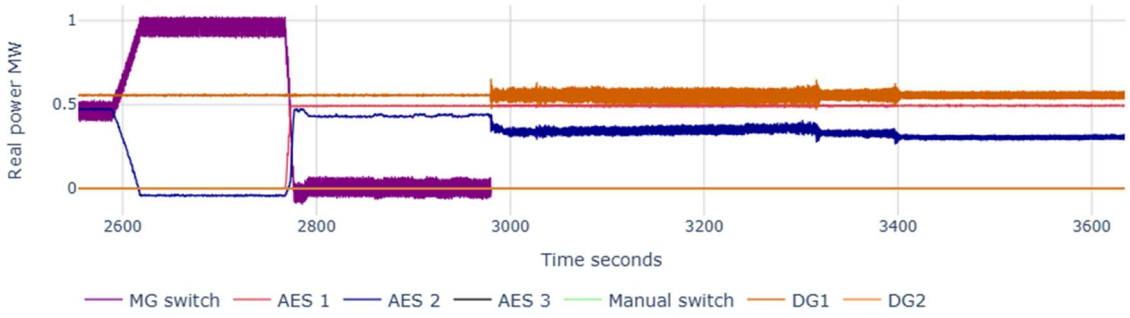

Figure 25. Inverter output powers and the power flow through the microgrid switch during planned islanding with a diesel generator online and without the ultracapacitor under heavy loading conditions.

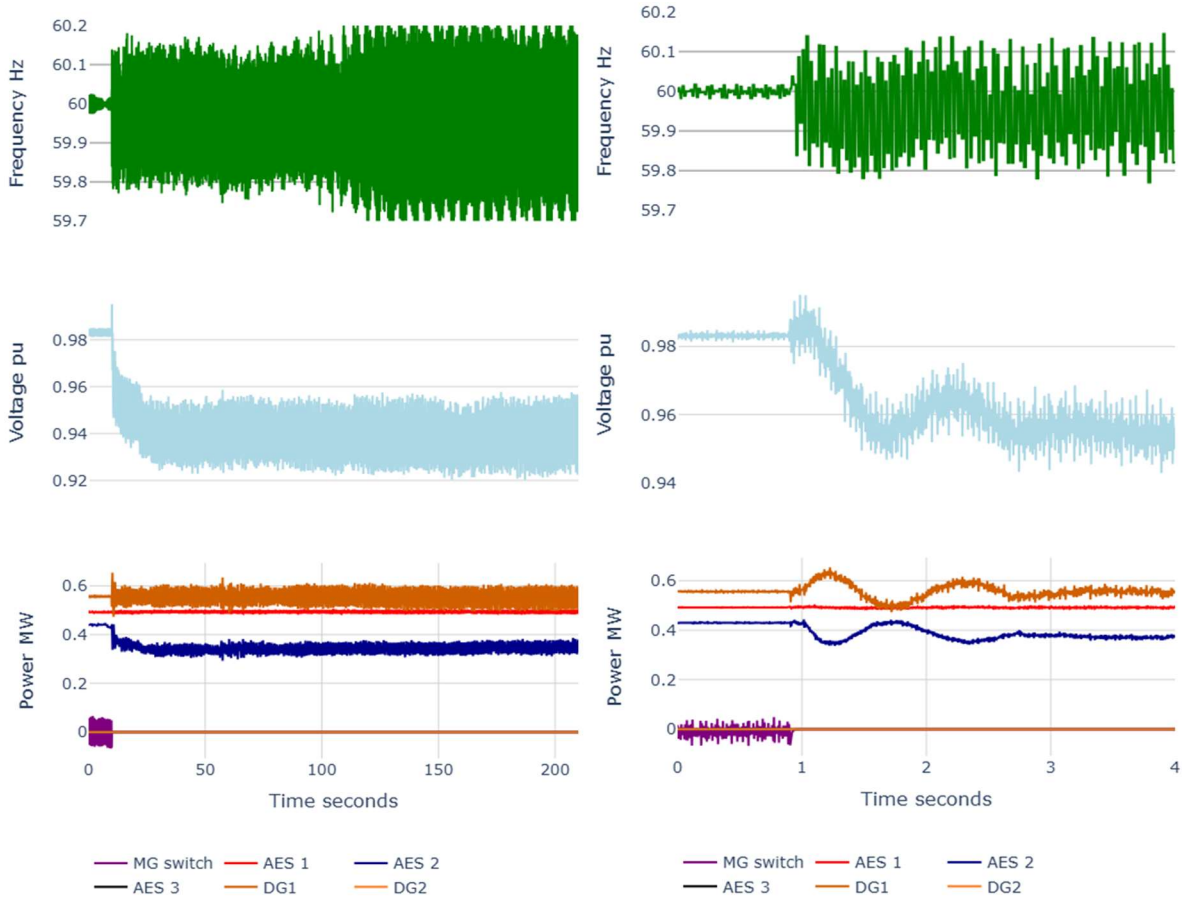

Figure 26. The microgrid frequency (top); microgrid voltage (center); and inverter output powers and the power flow through the microgrid switch during planned islanding with a diesel generator online and without the ultracapacitor under heavy loading conditions for about 3 min (left) and about 4 s (right).

3.3.2.3.2 Heavy Load With Ultracapacitor

Figure 27 and Figure 28 show a planned islanding event with the diesel generator and ultracapacitor, AES 3, online. We manually dispatch the diesel generator at 550 kW. The microgrid controller reduces the power flow through the microgrid switch to near zero before opening the microgrid isolation switch at 4,980 s. It dispatches GFL inverter AES 1 at its full power rating (500 kW), and it dispatches AES 2, which operates in GFL mode while grid-connected, to provide the rest of the net load (~400 kW) so that the power flow through the microgrid isolation switch is near zero. There are significant oscillations in power and frequency before and after islanding. The bottom plot shows the SOC of AES 3, and that it discharges more slowly right after islanding because its power oscillates between discharging and charging.

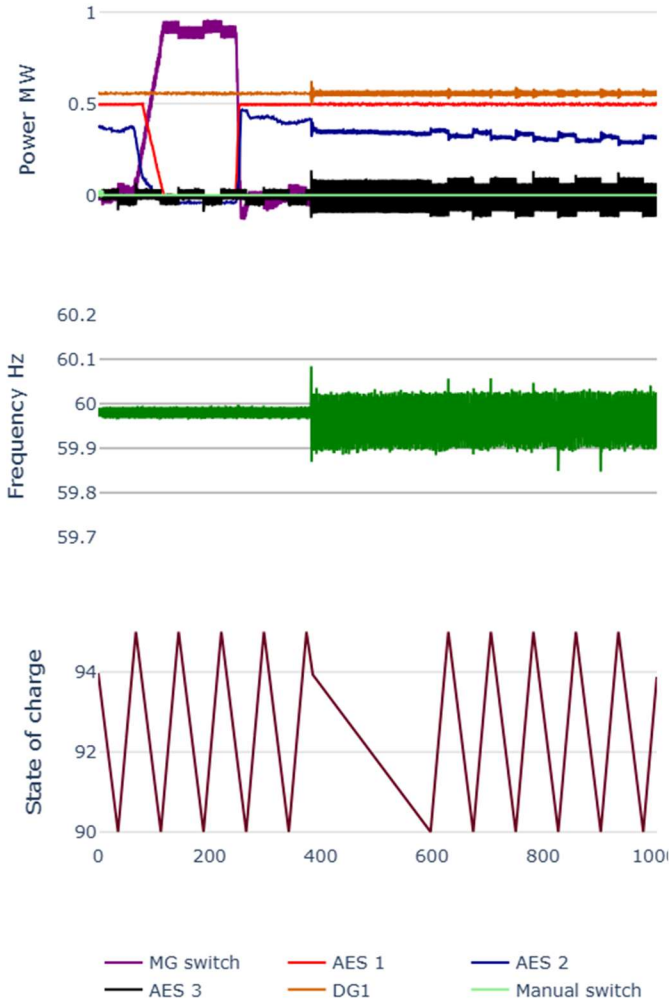

Figure 27. Inverter output powers and the power flow through the microgrid switch (top); the microgrid frequency (center); and ultracapacitor SOC (bottom) during planned islanding with a diesel generator online and with the ultracapacitor under heavy loading conditions.

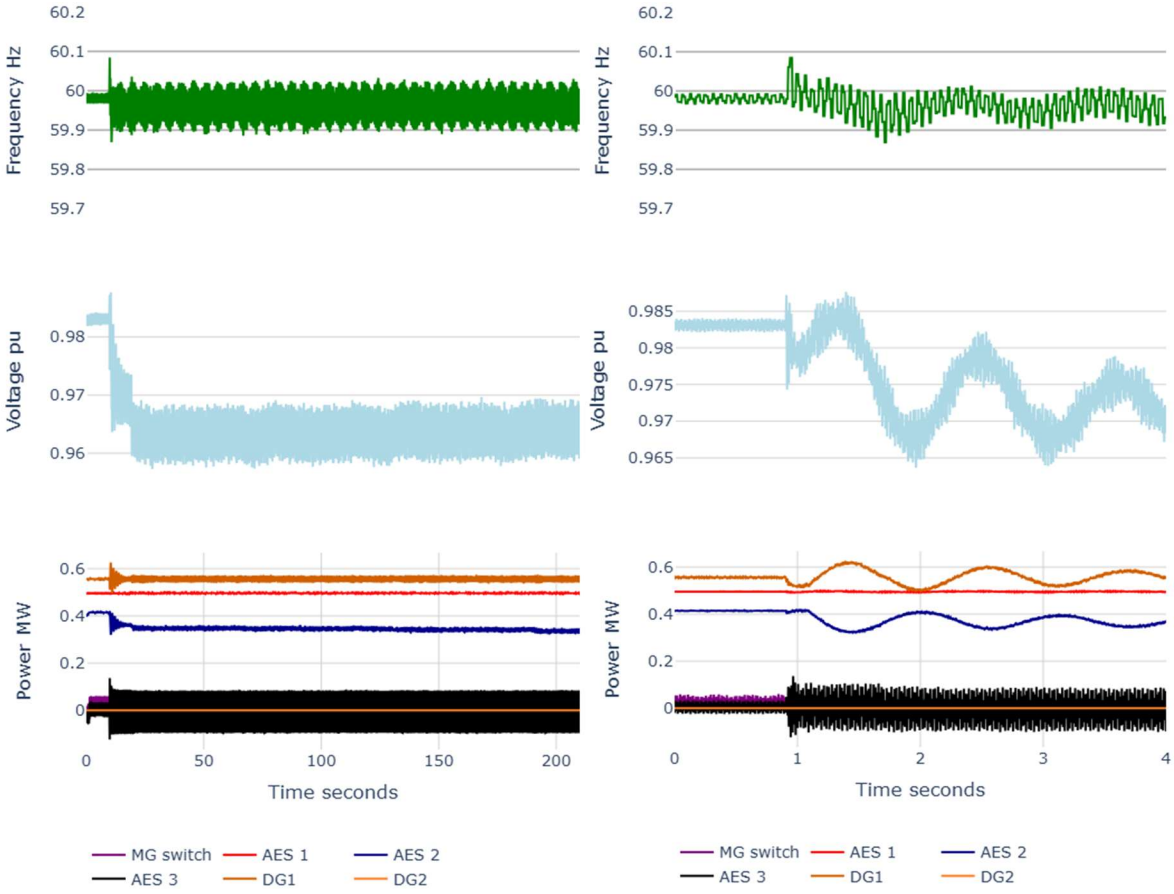

Figure 28. The microgrid frequency (top); microgrid voltage (center); and inverter output powers and the power flow through the microgrid switch during planned islanding with a diesel generator online and with the ultracapacitor under heavy loading conditions for about 3 min (left) and about 4 s (right).

3.3.3 Planned Islanding Results Summary

Table 3 summarizes the planned islanding experimental results. Green shading indicates when the different DERs are online. AES 2 always operates in GFM mode and AES 1 in GFL mode. AES 1 is dispatched by the microgrid controller and the diesel generator is dispatched manually. AES 2, operating in GFM mode, picks up the remaining load. When AES 3 is online, it operates in frequency regulation mode.

Table 3. Summary of planned islanding results

Load profile	AES 2 (GFM)	AES 3	AES 1 (GFL)	Diesel Generator	Result
Night	120 kW	Offline	500 kW	Offline	Stable island.
Night	160 kW	Online	500 kW	Offline	Stable island, AES 3 not triggered.
Light	100 kW	Offline	500 kW	Offline	Stable island.
Light	150 kW	Online	500 kW	Offline	Stable island. No observable response from AES 3.
Light, Cloudy	200 kW	Online	500 kW	Offline	Stable island. No observable response from AES 3.
Night	0 kW	Offline	240 kW	350 kW	Stable island, AES 1 dispatch lowered. Small steady state oscillations observed in DER output before and during island.
Light	0 kW	Offline	300 kW	350 kW	Stable island, AES 1 dispatch lowered. Steady state oscillations observed in DER output before and during island.
Heavy	400 kW	Offline	500 kW	550 kW	Stable island with significant steady state oscillations observed in DER output before and during island.
Heavy	400 kW	Online	500 kW	550 kW	Stable island with significant steady state oscillations observed in DER output before and during island. No discernible response from AES 3 due to oscillations.

3.4 Load Step Results

We simulated load steps with the ultracapacitor, AES 3, online, in islanded operation because this results in larger frequency variations than during islanding.

3.4.1 Light Load

For load steps under light load conditions, we used constant loads and PV outputs in the simulation. The starting net load is about the same as during the planned islanding experiment under light load conditions. The load is stepped up from 685 kW to 885 kW (i.e., a step up of 200 kW). The results are shown in Figure 29. The MGC dispatches the GFL inverter, AES 1, at its rated output power of 500 kW. The AES 3 output power changes from charging at about 25 kW to discharging, peaking at about 32 kW, when the load is stepped up. The frequency drops as low as 59.58 Hz and is restored above 59.94 Hz within 75 msec; it is above 59.9 Hz by the time AES 3 would have reached its maximum discharge rate, as shown in Figure 12. The response rates are similar for AES 2 and AES 3, which is to be expected because they use inverters from the same manufacturer and family of products but with different ratings.

The frequency with the PMU measurement input to AES 3 showed significant oscillations after a load step, so further study is warranted with a filtered PMU measured frequency as an input. AES 2 regulates the frequency quickly and accurately and AES 3 contributes when the frequency is outside of its frequency dead band, but it does not reach its rated output power because its response time is longer than the dwell time of frequency below the frequency deadband.

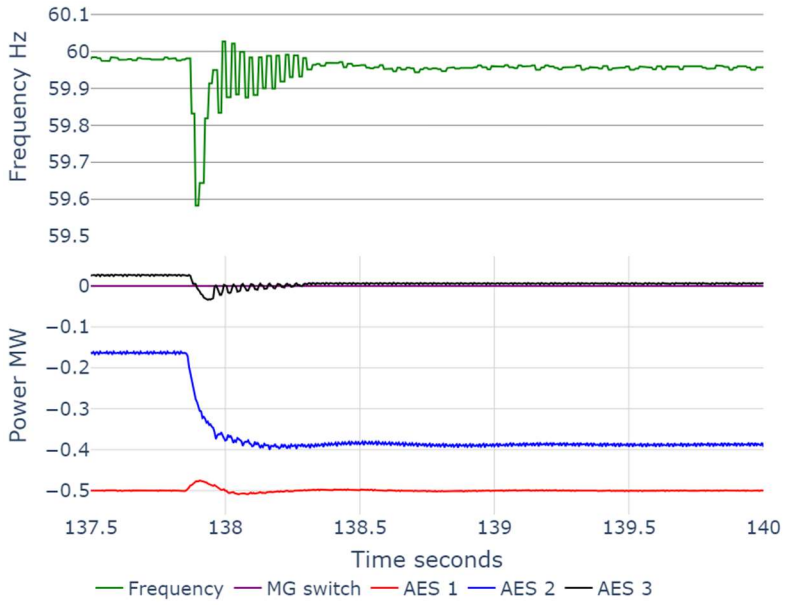

Figure 29. Microgrid frequency (top) and inverter powers (bottom) during a load step of 200 kW in islanded operation with the ultracapacitor under light load conditions.

3.4.2 Heavy Load

For heavy load, we introduced load steps after the conclusion of the planned islanding experiment under heavy loading conditions with the ultracapacitor described in Section 3.3.2.3.2. Figure 30 shows the inverter and diesel generator output powers, microgrid frequency, and ultracapacitor SOC. Figure 31 shows the load step down (left) and load step up (right) over 30 s.

Stable operation is maintained, but significant oscillations are observed and the frequency oscillations exceed the ultracapacitor deadband, so its ability to provide frequency support is negatively impacted. As noted in Section 3.3.2.1, further study is warranted on the interactions of the RSCAD generator model with other elements.

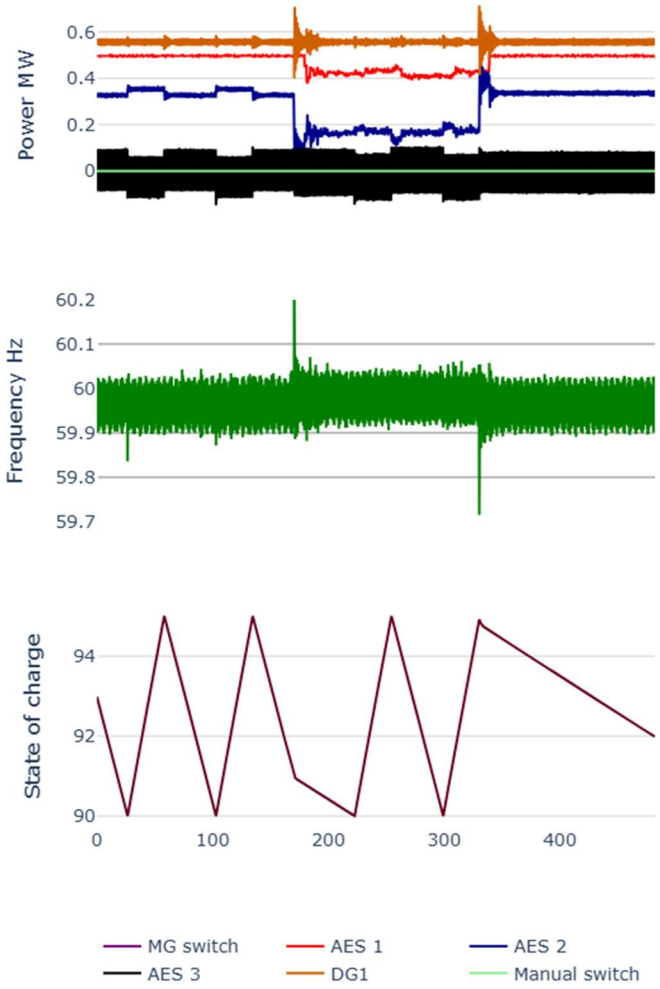

Figure 30. Inverter and diesel generator output powers (top); the microgrid frequency (center); and ultracapacitor SOC (bottom) during load steps in islanded operation with the ultracapacitor under heavy loading conditions.

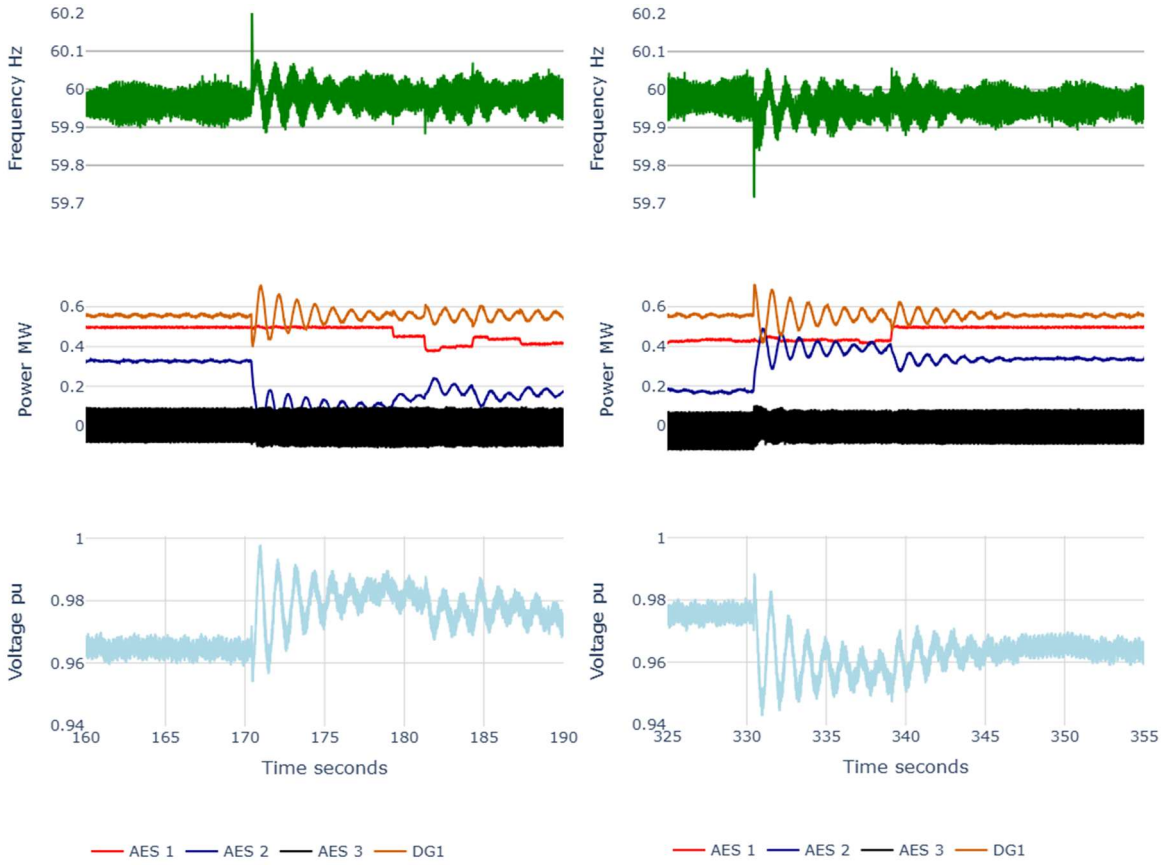

Figure 31. The microgrid frequency (top); inverter output powers and the power flow through the microgrid switch (center); and microgrid voltage during a load step down (left) and load step up (right) in islanded operation with a diesel generator online and with the ultracapacitor under heavy loading conditions for about 30 s.

3.5 Black Start Results

We performed a black-start simulation under light load conditions with the ultracapacitor and diesel generators offline. We dispatched the GFL inverter, AES 1, manually, and we closed the breakers manually in the RSCAD simulation. After we closed each breaker, we verified that we observed stable voltage and then manually activated the PV systems in the newly energized part of the feeder. Figure 32 shows an anonymized version of the RSCAD model showing the section of the feeder that we energized during the black-start test. We followed the following sequence for the black-start test:

1. Open all breakers in RSCAD model downstream of the 12 kV bus
2. Turn on the DC source to the inverter
3. Initiate black start sequence in the microgrid controller
4. Turn on the voltage amplifier and close the physical breaker to connect the GFM inverter hardware (AES 2) to the amplifier
5. Close breaker 10
6. Check for stable voltage, then turn on PV5, PV6 and PV21
7. Check for stable voltage, then close breaker 11
8. Check for stable voltage, then turn on PV7
9. Check for stable voltage, then close breaker 14
10. Check for stable voltage, then turn on PV12
11. Check for stable voltage, then close breaker 12
12. Check for stable voltage, then turn on PV8 and PV9.

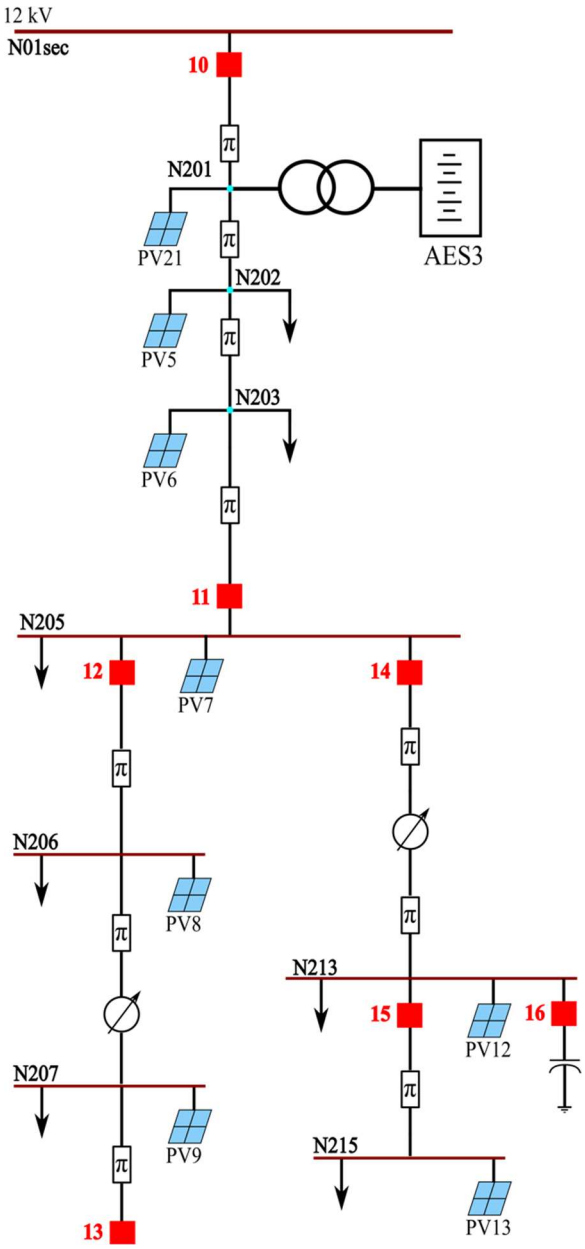

Figure 32. Anonymized version of the RSCAD model showing loads and breakers used for the black-start test.

Figure 33 shows the microgrid voltage and frequency, measured at the 12-kV bus, during the black-start experiment, showing formation of the island and stable operation. Before the inverter initiates the black-start mode, the voltage at the bus is zero, and there is no waveform from which the frequency could be measured. Therefore the frequency value oscillates around 60 Hz before the frequency measurement gets an actual voltage waveform.

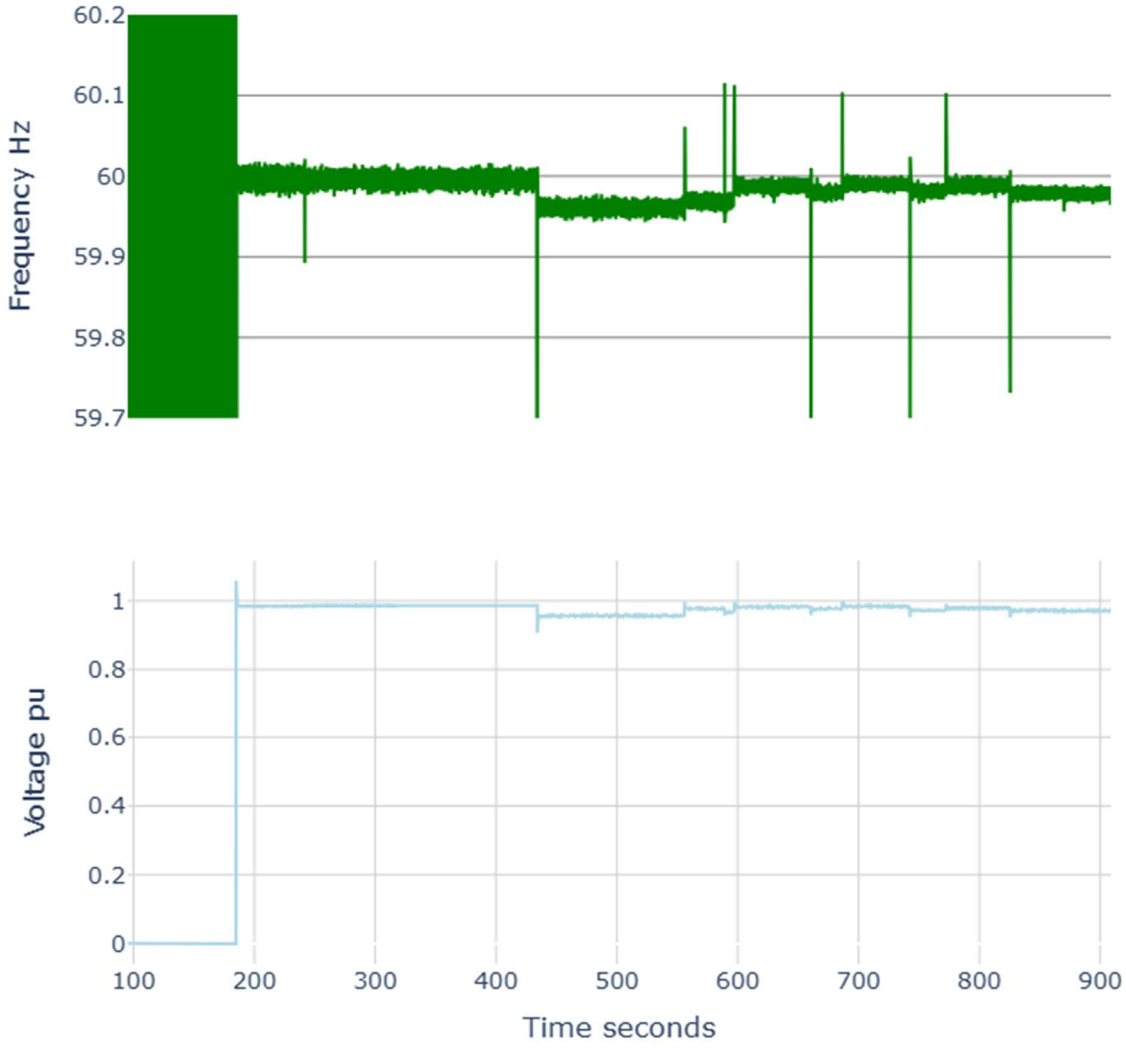

Figure 33. Microgrid frequency (top) and voltage (bottom) during the black-start experiment, showing the establishment of voltage and frequency for the microgrid.

Figure 34 shows the microgrid frequency, inverter output power, and microgrid voltage for the portion of the experiment after the 12-kV bus is energized. Before breaker 10 is closed, there are no energized loads. The GFM inverter. AES 2, output power increases at ~430 s when breaker 10 is closed, to supply power to the first energized section. The GFL inverter, AES 1, is manually dispatched at ~ 550 s, resulting in a change in output power of the GFM inverter to maintain generation-load balance. The PV systems in the first energized section are activated at ~ 590 s, causing a slight reduction in the output power of AES 2. PV inverters would take between 1 and 5 min to come online in the field; here they are brought online sooner for the sake of limiting the duration of the experiment and the amount of data to collect.

The output power of AES 1 is manually increased at ~ 600 s, which is prior to closure of the next breaker to ensure that enough generation capacity is online. Then breaker 11 is closed at ~ 670 s and the GFM inverter picks up that load. The next set of PV systems are brought online shortly afterward, resulting in a small drop of power provided by AES 2. This sequence is repeated with GFL inverter dispatch at ~690 s, closure of breaker 14 at ~750 s, and PV systems online at ~760 s; and then again with a GFL inverter dispatch at ~780 s, closure of breaker 12 at ~820 s, and PV systems online at ~830 s. There are smaller changes in AES 2 output power due to load and PV profile changes every 1 min.

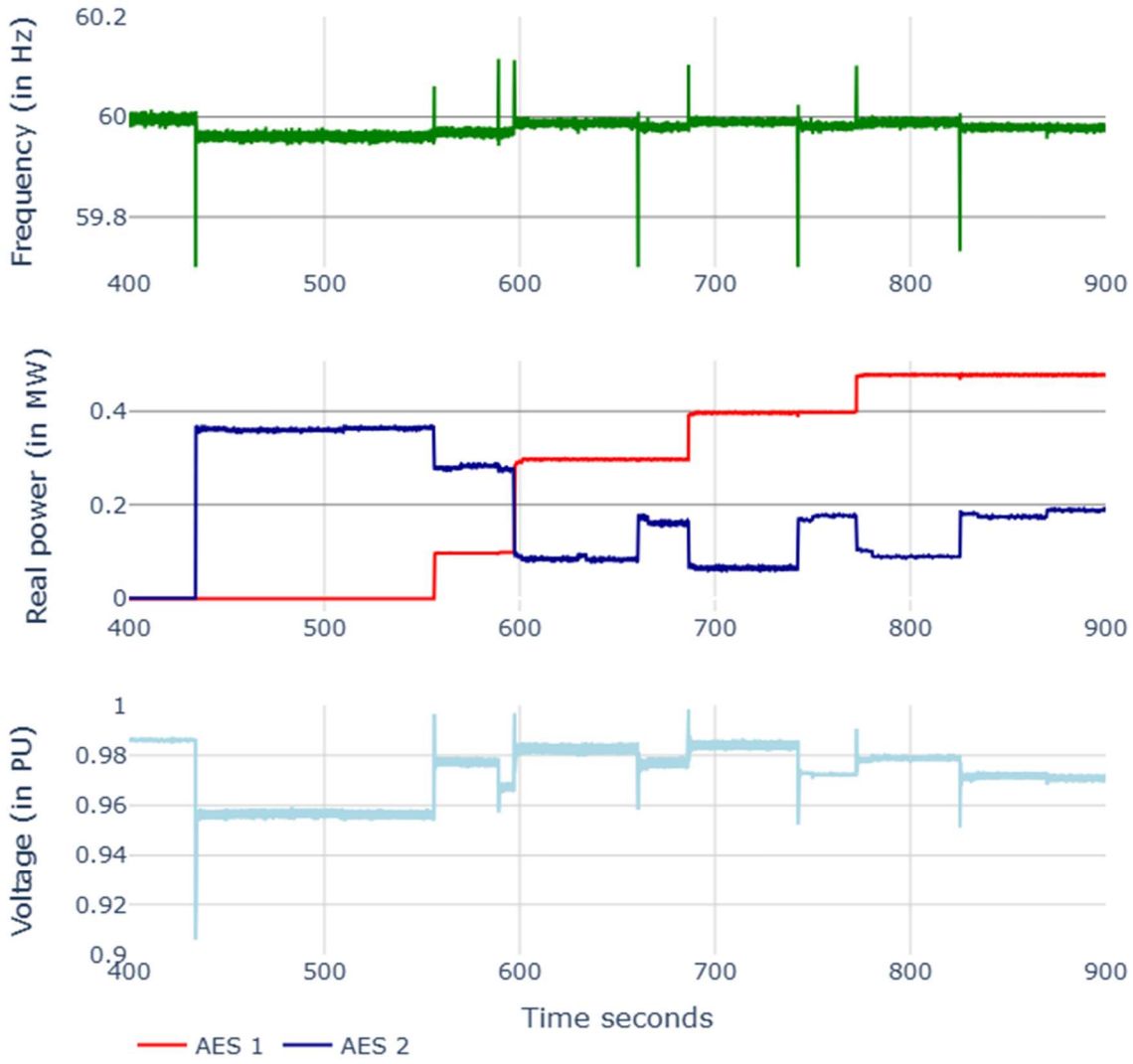

Figure 34. The microgrid frequency (top); inverter output powers (center); and microgrid voltage during the black-start experiment, after the island has been established.

The voltage and frequency are maintained within limits throughout all load and generation changes. The most significant transition is when the first load is added, shown in more detail in Figure 35 over 4 s. There is a significant transient in frequency and voltage, but they are within voltage limits within 100 msec.

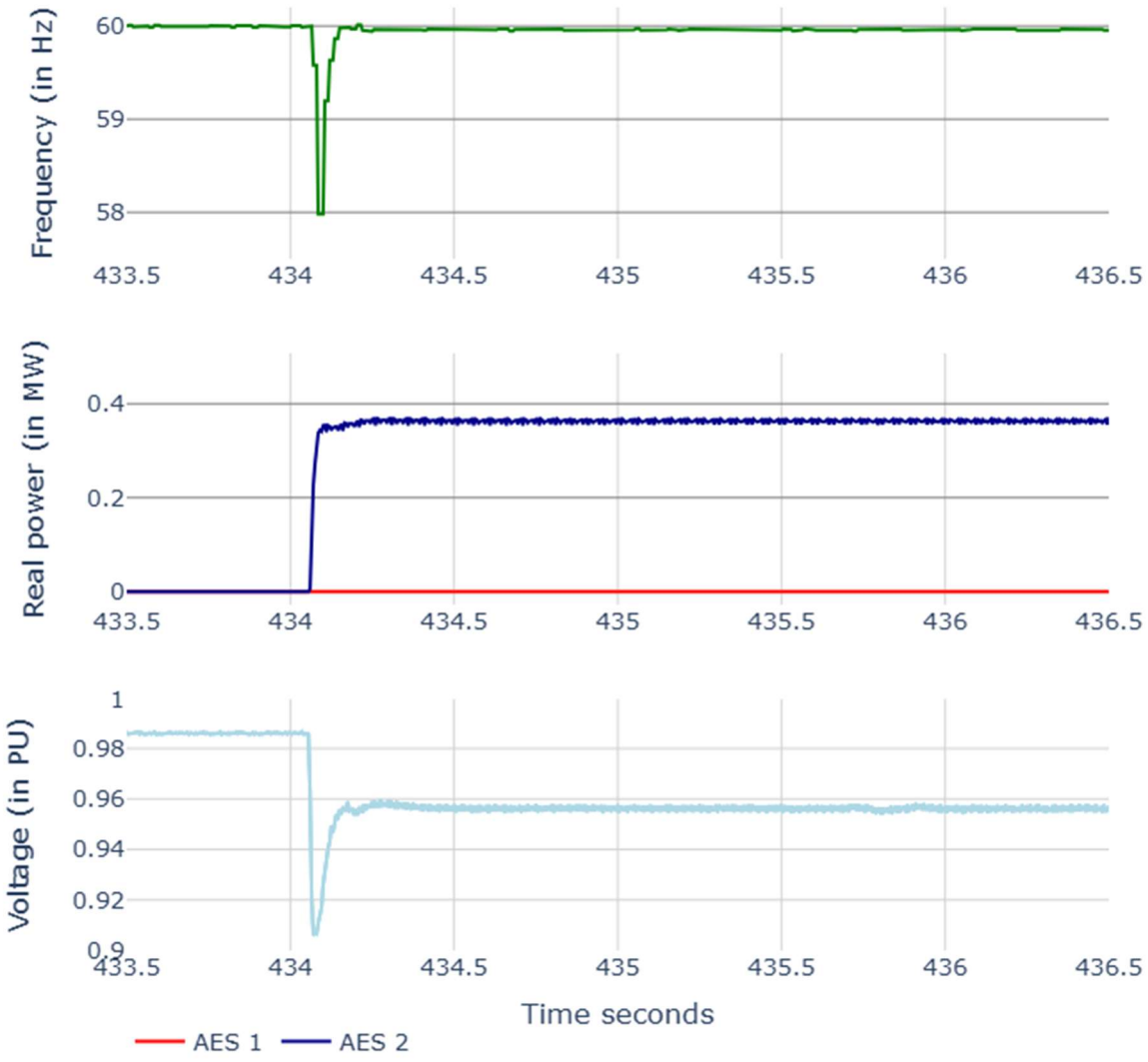

Figure 35. The microgrid frequency (top); inverter output powers (center); and microgrid voltage during the black-start experiment, when the first load is picked up.

4 Conclusions

This report presents results from HIL simulations of the SDG&E Borrego Springs Microgrid. It provides details on the experimental setup that uses PHIL and CHIL devices that closely represent the field power hardware and controls. It presents HIL simulation results of planned islanding, load steps in islanded operation and black start with only BESS sources that show the effectiveness of the inverters in maintaining the island and managing the microgrid frequency.

The key findings of this work are:

- As microgrids continue to proliferate, particularly those that rely on an inverter-based resource to act as a voltage/frequency leader, there is a need for PHIL interfaces with GFM inverters that enable HIL simulations with seamless transitions between islanded and grid-connected microgrid operation. Such an interface is particularly challenging for inverters that need to switch between GFL and GFM modes. As a result, NREL developed two PHIL interfaces that meet these requirements, and we used the method with a voltage-mode power amplifier and power inductor that together act as a current source for the Borrego Springs Microgrid HIL simulations.
    - This report describes the experimental results of the PHIL interface including load steps during islanded operation, inverter set point changes during grid-connected operation, and transitions between GFM and GFL inverter modes as the microgrid transitions between islanded and grid-connected operation.
    - The accuracy of the voltage amplifier interface method is not sufficient at low power levels, and this will require attention by those who choose to implement this method.
- The ultracapacitor, AES 3, did not have as significant a contribution as we expected based on the observed frequency variations. The GFM inverter, AES 2, responds almost immediately to stabilize the frequency, so the frequency is below 59.94 Hz for less than 100 msec; and it takes AES 3 190 msec to reach its maximum output power of 200 kW. Therefore, the lack of response from AES 3 is believed to be due to the slower dynamic response in the ultracapacitor RSCAD model's controls.
- We observed steady state oscillations in the diesel generator output power during islanded operation, along with oscillations in the inverter output powers. No such oscillations were observed without the diesel generator. Prior to islanding, oscillations in the power flow through the microgrid switch are observed, and we suspect that there is some undesirable interaction between the diesel generator and the dynamic load models in RSCAD, but we did not have time to fully investigate this. We recommend that this be studied in more depth.
- HIL simulations provide valuable insights to develop safe operating procedures and de-risk field tests and operations. Broadly, these promising results will improve the ability of grid operators to integrate increasing amounts of solar generation into the grid in a cost-effective, secure, resilient, and reliable manner.

NREL made significant contributions to the field of PHIL interfaces through this project.

- NREL extended a previously-developed PHIL interface for GFM inverters to enable simulations of seamless transitions between islanded and grid-connected operation. Such interfaces are particularly challenging when the inverters need to switch modes, i.e., between GFL and GFM as the microgrid transitions between grid-connected and islanded operation. The PHIL interface we used is suitable for those who need a solution that uses a voltage-mode power amplifier.

This report also identified a few areas in which future work is warranted, namely to:

- Study the PHIL interfaces with multiple GFM inverters in a microgrid.

- Address the PHIL interface accuracy deterioration at lower power, possibly by adding adaptive gains.
- Study the interactions between the ultracapacitor model and the network model in RSCAD and their effect on the voltage level during islanded operation.
- Address the steady state oscillations observed when the diesel generator model in RSCAD is included in the simulations.

In addition, NREL will continue to use the PHIL experimental setup developed for the Borrego Springs for a project focused on the grid integration of grid-forming fuel cell inverters.

References

[1] J. Wang, A. Pratt, K. Prabakar, B. Miller, and M. Symko-Davies, "Development of an integrated platform for hardware-in-the-loop evaluation of microgrids prior to site commissioning," *Applied Energy*, vol. 290, 2021.

[2] K. Prabakar, Y. N. Velaga, R. Flores, J. Brouwer, J. Chase, and P. Sen, "Enhancing distribution system resiliency using grid-forming fuel cell inverter," in *Proc. 2022 IEEE Rural Electric Power Conference (REPC)*, pp. 38–42.

[3] K. Prabakar, A. Pratt, et al., "Site-specific evaluation of microgrid controller using controller and power-hardware-in-the-loop," in *Proc. 2019 45th Annual Conference of the IEEE Industrial Electronics Society (IECON)*, pp. 6463–6468.

[4] J. Hernandez-Alvidrez, et al., "Method to interface grid-forming inverters into power-hardware-in-the-loop setups," in *Proc. 2020 IEEE 47th Photovoltaic Specialists Conference*, pp. 1804–1810.

[5] N. Ainsworth, et al., "Modeling and compensation design for a power hardware-in-the-loop simulation of an ac distribution system," in *Proc. 2016 North American Power Symposium*, pp. 1–6.

[6] G. Lauss, et al., "Characteristics and design of power hardware-in-the-loop simulations for electrical power systems." *IEEE Trans. Ind. Electron.*, vol. 63, no. 1, pp. 406–417, Jan. 2016.

[7] Y. Lin, et al., "Research roadmap on grid-forming inverters," National Renewable Energy Laboratory, Golden, CO, Tech. Rep. NREL/TP-5D00-73476, 2021.

[8] S. Chakraborty, et al., "A novel power-hardware-in-the-loop interface method for grid-forming inverter systems," in *Proc. 2022 48th Annual Conference of the IEEE Industrial Electronics Society (IECON)*, pp. 1–6.

[9] Z. Feng, et al., "Current-type power hardware-in-the-loop interface for black-start testing of grid-forming converter," *Proc. 2022 48th Annual Conference of the IEEE Industrial Electronics Society (IECON)*, pp. 1–7.

[10] A. Pratt, K. Prabakar, S. Ganguly, and S. Tiwari, "Power hardware-in-the-loop interfaces for inverter-based microgrid experiments including transitions," in *Proc. 2023 IEEE Energy Conversion Congress and Exposition (ECCE)*, pp. 537–544.

[11] A. Pratt, K. Prabakar, and M. Symko-Davies, "Power-hardware-in-the-loop experiments of a microgrid with a grid-forming battery inverter," accepted to the IEEE PES General Meeting, July 27–31, 2025, Austin, TX.

[12] L. Abcede, A. Pratt, K. Prabakar, and K. McGrath, "Interoperable, inverter-based distributed energy resources enable 100% renewable and resilient utility microgrids," in *Proc. 2025 IEEE Grid Edge Technologies Conference and Exposition*, pp. 1–5.

This material is based upon work supported by the U.S. Department of Energy Office of Energy Efficiency and Renewable Energy (EERE) under the Solar Energy Technologies Office (SETO) Award Number DE-EE0009027 to SDG&E and the National Renewable Energy Laboratory, under Contract No. DE-AC36-08GO28308. The views expressed herein do not necessarily represent the views of the U.S. Department of Energy or the United States Government.

Full Scale Simulation Report

Transient Stability Study of Borrego Springs Microgrid With 100% Renewables

Yaswanth Nag Velaga, Jing Wang

This material is based upon work supported by the U.S. Department of Energy Office of Energy Efficiency and Renewable Energy (EERE) under the Solar Energy Technologies Office (SETO) Award Number DE-EE0009027 to SDG&E and the National Renewable Energy Laboratory, operated by Alliance for Sustainable Energy, LLC, under Contract No. DE-AC36-08GO28308. The views expressed herein do not necessarily represent the views of the U.S. Department of Energy or the United States Government.

Acknowledgments

The authors acknowledge the substantial contributions from the staff at San Diego Gas & Electric Company (SDG&E), including Laurence Abcede, Kimberly McGrath, Andrew Moradpour, Beverly R. Raposa, Jose J. Cardenas, and Nagadev Shanmukh. They provided power system model and data, engineering input and feedback, and field operational practice.

The authors also thank Robert Reedy of the U.S. Department of Energy Office of Energy Efficiency and Renewable Energy Solar Energy Technologies Office for his continuous support and very helpful insights for this project.

List of Acronyms

AVR	automatic voltage regulator
BESS	battery energy storage system
CI	constant impedance
CP	constant power
DER	distributed energy resource
EMT	electromagnetic transient
GFL	grid-following
GFM	grid-forming
IBR	inverter-based resource
IEEE	Institute of Electrical and Electronics Engineers
LG	line to ground
LLG	double line to ground
LLLG	triple line to ground
LN	line to neutral
MVA	megavolt ampere
MVAR	megavolt ampere reactive
p.u.	per unit
PCC	point of common coupling
PD	proportional-derivative
PI	proportional-integral
PID	proportional-integral-derivative
PLL	phase-locked loop
PQ	power control
PV	photovoltaic
RMS	root mean square
SDG&E	San Diego Gas & Electric Company
SES	storage energy system
SOGI	second-order generalized integrator
VAR	volt ampere reactive
VF	voltage-frequency

Executive Summary

As the inverter-based resources in the San Diego Gas & Electric Company Borrego Springs Microgrid become the dominant generation units and the renewable generation deployment level increases to 100%, the need for more accurate and detailed simulations becomes increasingly critical to ensure reliable operations. The operations of multiple grid-forming (GFM) and grid-following (GFL) inverters within a power system is not well understood under dynamic operating conditions, such as islanding operation and black start; therefore, full-scale electromagnetic transient (EMT) modeling and simulation is developed to investigate the stability of the system under various dynamic operating conditions and to identify potential stability and reliability risks.

Through the full-scale EMT simulation, we also aim to demonstrate the capability of the GFM battery inverter (the islanding leader, SES2) through a more comprehensive simulation of the Borrego Springs Microgrid. In addition, we evaluate the effectiveness of the microgrid control system—including the controls of the two battery storage energy systems (SES), SES1 and SES2, and the controls of the ultracapacitor energy storage system, SES3—in reducing the variability of the frequency and voltage of the microgrid, especially during islanding. SES2 is the island leader and is black-start capable. In the baseline operation, SES1 runs in GFL mode with dispatched power; SES2 runs in GFL mode with zero power generation dispatch when the microgrid is grid-connected and as the GFM islanding leader when the microgrid is islanded; and SES3 runs in frequency envelope mode for fast frequency support, especially during the planned/unplanned islanding operations. Because this is a pure software simulation, we use a simple microgrid controller developed in the PSCAD simulation software to perform the functions that will be performed by the Borrego Springs Microgrid local area distribution controller in the field.

In this report, we simulate four types of dynamic events: planned islanding and unplanned islanding, black start, and various contingencies in islanded mode. For each dynamic event, representative load scenarios are simulated, including morning (photovoltaic ramping), noon (high solar, low net load), and night (no solar, high load). The EMT simulation provides insights for field deployment—specifically, the high-fidelity model provides results to predict the potential stability and reliability risks and suggests possible mitigation measures (e.g., generation and load balancing, tuning the SES control parameters). In addition, investigating how the three battery inverters work together with appropriate operation modes to stabilize the microgrid system during dynamic events—especially unplanned islanding operation—are of great interest for this project.

Overall, this full-scale EMT simulation of the real-world Borrego Springs Microgrid makes significant contributions to this project and to similar microgrid projects. The main contributions of the PSCAD EMT simulation are to study the stability and reliability of the 100% renewable microgrid under various dynamic events, which will provide insights for field deployment. The key learnings are summarized in this report.

Table of Contents

List of Figures

List of Tables

1 Introduction and Background

1.1 Borrego Springs 100% Renewable Microgrid

The town of Borrego Springs is fed by a single, radial 69-kV transmission line that is approximately 30 miles long and includes an elevation change of approximately 5,000 feet. As part of the Colorado Desert subregion of the Sonoran Desert, the area experiences high winds and monsoon storms that lead to long-duration outages during high temperatures [1]. San Diego Gas & Electric Company (SDG&E) developed the Borrego Springs Microgrid to provide reliable power and energy resilience for the 2,800 residents. At the outset, the microgrid included two diesel generators as the grid-forming (GFM) sources to provide resilience and reliability in islanded mode. SDG&E is currently working toward grid resilience with a 100% renewable microgrid through the addition of battery energy storage systems (BESS) with advanced GFM inverters. With this goal, one new BESS with a GFM battery inverter will replace the diesel generators as the islanding leader in islanded operation. The other two inverters are also capable of operating in GFM mode: One inverter has battery storage and is configured as a dispatchable generation source to meet energy demand, and the other inverter has ultracapacitor storage and is configured as the fast frequency support asset to arrest system frequency excursions during planned and unplanned islanding operation. For solar generation, the Borrego Springs Microgrid aims to incorporate a third-party 26-MW photovoltaic (PV) facility, which also includes a 6.5-MW concentrating solar power facility and many distributed rooftop PV units owned by its customers. Combining storage and PV creates a unique opportunity to leverage GFM technology to potentially allow the microgrid to operate with 100% renewable generation to energize portions of the grid and provide power to customers during an outage, increase renewable resource energy contributions, and improve power system reliability and resilience.

1.2 Purpose and Importance of Electromagnetic Transient Simulation

This project is a partnership between the U.S. Department of Energy Office of Energy Efficiency and Renewable Energy Solar Energy Technologies Office and SDG&E to achieve the goal of 100% renewable microgrid operation in Borrego Springs. (1) This project is researching and validating innovative microgrid technologies that enable distributed energy resources (DERs) with the ability of GFM battery inverters to contribute to grid stability and resilience by maintaining voltage and frequency during transient conditions, especially microgrid islanding. (2) A second component is the evaluation and design of a standard interface for various DERs to decrease the complexity of interfacing between a DER management system and the edge devices. (3) The third key component is an evaluation of past islanding attempts coupled with the development of controls for an appropriately sized battery to decrease frequency and voltage variability within the island, avoiding the activation of protection equipment.

The project focuses on achieving these goals through a combination of electromagnetic transient (EMT) simulations, hardware-in-the-loop simulations, and field tests. This report focuses on the EMT simulations. The objective of the EMT simulations is to evaluate the transient stability of the Borrego Springs Microgrid to demonstrate the effectiveness of the GFM battery inverter controls through more comprehensive simulations of the microgrid [2].

EMT simulations are complementary to hardware-in-the-loop simulations to test the microgrid's stability and reliability under dynamic events—especially for scenarios that are hard to complete in hardware-in-the-loop due to potential hardware damage—and to perform a comprehensive study to fully understand the stability and reliability of the Borrego Springs Microgrid under various dynamic scenarios [3], [4].

As the inverter-based resources (IBRs) in the Borrego Springs Microgrid become the dominant generation units and the renewable deployment level increases to 100%, the need for more accurate and detailed simulations becomes increasingly critical to ensure reliable operations [5]. In particular, the operation of multiple GFM and grid-following (GFL) inverters within a power system is not well understood under dynamic operating conditions, such as islanding and black starts [6]; therefore, full-scale EMT modeling and simulation can be used to investigate the stability of the system under various dynamic operating conditions and to identify potential reliability risks.

In addition, investigating how the three storage energy system (SES) battery inverters work together with appropriate operation modes to stabilize the microgrid system during dynamic events—especially unplanned islanding operation—is of great interest for this project. Moreover, the testing results of the EMT simulation provide insights for field deployment, including potential instability risks and recommendations to tune the control parameters of the islanding leader to stabilize the microgrid system under dynamic events.

1.3 Challenges of Electromagnetic Transient Simulation

The power system model of the Borrego Springs Microgrid has more than 300 nodes. The three substation energy storage systems (SES1, SES2, and SES3) are modeled in detail. At least 20 GFL PV inverters at the 26-MWac PV installations are modeled explicitly in PSCAD, including their controls. The 6.5-MW concentrating solar power facility is modeled in detail. At least 80 customer-owned rooftop solar installations are modeled in detail as well. The simulation therefore exceeds 100 inverters and 400 nodes. The original power system model is in Synergi. Because no tool is available to convert the existing model data format (Synergi) to the PSCAD data format, we manually develop the power system model based on the updated RSCAD model developed by Quanta for SDG&E that was converted from Synergi. To complete the detailed model of the Borrego Springs Microgrid, we follow these three steps: (1) Start with the passive network and ensure that the power flow matches the passive network model in RSCAD. (2) Add the dynamic model of DERs and verify the DER model one by one. (3) Evaluate the overall stability and power quality of the microgrid model for both grid-connected and islanded mode.

To build such a complex model, we faced a few major challenges. These are summarized in Table 1 with the corresponding solutions.

Table 1. Challenges and Solutions of EMT Simulations

Challenge	Solution
Simulation of full network with 105 DERs	The network is divided into three projects in PSCAD interlinked through a cable model.
Black start of the grid connection	An accelerated black-start sequence is performed to reduce the overall simulation time. For example, the rooftop PV is reconnected to the grid 5 seconds after the grid voltage recovers rather than 5 minutes based on the IEEE 1547-2003 requirements.
Stability of the Borrego Springs network	The control parameters of the PID controller of the SES2 GFM inverter are tuned to simulate the stable cases.

2 PSCAD Modeling of the Microgrid

The circuit topology of the microgrid is shown in Figure 1. The passive network of the Borrego Springs Microgrid was developed in PSCAD based on the RSCAD model [2]. The microgrid consists of a 69-kV distribution substation; step-down transformers; three main circuits; and various IBRs, including a 26-MW PV facility (PV1), a 6.5-MW concentrating PV system (PV2), 5.4 MW of rooftop and distributed PV (based on 2019 load data), two 1.8-MW diesel generators (Gen1 and Gen2), two utility-scale BESS (SES1 and SES2) rated at 0.5 MVA/1.5 MWh and 1 MVA/3 MWh, respectively, and a 0.5-MVA/3-minute ultracapacitor energy storage system (SES3) in the microgrid yard. SES1, SES2, and SES3 all have the same inverters, which are capable of operating in either GFM or GFL mode. The two diesel generators are not used in grid-connected mode, and they are backup generation in an islanded microgrid in case the BESS have low states of charge, or the load exceeds the capacity of the BESS. They operate as GFL dispatchable resources when they are used. Each circuit has three-phase dynamic load (constant power and impedance), and Ckt1 and Ckt3 have pump load modeled as induction motors. The following sections discuss the modeling of the load, the diesel generators, the PV inverters, and the BESS.

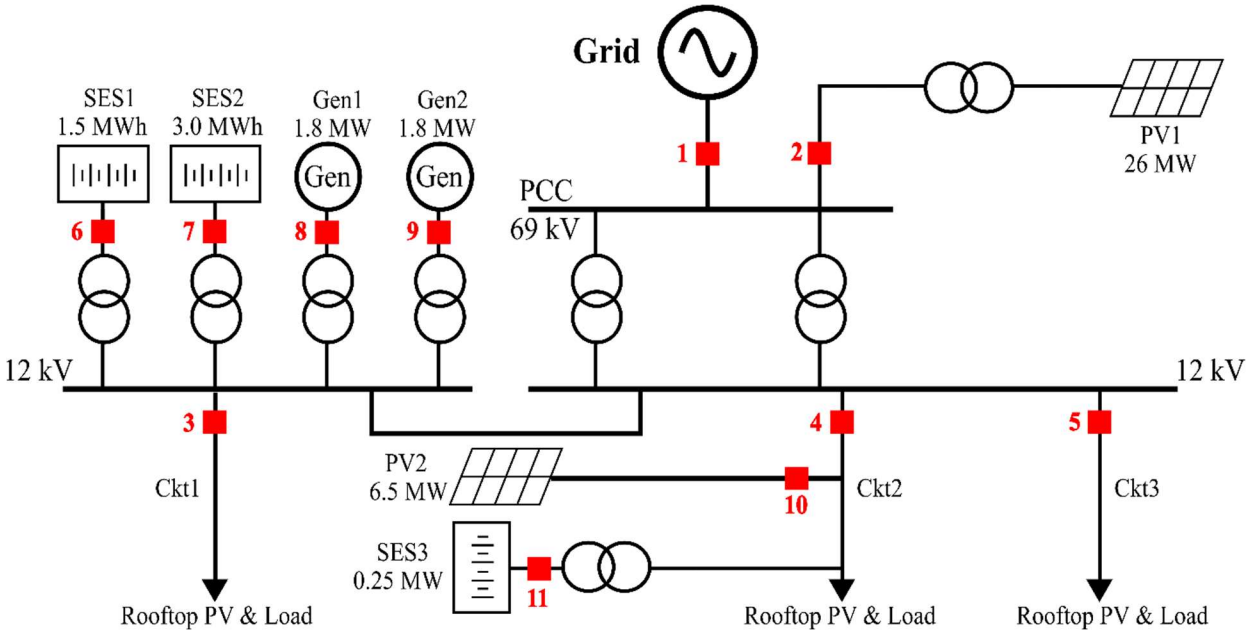

Figure 1. Simplified one-line diagram of the Borrego Springs Microgrid

2.1 Network Model

Load in the RSCAD model of the Borrego Springs Microgrid is modeled as unbalanced ZIP load that varies throughout the simulation. A ZIP model represents the relationship between the voltage magnitude and power in a polynomial equation that combines constant impedance (Z), current (I), and power (P) components. In the Borrego Springs model, the constant current load is zero. The PSCAD simulation tool has only a balanced ZIP load that cannot be varied during the simulation run. To emulate the load behavior in PSCAD, three-phase unbalanced constant impedance and power load were developed [7].

2.1.1 Constant Impedance

Varying passive elements (R, L, and C) are used to model the constant impedance load. The resistance element is used to represent the active power load. For any active power (P) and nominal voltage (V_{nom}), the resistance is calculated using Eq. 1:

$$R = \frac{V_{nom}^2}{P} \quad (1)$$

Similarly, inductance is used to represent the lagging reactive power. For the lagging reactive power (Q), nominal voltage (V_{nom}), and frequency (f), the inductance is calculated using Eq. 2:

$$L = \frac{V_{nom}^2}{Q * 2\pi f} \quad (2)$$

To model the leading power factor load, capacitance is used. For the leading reactive power (Q), nominal voltage (V_{nom}), and frequency (f), the capacitance is calculated using Eq. 3:

$$C = \frac{Q}{V_{nom}^2 * 2\pi f} \quad (3)$$

The three-phase unbalanced constant impedance load representation in PSCAD is shown in Figure 2.

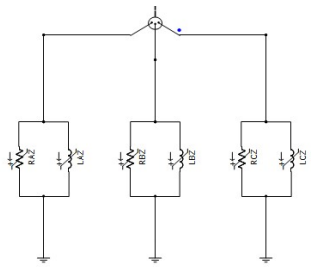

Figure 2. PSCAD model of a constant impedance load

2.1.2 Constant Power Load

A single-phase controllable current source is used to model the unbalanced dynamic power load. The current injection required to maintain constant power is derived from $S=V\angle\delta I\angle\beta$^*, where V is the terminal phase voltage, and δ and β are the voltage and current angles, respectively. For single-phase P and Q, the current is calculated using Eq. 4. Each instantaneous phase current is calculated using Eq. 5, where ω is the angular frequency:

$$I_{rms}\angle\beta = \frac{P}{V}\angle\delta - j\frac{Q}{V}\angle\delta \quad (4)$$

$$I_{inst} = \sqrt{2}\, I_{rms} \cos(\omega t + \delta + \beta) \quad (5)$$

The current angle (β) is calculated from Eq. 4, and the voltage angle (δ) is obtained from a single-phase phase-locked loop (PLL). Because a single-phase PLL is not available in PSCAD, a

second-order generalized integrator (SOGI) single-phase PLL is developed (Figure 3) to track the A, B, and C phase voltage angles and ω.

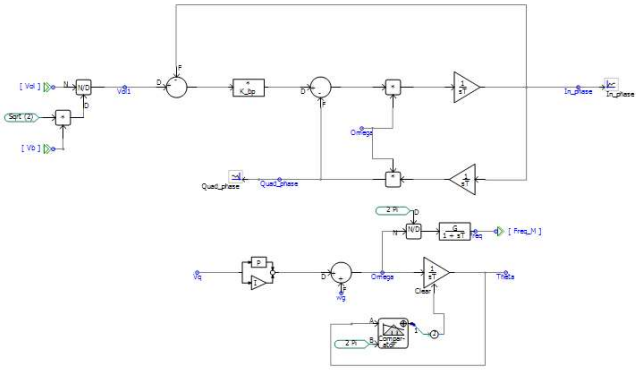

Figure 3. SOGI PLL control logic

Using Eq. 4, current injections for A, B, and C are calculated in Eq. 5, Eq. 6, and Eq. 7. The value of I_{rms} for each phase in Eq. 5, Eq. 6, and Eq. 7 is calculated from the respective P and Q, as shown in Eq. 3. When the terminal voltage (V) changes, the current injection in Eq. 5, Eq. 6, and Eq. 7 changes to maintain constant power at the terminal. This model can receive the load profile to vary the load consumption.

$$I_{inst\_Ap} = \sqrt{2}\, I_{rms\_Ap} \cos\left(\omega_{Aph} t + \delta_{Ap} + \beta_{Aph}\right) \quad (5)$$

$$I_{inst\_Bp} = \sqrt{2}\, I_{rms\_Ap} \cos\left(\omega_{Bph} t + \delta_{Bp} + \beta_{Bp}\right) \quad (6)$$

$$I_{inst\_Cp} = \sqrt{2}\, I_{rms\_Aph} \cos\left(\omega_{Cph} t + \delta_{Cph} + \beta_{Cp}\right) \quad (7)$$

Because time domain programs like PSCAD calculate instantaneous power, there will be a double-the-fundamental-frequency component in the P and Q measurements. The active and reactive power measurements need to be filtered to retain only the fundamental frequency component to compare against the power reference. For balanced load, the double-the-fundamental-frequency component becomes zero. The control block for the Phase A implementation in PSCAD is shown in Figure 4. A similar control logic is implemented for phases B and C.

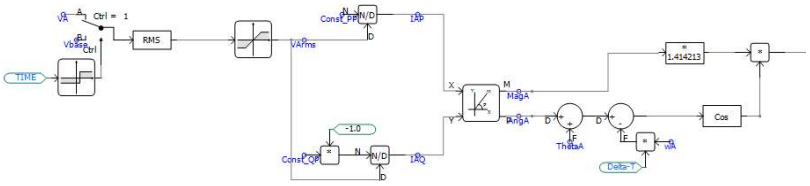

Figure 4. SOGI PLL control logic

2.1.3 Validation of Passive Network Model

The three feeders under consideration (Ckt1, Ckt2, and Ckt3) are operated in radial mode because the breakers between the feeders are normally open. The accuracy of the PSCAD model is compared to the RSCAD power flow results for one load scenario. The real power, reactive power, and voltages are measured at the 69-kV source and at the head of feeders 1, 2, and 3 and

at nodes N101, N201, and N301, respectively. Measurement points are also located in each feeder at branching nodes. The model comparison results are shown in Table 2 through Table 5.

Table 2. The 69-kV Source Validation

Feeder Head	RSCAD	PSCAD	Error (%)
Active power (MW)	7.075	6.971	1.47
Reactive power (MVAR)	-1.3	-1.38	-6.15
Voltage LN (kV)	40.94	40.93	0.02

Table 3. Feeder Ckt1 Validation

	Active Power			Reactive Power			Voltage LN		
Node	RSCAD (MW)	PSCAD (MW)	Error (%)	RSCAD (MVAR)	PSCAD (MVAR)	Error (%)	RSCAD (kV)	PSCAD (kV)	Error (%)
101	1.928	1.927	0.05	-1.885	-1.885	0.00	7.185	7.183	0.03
1041	1.721	1.719	0.12	-2.07	-2.071	-0.05	7.24	7.24	0.00
1091	1.038	1.039	-0.10	-0.9652	-0.9666	-0.15	7.24	7.241	-0.01
111	0.7761	0.7765	-0.05	-1.054	-1.055	-0.09	7.219	7.22	-0.01
105	-0.6697	-0.6688	0.13	-1.113	-1.113	0.00	7.238	7.239	-0.01
107	-0.6079	-0.6075	0.07	-1.134	-1.134	0.00	7.238	7.239	-0.01

Table 4. Feeder Ckt2 Validation

	Active Power			Reactive Power			Voltage LN		
Node	RSCAD (MW)	PSCAD (MW)	Error (%)	RSCAD (MVAR)	PSCAD (MVAR)	Error (%)	RSCAD (kV)	PSCAD (kV)	Error (%)
201	1.802	1.803	-0.06	-0.6723	-0.6712	0.16	7.183	7.182	0.01
2031	-1.493	-1.495	-0.13	-0.8013	-0.8002	0.14	7.159	7.157	0.03
208	0.6075	0.6078	-0.05	-1.095	-1.095	0.00	7.152	7.151	0.01
2051	0.5109	0.512	-0.22	0.1808	0.1708	5.53	7.159	7.157	0.03
206	-0.909	-0.9098	-0.09	0.9946	0.9945	0.01	7.156	7.155	0.01
2132	-0.349	-0.3495	-0.14	-0.1152	-0.1153	-0.09	7.123	7.122	0.01

Table 5. Feeder Ckt3 Validation

	Active Power			Reactive Power			Voltage LN		
Node	**RSCAD (MW)**	**PSCAD (MW)**	**Error (%)**	**RSCAD (MVAR)**	**PSCAD (MVAR)**	**Error (%)**	**RSCAD (kV)**	**PSCAD (kV)**	**Error (%)**
301	2.041	2.044	-0.15	-0.5415	-0.5407	0.15	7.137	7.137	0.00
305	-1.578	-1.58	-0.13	-0.7262	-0.7254	0.11	7.08	7.08	0.00
306	-1.205	-1.206	-0.08	-0.3981	-0.3973	0.20	7.002	7.003	-0.01
309	0.6398	0.6409	-0.17	0.21	0.2099	0.05	6.98	6.9807	-0.01
311	0.3612	0.3619	-0.19	-1.139	-1.137	0.18	7.081	7.082	-0.01

Low-error voltages in each feeder validate the accuracy of the line parameters and load models. Except for the reactive power at one node, the maximum model validation error of 0.2% among feeders A, B, and C shows that the PSCAD passive model closely resembles the RSCAD model. The feeder head reactive power error is -6.15%, which seems high; however, the absolute error in reactive power is 0.08 MW, which is similar to the absolute error in the active power (0.104 MW). Because the reactive power is low (-1.3 MVAR), the calculated error is relatively high. Note that this error in the reactive power is from the magnetizing power of the two transformers connected to the feeder head/the utility grid and one transformer connected to the PV plant. The comparison among three circuits—Ckt1, Ckt2, and Ckt3—shows that the reactive power at the beginning of each circuit matches these two models. At node N2051 in Feeder B, the reactive power error is approximately 5.5%. Further investigation of the upstream and downstream nodes around N2051 revealed that the reactive power error is less than 0.2%. Due to the low error at all other nodes in Ctk3, the N2051 reactive power mismatch was determined to be because of a measurement issue. This issue will be further investigated along with the reactive power mismatch at the source. The accuracy of the PSCAD model is validated by the fact that the error is very low in all three feeders. This also validates the accuracy of the developed load models (constant impedance and current). Therefore, the PSCAD model is a close approximation of the Borrego Springs model.

The Borrego Springs network has several transformers that consume reactive power. The approximate values of the reactive power consumption in the simulation are shown in Table 6. The total reactive power requirement for the transformers is approximately 1.84 MVAR in addition to the network load.

Table 6. Transformer Reactive Power Consumption

Transformer	Reactive Power (MVAR)
69/12-KV transformers	0.196
SES1 and SES2	0.05
SES3	0.022
PV1	1.26
Rooftop PV transformer	0.3
Total	**1.84**

2.2 Diesel Generators

The two diesel generators (Gen1, Gen2), shown in Figure 1, are modeled in PSCAD, and the control schematics for the generators are shown in Figure 5. These generators are rated at 1.825 MVA each and operate at 480-V nominal voltage. The diesel generators are connected through a step-up transformer at 0.48/12 kV to connect to the medium-voltage grid. The circuit breaker connected at the diesel generator terminal is called "GCB," and the breaker on the 12-kV side of the network is called "Grid."

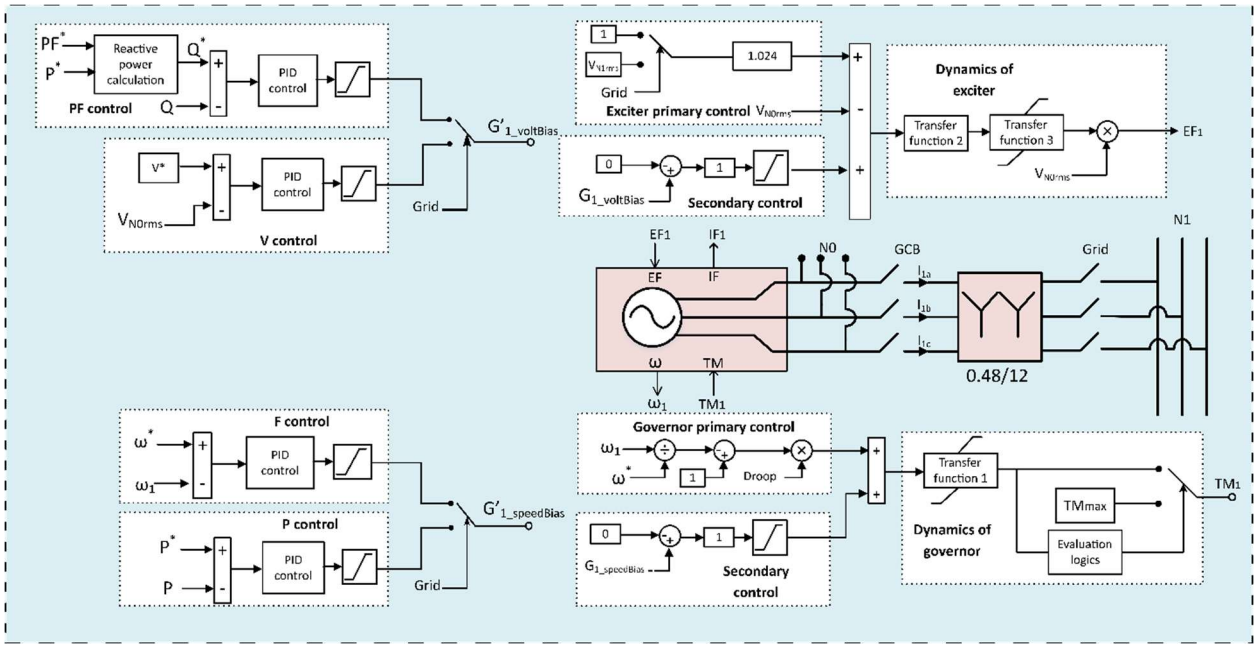

Figure 5. Schematic diagram of the diesel generator control block

The diesel generator control schematics shown in Figure 5 consists of a governor and exciter and primary and secondary controls. The governor regulates the diesel generator's throttle to control the power/frequency, and the exciter controls the diesel generator's voltage and volt ampere reactive (VAR). The dynamics of both the governor and exciter are represented using transfer functions. The outputs of the governor and exciter are the torque (TM1) and field voltage (EF1), which are given as inputs to the synchronous machine shown in Figure 5. The governor primary control is a droop control that uses an adjustable parameter of 2.2%. The exciter primary control

has a 1.024 gain to maintain 1-per-unit (p.u.) rated voltage on the grid side (N1). $G_{1\_speedbias}$ and $G_{1\_voltbias}$ are the speed bias and voltage bias generated from the secondary control to adjust the diesel generator's speed and voltage, respectively. Rate limiters and proportional-integral-derivative (PID) controls are the main parameters that need to be tuned to achieve the desired transient response.

The diesel generators have three operation modes: startup and synchronization (voltage-frequency [VF] control), grid-connected (PQ control), and isochronous (VF control). The model shifts between the control modes based on the grid and diesel generators' breaker statuses. More details on the diesel generator modeling can be found in the published paper for diesel generator testing [8].

2.3 Distributed Energy Resource Modeling

2.3.1 Grid-Following Photovoltaic Inverters

PV1, PV2, and the rooftop PV are modeled as GFL inverters. All GFL inverters are average models of a controlled voltage source followed by a filter. The control block diagram is shown in Figure 6. The inverter receives the power set points (P_{ref}, Q_{ref}), which generate the direct-quadrature (*dq)* current references (I_d^*, I_q^*) using the Park transformation and are passed through the dynamic current limiter. The referenced currents generated from the power references are compared to the derived currents (I_{d_mea}, I_{q_mea}), which are calculated from the current measurements. The current controller consists of a proportional-integral (PI) controller and grid voltage feed-forward terms that together minimize the error and generate the *dq* voltage references (V_d, V_q). These voltages in the synchronous reference frame are then converted to natural reference frame voltages (*abc*) using the inverse Park transformation.

The PV1 model has an LCL filter, consisting of two series inductors and a shunt capacitor connected at the midpoint between the inductors, with the parameters obtained from the field. This model can work in either *PQ* control mode or with a smart inverter function (volt-VAR with VAR priority and active power maximum power point tracking). PV2 is a legacy and noncontrollable facility, and it works in unity power factor mode. The distributed rooftop PV units operate in unity power factor mode. PV2 and the rooftop PV are modeled using an L filter.

The 26-MW PV facility, PV1, consists of 54 inverters of 500 kW each in the field, but it is aggregated and modeled using 20 inverters of 1.3 MW each in PSCAD. The 4.5 MW of rooftop PV are distributed at customer sites in the field, but the rooftop PV is aggregated in PSCAD. There are 22 total rooftop PV systems in the RSCAD model, which were disaggregated and modeled using 82 inverters of different ratings and placed at the same locations as in the RSCAD model.

The voltage and frequency trip and ride-through settings are included in the PSCAD model. The inverters of PV1 comply with the Institute of Electrical and Electronics Engineers (IEEE) Std 1547-2018 in the field, and therefore those settings are used in PSCAD [9]. The rooftop PV units are a mix of legacy and more modern inverters, but because they are aggregated in the PSCAD model, that could not be reflected, and therefore they are all modeled as IEEE Std 1547-2003 compliant.

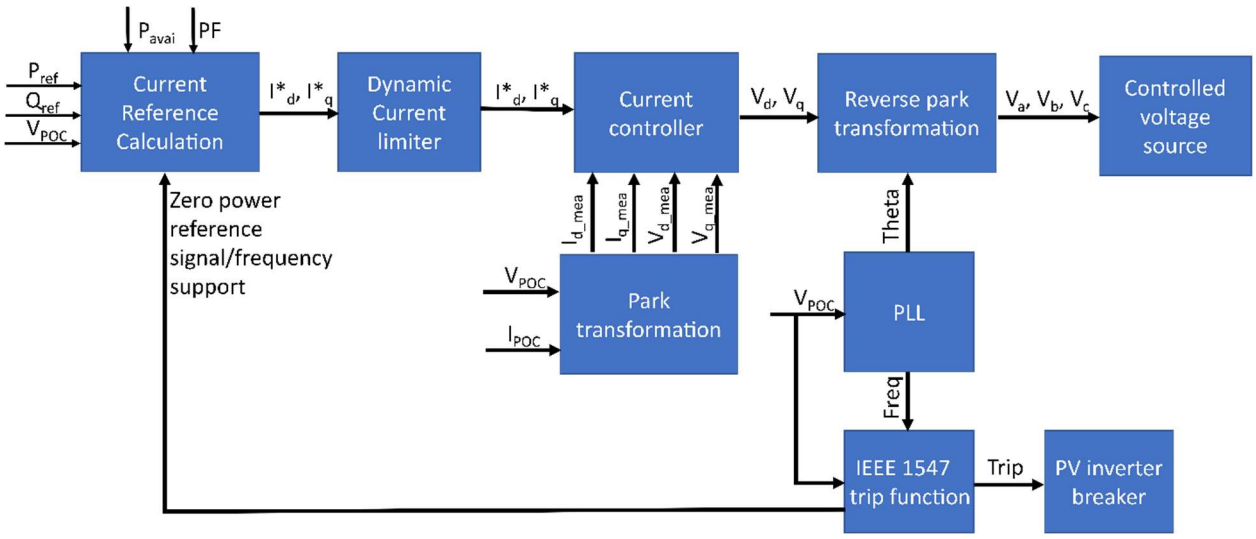

Figure 6. GFL inverter control block diagram

2.3.2 Grid-Forming Inverter

SES1, SES2, and SES3 are modeled as GFM inverters. The PSCAD model of the GFM inverter was developed to represent the state of the art in GFM inverters. We were unable to use an inverter model provided by the manufacturer, so we used a model developed by the National Renewable Energy Laboratory that was reviewed and approved as sufficiently representative of the field inverter by the manufacturer and SDG&E. The control diagram of the GFM inverter model is shown in Figure 7. This GFM inverter model has a traditional double-loop structure with an outer loop for power control (PQ control) or voltage control (VF control), depending on the operation mode, and an inner current loop. There are three operation modes of the inverter model: startup (VF control), grid-connected (PQ control), and islanding leader (VF control). The model can shift between the control modes based on the point of common coupling (PCC) circuit breaker status. In PQ control mode, the GFM inverter is IEEE Std 1547-2018 compliant.

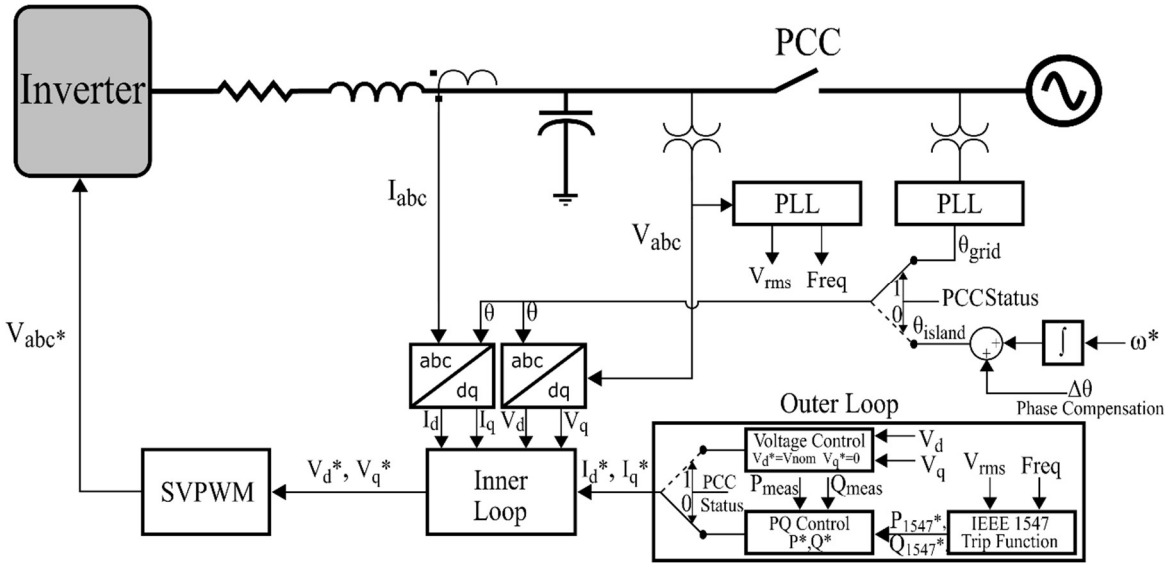

Figure 7. GFM inverter control block diagram

The GFM inverter is initialized in VF control to start up and connect to the network by closing the PCC breaker after synchronization. When the PCC breaker is closed, the outer loop control shifts from VF to PQ mode following the power set points. If the inverter is the island leader and it is in islanded operation, it shifts from PQ to VF mode when the PCC breaker is opened, and then ω is determined from the selected operation mode, i.e., isochronous mode or droop relationship. One important feature of this control structure is that the phase angle for the Park transformation (abc/dq0) switches between a grid-connected GFL angle (θ_{grid}) and an islanded self-generated angle (θ_{island}). To have a smooth islanding transition, the phase angle difference between the grid phase angle and the self-generated phase angle is calculated and added to the GFM inverter phase angle after the PCC circuit breaker is opened. The current references generated from the outer loop (I_d^*, I_q^*) are passed onto the inner current loop, which include a PI control and a grid voltage feed-forward term. Finally, the voltage references from the inner current loop are converted to three-phase voltage signals for the pulse-width modulation (PWM)generation to control the average switching model.

The inverter model is also equipped with additional grid-supporting functions in GFL mode. These are discussed in the following subsections.

Active/reactive power priority: Under normal operation, GFL inverters track the power reference commands subject to the maximum current limit. During frequency or voltage contingency events, inverters are required to support the grid by generating/absorbing active or reactive power; therefore, the active power (P) or reactive power (Q) reference command is implemented using current-limiting logic to prioritize one over the other. In an active power priority scenario, the model prioritizes the active power set point, and the reactive power is limited to the remaining device capacity. With reactive power priority, the model provides reactive power output in response to the voltage measurements at the terminal. The amount of power injection is determined from a predefined volt-VAR curve subject to the device rating. The reactive power output is changed once per second to minimize the oscillations. At the same time, the active power is curtailed if there is less capacity of active power than the commanded active power because of VAR priority. Note that SES3 uses a frequency fast response function to support and maintain the frequency during islanding operation.

Ride-through mode: During grid-connected mode, inverter tripping under grid disturbances can cause grid instability, leading to blackouts; therefore, interconnection standards require inverters to ride through disturbances and restore power to the pre-disturbance levels [9]. During voltage disturbances, voltage sags at the inverter terminals trigger voltage ride-through mode. For voltages outside the continuous operating range, the model stays connected in constant power mode or enters cessation mode. During frequency disturbances, the model responds by increasing/decreasing the active power based on a droop relationship. The magnitude of the active power is calculated from the equations described in Table 23 of IEEE Std 1547-2018.

2.4 IEEE Std 1548-2018 Ride-Through Modeling

GFM and utility-scale inverters are equipped with IEEE Std 1547-2018 ride-through and trip settings. The ride-through and trip requirements for voltage and frequency are defined according to IEEE Std 1547-2018. Category III requirements are selected for the modeling. The ride-through requirements for voltage and frequency are modified for undervoltage and frequency to

avoid gaps in the default settings, as shown in Table 7 and Table 8, respectively. Figure 8 and Figure 9 show the selected simulation results for undervoltage and underfrequency.

Table 7. Modified Voltage Ride-Through Requirements

Voltage Range (p.u.)	Operating Mode	Minimum Ride-Through Time (s)	Maximum Response Time (s)
V > 1.20	Cease to energize	N/A	0.16
1.10 < V ≤ 1.20	Momentary cessation	12	0.083
0.88 ≤ V ≤ 1.10	Continuous operation	Infinite	N/A
0.50 ≤ V < 0.88	Mandatory operation	21	N/A
V < 0.50	Momentary cessation	1	0.083

Table 8. Modified Frequency Ride-Through Requirements

Frequency Range (Hz)	Operating Mode	Minimum Ride-Through Time (s)
f > 62	N/A	N/A
61.2 < f ≤ 62	Mandatory operation	300
58.5 ≤ f ≤ 61.2	Continuous operation	Infinite
56.5 ≤ f < 58.5	Mandatory operation	300
f < 56.5	N/A	N/A

Undervoltage mandatory operation (0.5 ≤ V < 0.88): As shown in Figure 8, when the terminal voltage decreases below 0.88 p.u., the active and reactive power references (P_{ref} and Q_{ref}) do not change. The power measurements (P_{meas} and Q_{meas}) change because the decrease in voltage is compensated by an increase in current until reaching a maximum limit (1.2 p.u.). In this case, the model is running on active power priority, so the reactive power becomes zero. The inverter model continues to inject power until it trips 21 seconds after the event starts, as required by the IEEE Std 1547-2018 trip settings. The trip time duration between the markers is noted.

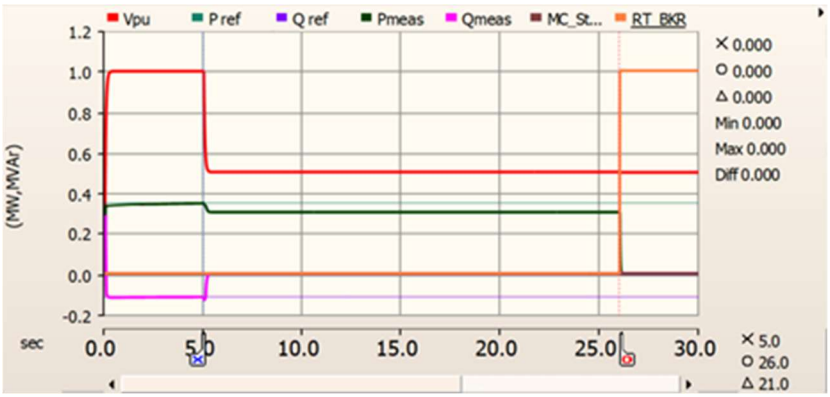

Figure 8. Undervoltage mandatory operation event

Underfrequency continuous operation (58.5 ≤ f < 61.2): When the frequency deviates from the nominal, the inverter model responds by increasing/decreasing the active power based on the low-/high-frequency droop relationship. The magnitude of the active power change is calculated from the equations described in Table 23 of IEEE Std 1547-2018. In this case, the frequency changes from 60 Hz (1 p.u.) to 59 Hz (0.9833 p.u.) 5 seconds into the simulation, as shown in Figure 9. The inverter increases the active power reference due to the low-frequency condition. The reactive power reference stays the same throughout the simulation. The inverter stays connected based on the requirement of the standard. It disconnects when the frequency drops below the continuous operating range.

Figure 9. Underfrequency continuous operation event

2.5 Microgrid Simulation With 100% Distributed Energy Resources

2.5.1 Network Parallelization

The full network of the Borrego Springs Microgrid contains distributed rooftop PV (82 inverters), utility-scale PV (PV1, 20 inverters), (PV2), and SES1, SES2, and SES3. To simulate the whole Borrego Springs Microgrid with 105 DERs, the system needs to be split into multiple projects to enhance the simulation speed and time. In PSCAD, the boundaries of these projects are defined via distributed parameter transmission lines and cables; therefore, the PI models of the lines connecting the Ckt2 and Ckt3 feeders are modeled as distributed lines of 1-km length each to split the network. The distributed lines are modeled to match the resistance and inductance parameters of the existing lines. Even though these distributed lines added fictitious

capacitance to the line, its impact is minimal on the overall reactive power flow. Figure 10 shows the network split in PSCAD. Project 1 comprises the grid, Ckt1, the BESS, and other generation sources. Projects 2 and 3 consist of the Ckt2 and Ckt3 networks along with rooftop PV. Due to the short line length (1 km) connecting projects 2 and 3, the time step is adjusted to 25 µs.

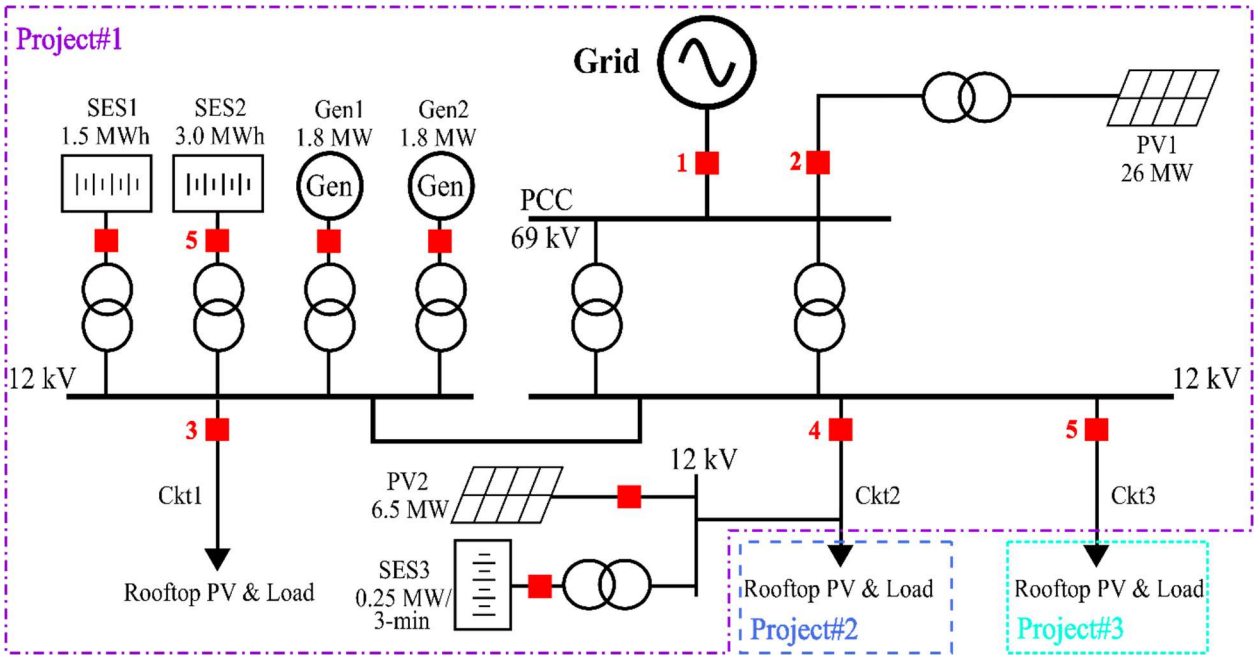

Figure 10. Borrego Springs network parallel simulation in PSCAD

2.5.2 Simulation Model Configuration

The full network model of the Borrego Springs Microgrid is divided into three individual projects at transmission lines connecting projects 2 and 3, as shown in Figure 10. Four different scenarios (listed in Table 13) need to be simulated to evaluate the stability of the full network. The simulation time step for all scenarios is 25 µs. Each scenario has different test cases that were developed based on the availability of the generation sources and microgrid load scenarios. The microgrid load and irradiance data for morning, noon, night are taken from the July 29, 2019, load data provided by SDG&E (see Figure 11 (a) & (b) and Figure 12). The solar generation and load data used for the simulation scenarios are listed in Table 9. The rooftop PV installed in each feeder is aggregated on the primary side of the transformer at 12 kV. Table 10, Table 11, and Table 12 show the rooftop PV installed capacity at various nodes in Ckt1, Ckt2, and Ckt3, respectively. The number of PV units in the table signifies the number of GFL inverters used to represent the PV. All the test cases for each scenario are listed in Table 14, Table 15, Table 19, and Table 22 . The model configuration, setup, and simulation duration for each test scenario are discussed in the following sections.

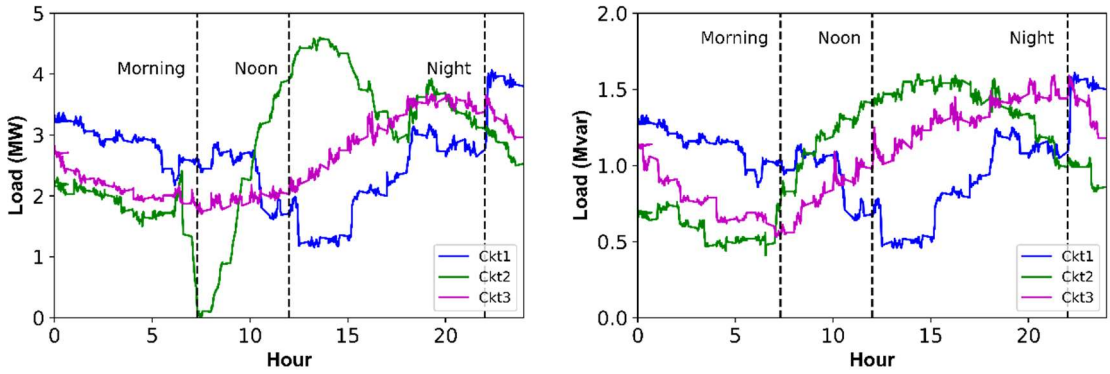

Figure 11. Load profile of Ckt1, Ckt2, and Ckt3 for July 29, 2019

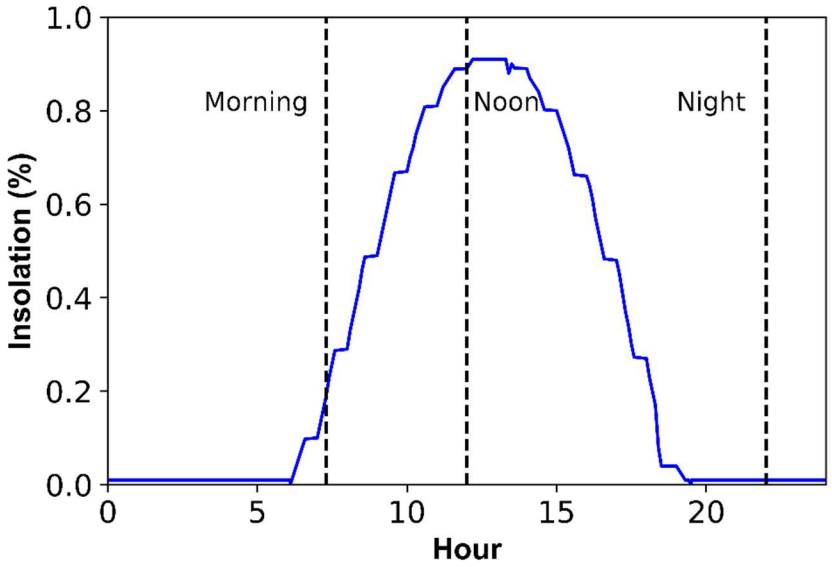

Figure 12. Solar insolation profile for July 29, 2019

Table 9. Solar and Load Data for the Morning, Noon, and Night Test Scenarios

Loading	Active Power (MW)	Reactive Power (Mvar)	Solar Insolation (p.u.)
Morning	5.25	2.5	0.2
Noon	8.8	3.5	0.9
Night	9.2	3.5	0

Table 10. Rooftop PV on Ckt1

Generation (kW)	Number of PV Units
8.95	1
1133	4
605	4
272	4

Table 11. Rooftop PV on Ckt2

Generation (kW)	Number of PV Units
7	1
42	4
68	4
33.81	4
32	4
125	4
254	4
230	4
64	4
97	4
428	4
60	4

Table 12. Rooftop PV on Ckt3

Generation (kW)	Number of PV Units
44.48	4
60	4
187	4
365	4
994	4
328	4

Planned islanding: For each load scenario, the load scaling factors for each circuit are derived from the passive network model simulation. Next, the generation sources are enabled/disabled depending on their availability. The rooftop and PV2 sources generate power based on the solar irradiance data, and PV1 is dispatched based on the need as well as the available power from the solar irradiance data. The simulation starts with the main PCC breaker closed and the GFM (SES2) breaker open. The operating conditions, such as P/Q priority and the ride-through parameters, are set prior to the simulation run. The initial transients from the model initialization

settle within approximately 0–2 seconds. At 2 seconds, a command is given to SES2 to start the synchronization with the grid and close the breaker. SES2 adjusts its voltage and frequency based on the PCC quantities. When the voltage, frequency, and phase angle are within the set quantities, the breaker automatically closes, and SES2 is connected to the breaker. When the PCC breaker is closed, SES2 operates in GFL mode and changes to GFM as soon as the PCC breaker opens. At 5.6 seconds, the PCC breaker opens to create the microgrid island where SES2 acts as a GFM inverter. The simulation is run for an additional 4.4 seconds after the PCC breaker opens to allow any oscillations to settle. The total simulation run is kept at 10 seconds.

When the diesel generator operates as a GFM in test cases 2, 3, 7, and 8, SES1 and SES2 are offline. All initial conditions and sequences of events are similar to the conditions previously discussed. Compared to an inverter, the diesel generator takes more time (approximately 9 seconds) to adjust its voltage and frequency to synchronize and close the breaker. In this case, the PCC breaker opens at 12 seconds, and the total simulation duration is kept at 20 seconds so that the diesel generator response can be captured.

Unplanned islanding: Load scaling factors derived in the planned islanding are used for the unplanned islanding test cases. Depending on the availability of the generation sources, PV1, PV2, and SES3 are enabled/disabled. Because the islanding events are unplanned, the dispatches of the generation sources are kept the same during grid-connected and islanded mode. SES1 stays connected, but the power dispatch is kept the same. The PCC breaker is set to open at 5.6 seconds, and the total duration of the simulation is set at 10 seconds.

Black start: For three test cases, load factors derived in the planned islanding scenario are used. The sequence of power restoration to load in the network is given by SDG&E. The dispatch of the GFL source SES1 is calculated from the load prior to the breaker switching. For the next load in the sequence, the SES1 and SES2 generation levels are revised after any rooftop PV comes online after the last load switching. When the SES1 resource is fully used, SES2 picks up the load until it reaches its capacity. At every step in the load sequence with SES1, two generation levels are validated from the simulation. The total simulation duration varies based on the number of loads energized in the black-start sequence.

Contingency events: The contingency scenarios are simulated after establishing the stable islanded microgrid. The simulation is initialized using the snapshot taken from the respective planned islanding scenarios. The snapshot is captured when the microgrid is islanded and stable. Later, the respective contingency event (fault, load rejection generation drop-off, etc.) is simulated to study the GFM response. The total duration of the simulation varies depending on the time it takes for the microgrid to stabilize.

3 Testing Scenarios

At the request of our project partner (SDG&E), we focus on the simulation evaluation to study the behavior of multiple GFM and GFL inverters under dynamic conditions—such as black-start, islanding, and contingency events (e.g., load rejection and sudden cloud cover)—during islanded operation. Each simulation scenario runs approximately 20–60 seconds, and the simulation time step is 25 µs. The time of 20 seconds was decided based on the settling time of the system from other projects with a similar network setup; therefore, we focus on the following four scenarios to evaluate the transient stability of the Borrego Springs Microgrid system. Table 13 summarizes all the testing scenarios for this project.

Table 13. Testing Scenarios

Scenario	Description
Black start	A black start is a very important scenario, especially to test the capability of the GFM and black-start-capable battery inverter and islanding leader, SES2. SDG&E provides the field sequence/restoration steps. This scenario has a series of dynamic operations of reconnecting DERs and load; therefore, the simulation time might be longer than 60 seconds. We also anticipate having to speed up the restoration sequence compared to what would be done in the field to keep the total simulation time reasonable.
Planned islanding	This is the most critical scenario to test for the Borrego Springs Microgrid. In this case, the microgrid controller reduces the power flow across the PCC to near zero before opening the microgrid switch. A disconnection logic is developed to control the PCC circuit breaker. Three different load conditions are simulated: morning, noon, and night. For each load condition, a combination of the availability of different grid assets is designed to investigate all possible situations.
Unplanned islanding	Unplanned islanding might happen, and it is important to test the stability of the microgrid system. For example, if a fault happens in the main grid, the PCC relay will open the PCC switch. Three different load conditions are simulated: morning, noon, and night. For each load condition, a combination of the availability of different grid assets is designed to investigate all possible situations.
Contingency events	This tests the islanded microgrid under selected disturbance events to evaluate the disturbance metrics of the microgrid. Events include: • Faults (line to ground [LG], double line to ground [LLG], triple line to ground [LLLG]) • Loss of generation (e.g., SES1) • Load rejection. For each event, three different load conditions are simulated: morning, noon, and night.

4 Black Start

A black start in power systems refers to restarting the network after a blackout event. The ability to restart the network improves resilience and has significant economic and societal consequences [10]. The Borrego Springs Microgrid network is simulated under various black-start scenarios, as shown in Table 14. These scenarios assess the black-start performance of SES2 (GFM) and validate the proposed sequence/restoration steps. The SES2 current limit is changed from 1.2 p.u. to 1.5 p.u. for the black-start cases. From among all the circuits shown in Figure 10, the Ckt1 load is higher than those of Ckt2 and Ckt3. From among all the simulation scenarios shown in Table 14, Ckt1 is not totally restored due to insufficient generation to pick up the bigger load. So, only the restoration of Ckt1 in the morning scenario is discussed in Section 4.1. The black start of all circuits under the morning, noon, and night scenarios is discussed in Section 4.2.

Table 14. Black-Start Operation Test Cases

Test No.	Loading	PV1	PV2	Rooftop PV	Diesel	SES1 and SES2	SES3
1	Morning	Offline	Offline	On	On	On	On
2	Noon	Offline	Offline	On	Offline	On	On
3	Night	Offline	Offline	Offline	On	On	On

4.1 Black Start of Only Ckt1

In this scenario, the microgrid system is blacked out, and the PCC circuit breaker opens to test the black-start capability of SES2. The objective is to use SES2 as a GFM source and SES1 as a GFL source to fully energize Ckt1, which includes rooftop PV, so the diesel generators are offline for these simulations. Ckt1 has a radial structure, as shown in Figure 13, which includes three zones that were identified based on the switching sequence. Zone 1 has light balanced load and rooftop PV, and zones 2 and 3 both have heavy unbalanced load and rooftop PV. In PSCAD, each Ckt1 load in Figure 13 is modeled as constant power (CP) and constant impedance (CI). The circuit load data and installed rooftop PV capacity are shown in Figure 13. Note that the breakers are numbered in the sequence in which they operate.

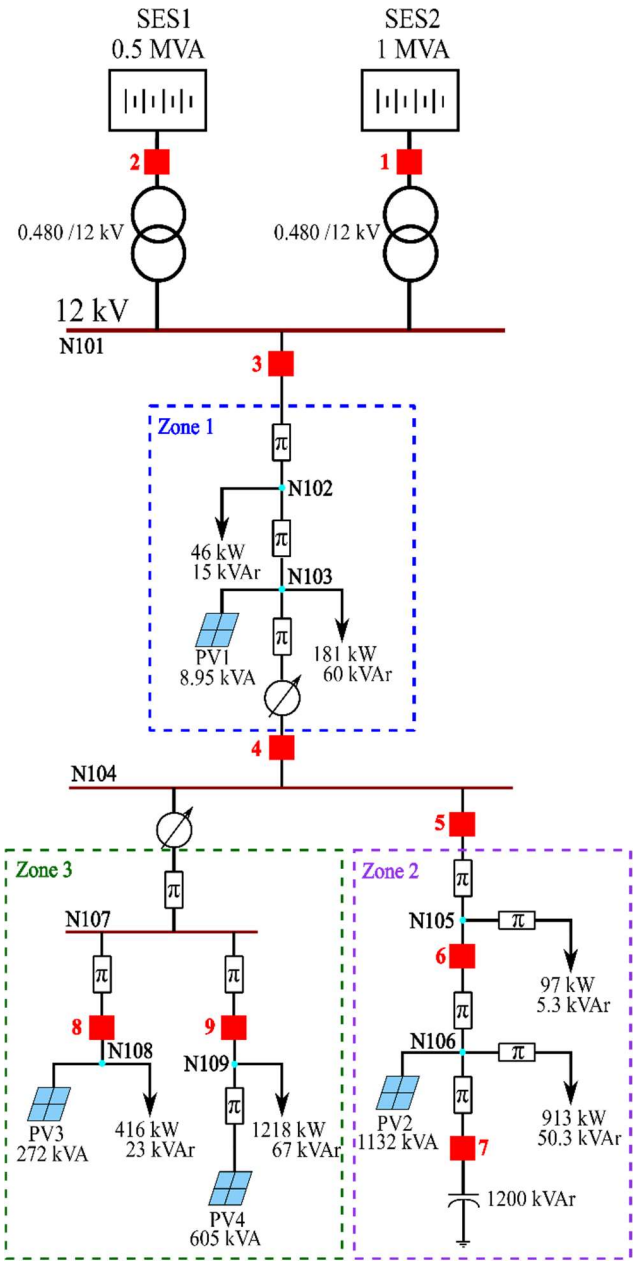

Figure 13. Borrego Springs Ckt1 one-line diagram

The accelerated black-start sequence is performed as follows:

1. SES2: Start the simulation and enable SES2 in startup (VF control) mode so that it can serve as a black-start GFM source. SES2 ramps up and energizes the 480-V bus. BKR1 closes at 1.5 seconds to connect with the grid transformer and energize the 12-kV bus.
2. SES1: With the 12-kV bus energization, close BKR2 at 2.5 seconds to connect SES1 in PQ control mode. SES2 is in standby mode, with zero power generation.
3. Zone 1: Close BKR3 to energize nodes N102 and N103 at 4 seconds; all four loads (two constant power, two constant impedance) are connected at the same time. The rooftop PV comes online at 12 seconds with an 8-second delay after the N103 energization; the

rooftop PV starts with zero power output, and it ramps up to 60% of capacity based on the assumed solar insolation conditions with unity lagging power factor.

4. Close BKR4 at 15 seconds to energize nodes N104 and N107.
5. Zone 2: Close BKR5 and BKR6 at 17 seconds and 25 seconds, respectively, to energize the Zone 2 nodes.
6. To reduce the power output from SES2, increase the SES1 contribution by changing the power reference commands at 27 seconds to 0.8 p.u. and 0.95 lagging power factor.
7. Before PV2 comes online, switch the capacitor bank in Zone 2 at 29 seconds to contribute 1.2-MVAR reactive power for voltage stability.
8. The larger PV (PV2) in Zone 2 comes online at 33 seconds with 60% generation and 0.95 power factor operation.
9. Zone 3: Connect the N108 load by closing BKR8 at 40 seconds and connect the aggregated rooftop PV to the circuit at 48 seconds.
10. Connect the final load in the circuit by closing BKR9 at 55 seconds; subsequently, the rooftop PV at N109 generates 60% of capacity from 63 seconds.

Figure 14 shows the voltage, frequency, and active and reactive power measurements of the primary side of the transformer that connects to SES2. The voltage and frequency measurements show that the overall black-start process is successful. These measurements show noise from 27 seconds with the addition of the Zone 2 and Zone 3 unbalanced load. This load causes negative-sequence harmonics, but the positive-sequence dq0 control in the SES2 inverter can control only the fundamental frequency component. A notch filter tuned to suppress the second harmonic is applied to the dq voltage measurements to filter out the second harmonic caused by the negative-sequence component. Due to the presence of third and fourth harmonics, the measurements become noisier with each addition of unbalanced load.

During the black-start process, the voltage and frequency are maintained at 1 p.u. and 60 Hz, respectively. The transient spikes shown in Figure 14 are due to the connection of the capacitor banks and the rooftop PV. In particular, the connection of a capacitor bank at 29 seconds causes a big transient spike in frequency and is also reflected in the voltage measurements. The connection of the end-of-line PV at N106 with a large capacity of 700 kW causes another spike in voltage and frequency (at 33 seconds). Most transients in the voltage and frequency measurements are caused by the addition of the rooftop PV units, which indicates interactions between the GFM and GFL inverters. Note that PV2, PV3, and PV4 have four GFL units connected in parallel. The active power output of SES2 shows a more expected response, increasing power with load connected and decreasing power with PV connected. The reactive power output shows a big transition from supplying reactive power to absorbing at 29 seconds because of the 1.2-MVAR capacitor bank switching.

Figure 14 also shows the voltage and power measurements at N106. The node is energized at 27 seconds, and the voltage ramps up to 0.98 p.u. until the capacitor bank switches. Due to the reactive power from the capacitor bank, the voltage at N106 is maintained between 1 p.u. and 1.02 p.u. The active power demand at N106 increases to 650 kW at 29 seconds, but it decreases

to near zero because of large rooftop PV coming online at 33 seconds. Overall, the results presented in Figure 14 indicate a successful fast black start of Ckt1.

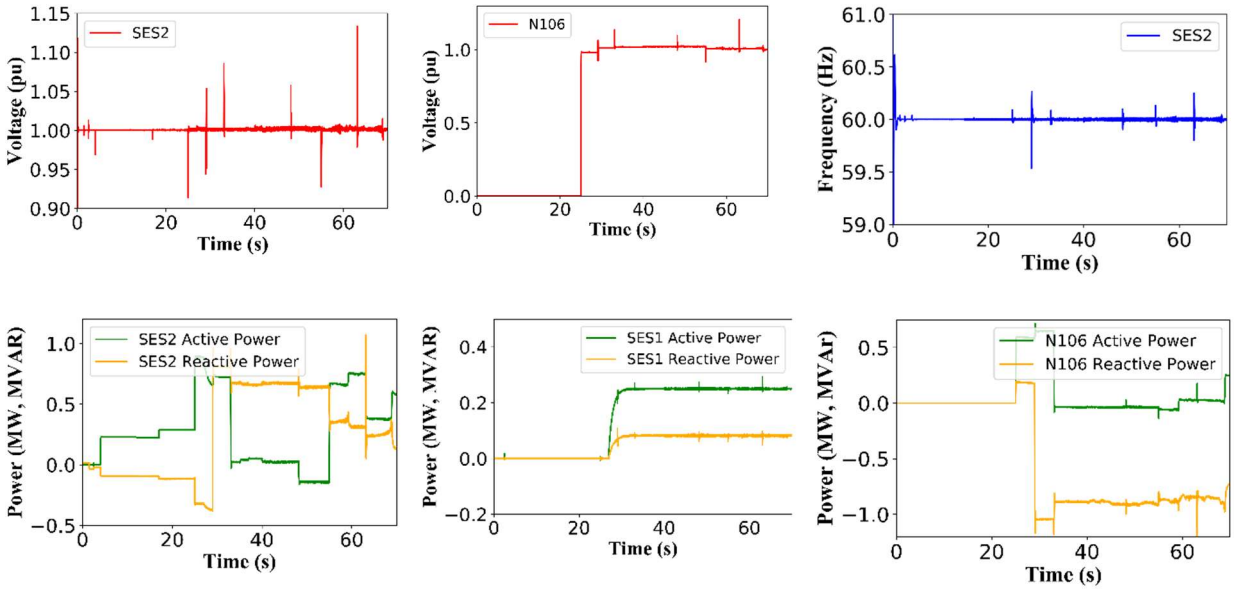

Figure 14. SES2, SES1, and end-of-feeder voltage, frequency, and power measurements

4.2 Black Start of the Whole Microgrid

SES2, SES1, the rooftop PV, and the capacitor banks are used as generation sources. In this case, SES2 operates as a GFM source; SES1 and the rooftop PV operate as GFL resources. The sequence of load coming online is based on the black-start sequence of the 12-kV bus provided by SDG&E with the 69-kV bus unavailable. The sequence starts with Ckt2, shown in Figure 15, because the microgrid's critical loads are located in Ckt2, then proceeds to Ckt3, shown in Figure 16, and then to Ckt1, shown in Figure 13.

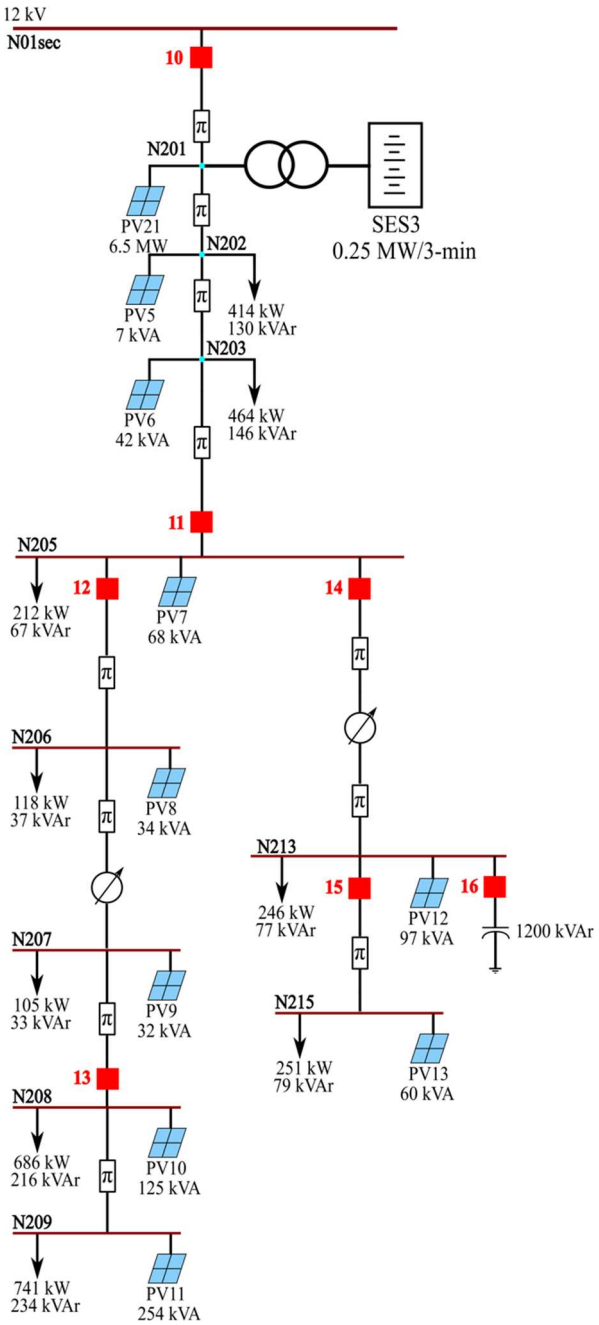

Figure 15. Borrego Springs Ckt2 one-line diagram

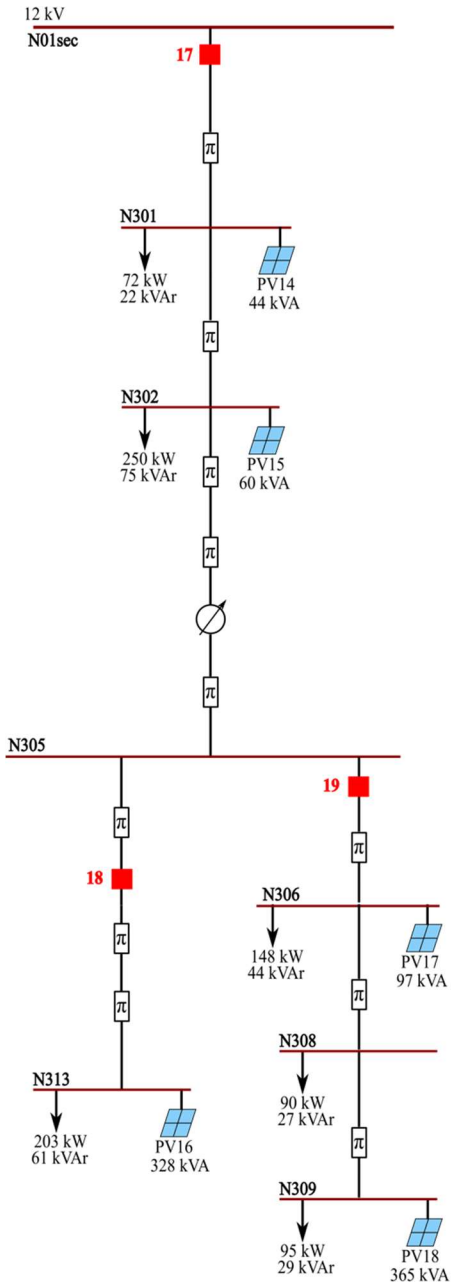

Figure 16. Borrego Springs Ckt3 one-line diagram

In PSCAD, an accelerated black start is performed to reduce the total simulation time. The main assumptions for the black-start simulation are:

- Ckt1, Ckt2, and Ckt3 are operated as radial feeders. The intertie switches are assumed to be open.
- The state of charge of SES1 and SES2 is assumed to be 100%.
- The rooftop PV operates at 0.95 lagging power factor and comes online 5 seconds after the connecting bus is energized.
- PV2 is offline.
- The overcurrent limit of SES2 (GFM) is set to 1.5 p.u.

4.2.1 Morning Scenario

The black-start sequence of the simulation is shown in

Figure 17, including the load pickup for the respective circuits and the status of SES1 and SES2. The rooftop PV comes online 5 seconds after the connected bus is energized. An accelerated black start is performed to reduce the overall simulation time.

Seq	Time (s)	Breaker Switching	PV Switching	Pload	Qload	SES1		PV2		Capacitor Banks	Rooftop PV		SES2		
						Pgen	Qgen	Pgen	Qgen	Qgen	Pgen	Qgen	Pgen	Qgen	S (MVA)
1	5	10		0.00	0.09	0.00	0.00	0.00	0.00	0.00	0.00	0.00	0.00	0.09	0.09
2	10		PV5	0.00	0.00	0.00	0.00	0.00	0.00	0.00	0.00	0.00	0.00	0.09	0.09
3	13	11		0.00	0.05	0.00	0.00	0.00	0.00	0.00	0.00	0.00	0.00	0.14	0.14
4	18		PV6, PV7	0.00	0.00	0.00	0.00	0.00	0.00	0.00	-0.04	0.01	-0.04	0.15	0.16
5	23	12		0.02	0.05	0.00	0.00	0.00	0.00	0.00	0.00	0.00	-0.02	0.20	0.20
6	28		PV8, PV9	0.00	0.00	0.00	0.00	0.00	0.00	0.00	-0.04	0.01	-0.06	0.21	0.22
7	30			0.00	0.00	-0.50	0.00	0.00	0.00	0.00	0.00	0.00	-0.56	0.21	0.60
8	33	13		0.15	0.32	0.00	0.00	0.00	0.00	0.00	0.00	0.00	-0.41	0.53	0.67
9	38		PV10, PV11	0.00	0.00	0.00	0.00	0.00	0.00	0.00	-0.23	0.07	-0.63	0.61	0.88
10	43	17		0.33	0.18	0.00	0.00	0.00	0.00	-1.20	0.00	0.00	-0.30	-0.42	0.51
11	48		PV14, PV15	0.00	0.00	0.00	0.00	0.00	0.00	0.00	-0.06	0.02	-0.36	-0.40	0.54
12	50	14		0.08	0.06	0.00	0.00	0.00	0.00	0.00	0.00	0.00	-0.29	-0.33	0.44
13	55		PV12	0.00	0.00	0.00	0.00	0.00	0.00	0.00	-0.06	0.02	-0.34	-0.32	0.47
14	57	15		0.08	0.06	0.00	0.00	0.00	0.00	0.00	0.00	0.00	-0.27	-0.25	0.37
15	62		PV13	0.00	0.00	0.00	0.00	0.00	0.00	0.00	-0.04	0.01	-0.30	-0.24	0.39
16	63	18		0.21	0.11	0.00	0.00	0.00	0.00	0.00	0.00	0.00	-0.09	-0.13	0.16
17	68		PV16	0.00	0.00	0.00	0.00	0.00	0.00	0.00	-0.20	0.06	-0.29	-0.07	0.30
18	69	19		0.35	0.18	0.00	0.00	0.00	0.00	0.00	0.00	0.00	0.06	0.11	0.13
19	74		PV17, PV18	0.00	0.00	0.00	0.00	0.00	0.00	0.00	-0.33	0.11	-0.27	0.22	0.35
20	75	3		0.23	0.07	0.00	0.00	0.00	0.00	0.00	0.00	0.00	-0.04	0.30	0.30
21	80		PV1	0.00	0.00	0.00	0.00	0.00	0.00	0.00	-0.01	0.00	-0.05	0.30	0.30
22	82	8		0.42	0.14	0.00	0.00	0.00	0.00	0.00	0.00	0.00	0.37	0.43	0.57
23	87		PV3	0.00	0.00	0.00	0.00	0.00	0.00	0.00	-0.16	0.05	0.20	0.49	0.53
24	88	9		1.22	0.39	0.00	0.00	0.00	0.00	0.00	0.00	0.00	1.42	0.88	1.67

Figure 17. Morning scenario black-start sequence

The results for the whole microgrid system black-start sequence are shown in two separate time blocks (45 seconds). Figure 18 shows the simulation results for SES2 (GFM) and SES1 (GFL). The observed transients are related to the load pickup shown in

Figure 17. With each recloser switching, SES2 increases its active and reactive power output until the rooftop PV comes online. At approximately 15–16 seconds in Figure 18 (a)–(c), a transient causes SES2 to supply more power. This is caused by the interactions between the load

picked up at 13 seconds and SES2. To reduce the active power load of SES2, SES1 is brought online at 30 seconds with full power generation (see Figure 18 (f)). The power and voltage show oscillations up to 0.25 MW and 0.2 p.u., respectively. The source behind the oscillations is investigated. The root-mean-square (RMS) current in Figure 18 (d) shows that SES2 does not exceed its current capacity of 1.2 kA.

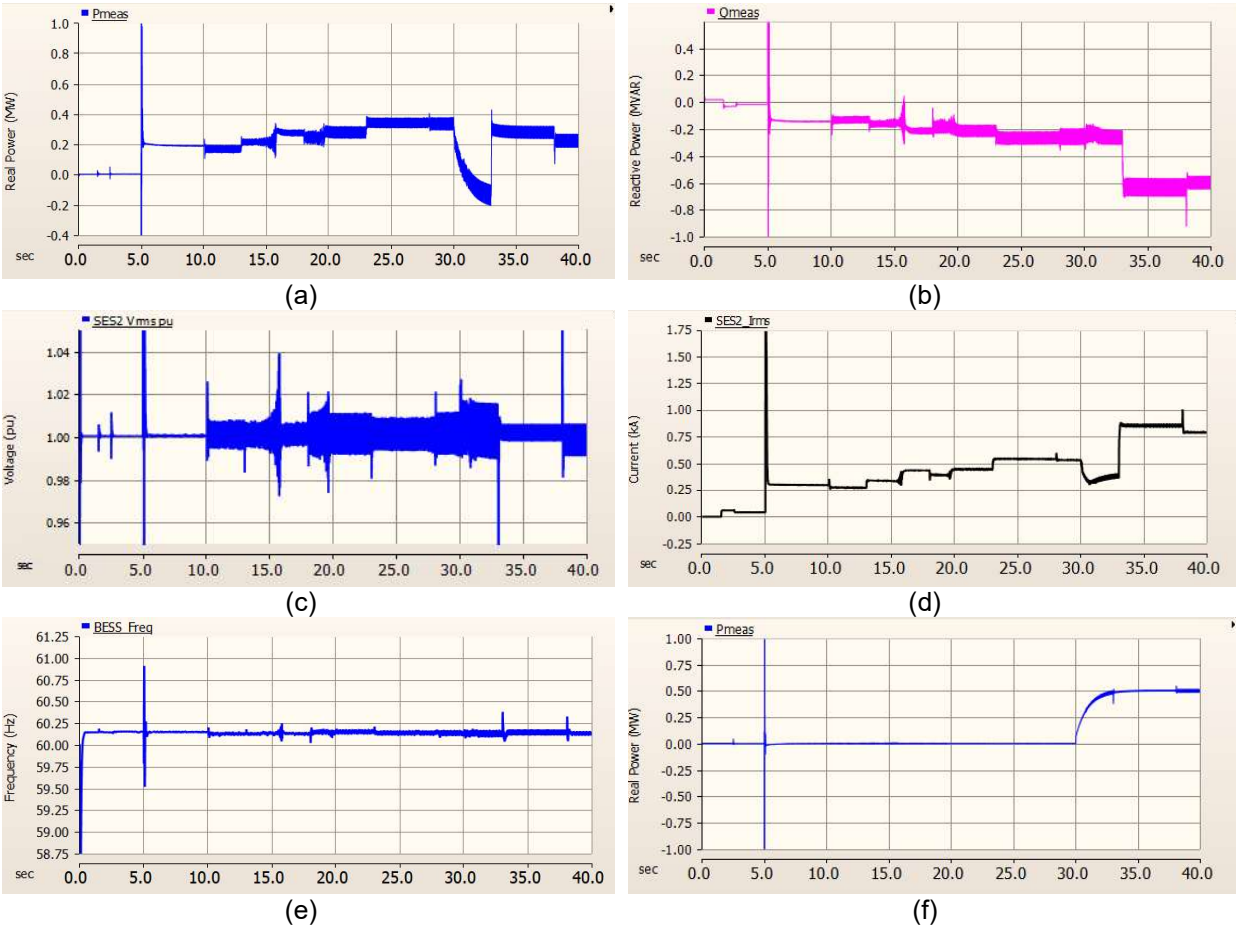

Figure 18. Morning scenario black-start sequence from 0–40 seconds: (a) and (b) SES2 GFM active and reactive power, (c) and (d) SES2 RMS voltage and current, and (e) and (f) SES2 frequency and SES1 (GFL) active power

The second part of the black-start sequence occurs from 40–90 seconds, as shown in

Figure 17. The power, voltage, current, and frequency measurements of SES2 are shown in Figure 19 (a)–(f). To reduce the reactive power load on SES2, the capacitor bank in Ckt3 switches on at 43 seconds to supply 1.2 MVAR, and, as a result, the SES2 reactive power changes from generating to absorbing (see Figure 19 (b)). The current measurements in Figure 19 (d) show that SES2 does not exceed its current rating but approaches the limits after 74 seconds.

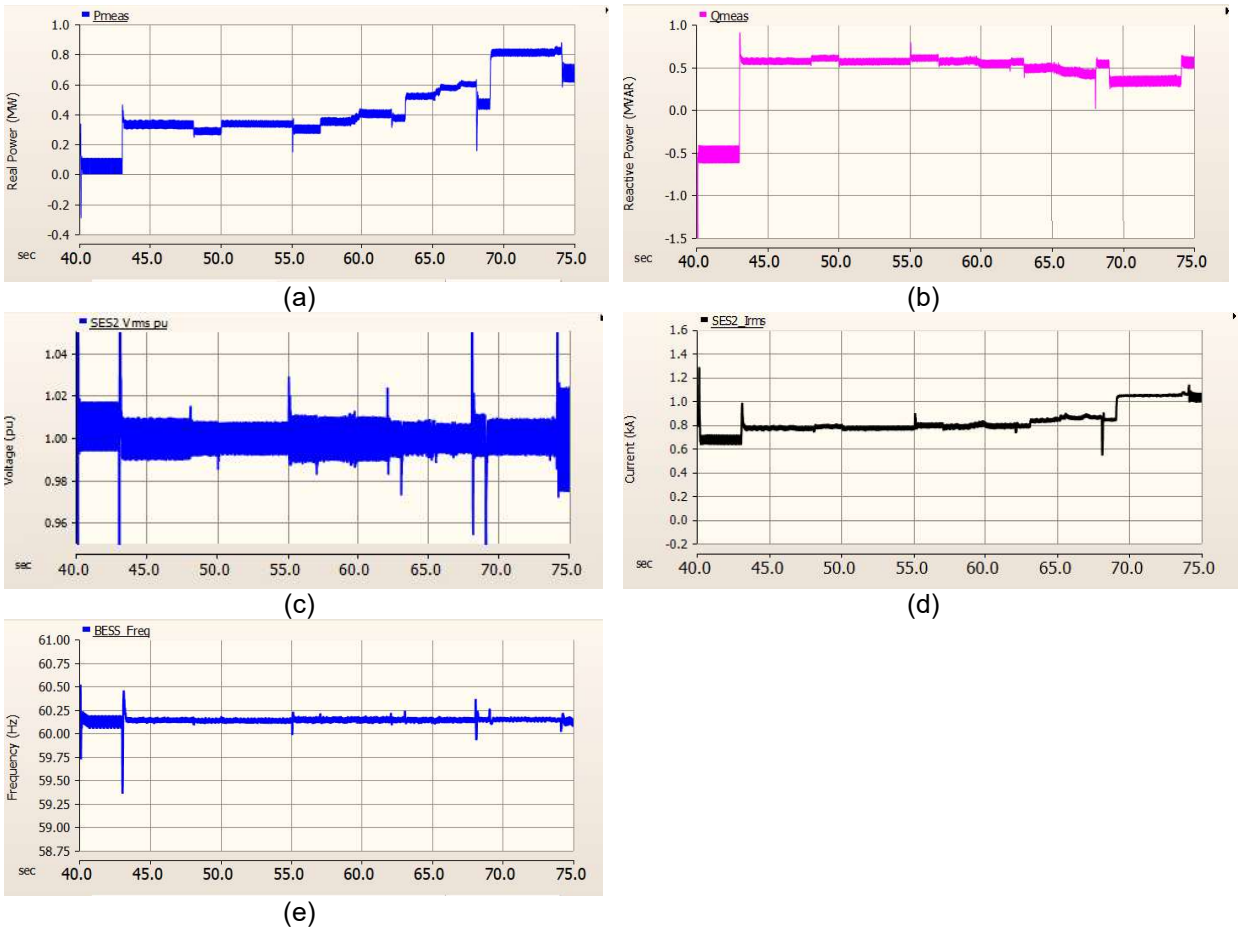

Figure 19. Morning scenario black-start sequence from 45–88 seconds: (a) and (b) SES2 GFM active and reactive power, (c) and (d) SES2 RMS voltage and current, and (e) SES2 frequency

During the full system black-start simulation, the SES2 GFM BESS shows oscillations in the power and voltage measurements (Figure 18 and Figure 19). The oscillations increase as SES2 picks up more load in the sequence. The origin of these oscillations is investigated through four scenarios: (1) aggregated rooftop PV, (2) constant impedance load, (3) aggregated PV and constant impedance load, and (4) constant impedance load and no rooftop PV.

1. **Scenario 1: Aggregated rooftop PV.** The distributed rooftop at each node is aggregated to observe the interactions between the rooftop PV and SES2. Due to the long simulation times, only the first 20 seconds of the black-start simulation are performed. Three loads and PV at three nodes of Ckt2 (see Figure 1) are turned on during the 20-second simulation. The power oscillations have decreased from 75 kW to 40 kW (Figure 20 (a)).
2. **Scenario 2: Constant impedance load.** The full simulation of the Borrego Springs model in PSCAD contains dynamic load. Dynamic load tends to introduce oscillations in the measurements. The dynamic load at three nodes in Ckt2 is replaced by constant impedance load. The power oscillations have further decreased to 25 kW (Figure 20 (b)).
3. **Scenario 3: Aggregated PV and constant impedance load.** Scenario 1 and Scenario 2 are simulated by replacing the dynamic load with constant impedances and aggregating

the rooftop PV at three nodes in Ckt2. The results do not show any improvement in the power oscillations compared to Scenario 2 (Figure 20 (c)).

4. **Scenario 4: Constant impedance load and no rooftop PV.** Scenario 2 is simulated again without the rooftop PV. The power measurements do not show any oscillations (Figure 20 (d)).

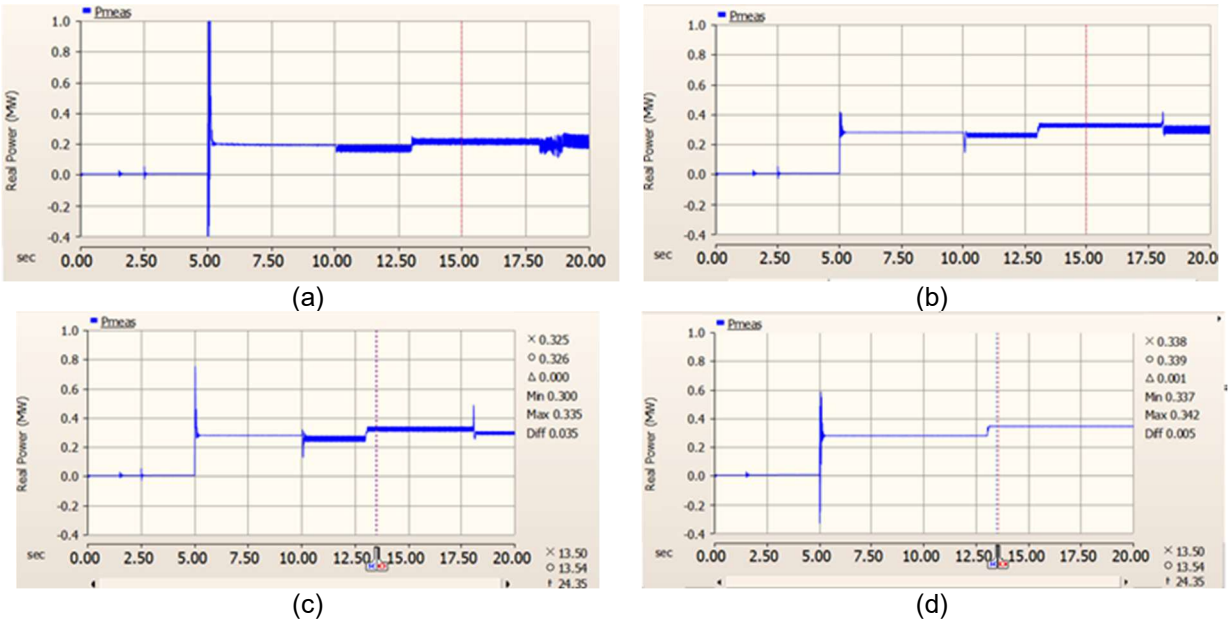

Figure 20. SES2 power measurements: (a) Scenario 1, (b) Scenario 2, (c) Scenario 3, and (d) Scenario 4

The Scenario 2 and Scenario 3 results show that aggregated versus distributed PV does not reduce the power oscillations. By changing the dynamic load to constant impedance, the oscillations can be reduced from 75 kW to 25 kW; however, it is evident that Scenario 4 shows a marked improvement in oscillations in power measurements. The results demonstrate that the PV inverters and dynamic loads interact with the BESS (GFM).

4.2.2 Noon Scenario Without Diesel Generator

For the black-start simulation in the noon scenario, the major generation sources, PV1 and PV2, and the diesel generator are offline. SES1 and SES2 and the rooftop PV are the only generation sources to restore the load.

Figure **21** shows the restoration sequence in the simulation.

Seq	Time (s)	Breaker Switching	PV Switching	SES1				PV2		Capacitor Banks	Rooftop PV		SES2		
				Pload	Qload	Pgen	Qgen	Pgen	Qgen	Qgen	Pgen	Qgen	Pgen	Qgen	S (MVA)
1	3.5	10		0.88	0.28	0.00	0.00	0.00	0.00	0.00	0.00	0.00	0.88	0.28	0.92
2	5.5		PV5	0.00	0.00	0.00	0.00	0.00	0.00	0.00	-0.04	0.00	0.84	0.28	0.88
3	6.5			0.00	0.00	-0.45	-0.21	0.00	0.00	0.00	0.00	0.00	0.39	0.07	0.39
4	8.5	11		0.21	0.07	0.00	0.00	0.00	0.00	0.00	0.00	0.00	0.60	0.13	0.61
5	10.5		PV6, PV7	0.00	0.00	0.00	0.00	0.00	0.00	0.00	-0.06	0.00	0.54	0.13	0.55
6	11.5	12		0.22	0.07	0.00	0.00	0.00	0.00	0.00	0.00	0.00	0.76	0.20	0.79
7	13.5		PV8, PV9	0.00	0.00	0.00	0.00	0.00	0.00	0.00	-0.06	0.00	0.70	0.20	0.73
8	15.5	13		1.64	0.45	0.00	0.00	0.00	0.00	0.00	0.00	0.00	2.34	0.65	2.43

Figure 21. Noon scenario without diesel generator black-start sequence

From the sequence shown in **Figure 21**, Ckt2 is energized by closing BKR10 3.5 seconds into the simulation. Due to the high load at noon, SES2 picked up the approximate 1-MVA load that caused the voltage and frequency transients shown in Figure 22. SES1 is used to pick up part of the load by supplying 0.4 MW and 0.2 MVAR. More breakers are closed at 8.5 seconds and 11.5 seconds to energize the load farther down the feeder. Because there are no big rooftop units on Ckt2, SES2 is loaded at 0.73 p.u. at the end of 13.5 seconds. Figure 22 (e) and (f) show the active and reactive power generation from SES2. All capacitor banks are located at the end of the feeder; therefore, all the load needs to be shared by SES1 and SES2. Further, closing BKR13 at 15.5 causes SES2 to exceed its capacity, so the black-start simulation is stopped at 14 seconds.

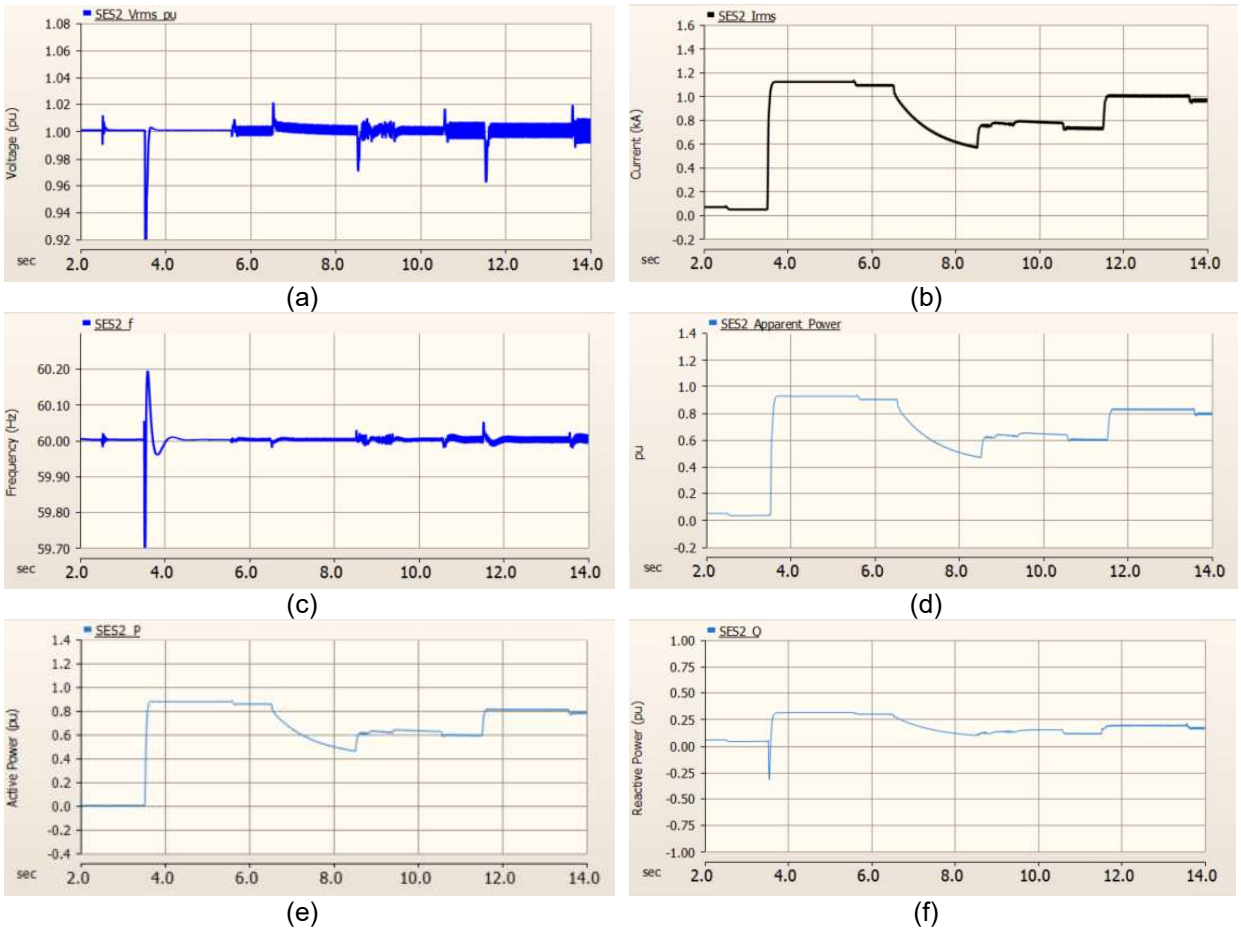

Figure 22. Noon scenario without diesel generator black-start sequence: (a) and (b) SES2 GFM RMS voltage and current, (c) and (d) SES2 frequency and apparent power, and (e) and (f) SES2 GFM active and reactive power

4.2.3 Night Scenario Without Diesel Generator

In the case of the night scenario, only SES1 and SES2 are available as generation sources. The diesel generator is assumed to be offline. Compared to the noon scenario, the night simulation results show a close resemblance except for the SES2 load. Figure 23 shows the black-start sequence in the simulation. Figure 24 (a)–(f) show the night scenario simulation results. The restoration of load is similar to the noon scenario except the rooftop PV is offline. SES2 will exceed the capacity after switching on BKR13, so the simulation is stopped at 14 seconds. The voltage and frequency in Figure 24 (a) and (c) do not show any oscillations compared to the noon scenario results shown in Figure 22 because the rooftop PV is offline. The source of the oscillations is discussed in the morning scenario (Section 4.2.1).

						SES1		PV2		Capacitor Banks	Rooftop PV		SES2		
Seq	Time(s)	Breaker Switching	PV Switching	Pload	Qload	Pgen	Qgen	Pgen	Qgen	Qgen	Pgen	Qgen	Pgen	Qgen	S (MVA)
1	3.5	10		0.60	0.19	0.00	0.00	0.00	0.00	0.00	0.00	0.00	0.60	0.19	0.63
			PV5	0.00	0.00	0.00	0.00	0.00	0.00	0.00	0.00	0.00	0.60	0.19	0.63
2	7	11		0.15	0.05	0.00	0.00	0.00	0.00	0.00	0.00	0.00	0.75	0.24	0.79
			PV6, PV7	0.00	0.00	0.00	0.00	0.00	0.00	0.00	0.00	0.00	0.75	0.24	0.79
3	10			0.00	0.00	-0.50	0.00	0.00	0.00	0.00	0.00	0.00	0.25	0.24	0.35
4	12	12		0.15	0.05	0.00	0.00	0.00	0.00	0.00	0.00	0.00	0.40	0.29	0.50
			PV8, PV9	0.00	0.00	-0.50	0.00	0.00	0.00	0.00	0.00	0.00	0.40	0.29	0.50
		13		1.13	0.30	0.00	0.00	0.00	0.00	0.00	0.00	0.00	1.53	0.59	1.64

Figure 23. Night scenario without diesel generator black-start sequence

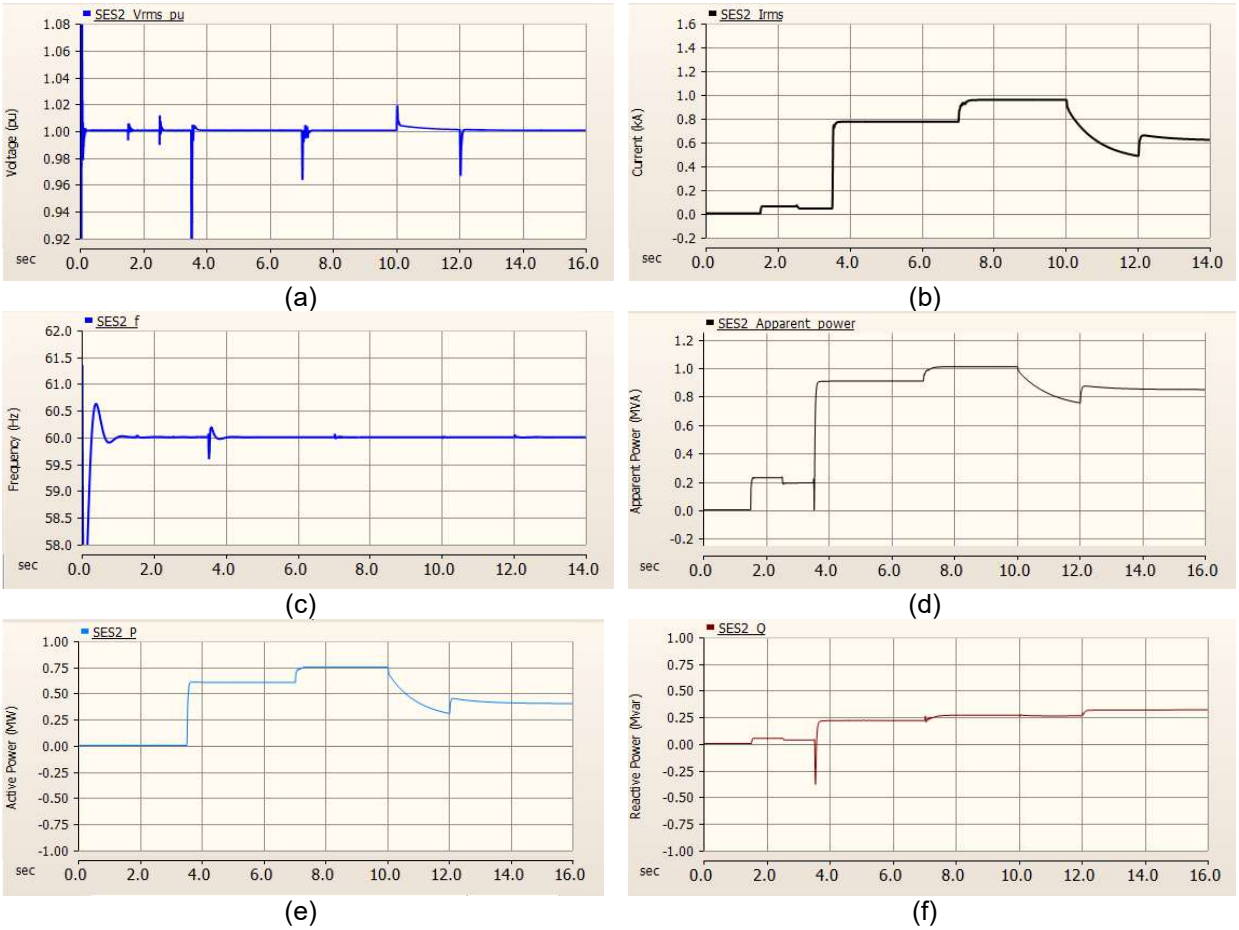

Figure 24. Night scenario without diesel generator black-start sequence: (a) and (b) SES2 GFM RMS voltage and current, (c) and (d) SES2 frequency and apparent power, and (e) and (f) SES2 GFM active and reactive power

4.2.4 Night Scenario With Diesel Generator

In this scenario, SES1 and SES2 are available, and the diesel generator is used to pick up more load than in the previous scenario (Section 4.2.3). The black-start sequence is performed as shown in **Figure 25**. The representative simulation results are shown in Figure 26.

					SES1		Desert Green		Capacitor Banks	Rooftop PV		Diesel		SES2		
Seq	Time (s)	Breaker Switching	Pload	Qload	Pgen	Qgen	Pgen	Qgen	Qgen	Pgen	Qgen	Pgen	Qgen	Pgen	Qgen	S (MVA)
1	20	10	0.60	0.00	0.00	0.00	0.00	0.00	0.00	0.00	0.00	0.00	0.00	0.60	0.00	0.60
2	25	11	0.15	0.05	0.00	0.00	0.00	0.00	0.00	0.00	0.00	0.00	0.00	0.75	0.05	0.75
3	27		0.00	0.00	-0.50	0.00	0.00	0.00	0.00	0.00	0.00	0.00	0.00	0.25	0.05	0.25
4	32	12	0.15	0.05	0.00	0.00	0.00	0.00	0.00	0.00	0.00	0.00	0.00	0.40	0.10	0.42
5	36		0.00	0.00	0.00	0.00	0.00	0.00	0.00	0.00	0.00	-0.55	0.00	-0.15	0.10	0.17
6	46	13	1.13	0.30	0.00	0.00	0.00	0.00	0.00	0.00	0.00	0.00	0.00	0.98	0.40	1.06
7	50		0.00	0.00	0.00	0.00	0.00	0.00	0.00	0.00	0.00	-0.37	0.00	0.61	0.40	0.73
8	60		0.00	0.00	0.00	0.00	0.00	0.00	0.00	0.00	0.00	-0.54	0.00	0.07	0.40	0.40
9	70	17	1.02	0.35	0.00	0.00	0.00	0.00	0.00	0.00	0.00	0.00	0.00	1.09	0.75	1.32
10	75		0.00	0.00	0.00	0.00	0.00	0.00	-1.20	0.00	0.00	0.00	0.00	1.09	-0.45	1.18
11	80		0.00	0.00	0.00	0.00	0.00	0.00	0.00	0.00	0.00	-0.37	0.00	0.72	-0.45	0.85
12	95	14	0.17	0.05	0.00	0.00	0.00	0.00	0.00	0.00	0.00	0.00	0.00	0.89	-0.40	0.98
13	105	15	0.17	0.05	0.00	0.00	0.00	0.00	0.00	0.00	0.00	0.00	0.00	1.06	-0.35	1.12
14	120	18	0.64	0.22	0.00	0.00	0.00	0.00	0.00	0.00	0.00	0.00	0.00	1.70	-0.13	1.71

Figure 25. Night scenario with diesel generator black-start sequence

In the previous scenario, only four loads in Ckt2 are picked up due to low generation. In this scenario, one diesel generator rated at 1.825 MW is used alongside SES1 and SES2 to pick up more load during the night. As shown in **Figure 25**, the black-start sequence starts at 20 seconds of simulation time. Prior to the load pickup, SES2 is first connected to the network, and then the diesel generator synchronization is initiated to connect to the network. Figure 26 (a)–(g) show the transient at 20 seconds due to the 0.60-MW load coming online with the BKR10 switching. When the next breaker in the sequence switches at 25 seconds, SES2 has reached three-fourths capacity. SES1 is brought online at 27 seconds to supply 0.5 MW and reduce the burden on SES2. Figure 26 (b), (e), and (f) show SES2 reducing the output at 27 seconds due to SES1 coming online. Prior to the big load coming online at 46 seconds, the diesel generator is used to supply 0.55 MW and keep the SES2 load low. With the switching of BKR13, SES2 reaches its full capacity, and there is no headroom available to pick up more load. So, the diesel generator real power set points are changed to inject an additional 0.37 MW from the previous set point. The generation levels of the diesel generator shown in **Figure 25** are the additional power (MW) that is required from the previous set point. These set points are incrementally changed to avoid a large transient response and to smooth the response from the diesel generator. Figure 26 (g) shows the gradual change in the power injection from the diesel generator.

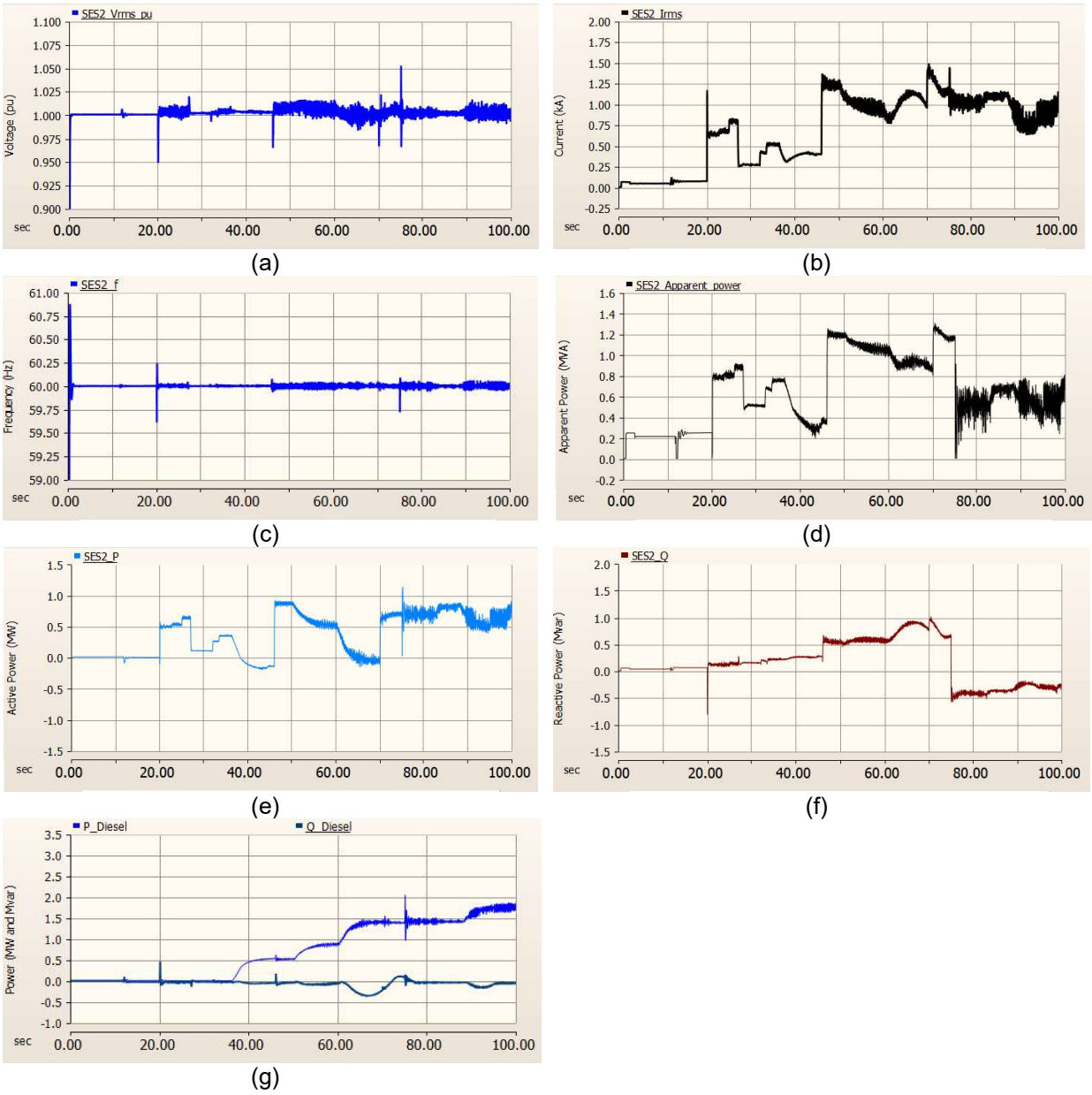

Figure 26. Night scenario with diesel generator black-start sequence: (a) and (b) SES2 GFM RMS voltage and current, (c) and (d) SES2 frequency and apparent power, (e) and (f) SES2 GFM active and reactive power, and (g) diesel active and reactive power

When BKR17 switches at 70 seconds of simulation time, SES2 briefly exceeds its capacity at 1.32 MVA. Because the black-start current capacity of the inverter is assumed to be 1.5 p.u., the simulation is continued to further pick up more load. With the switching of BKR 15, SES2 further exceeds its capacity to reach 1.2 MVA. The simulation is stopped at 120 seconds because of the big load in the sequence thereafter, which will cause SES2 to supply 1.7 MVA.

4.3 Summary of Black-Start Scenarios

The GFM inverter has one inner and two outer loops (grid-connected and islanded). The inner loop and grid-connected mode outer loop are based on a PI controller structure, whereas the islanded mode outer loop is based on a PID controller structure. To simulate the black-start scenarios, the SES2 (GFM) outer loop is tuned between the PI and PID controllers in Figure 7. For the morning and noon scenarios without the diesel generator, the SES2 outer loop is tuned to the PI controller, and the derivative constants are kept at zero. For the night scenario, the diesel generator is connected in GFL mode to pick up the load. In this scenario, the PID controller is tuned like the PI controller in the morning and noon scenarios. Derivative constants are required to have a stable microgrid upon connecting the diesel generator to the microgrid.

5 PSCAD Simulation of Microgrid

This chapter focuses on three scenarios to evaluate the transient stability of the Borrego Springs Microgrid system: planned islanding, unplanned islanding, and contingency events, such as faults and solar insolation changes in islanded operation. The black-start simulation scenario is discussed in Section 4. The starting condition for all the tests except for black starts is grid-connected operation. Each simulation scenario runs approximately 10–20 seconds, and the simulation time step is 25 μs.

5.1 Planned Islanding

For the planned islanding of the Borrego Springs Microgrid, the different test cases are shown in Table 15. These were developed based on the availability of the generation sources and microgrid load scenarios. To include representative testing conditions, morning (high load and low PV), noon (low load and high PV), and night (high load and no PV) load scenarios are considered. The load for each scenario is selected from the load profile for July 29, 2019.

As shown in Table 15, each load scenario has four scenarios depending on the availability of the generation sources. SES1, SES2, and SES3 are energy storage systems. SES1 is a GFL source. SES2 is the islanding leader—the GFM source. And SES3 is primarily used to assist SES2 in the ride-through frequency transients during islanding operation. Note that SES2 is controlled to generate zero power in grid-connected mode. Borrego Springs has 5.5 MW of installed rooftop capacity throughout the entire network. The 6.5-MW PV plant is non-dispatchable, whereas the 26-MW PV plant is dispatchable. One representative simulation result from each load scenario is discussed in this section.

Table 15. Planned Islanding Operation Test Cases

Test No.	Loading	26-MW PV Facility	6.5-MW PV Facility	Rooftop PV	Diesel	SES1 and SES2	SES3
1	Morning	On	On	On	On	Offline	Offline
2	Morning	On	Offline	On	Offline	On	On
3	Morning	On	Offline	On	On	Offline	Offline
4	Morning	On	On	On	Offline	On	On
5	Morning	On	On	On	Offline	On	Offline
6	Morning	On	Offline	On	Offline	On	Offline
7	Noon	On	On	On	Offline	On	On
8	Noon	On	On	On	On	Offline	Offline
9	Noon	On	Offline	On	On	Offline	Offline
10	Noon	On	Offline	On	Offline	On	On
11	Noon	On	On	On	Offline	On	Offline
12	Noon	On	Offline	On	Offline	On	Offline
13	Night	Offline	Offline	Offline	Offline	On	On
14	Night	Offline	Offline	Offline	Offline	On	Offline

5.1.1 Scenario 1: Test 1—Morning

In this scenario (7:30 a.m.), the diesel generator is online and acting as a GFM in islanded mode. SES1, SES2, and PV2 are offline. This scenario serves as the baseline to compare the inverter-based GFM to the conventional generation-based GFM. The total load of the microgrid for the morning scenario is 5.25 MW, 2.5 MVAR. The solar irradiance from the profile data is 19%; therefore, the rooftop PV and 26-MW solar facility are generating 4 MW (19% as per solar irradiance). Each circuit has one capacitor bank with 1.2 MVAR turned on to supply the needed reactive power.

The diesel generator operates as the islanding leader for the microgrid. Figure 27 shows the simulation results of the microgrid. Figure 27 (a) shows the instantaneous waveform the moment the PCC breaker opens. The initial transients in Figure 27 (b) show the PCC voltage reducing to 0.9 p.u. and quickly recovering to 0.98 p.u. The RMS voltage shows small oscillations after the recovery because of the PID control action to reduce the error. Figure 27 (b) shows the PCC frequency experiencing an overshoot and undershoot before reaching the steady-state value. Compared to the SES2 response shown in Figure 33 (c), the frequency slowly increases because of the slow governor response.

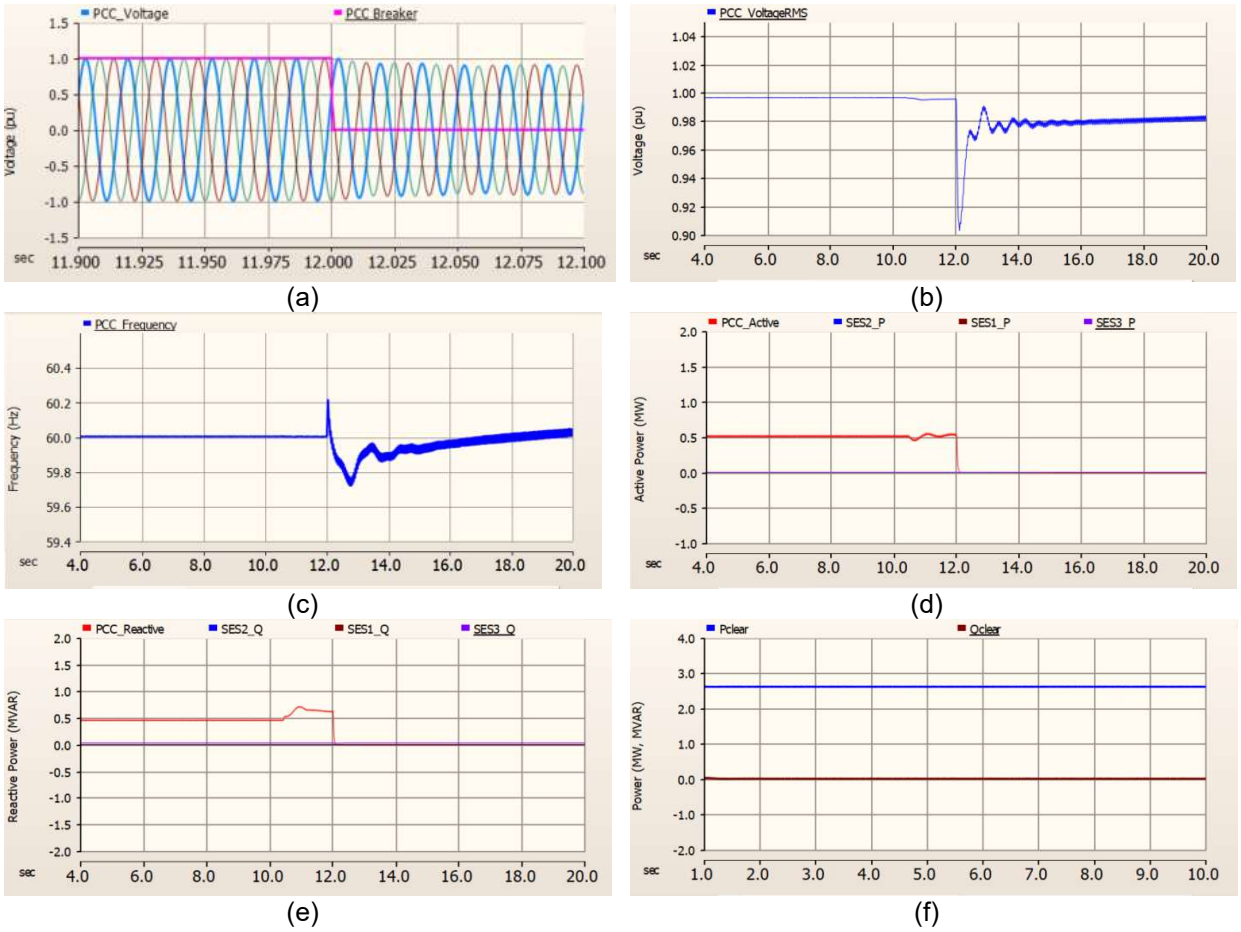

Figure 27. Morning planned islanding scenario with diesel generator (baseline): (a) microgrid PCC instantaneous voltage; (b) microgrid PCC RMS voltage; (c) microgrid PCC frequency; (d) PCC and SES1, SES2, and SES3 active power; (e) PCC and SES1, SES2, and SES3 reactive power; and (f) PV1 active power

Figure 28 shows the diesel generator active and reactive power generation. When the PCC breaker is opened, the diesel generator overshoots and eventually settles to supply approximately 0.5 MW within less than 2 seconds; however, the reactive power generation response shows the automatic voltage regulator (AVR) controller's slow and damped response. Figure 29 shows the recovery of the end-of-feeder voltages to steady state after islanding. Due to the slow response of the AVR, the voltage takes more than 6 seconds to reach steady state.

Figure 28. Morning planned islanding scenario with diesel generator (baseline): diesel generator active and reactive power

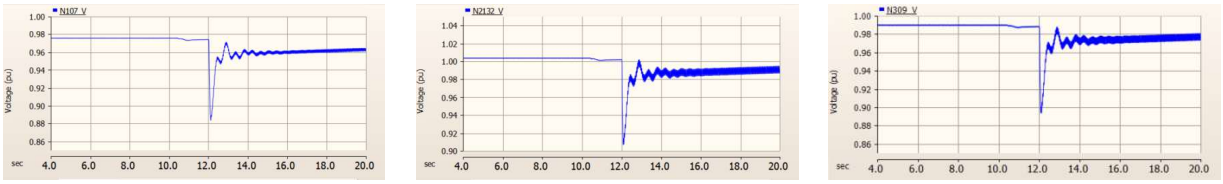

(a) (b) (c)

Figure 29. Morning scenario with diesel generator: (a)–(c) end-of-feeder node voltages at Ckt1, Ckt2, and Ckt3

5.1.2 Scenario 1: Test 3—Morning

In this morning scenario, the diesel generator is acting as the GFM instead of SES2. PV1, PV2, and the rooftop PV are the additional generation sources available to support the Borrego Springs network. This scenario serves as a base case for Scenario 4 in Table 15 because SES2 acts as a GFM source; therefore, the rooftop, PV1, and 26-MW solar PV facility are generating approximately 5 MW (19% as per solar irradiance). Each circuit has one capacitor bank with 1.2 MVAR turned on to supply the needed reactive power.

Figure 30 shows the simulation results of the planned islanding scenario with the diesel generator acting as the GFM. Figure 30 (b) shows the PCC voltage of the islanding scenario after it reaches steady state within less than 2 seconds after islanding. Figure 30 (c) shows that there is excess generation, due to which the PCC frequency is greater than 60 Hz.

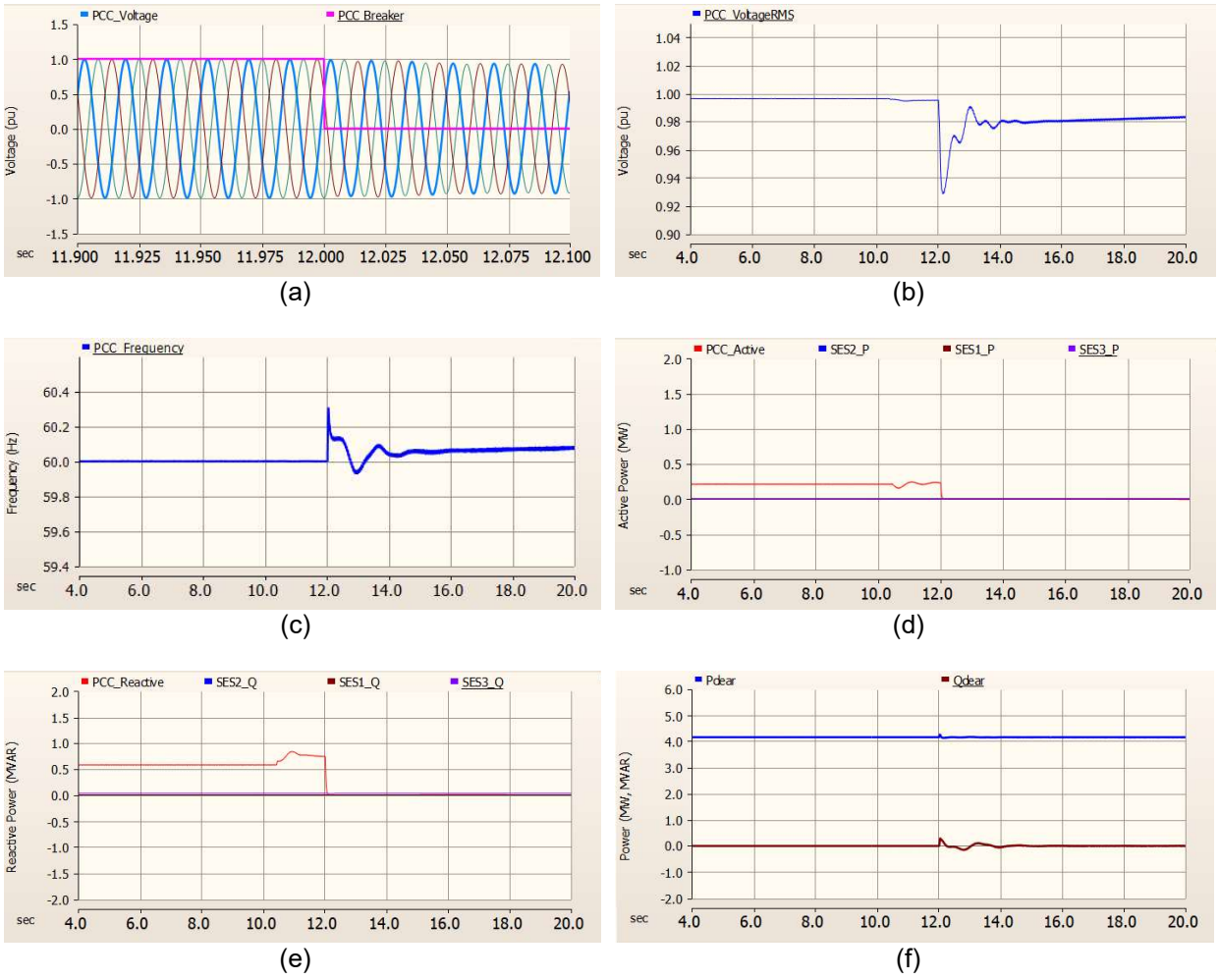

Figure 30. Morning planned islanding scenario with diesel generator and PV2: (a) microgrid PCC instantaneous voltage; (b) microgrid PCC RMS voltage; (c) microgrid PCC frequency; (d) PCC and SES1, SES2, SES3 active power; (e) PCC and SES1, SES2, SES3 reactive power; and (f) PV1 active power

Figure 31 shows the diesel generator active and reactive power generation. The oscillations shown in the diesel generator power plot after the PCC breaker opening damp out within less than 4 seconds. Figure 32 shows the recovery of the end-of-feeder voltages in the network and the diesel generator's ability to support the microgrid.

Figure 31. Morning planned islanding scenario with diesel generator (baseline): diesel generator active and reactive power

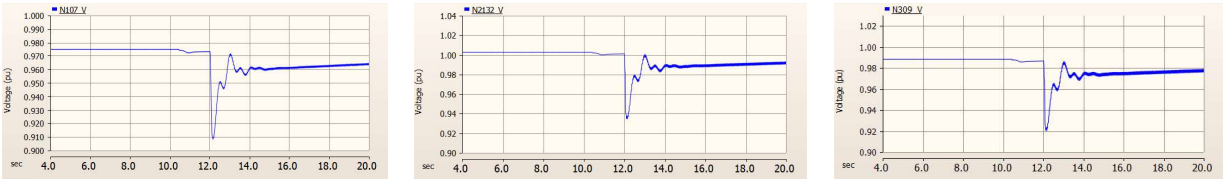

(a) (b) (c)

Figure 32. Morning scenario with diesel generator: (a)–(c) end-of-feeder node voltages at Ckt1, Ckt2, Ckt3

5.1.3 Scenario 1: Test 4—Morning

In the morning scenario (7:30 a.m.), the diesel generator is offline. The total load of the microgrid for the morning scenario is 3.126 MW, 2.362 MVAR. The solar irradiance from the profile data is 19%; therefore, the rooftop, 6.5-MW PV, and 26-MW PV systems generate 19% of power based on their capacities. Each circuit has one capacitor bank with 1.2 MVAR turned on to supply the needed reactive power. Table 16 shows the generation and load for the morning scenario.

Table 16. Generation and Load for Morning Planned Islanding Scenario

Description	Active Power (MW)	Reactive Power (MVAR)
Load	5.25	2.5
SES1	0.5	0
Rooftop	1.087	0
6.5 MW PV	1.24	0
Capacitors	0	3.6
26-MW PV facility	2.86	0

For the planned islanding, the goal is to reduce the PCC power flow to near zero. Overall, the total generation is larger than the total load demand; therefore, the 26-MW PV facility is curtailed from 20% to 11%, and SES1 is set to generate 0.5 MW at full capacity. Note that the minimal power generation for the 26-MW PV plant is 10%. The Borrego Springs Microgrid has large transformers that require reactive power, and there are active power losses from the lines and transformers. Based on the steady-state power flow study, the transformers in the network consume approximately 1 MW and 1.84 MVAR (Table 6); therefore, the active and reactive power required from SES2 after islanding is approximately -0.25 MW and 0.6 MVAR, respectively.

SES2 operates as the islanding leader for the microgrid. The simulation starts in grid-connected mode, and SES2 starts in VF mode, then synchronizes (syncs) to the grid and changes to power control (PQ) mode after its breaker closes. At 5.6 seconds of the simulation, the PCC breaker is intentionally opened, which drives SES2 to change to VF mode and operate as the islanding leader. Representative results of the simulation are shown in Figure 33 (a)–(f).

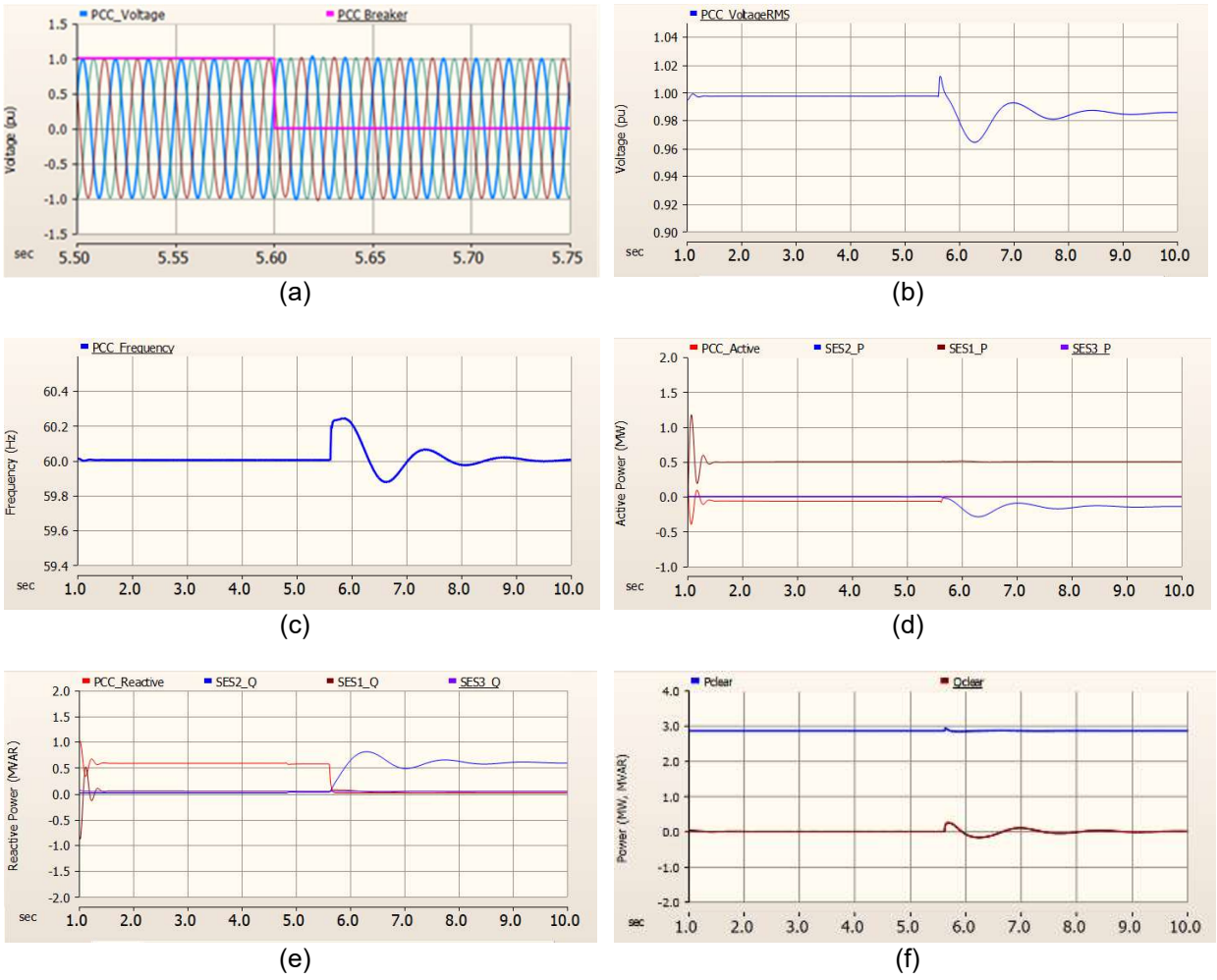

Figure 33. Morning planned islanding scenario: (a) microgrid PCC instantaneous voltage; (b) microgrid PCC RMS voltage; (c) microgrid PCC frequency; (d) PCC and SES1, SES2, and SES3 active power; (e) PCC and SES1, SES2, and SES3 reactive power; and (f) PV1 active power

Figure 33 (a) shows the microgrid voltage waveform when the PCC circuit breaker is opened. There are no noticeable transients in the voltage waveform, which indicates a smooth and successful transition during this planned islanding. Figure 33 (b) shows the RMS value of the microgrid voltage, which has a very small overshoot and undershoot. Figure 33 (c) shows that the microgrid frequency exhibits an overshoot the instant the PCC breaker opens and undershoots to approximately 59 Hz. After 3 seconds in islanded operation, the frequency settles at 60 Hz. The microgrid voltage and frequency in Figure 33 (b) and (c) show damped oscillations, and the system settles within less than 4 seconds from the moment the PCC circuit breaker opens. Figure 33 (d) shows the active power through the PCC and for SES1, SES2, and SES3. The active power at the PCC is close to zero when the PCC circuit breaker is open. Note that SES2 needs to absorb excess generation because of its load-following capability as the GFM source. Figure 33 (e) shows the reactive power through the PCC and for SES1, SES2, and SES3. The reactive power at the PCC is more than 0.5 MVAR when the PCC circuit breaker is opened. This is a big challenge for the microgrid; however, SES2 has enough capacity to output the reactive power needed, and it is fast enough to take over the burden from the main grid.

Figure 34 shows the end-of-feeder RMS voltage for each circuit. The results show that the three end-of-feeder voltages are maintained within acceptable limits (approximately 0.95–1.05 p.u.). The results further validate the stability of the microgrid after the planned islanding operation.

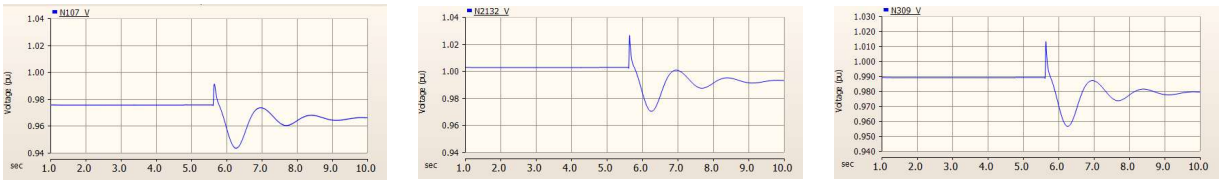

(a) (b) (c)

Figure 34. Morning scenario: (a)–(c) end-of-feeder node voltages at Ckt1, Ckt2, and Ckt3

In this scenario, the results show that a planned islanding event can be carried out without any issues due to careful power dispatch and that SES2 has enough capacity to handle the power demand during islanding operation. Due to the 26-MW PV plant capacity, the generation must be curtailed to the minimum power (10%). Other test cases of morning scenarios also show successful operation of the planned islanding.

5.1.4 Scenario 2: Test 7—Noon

In the noon scenario, all generation sources are available except for the diesel generation. The microgrid load from the noon scenario is almost double that of the morning scenario, and the solar irradiance increases from 19% to 89%, so all PV units generate 89% of power. The 26-MW PV plant is totally curtailed or shut down because of the excessive power generated from the rooftop PV and the 6.5-MW PV facility. Table 17 shows the total generation and load for the noon planned islanding scenario.

Table 17. Generation and Load for Noon Planned Islanding Scenario

Description	Active Power (MW)	Reactive Power (MVAR)
Load	8.8	3.5
SES1	0	0.5
Rooftop	4.9	0
6.5-MW PV	5.85	0
Capacitors	0	4.8
26-MW PV facility	0	0

Initially, three capacitors with a total reactive power of 3.6 MVAR are connected. To compensate for the reactive power from the transformers, SES1 is dispatched to supply 0.5-MVAR reactive power.

The original simulations show that the voltage is unstable after the transition from grid-connected to islanded mode. An effort is made to tune the SES2 control parameters, such as the PID control parameters; however, that still cannot resolve the stability problem. We understood that SES2 is the islanding leader, and its reactive power output affects its voltage stability; therefore, one more capacitor is turned on for Ckt1, which eventually resolves the voltage stability issue. This is because more reactive power is needed from the transformers (69/12 kV,

12/0.48 kV, and 69/4.6 kV), and a reactive power source near SES2 helps to maintain its voltage. Figure 35 (a)–(f) show representative results of the simulation with four capacitors connected to the network.

The instantaneous voltage waveforms in Figure 35 (a) show the smooth transients during the planned islanding operation. Figure 35 (b) shows the PCC voltage RMS, which indicates that the PCC voltage slightly exceeds the lower operation limit of 0.95 p.u. Figure 35 (c) shows the PCC frequency, which has similar transients as the morning scenario shown in Figure 33 (c). The active power measurements shown in Figure 35 (d) indicate that SES2 absorbs excessive active power after the PCC circuit breaker opens. SES2 generates reactive power to balance and sustain the microgrid, as shown in Figure 35 (e). Figure 35 (f) shows the PV1 curtailment during the entire simulation. Figure 36 shows the end-of-feeder voltage RMS for Ckt1, Ckt2, and Ckt3. The Ckt1 results show that the voltages at the end of the feeder are maintained within the acceptable limits (approximately 0.95–1.05 p.u.).

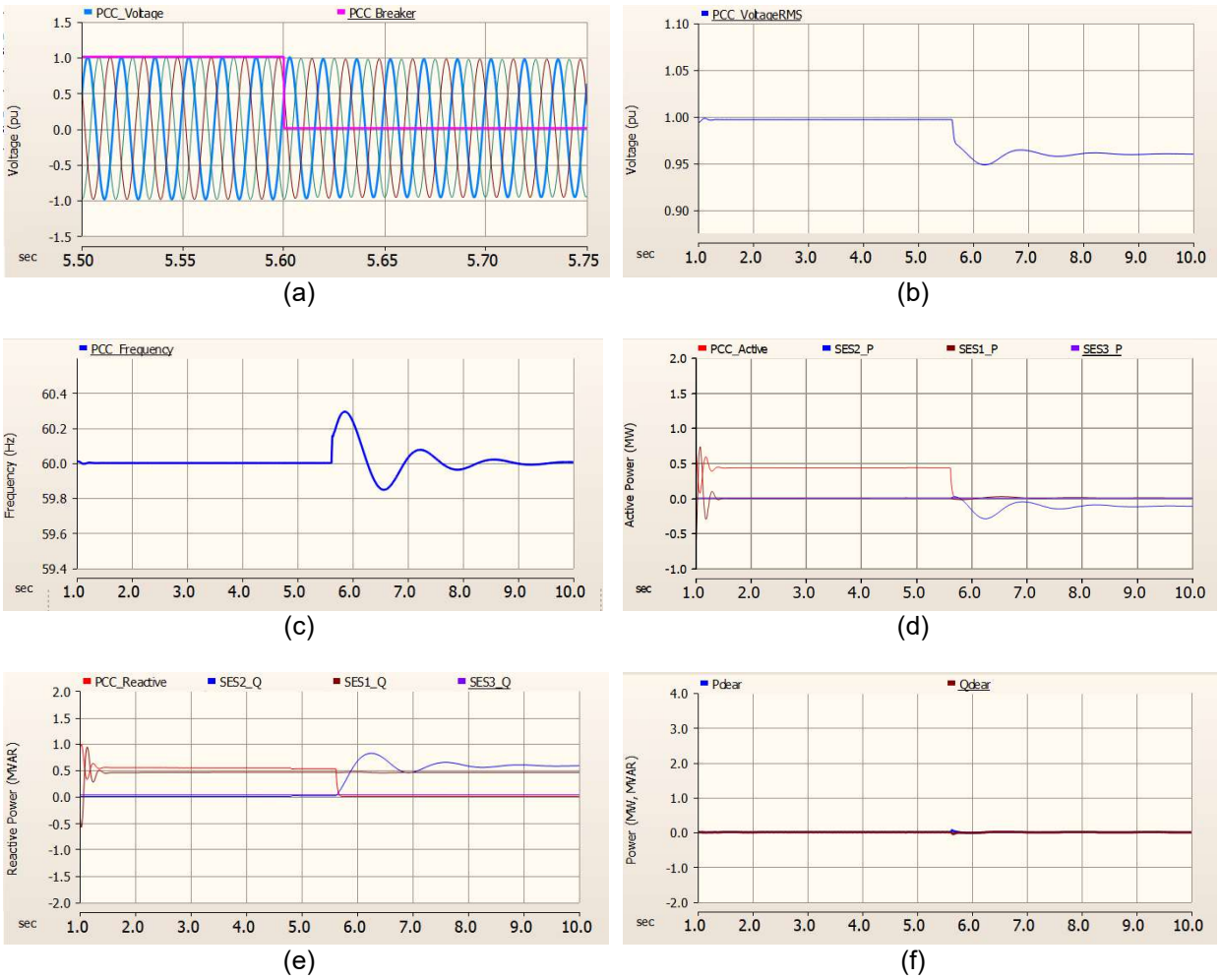

Figure 35. Noon planned islanding scenario: (a) microgrid PCC instantaneous voltage; (b) microgrid PCC RMS voltage; (c) microgrid PCC frequency; (d) PCC and SES1, SES2, and SES3 active power; (e) PCC and SES1, SES2, and SES3 reactive power; and (f) PV1 active power.

Figure 36 (a)–(c) show the end-of-feeder RMS voltages for each circuit. The results show that the Ckt1 and Ckt3 end-of-feeder voltages are maintained within the acceptable limits (approximately 0.95–1.05 p.u.); however, from grid-connected to islanded mode, the Ckt2 end-of-feeder voltage drops from 0.96 p.u. to 0.92 p.u. To keep the voltage within the operation limits, there is a need to regulate the end-of-feeder voltage for Ckt2, such as turning on the volt-VAR smart inverter function of the rooftop PV in Ckt2.

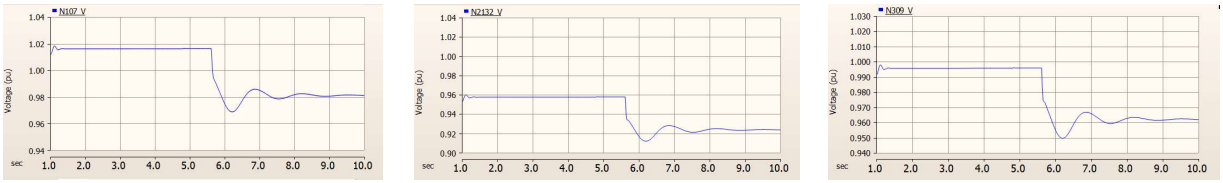

Figure 36. Noon scenario: (a)–(c) end-of-feeder node voltages at Ckt1, Ckt2, and Ckt3

In this scenario, the results show that a planned islanding event can be carried out without any issues thanks to careful power dispatch and that SES2 has enough capacity to handle the power demand during islanding operation. Due to the excess power generation available from PV1 and the minimum operating capacity of 10%, PV1 is fully curtailed during the entire simulation. Other test cases of noon scenarios also show the successful operation of the planned islanding.

5.1.5 Scenario 2: Test 8—Noon

In this scenario, SES1 and SES2 are offline, and PV1 and the rooftop PV are additional generation sources available to support the diesel generator. Even though PV1 is available, due to the excess generation, PV1 is fully curtailed. The total generation is more than the total load available in this scenario. Figure 37 (b) shows that the voltage experiences oscillations but eventually reaches steady state. Figure 37 (c) shows that the frequency is not stable, so this scenario is not successful. Figure 38 shows the diesel generator's power oscillations after the islanding event. Figure 39 (a)–(c) show the Ckt1, Ckt2, and Ckt3 end-of-feeder voltages. All voltages show oscillations after separation but settle within approximately 6 seconds.

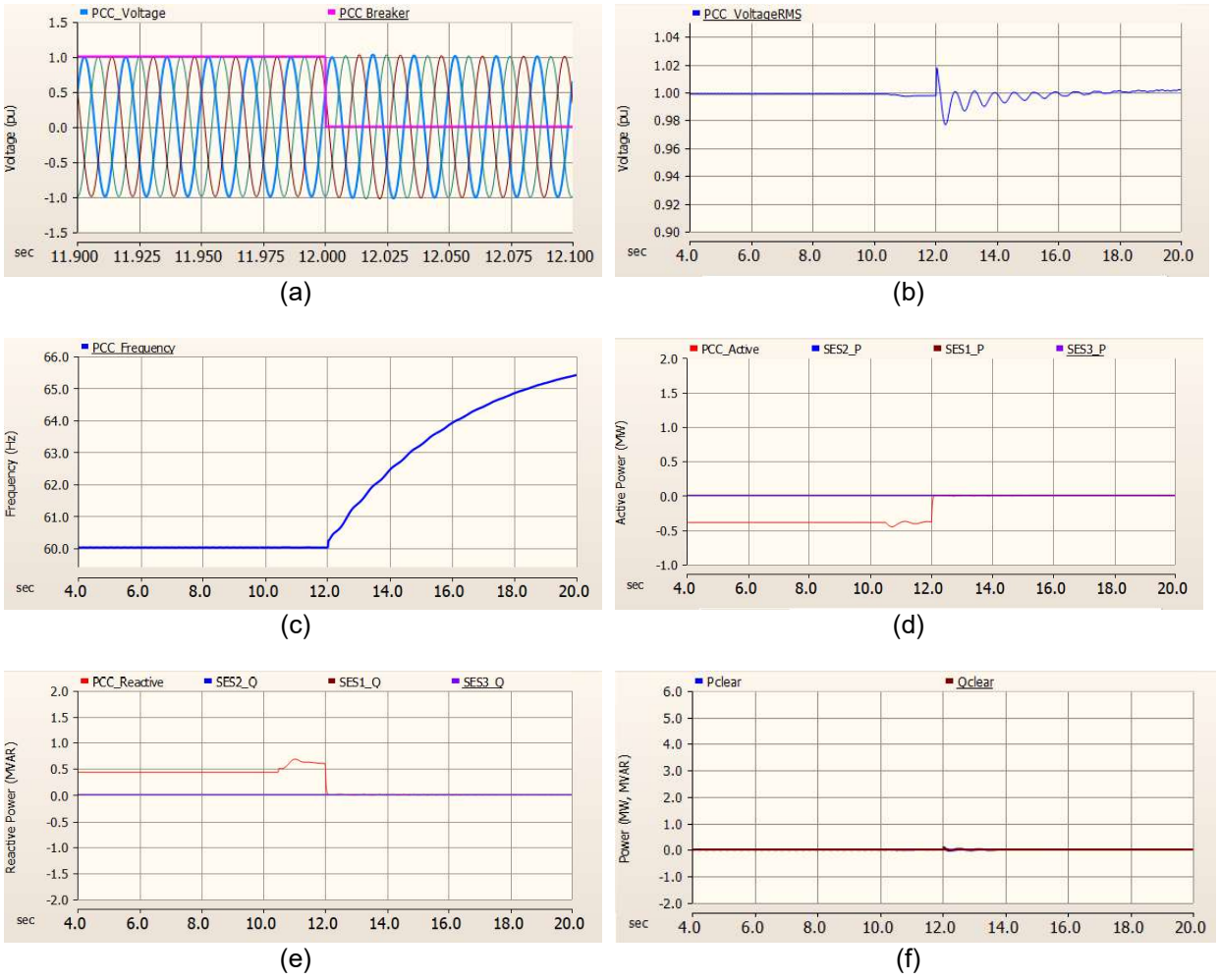

Figure 37. Noon planned islanding scenario: (a) microgrid PCC instantaneous voltage; (b) microgrid PCC RMS voltage; (c) microgrid PCC frequency; (d) PCC and SES1, SES2, and SES3 active power; (e) PCC and SES1, SES2, and SES3 reactive power; and (f) PV1 active power

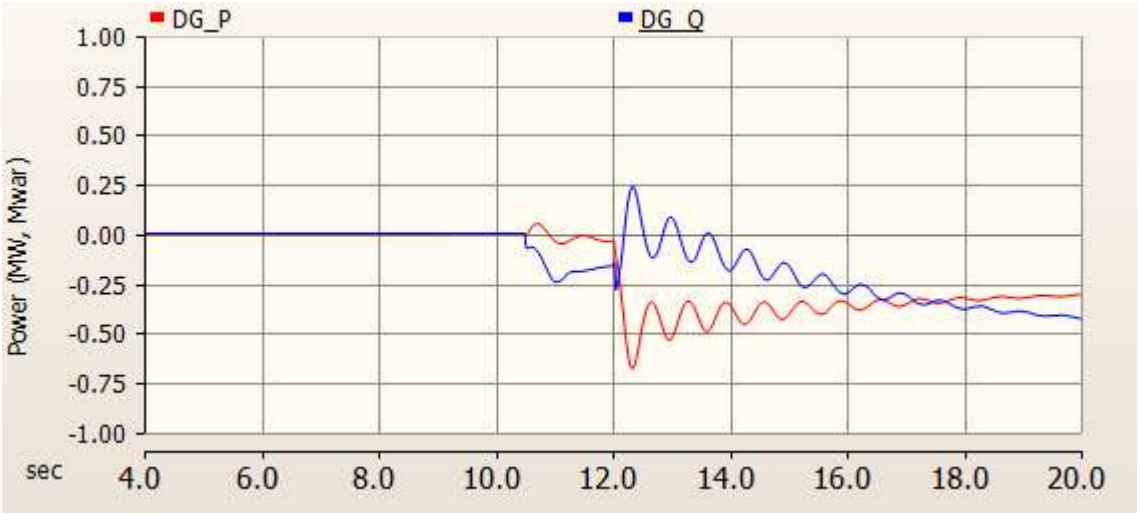

Figure 38. Morning planned islanding scenario with diesel generator (baseline): diesel generator active and reactive power

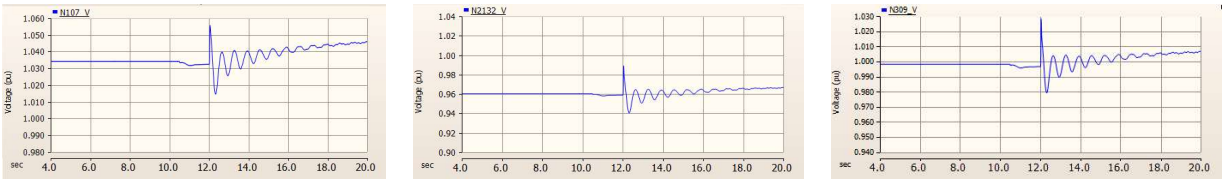

(a) (b) (c)

Figure 39. Noon scenario: (a)–(c) end-of-feeder node voltages at Ckt1, Ckt2, and Ckt3

5.1.6 Scenario 2: Test 9—Noon

In this scenario, SES1 and SES2 are offline, and the diesel generator is the GFM resource during the islanding. PV1, PV2, and the rooftop PV are the other generation sources available. PV1 is curtailed to reduce the excess generation. The total load of the network is the same as the other noon scenarios shown in Table 17. Figure 40 (a)–(f) show the simulation results. Figure 41 shows the diesel generator response after the islanding event. The diesel generator's power oscillates and settles at 0.6 MW and 0.4 MVAR, which is slightly less than the grid-supplied power. Figure 42 (a)–(c) show that the end-of-feeder voltages are within the acceptable limits (0.95 p.u. to 1.05 p.u.).

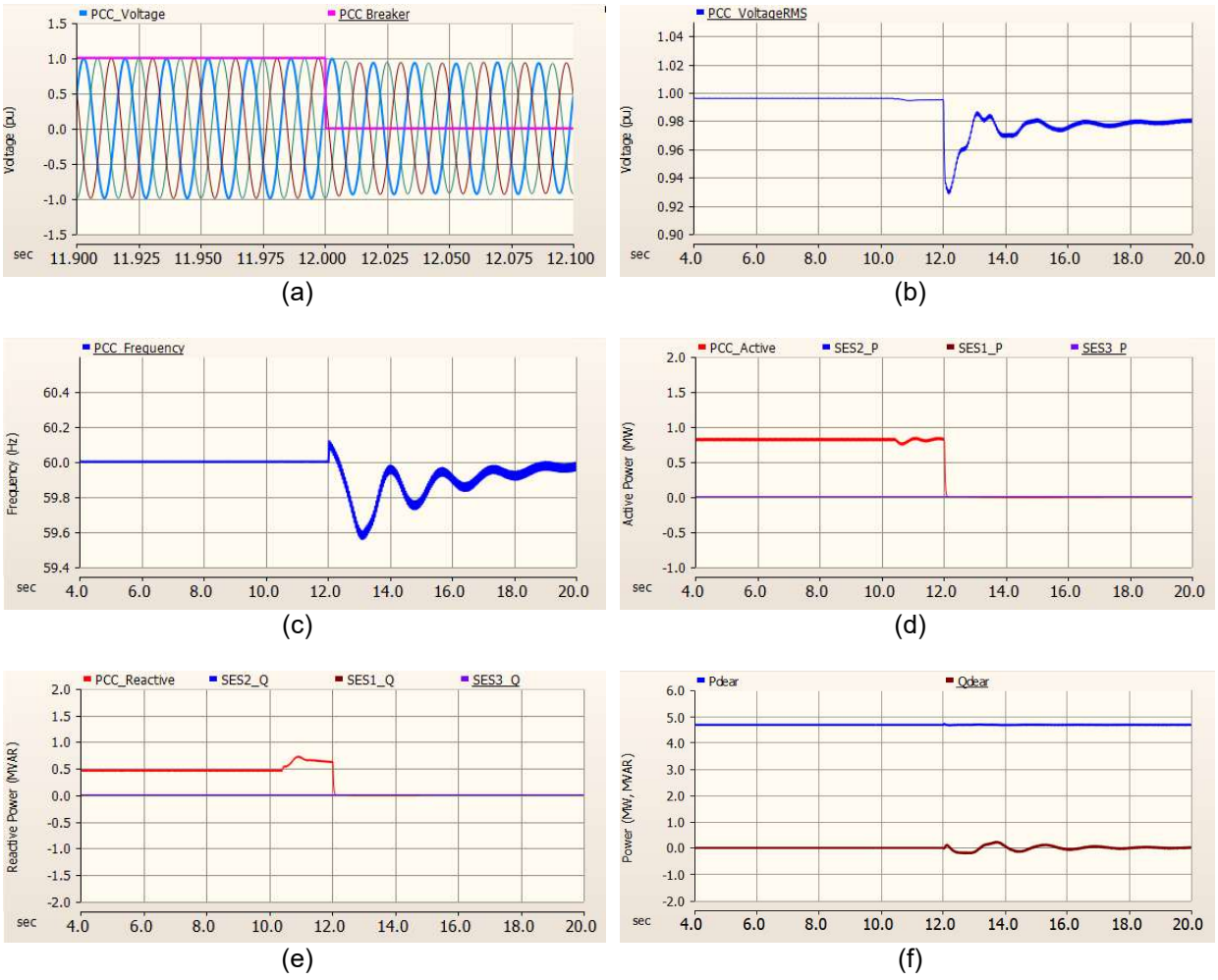

Figure 40. Noon planned islanding scenario: (a) microgrid PCC instantaneous voltage; (b) microgrid PCC RMS voltage; (c) microgrid PCC frequency; (d) PCC and SES1, SES2, and SES3 active power; (e) PCC and SES1, SES2, and SES3 reactive power; and (f) PV1 active power

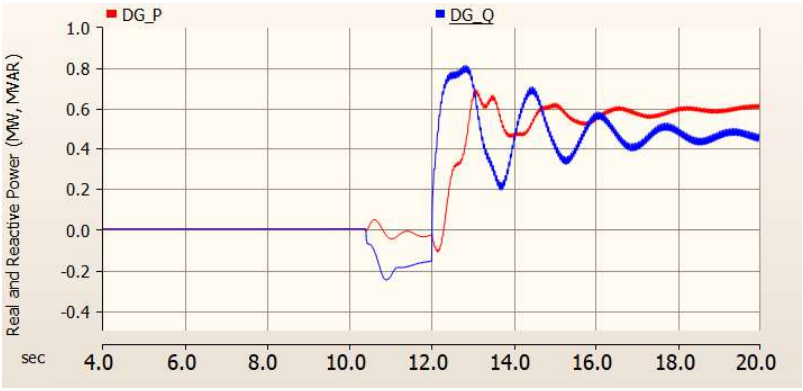

Figure 41. Noon planned islanding scenario with diesel generator (baseline): diesel generator active and reactive power

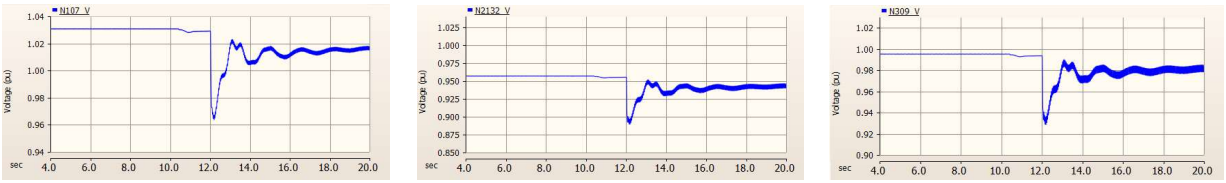

(a) (b) (c)

Figure 42. Noon scenario with diesel generator: (a)–(c) end-of-feeder node voltages at Ckt1, Ckt2, and Ckt3

5.1.7 Scenario 3: Night

Because there is no solar irradiance, the generation from the PV1, PV2, and the rooftop PV are assumed to be zero. SES1 and SES2 are the only sources available, with a combined capacity of 1.5 MVA. The microgrid has 9.2 MW and 3.5 MVAR of total load at night (10:00 p.m.). To support the microgrid operation, a sequence of load shedding is performed based on load prioritization, which is provided by SDG&E. Due to the reactive power requirement from the 26-MW PV1 facility and the 69/12-kV transformers, only the 12-kV bus is energized.

After shedding the loads, only three breakers in Ckt2 are closed. It is assumed that all the breakers that are required to shed load are open before the simulation starts. This reduces the total simulation time. All the capacitor banks are also lost because they are all located at the end of the feeders, and when the load-shedding breakers are open, the reactive power sources from the capacitor banks are lost.

The initial simulation results show that the voltage collapses in the microgrid to 0.75 p.u. SES2, the islanding leader, cannot maintain the nominal voltage at 1 p.u. To find a feasible solution, an effort is made to tune the control of SES2. To correct the voltage error of SES2, the PI control for the outer loop is tuned instead of the proportional-derivative (PD) control. Note that the PD control works for the full simulation in the morning and noon scenarios. To resolve the issue, we tuned the PI control for the outer loop so that SES2 can maintain the voltage close to 1 p.u., but the oscillations are not damped. Finally, the PID control of SES is tuned to control the voltage magnitude in the microgrid and damp the oscillations.

Because the 69-kV breakers are open, PCC measurements are taken at the 12-kV side of the microgrid. Figure 43 (a) and (b) show that the voltage dips but subsequently recovers to maintain 1-p.u. voltage. To reduce the voltage dip during the transition period, the integrator constants in the PID control were further tuned, but there is marginal improvement. Figure 44 (a)–(b) show the active and reactive power at the PCC and SES1, SES2, and SES3. There is a large amount of power at the PCC when the circuit breaker opens. Figure 44 (a) shows the change in power levels before opening the PCC breaker at 5.6 seconds. SES1 is dispatchable, and its output power is dispatched to keep the PCC power flow to a minimum value during the islanding operation and then supply the active and reactive power to the load. This scenario shows an extreme case where there is not enough generation and there is very little flexibility to balance the generation and load; however, with careful dispatch and tuning of SES2, the microgrid system survives this planned islanding operation.

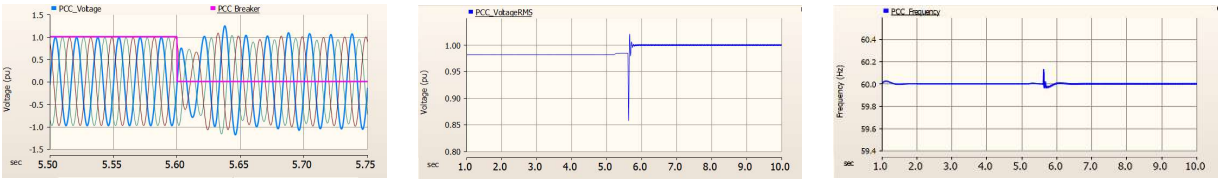

(a) (b) (c)

Figure 43. Night scenario: (a) Microgrid PCC instantaneous voltage, (b) microgrid PCC RMS voltage, and (c) microgrid PCC frequency

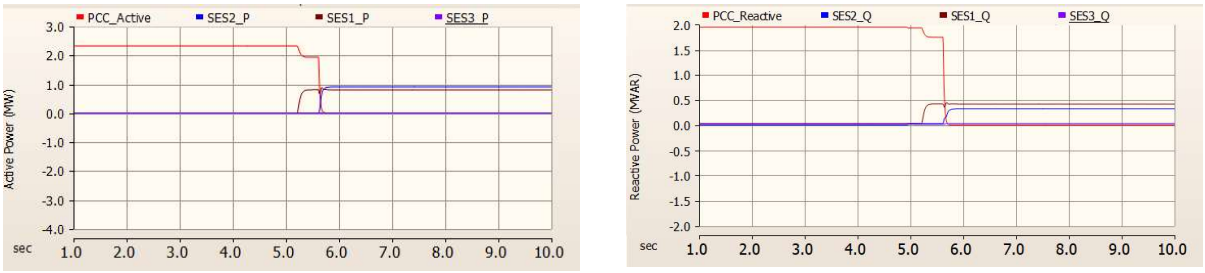

(a) (b)

Figure 44. Night scenario: (a)–(b) Microgrid PCC and SES1, SES2, and SES3 active and reactive power

5.1.8 Observations and Conclusions

The planned islanding operation of the Borrego Springs Microgrid was evaluated under different scenarios based on the availability of SES1, SES2, SES3, the 26-MW PV facility (PV1), the 6.5-MW PV facility (PV2), and the rooftop generation sources.

In these studies, the simulations assume that the energy storage systems' state of charge of SES1, SES2, and SES3 is high before starting the planned islanding. Before opening the PCC breaker, the power flow through the circuit breaker is kept low (<50 kW). Also, the simulations tried to keep the power output from SES2 below 50% of capacity so that additional capacity can be used in case of any transients/sudden events. There is no direct control over the PV facilities, and the 26-MW PV facility has a minimal load constraint of 10%, which reduces the flexibility to balance the generation and load. SES1 is used as the main dispatchable source to meet the additional requirements after the 26-MW PV facility. The outcomes are summarized in the following sections and in Table 18.

5.1.8.1 Morning

In the morning scenario (7:30 a.m.), solar is ramping up, and the microgrid load (3.1 MW, 2.3 MVAR) is low compared to the other scenarios. One important observation for all scenarios is that the capacitors need to be online to generate sufficient reactive power. One capacitor from each feeder is required to be online for the morning scenarios. PV1 needs to be curtailed from 20% generation to 15% or 10%, depending on the status of PV2. Another observation is that excessive reactive power affects the system's voltage stability. Each capacitor bank is 1.2 MVAR without intermediate steps and as a result there is not enough granularity to regulate the system voltages. Dispatchable sources, such as SES1 and the 26-MW PV, can be better options

to regulate/maintain the system voltages. In addition, SES3 affects the system stability as well. When SES3 is offline, the small oscillations in the power measurements are reduced.

5.1.8.2 Noon

In the noon scenarios, solar generation is high (90% generation), and the total load is almost double that of the morning scenarios. In this case, the generation from PV2 and the rooftop PV is more than the required active power from the load, so PV1 needs to shut down; however, the reactive demand is also high. Four capacitor banks are on: Two are enabled for Ckt1, and one each is enabled for Ckt2 and Ckt3.

5.1.8.3 Night

In the night scenarios, the load is the highest, and there is no solar power to support full microgrid operation. Load shedding is required before starting the planned islanding. The 69-kV bus is also de-energized because of the additional reactive requirement from two 69/12-kV and PV1 transformers. SES1 and SES2 are used as the generation to support the 1.5-MVA load. There is no capacitor bank on because the sectionalizers are open to shed the load.

Table 18. Learnings and Findings of the Planned Islanding

Test No.	Results	Learnings and Findings
1	*Successful planned islanding operation with diesel generator as GFM asset.* When the PCC circuit breaker is opened, the active and reactive power at the PCC are close to 500 kW and 500 kVAR, respectively. The PCC voltage and frequency reach steady state in about 6 seconds. The voltages at the end of the three circuits are maintained above 0.95 p.u.	(1) The 26-W PV facility is curtailed from 0.2 to 0.1 due to excess generation. (2) The PCC voltage and frequency exhibit small oscillations and reach steady state within 6 seconds due to the slow response of the governor and AVR.
2	*Successful planned islanding operation, but the system exhibits some oscillations*. When the PCC circuit breaker is opened, the active and reactive power at the PCC are close to zero and 500 kVAR, respectively. The microgrid reaches steady state within 4 seconds after the PCC circuit breaker is opened. The PCC voltage and frequency show oscillations even after reaching steady state. SES2 absorbs a small amount of excessive active power and generates approximately 500-kVAR reactive power after the islanding operation. The voltages at the end of the three circuits are maintained above 0.95 p.u.	(1) The 26-MW PV facility is less curtailed (from 0.2 to 0.15) because the 6.5-MW PV facility is offline. (2) SES2 can act as a slack bus to balance the generation and load to maintain the system. (3) Before the islanding operation, the PCC frequency and head of circuits already exhibit some oscillations, and the oscillations worsen after the islanding operation.
3	*Successful planned islanding operation*. When the PCC circuit breaker is opened, the active and reactive power at the PCC are close to 200 kW and 550 kVAR, respectively. The PCC voltage settles at 0.98 p.u. from the islanding event. The PCC frequency overshoots to 60.3 Hz the moment the PCC breaker opens and settles at 60.1 Hz within 6 seconds. The voltages at the end of the three circuits are maintained above 0.95 p.u.	(1) The 26-W PV facility is curtailed from 0.2 to 0.16. (2) The PCC voltage and frequency exhibit small oscillations and reach steady state within 6 seconds due to the slow response of the governor and AVR.

4	*Successful planned islanding operation*. When the PCC circuit breaker is opened, the active and reactive power at the PCC are close to zero and 550 kVAR, respectively. The microgrid reaches steady state within 4 seconds after the PCC circuit breaker is opened. The microgrid voltage and frequency show smooth transients with a small undershoot (0.97 p.u.) in voltage, and the microgrid frequency nadir is 60 Hz and overshoots to 60.42 Hz. (The frequency is 60.18 Hz in grid-connected mode.) The voltages at the end of the three circuits are maintained above 0.95 p.u.	Low load and low PV. (1) The PCC power flow needs to be minimized during the islanding operation. (2) The 26-MW PV facility needs to be curtailed (from 0.2 to 0.1) to reduce the excessive active power. (3) The transformers in the microgrid consume a significant amount of reactive power, and the capacitor banks need to turn on to supply the reactive power demand. SES1 can be used to buffer and fine-tune to balance the reactive power demand and generation.
5	*Successful planned islanding operation*. When the PCC circuit breaker is opened, the active and reactive power at the PCC are close to zero and 550 kVAR, respectively. The microgrid reaches steady state within 4 seconds after the PCC circuit breaker is opened. The PCC voltage and frequency show smooth transients with a small undershoot (0.97 p.u.) in voltage, the PCC frequency nadir of 60 Hz (60.18 Hz in grid-connected mode), and an overshoot of 60.42 Hz. The voltages at the end of the three circuits are maintained above 0.95 p.u.	Unlike Scenario 1, SES3 is offline. The frequency is stable and maintained close to nominal, so there is no need to use SES3.
6	*Successful planned islanding operation.* When the PCC circuit breaker is opened, the active and reactive power at the PCC are close to zero and 550 kVAR, respectively. The microgrid reaches steady state within 4 seconds after the PCC circuit breaker is opened. The PCC voltage and frequency show smooth transients with a small undershoot (0.97 p.u.) in voltage, the PCC frequency nadir of 60 Hz (60.18 Hz in grid-connected mode), and an overshoot of 60.42 Hz. There are no oscillations in the PCC voltage and frequency. The voltages at the end of the three circuits are maintained above 0.95 p.u.	Unlike Scenario 2, SES3 is offline. (1) The 26-MW PV facility is less curtailed (from 0.2 to 0.167) because PV2 is offline. (2) SES2 can act as a slack bus to balance the generation and load to maintain the system. (3) Each circuit has one capacitor bank on. (4) There is no need to use SES3.
7	*Successful planned islanding operation*. When the PCC circuit breaker is opened, the active and reactive power at the PCC are 450 kW and 500 kVAR, respectively. The microgrid reaches steady state within 4 seconds after the PCC circuit breaker is opened. The PCC voltage and frequency show smooth transients with a small undershoot (0.95 p.u.) in voltage, the PCC frequency nadir of 60 Hz (60.18 Hz in grid-connected mode), and an overshoot of 60.42 Hz. There are no oscillations in the PCC voltage and frequency. The voltages at the end of Ckt1 and Ckt3 are maintained above 0.95 p.u., and the end-of-circuit voltage for Ckt2 is 0.923 p.u.	There is high load and high PV. The general rule for reactive power dispatch: If the reactive power demand is less than 300 kVAR, SES2 is used; if the demand is between 300 and 500 kVAR, SES1 is used; otherwise, the 26-MW PV facility is used. (1) The 26-MW PV facility needs to be completely curtailed (from 0.9 to 0) to reduce the excessive active power. (2) SES1 is dispatched to generate 500-kVAR reactive power after the islanding operation. (3) Ckt1 has two capacitor banks on, and

		Ckt2 and Ckt3 each have one capacitor bank on. (4) A reactive power generation source with flexible dispatchability is needed to regulate the voltage at Ckt2, such as turning on the volt-VAR smart inverter function of the rooftop PV.
8	*Unsuccessful planned islanding operation*. When the PCC circuit breaker is opened, the active and reactive power at the PCC are -400 kW and 500 kVAR, respectively. The PCC voltage exhibits oscillations for 6 seconds before settling at 1 p.u. The PCC frequency increases beyond the operation limit, so the planned islanding is not successful.	(1) The 26-MW PV facility is curtailed from 0.9 to 0 because minimum power from the facility is 10% of capacity. The dispatched power is less than 10% of the PV1 capacity, so the facility is curtailed fully.
9	*Successful planned islanding operation.* When the PCC circuit breaker is opened, the active and reactive power at the PCC are 800 kW and 500 kVAR, respectively. The PCC voltage settles at 0.98 p.u. within 6 seconds. The PCC frequency shows a nadir of 59.6 Hz and exhibits oscillations before reaching steady state. The Ckt2 end-of-feeder voltage is slightly less than 0.95 p.u.	(1) The 26-MW PV facility is curtailed from 0.9 to 0.18. The 26-MW PV facility supplies the power generated by the 6.5-MW PV facility and additional active power to reduce the active power across the PCC breaker. (2) The diesel generator active and reactive power plots show the high oscillations compared to other scenarios.
10	*Successful planned islanding operation, but the system exhibits some oscillations*. When the PCC circuit breaker is opened, the active and reactive power at the PCC are 300 kW and -500 kVAR, respectively. The microgrid reaches steady state within 5 seconds after the PCC circuit breaker is opened. The PCC voltage and frequency show oscillations before the island operation and worsen after the islanding operation. The PCC voltage is steady before the islanding operation, but it shows oscillations after the islanding operation. SES2 absorbs a small amount of excessive active power and generates approximately 500-kVAR reactive power after the islanding operation. The voltages at the end of the three circuits are maintained above 0.95 p.u.; however, they exhibit very large oscillations (magnitude of 0.14 p.u.).	(1) The 26-MW PV facility is curtailed from 0.9 to 0.25. The 26-MW PV facility supplies the power generated by the 6.5-MW PV facility in Scenario 5 and additional active power to reduce the active power across the PCC breaker. It also supplies approximately 1-MVAR reactive power to take the power generated in SES1 from Scenario 5. (2) SES2 can act as a slack bus to balance the generation and load to maintain the system. (3) Ckt1 has two capacitor banks on, and Ckt2 and Ckt3 each have one capacitor bank on.
11	*Successful planned islanding operation.* The results are the same as Scenario 7.	Compared to Scenario 5, in this scenario, SES3 is offline. Because the frequency is maintained close to nominal, there is no need for SES3, and the system functions well without it.
12	*Successful planned islanding operation, but the system exhibits some oscillations*. When the PCC circuit breaker	Compared to Scenario 6, in this scenario, SES3 is offline, and

	is opened, the active and reactive power at the PCC are close to zero. The microgrid reaches steady state within 5 seconds after the PCC circuit breaker is opened. The PCC voltage and frequency show oscillations after the islanding operation, but the oscillations are smaller than those in Scenario 6. SES2 has active and reactive power output close to zero. The voltages at the end of the three circuits are maintained above 0.95 p.u. with reduced oscillations compared to Scenario 6.	the PCC power flow is closer to zero. This helps reduce the harmful transients during the islanding operation and avoids saturation of SES2.
13	*Successful planned islanding operation*. When the PCC circuit breaker is opened, the active and reactive power at the PCC are 2.4 MW and 2 MVAR, respectively. The microgrid reaches steady state within 0.5 seconds after the PCC circuit breaker is opened. The PCC voltage and frequency show smooth transients with an undershoot (0.85 p.u.) in voltage and a PCC frequency overshoot of 60.15 Hz. There are no oscillations in the PCC voltage and frequency.	There is high load and no PV. (1) Most load is disconnected because only 1.5 MW of power is available. (2) Significant effort is made to tune the voltage control of SES2. PID control must be used to maintain voltage stability. (3) This scenario shows an extreme case where there is not enough generation and there is very little flexibility to balance the generation and load; however, with careful dispatch and tuning of SES2, the microgrid system survives this planned islanding operation.
14	*Successful planned islanding operation*. The results are similar to Scenario 9.	Because the frequency is maintained as stable, there is no need for SES3; therefore, this scenario (with SES3 offline) shows the same results as Scenario 9.

5.2 Unplanned Islanding

The unplanned islanding scenarios simulate situations when the PCC circuit breaker is opened without any planned islanding operation. For example, a fault is imposed on the main grid, and the PCC relay detects the abnormal condition and opens the PCC switch, then the microgrid transitions to islanded mode. Note that the 26-MW PV facility, PV1, is not included in the simulation, as agreed with SDG&E. The unplanned islanding operation includes three scenarios, as listed in Table 19.

Table 19. Unplanned Islanding Operation Test Cases

Test No.	Loading	PV2	Rooftop	Diesel	SES1 and SES2	SES3
1	Morning	On	On	Offline	On	On
2	Noon	On	On	Offline	On	On
3	Night	Offline	Offline	Offline	On	On

Table 20 shows all three load scenarios. Unlike planned islanding, where SES1 and PV1 are used to regulate the power through the PCC breaker prior to islanding, no such changes are made in the unplanned islanding. Because this is an unplanned islanding scenario, all generation sources are not dispatched to reduce the power through the PCC breaker. In addition to SES2, PV2 and the rooftop PV are the other generation sources. Capacitor banks are used to supply the reactive power requirement of the network.

Table 20. Loading Scenarios for Unplanned Islanding

Loading	Active Power (MW)	Reactive Power (MVAR)
Morning	4.4	2.362
Noon	7.7	3.062
Night	9.2	3.5

Table 21. Rooftop and PV2 Active Power Generation for Unplanned Islanding

Generation	Rooftop Active Power (MW)	PV2 Active Power (MW)	Total Power (MW)
Morning	1.087	1.24	2.33
Noon	4.9	5.85	10.75
Night	0	0	0

5.2.1 Scenario 1: Morning

In the morning scenario, the solar inverters are generating approximately 20% of their rated power. SES1 is connected, but the power dispatch is assumed to be zero in grid-connected mode. PV2 is generating 20% of capacity (6.5 MW). One capacitor bank in each circuit is assumed to be connected to the network, with a combined capacity of 3.6 MVAR. Based on the SDG&E operation scenario, the 69-kV bus is offline, and only the 12-kV bus is energized. When the PCC breaker opens, all breakers that energize 69-kV buses simultaneously open. After the PCC breaker opens due to a fault or any abnormal situation, the load remains unchanged, and SES2, which is on standby, changes its mode of operation from GFL to GFM. In this scenario, SES2, PV2, and the rooftop PV, with a combined capacity of 3.4 MVA, and the capacitor banks, 3.6 MVAR, are the only generation sources to support the load. Figure 45 (e) and (f) show that the PCC power prior to the islanding operation is 3 MW and 0.5 MVAR. After islanding, SES2 needs to supply approximately 3 MW, but the rated capacity is 1 MW, so there is not enough generation available to support the full load in case of unplanned islanding. This is also shown in Table 20 and Table 21. Figure 46 (e) and (f) show that SES2 is operating at 1.2 p.u. of capacity because the overcurrent limit is set at 1.2 p.u. When it reaches full capacity, the current control loop saturates and acts as a constant current, thereby the voltage collapses. Figure 45 (b) Figure 46 (a) show the voltage collapsing from 1 p.u. to 0.78 p.u. as soon as the PCC breaker is opened. Because the voltage is below the operating limits, the unplanned islanding in the morning scenario will not be successful.

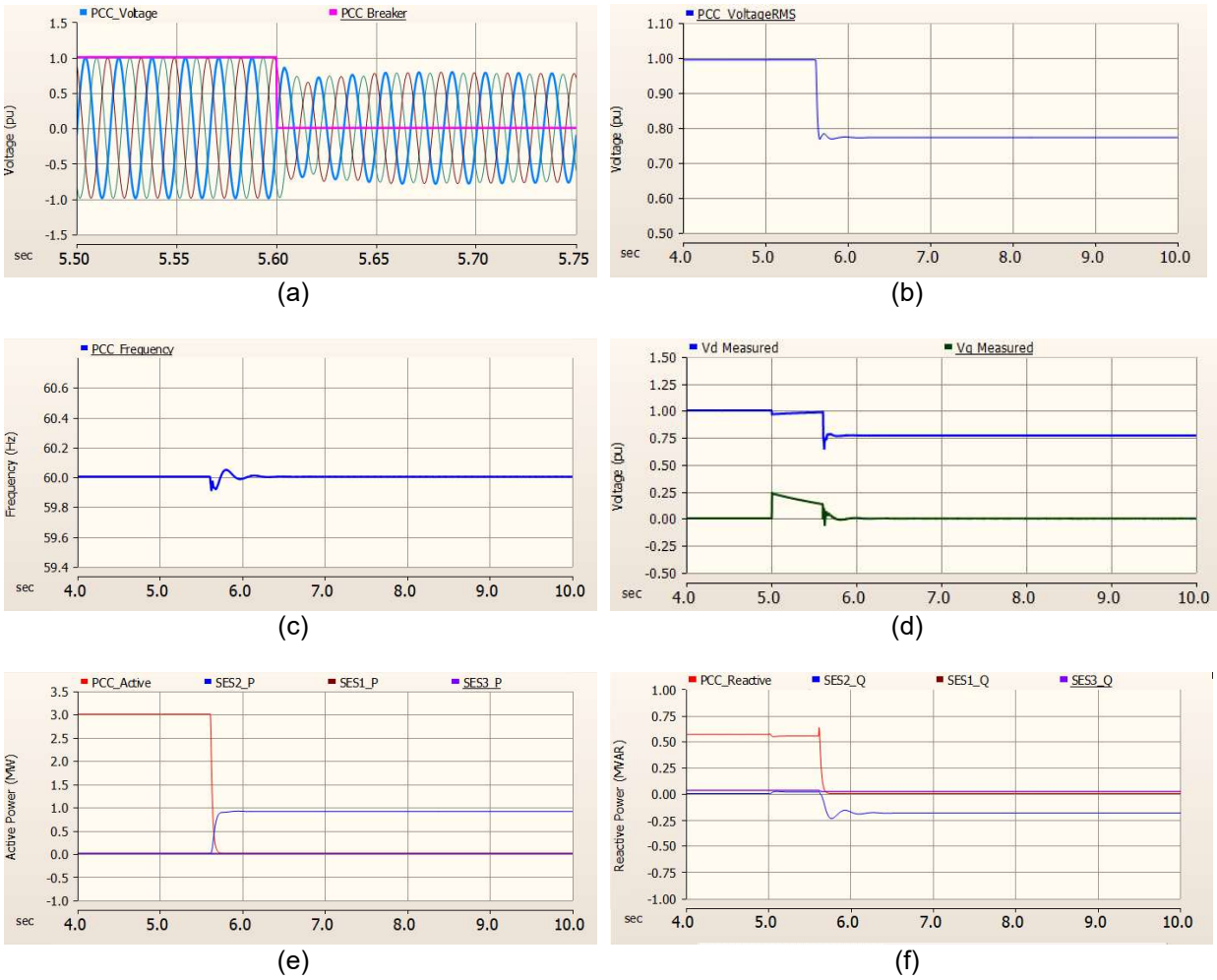

Figure 45. Morning unplanned islanding scenario: (a) microgrid PCC instantaneous voltage, (b) microgrid PCC RMS voltage, (c) microgrid PCC frequency, (d) SES2 Instantaneous voltage, and (e) and (f) active and reactive power generation sources

Figure 46 (b) shows the dq current references generated in the outer loop of SES2. The nominal current limit of the GFM inverter is assumed to be 1.2 p.u (2 kA). When the inverter reaches capacity, the dq current references generated from the outer control loop are limited. Various current-limiting techniques are available based on the synchronous reference frame or the natural reference frame. For SES2, the natural reference frame-based limiting technique is implemented. In simple terms, the dq current references are converted to three-phase currents, and the sine current limiter is applied before converting to the dq references again. Figure 46 (c) shows the current references in the three-phase currents at 1.2 p.u. Because the outer loop is saturated, the GFM inverter acts as a constant current source and loses its ability to maintain the voltage set point.

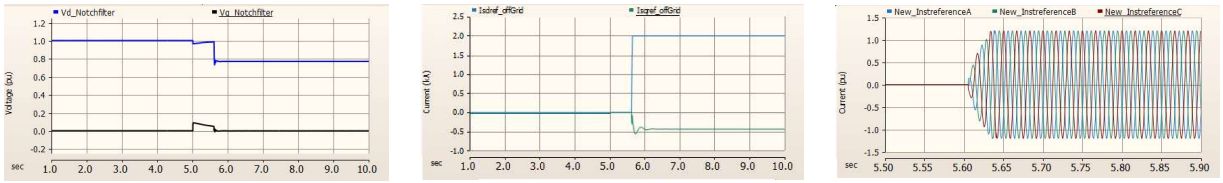

Figure 46. Morning unplanned islanding scenario: (a) SES2 dq voltages, (b) SES2 dq current references, and (c) instantaneous current references

5.2.2 Scenario 2: Noon

In the noon scenario, the rooftop PV and PV2 are generating approximately 90% of capacity. SES1 is connected to the network, but the power dispatch is assumed to be zero in grid-connected mode. Three capacitor banks are cumulatively generating 3.6 MVAR. The total available generation from all the generation sources excluding SES2 is 10.74 MW, 3.6 MVAR. Figure 47 shows the simulation results for the noon scenario. Figure 47 (e) and (f) show that SES2 is generating only half the capacity. With excess generation, the PCC voltage increases and is very close to the maximum operating voltage. This unplanned islanding scenario is stable because the voltage and frequency reached a new steady state, but the PCC voltage reached an operational limit, which can trigger overvoltage protection relays.

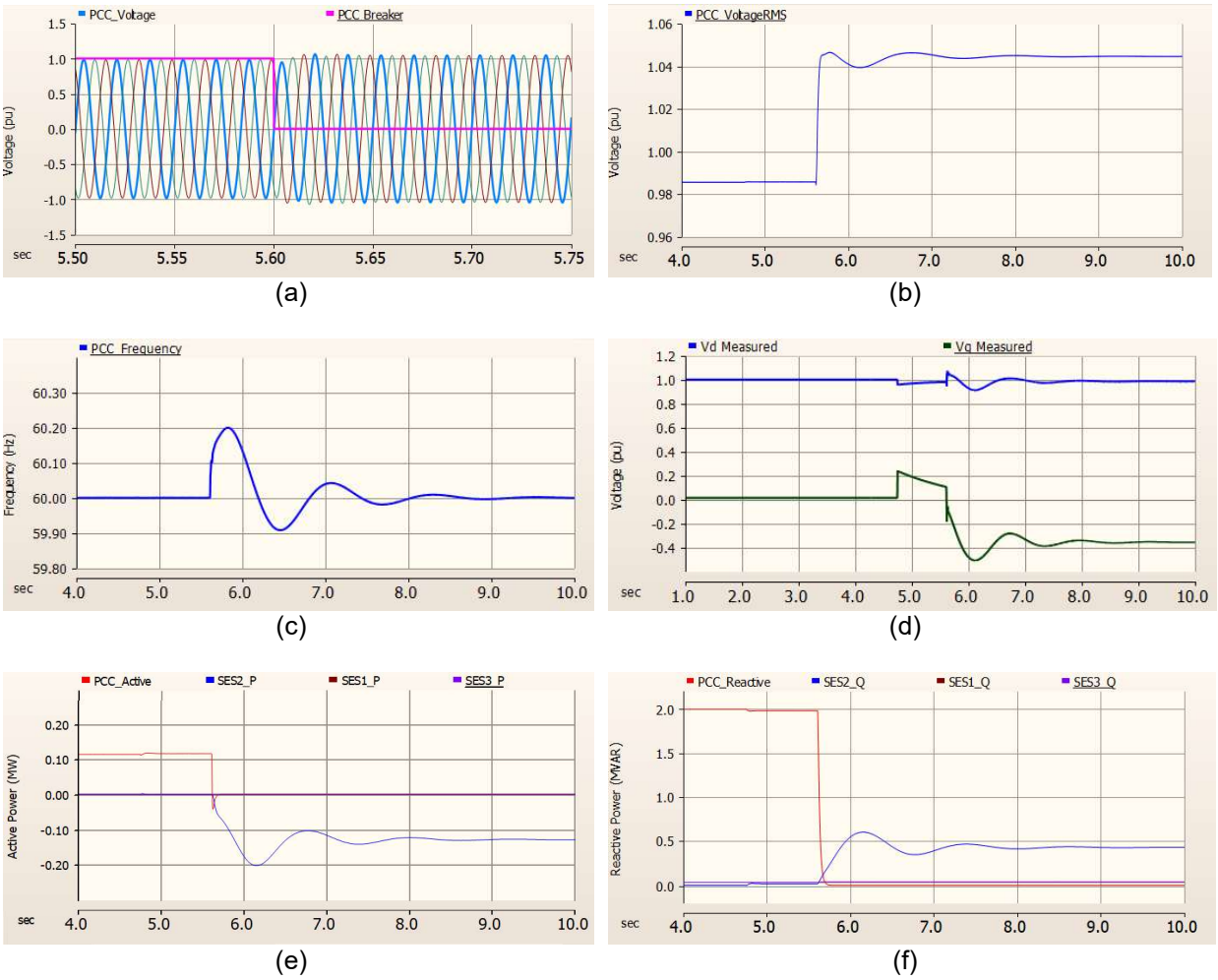

Figure 47. Noon unplanned islanding scenario: (a) microgrid PCC instantaneous voltage, (b) microgrid PCC RMS voltage, (c) microgrid PCC frequency, (d) SES2 dq voltage, and (e) and (f) active and reactive power generation sources

5.2.3 Scenario 3: Night

In the night scenario, the solar generation (rooftop, PV2) generates zero power (Table 21), and the load is very high (Table 20). SES2 and the capacitor banks are the only generation sources available to support the load after the unplanned islanding. Table 20 and Table 21 show that the available generation is only 10% of the active power demand; therefore, unplanned islanding in the night scenario will not be successful.

5.3 Contingency Events

This scenario tests the islanded microgrid under selected disturbance events to evaluate the transient stability of the microgrid. The events include:

1. Faults (LG, LLLG, and LLG)
2. Loss of generation (e.g., SES1)
3. Load rejection

4. Solar insolation transient conditions after islanding, e.g., clouds or rooftop PV coming online.

Table 22 summarizes the three testing scenarios. Note that the diesel generator is used only in the night scenario when there is not enough generation due to the loss of the solar generation.

Table 22. Contingency Event Test Cases

Test No.	Loading	PV2	Rooftop	Diesel	SES1 and SES2	SES3
1	Morning	On	On	Offline	On	On
2	Noon	On	On	Offline	On	On
3	Night	Offline	Offline	On	On	On

The islanded microgrid is tested under the four different contingencies described. It is assumed that the microgrid is successfully islanded and that the contingency events, such as faults, are applied thereafter. The simulation results show the stability of the islanded microgrid before applying any contingency events. In these scenarios, the PV1 branch and the 69/12-kV transformers are all de-energized.

5.3.1 Faults

In the noon scenario, SES1, the rooftop PV, and PV2 are the active power generation sources (see Table 17). The capacitor banks supply the reactive power to the network. Figure 48 shows the successful islanded microgrid's stability at 5.6 seconds of simulation time. Figure 48 (b) shows the PCC RMS voltage at the 12-kV bus, which shows an increase in voltage due to the overgeneration of active power.

Per SDG&E's inputs, LG and LLG faults with a fault impedance of 0.01 Ω are simulated on the end of the Ckt2 at N214. Initially, an LG fault is applied at 11.5 seconds of the simulation time for 10 cycles (0.166 seconds), and the results are shown in the following. It is assumed that the protection isolates the fault within 10 cycles. Figure 48 (a) shows the decrease in voltage on Phase A for 10 cycles and the recovery to nominal voltage. When one of the phase voltages reduces, the three-phase load in the network draws power from the remaining two phases. Due to an imbalance in the network, the voltage magnitude reduces differently for the other two phases. Figure 48 (b) shows the RMS voltage during the fault. The voltage magnitude decreases to 0.7 p.u. and recovers to the nominal voltage after the fault has been removed. Figure 49 (a) shows the subsequent SES2 dq voltages during the fault. Figure 49 (b) shows the SES2 current increasing in the faulted phase and the other two-phase current increasing due to the three-phase load. Figure 48 (c) shows the low-frequency transients during the fault and the recovery to the nominal value prior to the fault. SES1 and SES2 have ride-through enabled, which is shown in the active and reactive power measurements in Figure 48 (e) and (f). The simulation results show that the islanded microgrid can survive an LG fault for 10 cycles far from the generation sources.

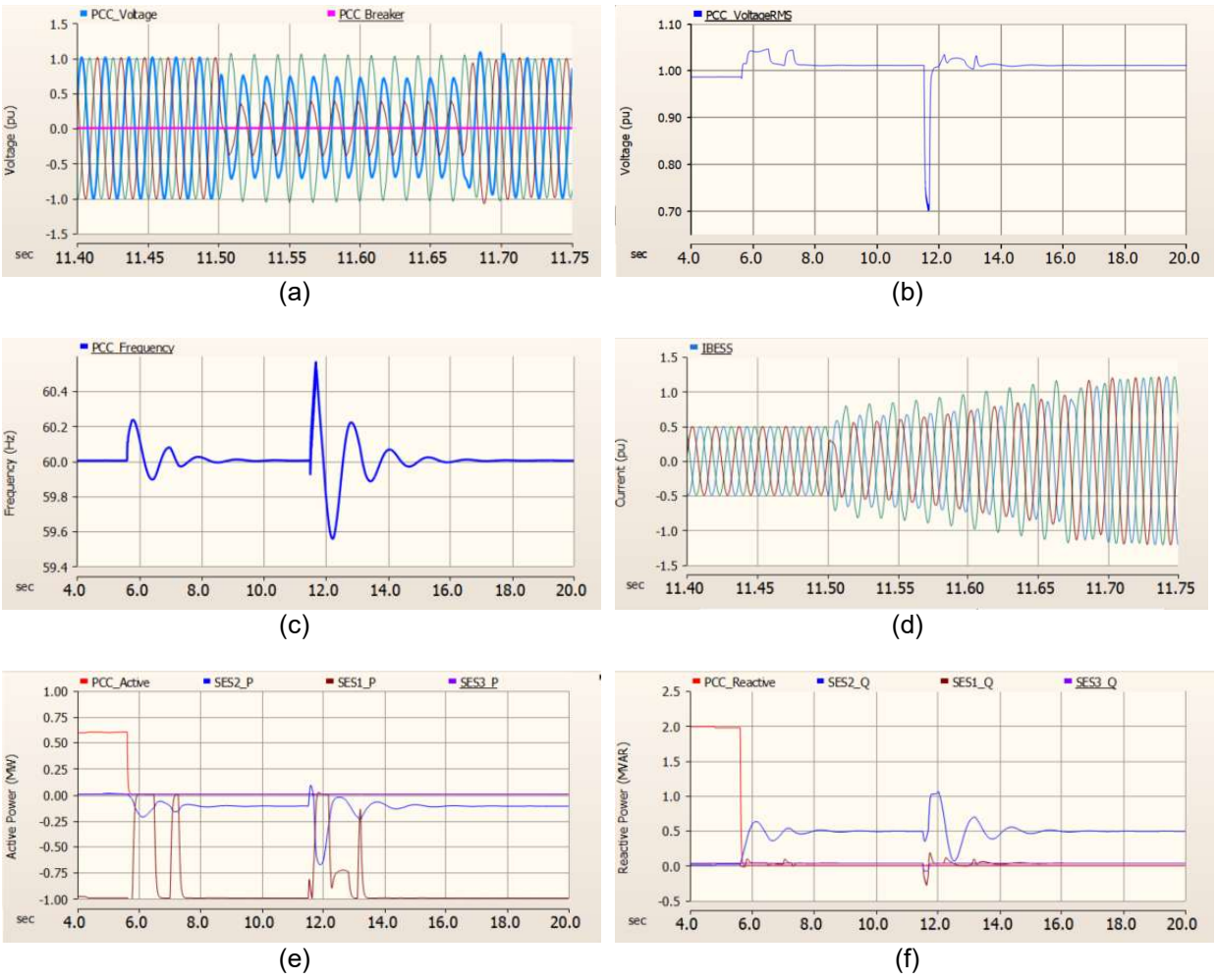

Figure 48. LG fault contingency for the noon scenario: (a) microgrid PCC instantaneous voltage, (b) microgrid PCC RMS voltage, (c) microgrid PCC frequency, (d) SES2 instantaneous current, and (e) and (f) active and reactive power generation sources

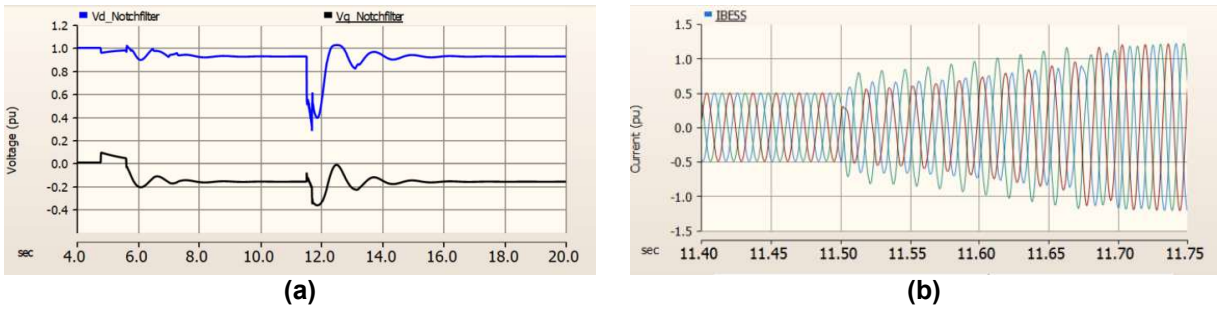

Figure 49. LG fault contingency for the noon scenario: (a) SES2 dq0 voltages and (b) SES2 current

Figure 50 shows the results for the LLG contingency event with a fault impedance of 0.01 Ω. An LLG fault is placed on Phase B and Phase C at 11.6 seconds. As the two-phase voltages collapse, SES2 cannot maintain the other phase voltage, and eventually the microgrid voltage collapses. Figure 51 (a) also shows the SES2 dq voltages collapsing during the fault. Figure 51 (b) shows the subsequent increase in SES2 current. Therefore, the microgrid cannot survive LLG faults.

GFM inverter controls require negative-sequence and virtual impedance control to ride through the severe faults [11].

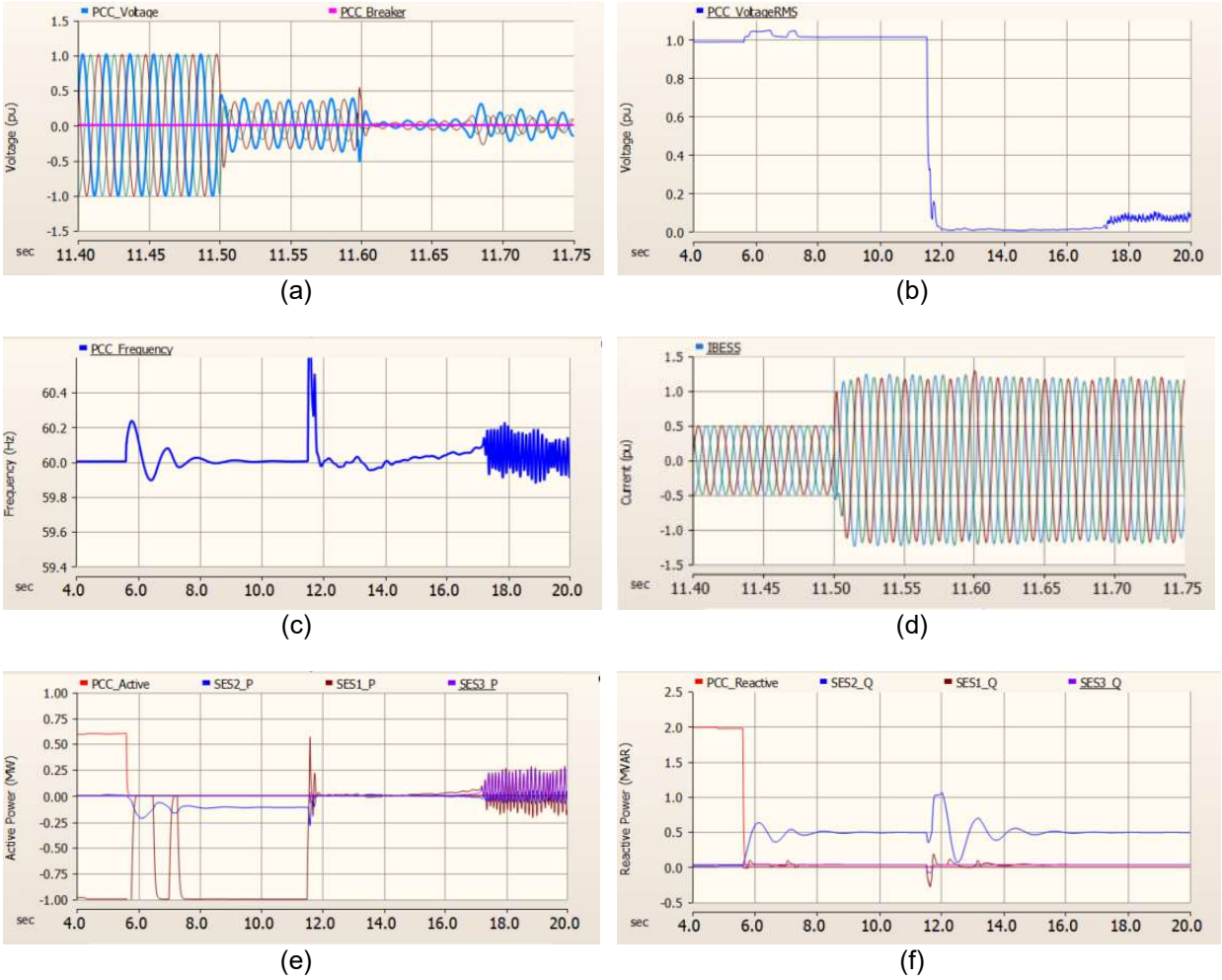

Figure 50. LLG fault contingency for noon scenario: (a) microgrid PCC instantaneous voltage, (b) microgrid PCC RMS voltage, (c) microgrid PCC frequency, (d) BESS instantaneous current, and (e) and (f) active and reactive power generation sources

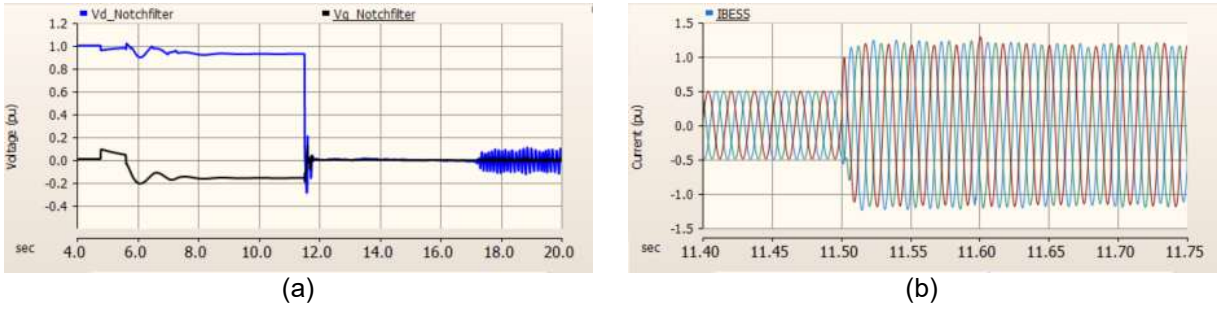

Figure 51. LLG fault contingency for noon scenario: (a) SES2 dq0 voltages and (b) SES2 current

5.3.2 Loss of Generation

As shown in the noon scenario results in Figure 52, the islanded microgrid is stable after the PCC breaker is opened. SES1 is operating at full capacity and absorbing real power. In this scenario, SES1 is assumed to be lost/offline after the stable microgrid event at 11.6 seconds. Figure 52 (b)

shows that the loss in SES1 causes the PCC voltage to increase due to excess generation. This phenomenon is observed in the unplanned islanding scenario. Overall, this simulation scenario shows that the microgrid is stable after SES1 is lost, but the PCC voltage has reached an operational limit, which can trigger overvoltage relays.

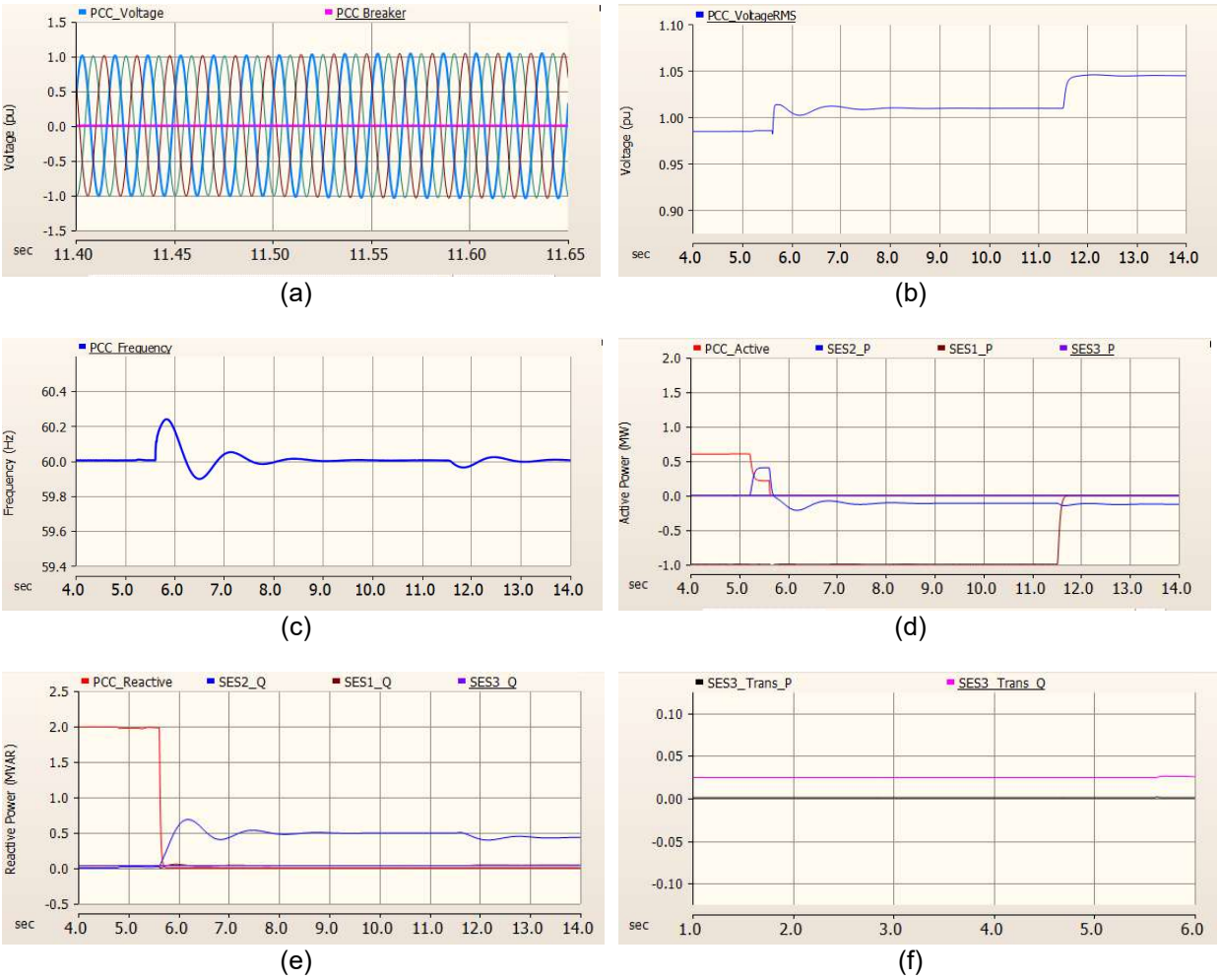

Figure 52. SES1 Loss of generation contingency event for the noon scenario: (a) microgrid PCC instantaneous voltage, (b) microgrid PCC RMS voltage, (c) microgrid PCC frequency, (d) and (e) active and reactive power generation sources, and (f) SES3 generation

5.3.3 Load Rejection

To study the transient stability response of SES2 (GFM) in case of a sudden load rejection, the simulation is performed under the noon load scenario. Due to the excess and non-dispatchable generation available under the noon scenario, a few changes are made to the available generation setup. The rooftop PV, SES1, and SES2 are assumed to be online. The combined active power generation that is available according to Table 23 is 6.4 MW, whereas the load is 8.8 MW. Even though three capacitor banks of 1.2 MVAR each can generate the sufficient reactive power required for the load shown in Table 23, the actual demand is more after considering the rooftop PV transformers (see Table 6). Four loads of combined power 3.41 MW and 1.1 MVAR are dropped from Ckt1, Ckt2, and Ckt3.

Table 23. Generation and Load for Load Rejection Scenario

Description	Active Power (MW)	Reactive Power (MVAR)
Load	8.8	3.5
SES1	0.5	0
Rooftop	4.9	0
6.5-MW PV	0	0
Capacitors	0	3.6
26-MW PV facility	0	0

Figure 53 shows the simulation results for the load rejection. The results show that the islanded microgrid is stable after the PCC breaker opens at 5.6 seconds. Prior to the load rejection, SES2 is loaded at 1.14 MVA, which is already a temporary overloading condition. At 10 seconds, a 0.5-MVA load is removed on Ckt2 to simulate a sudden load rejection. Figure 53 (d) and (e) show SES2 stabilizing in the active and reactive power generation within less than 1.5 seconds after the load has been removed. In response to the load being removed, SES2 decreases its active power generation and increases the reactive power absorption. After the load rejection, SES2 is at 1.16 MVA, which is a temporary overloading condition. This simulation results show that SES2 can respond to the contingency events provided that SES2 has the capacity to generate/absorb power.

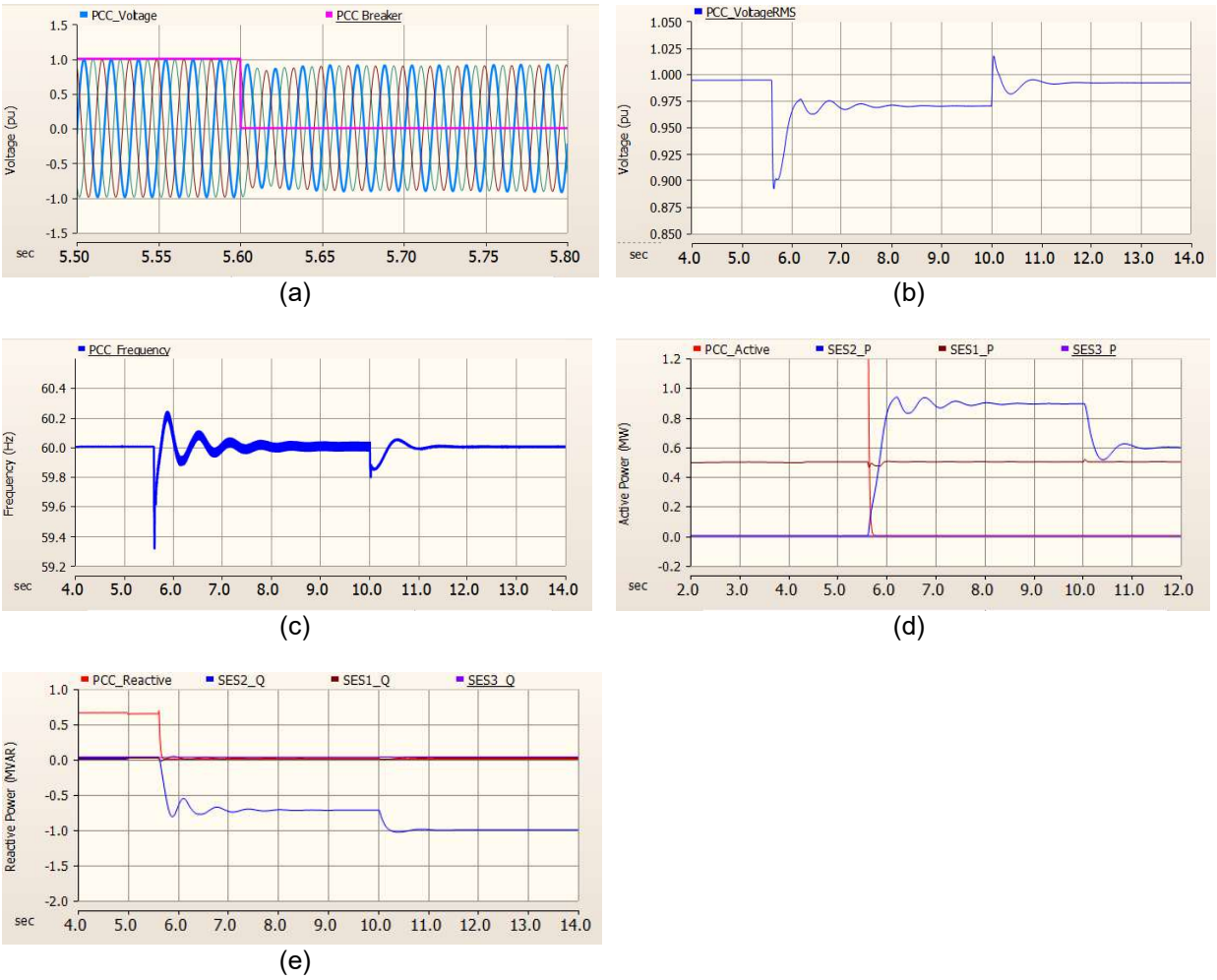

Figure 53. Load rejection event for the noon scenario: (a) microgrid PCC instantaneous voltage, (b) microgrid PCC RMS voltage, (c) microgrid PCC frequency, and (d) and (e) active and reactive power generation sources

6 Conclusion

6.1 Lessons Learned

This comprehensive EMT transient stability study provides insights into the system stability of the Borrego Springs Microgrid, especially the performance of the islanding leader, the SES2 GFM battery inverter. The lessons learned from this study are organized by EMT modeling and simulation scenarios, microgrid system transient stability, and the value for field deployment.

- EMT modeling and simulation scenarios:
    - Simulating the Borrego Springs network with 105 inverters is challenging, so the network is divided into three sections to simulate them in parallel. The sections are defined so that the DERs are distributed roughly equally across the three sections to reduce the overall simulation time.
    - For all the simulation scenarios, the capacitor banks (1.2 MVAR each) located at the end of the feeders are used to meet the reactive demand. Turning on/off the capacitor banks injects/stops injecting 1.2 MVAR of reactive power. In the planned islanding event, the lack of intermediate steps of reactive power from the capacitor banks causes SES2 to reach its full capacity (without the diesel generators), which means that SES2 does not have any capacity available for transients. In case of a black start, SES2 supports the active and reactive power, which means that part of the feeder is energized.
    - If the rooftop PV, the volt/VAR function can be used to support the voltage. It will reduce the dependence on the capacitor banks in conditions with low reactive power demand.
- Microgrid system transient stability:
    - Only one inverter, SES2, is operating in GFM mode during the islanding conditions. Prior to the planned islanding, power through the PCC breaker should be kept at a minimum to reduce the transients during the islanding operation. It is also important that the GFM loading level be kept at a minimum to ride through any transient/contingency events.
    - The stability of the microgrid system is highly dependent on the GFM inverter controls. For example, for all the simulation scenarios, the PID controller of the islanding leader needed to be properly tuned (PI versus PID) to have a stable microgrid. This is concerning because it is hard to find one set of control parameters that works for all the scenarios. In this project, NREL developed and utilized its own inverter model because the inverter manufacturer was unable to provide a PSCAD model. While the NREL inverter model is representative of state-of-the-art GFM inverters, our findings related to the inverter controls cannot be directly applied to the field inverter. Adaptive PID control in the GFM inverter might be needed to adaptively tune the PID control parameters to work with all the scenarios.
    - Through extensive EMT simulations, the stability of the Borrego Springs Microgrid can be summarized as:

i. The system operates well under planned islanding with SES2 as the islanding leader.
ii. It is hard for the system to survive unplanned islanding.
iii. A black start with only renewable resources can pick up the critical load in Ckt2 even at night, and the diesel generator can be successfully brought online to pick up more load.
iv. It is hard for the system to survive an LLG fault, but it can ride through LG faults, and the system can maintain stability with a large load rejection.

- Value for field deployment:
    - During islanded mode (without diesel generators), the reactive power demand requires at least three capacitor banks to supply the demand; therefore, the system should turn on three capacitor banks in grid-connected mode prior to the planned islanding.
    - The Borrego Springs Microgrid can achieve successful planned islanding for the morning, noon, and night scenarios with preplanned power dispatch; however, unplanned islanding is challenging, and the microgrid might survive only when there is enough generation and the imbalance between the generation and load is not significant.
    - Following the distribution operation procedure and load priority, a black start can be smoothly executed by reconnecting the grid elements one by one. For the morning scenario, the system can pick up approximately 1.8 MW and 1.2 MVAR native load including load from Ckt1, Ckt2, and Ckt3 without using the diesel generators. For the noon scenario, the system can pick up approximately 1.3 MW and 0.5 MVAR native load including load from Ckt1 without using the diesel generators. For the night scenario, the system can pick up 1 MW and 0.3 MVAR native load including load from Ckt1 without using the diesel generators, and the system can pick up 4 MW and 1.1 MVAR native load including load from Ckt1 and Ckt2 using one diesel generator. In the night scenario, the simulation is unstable when the second diesel is connected. This might be because there is not enough GFM capacity in the system. If SES1 can be used as a second GFM inverter, the system might be stable. This needs further investigation.
    - For fault events, the islanding leader can survive an LG fault; however, an LLG fault has more imbalance in the voltage, and the islanding leader, SES2, cannot survive. Similar to our observation on inverter controls for stability, fault ride-through is also very dependent on inverter controls, and because we used an NREL-developed inverter model, the performance in the field might differ. If issues are encountered in the field, virtual impedance control is recommended to cope with this situation. For the load rejection test with a large load disconnected, SES2 is able to automatically adjust to the load change and ride through the transients in the voltage and current.
    - During the black-start simulations, voltage and power oscillations are observed as more load is energized, which points to possible interactions between the load, rooftop PV, and BESS models in PSCAD; therefore, we do not expect this

behavior to occur in the field, but this phenomenon needs to be investigated if it occurs in field-testing.
    - Overall, SES2, the islanding leader and the only GFM source, can support the microgrid operation well enough to handle normal operations (e.g., planned islanding and black starts) and some abnormal operations (LG fault and some unplanned islanding). If one more GFM source can be added, the system might be capable of handling abnormal operations. In addition, the islanding leader, SES2, has a faster settling time than the diesel generator as the GFM source, and it can perform equivalent to the diesel generator; therefore, using a GFM inverter could replace the traditional diesel generator to make a 100% renewable microgrid feasible.

6.2 Future Work

This EMT model can serve as a baseline model for the Borrego Springs Microgrid to add more IBRs to the system as SDG&E plans to integrate more renewable resources, especially GFM inverters. With the updated EMT model, a transient stability study can be performed to investigate the stability and reliability of the microgrid from the following aspects:

- Study the best operation modes and droop settings for multiple GFM inverters with different capacities. Currently, a single islanding leader, a GFM inverter, is used even though other battery inverters are also GFM-capable. If multiple GFM inverters run in parallel, the best droop settings need to be investigated, especially under the worst scenario, e.g., unplanned islanding. Moreover, secondary control can be studied as well because reactive power sharing is a problem when multiple GFM inverters run in parallel.
- Troubleshoot and investigate any observed instability/oscillations in the field. A high-fidelity EMT model reflects the real-world power system, and the EMT model can recreate the instability/oscillations observed in the field. Through targeted troubleshooting, those observed problems can be mitigated.
- Perform specific EMT simulations to evaluate the capabilities of the microgrid with more IBRs, such as a black start and planned and unplanned islanding. For a black start, the most straightforward measure of the microgrid capability is how much load can be picked up under different loading conditions (morning, noon, and night). Planned and unplanned islanding tests whether the microgrid can survive under those conditions.

References

[1] Hilal Katmale, Sean Clark, Thomas Bialek, and Laurence Abcede, "Borrego Springs: California's First Renewable Energy-Based Community Microgrid," CEC-500-2019-013, Feb. 2019. [Online]. Available: https://www.energy.ca.gov/sites/default/files/2021-05/CEC-500-2019-013.pdf.

[2] Y. N. Velaga, J. Wang, A. Pratt, L. Abcede, and N. Shamukh, "Transient Stability Study of a Real-World Microgrid with 100% Renewables," in *2022 IEEE Energy Conversion Congress and Exposition (ECCE)*, Detroit, MI, USA: IEEE, Oct. 2022, pp. 1–8. doi: 10.1109/ECCE50734.2022.9947656.

[3] J. Wang, A. Pratt, K. Prabakar, B. Miller, and M. Symko-Davies, "Development of an Integrated Platform for Hardware-in-the-Loop Evaluation of Microgrids Prior to Site Commissioning," *Applied Energy*, vol. 290, p. 116755, May 2021, doi: 10.1016/j.apenergy.2021.116755.

[4] K. Prabakar *et al.*, "Site-Specific Evaluation of Microgrid Controller Using Controller and Power-Hardware-in-the-Loop," in *IECON 2019 - 45th Annual Conference of the IEEE Industrial Electronics Society*, Lisbon, Portugal: IEEE, Oct. 2019, pp. 6463–6468. doi: 10.1109/IECON.2019.8927354.

[5] H. Wang, M. Wang, Q. Cheng, S. Lv, and X. Ji, "Modeling Simulation and Inverter Control Strategy Research of Microgrid in Grid-Connected and Island Mode," *Energy Reports*, vol. 8, pp. 206–218, Nov. 2022, doi: 10.1016/j.egyr.2022.09.117.

[6] T. Orchi, M. Mahmud, and A. Oo, "Generalized Dynamical Modeling of Multiple Photovoltaic Units in a Grid-Connected System for Analyzing Dynamic Interactions," *Energies*, vol. 11, no. 2, p. 296, Jan. 2018, doi: 10.3390/en11020296.

[7] J. D. Rios Penaloza, J. A. Adu, A. Borghetti, F. Napolitano, F. Tossani, and C. A. Nucci, "Influence of Load Dynamic Response on the Stability of Microgrids During Islanding Transition," *Electric Power Systems Research*, vol. 190, p. 106607, Jan. 2021, doi: 10.1016/j.epsr.2020.106607.

[8] J. Wang *et al.*, "Diesel Generator Controller Evaluation via Controller-Hardware-in-the-Loop for Various Microgrid Operation Modes," in *2019 IEEE Power & Energy Society Innovative Smart Grid Technologies Conference (ISGT)*, Washington, DC, USA: IEEE, Feb. 2019, pp. 1–5. doi: 10.1109/ISGT.2019.8791660.

[9] "IEEE Standard for Interconnection and Interoperability of Distributed Energy Resources with Associated Electric Power Systems Interfaces," IEEE. doi: 10.1109/IEEESTD.2018.8332112.

[10] J. G. O'Brien *et al.*, "Electric Grid Blackstart: Trends, Challenges, and Opportunities."

[11] J. Wang, “Improved Control Strategy of Grid-Forming Inverters for Fault Ride-Through in a Microgrid System,” in *2022 IEEE Energy Conversion Congress and Exposition (ECCE)*, Detroit, MI, USA: IEEE, Oct. 2022, pp. 1–7. doi: 10.1109/ECCE50734.2022.9948153.